

**UNIVERSIDAD DE BURGOS**

**Departamento de Química**

**Área de Química Orgánica**

Design and synthesis of bioactive small  
molecule anionophores inspired on natural  
products

by

**Elsa Hernando Santa Cruz**

Thesis for the degree of Doctor of Philosophy

2017





ROBERTO QUESADA PATO, Profesor Titular del Área de Química Orgánica del Departamento de Química de la Universidad de Burgos.

INFORMA:

Que la presente memoria titulada *“Design and synthesis of bioactive small molecule anionophores inspired on natural products”* ha sido realizada en el Departamento de Química de la Universidad de Burgos, bajo su dirección, por la licenciada Elsa Hernando Santa Cruz y autoriza su presentación para que sea calificada como Tesis Doctoral.

Burgos, mayo 2017

Fdo.: Roberto Quesada Pato



*A mis padres,  
por estar siempre a mi lado*



## Acknowledgements

En primer lugar quiero agradecer a mi director, Roberto, la oportunidad que me dio para realizar esta tesis doctoral bajo su supervisión, apoyándome y motivándome durante estos años. A María, por resolverme dudas y ayudarme en todo lo que le fue posible a lo largo de este tiempo.

A todos mis compañeros de grupo y del laboratorio de la puerta de al lado, por estos años de trabajo compartido pero también de buenos ratos y risas. A Estela, Any y Ana por aquellos comienzos cuando todavía no sabíamos por donde nos daba el aire, a Rubén por esos días comiendo en que pretendíamos arreglar el mundo y en especial a Andrea por ser mi apoyo en todo momento y acabar convirtiéndose en mi amiga.

Agradezco a Marta, Jacinto y Pilar su disponibilidad siempre que he necesitado su ayuda.

A mis amigas y amigos por todos sus consejos que han resultado ser los mejores y por estar ahí cuando les he necesitado y cómo no, a ese último empujón de aire fresco que vino con Pablo.

Por último quiero agradecer a toda mi familia su apoyo y confianza en mí, porque sin ellos esto no hubiera sido posible.



## Abbreviations

A	absorbance
$\alpha$ -CD	$\alpha$ -cyclodextrin
ABC	ATP binding cassette
AcOEt	ethyl acetate
AE	anion exchanger
aq.	aqueous
ATP	adenosine triphosphate
Å	Angstrom
Bn	benzyl
Boc	tert-butyloxycarbonyl
BODIPY	boron-dipyrromethene
CB-7	cucurbit[7]uril
$C_c$	concentration of the concentrated solution
CD	cyclodextrin
$C_d$	concentration of the diluted solution
C.I.	coefficient interval
CF	5(6) carboxyfluorescein
CF	cystic fibrosis
CFTR	cystic fibrosis transmembrane conductance regulator
ClC	chloride channels
CSF	cerebrospinal fluid
CHCl <sub>3</sub>	chloroform
CH <sub>3</sub> CN	acetonitrile
COSY	correlation spectroscopy
Cp*RuCl	ruthenium catalysed reaction
CSCs	cancer stem cells

Cte.	constant
CuAAC	copper catalysed reaction
CyPLOS	cyclic phosphate-linked oligosaccharide
D	debye
DCE	1,2-dichloroethane
DCM	dichloromethane
DEF	diethylformamide
DEPT	distortionless enhancement by polarization transfer
DFT	density functional theory
Diss.	dissolved
DMF	dimethylformamide
DMPC	1,2-dimyristoyl- <i>sn</i> -glycero-3-phosphocholine
DMSO	dimethyl sulfoxide
DOSY	diffusion-ordered spectroscopy
DOPC	1,2-dioleoyl- <i>sn</i> -glycero-3-phosphocholine
DPPC	1,2-dipalmitoyl- <i>sn</i> -glycero-3-phosphocholine
DTTs	dithieno [3,2- <i>b</i> ;2' <i>3'</i> - <i>d</i> ] thiophenes
<i>e</i>	Euler number
EC <sub>50</sub>	half maximal effective concentration
em.	emission
ESI-FTICR-MS-MS	electrospray ionization Fourier-transform ion cyclotron resonance tandem mass spectrometry
Eq.	equation
eq. or equiv.	equivalents
exc.	excitation
EYPC	egg yolk- phosphatidylcholine
f	fluorescence emission at any time
FI	fluorescence intensity

FRET	fluorescence resonance energy transfer
FRT	fischer rat thyroid
$f_0$	initial fluorescence emission
Gluc.	gluconate
GUVs	giant unilamellar vesicles
h	hours
HMBC	heteronuclear multiple bond correlation
HMQC	heteronuclear multiple quantum coherence
H <sub>2</sub> O	water
HPTS	8-Hydroxypyrene-1,3,6-trisulfonic acid
HRMS	high resolution mass spectroscopy
[I]	initial rate
I.S.	ionic strength
ISE	ion selective electrode
ITC	isothermal titration calorimetry
K or K <sub>a</sub>	association constant
Kcal	kilocalories
KJ	kilojoules
K <sub>SV</sub>	Stern Volmer constant
L	liter
L <sub>α</sub>	liquid crystalline or fluid phase
L <sub>β</sub> and L <sub>β'</sub>	solid gel phases
L <sub>c</sub>	subgel phase
Log <i>P</i>	lipophilicity representation where <i>P</i> is the partition coefficient
LUVs	large unilamellar vesicles
λ	wavelength
M	molar

M <sup>+</sup>	metal cation
Me	methyl
MeOH	methanol
mg	milligram
MHz	megahertz
MIC	minimum inhibitory concentration
mM	millimolar
mL	milliliter
μL	microliter
μM	micromolar
MW	microwave
nm	nanometer
nM	nanomolar
NMR	nuclear magnetic resonance
NOESY	nuclear Overhauser effect spectroscopy
<i>o</i>	<i>ortho</i> position
OBn	benzyloxy
OMe	methoxy
<i>p</i>	<i>para</i> position
PC	phosphatidylcholine
PE	phosphatidylethanolamine
PG	phosphatidylglycerol
Pgs	pyrogallol[4]arenes
Ph	phenyl
pHi	intracellular pH
POPE	1-palmitoyl-2-oleoyl-sn-glycero-3-phosphoethanolamine
POPC	1-palmitoyl-2-oleoyl-sn-glycero-3-phosphocholine

POPG	1-palmitoyl-2-oleoyl-sn-glycero-3-phosphoglycerol
ppm	part per million
QSAR	quantitative structure activity relationship
RuAAC	ruthenium catalysed reaction
RT	retention times
SPH	sphingomyelin
$\sigma$	frequency
$t_{1/2}$	the time need to observe a change of 50 % in the fluorescence quenching of lucigenin
TBACl	tetrabutylammonium chloride
TBAF	tetrabutylammonium fluoride
TLC	thin layer chromatography
$T_m$	transition temperature
s	second
SA	acidity
SAR	structure activity relationship
SB	basicity
SCs	stem cells
SEC	size exclusion chromatography
SdP	dipolarity
SP	polarizability
SPH	sphingomyelin
SV	Stern Volmer
S.O.	safranin O
TBA	tetrabutylammonium
TEA	tetraethylammonium
THF	tetrahydrofuran
$T_c$	gel liquid crystal transition temperature

TREN	Tris(2-aminoethyl)amine
UV	ultraviolet
$v$	volume
$V_c$	volume of the concentrated solution
$V_d$	volume of the diluted solution
$V_m$	membrane potential
x 3	three times
$X^-$	anion
YFP	yellow fluorescence protein
°	grade

# Contents

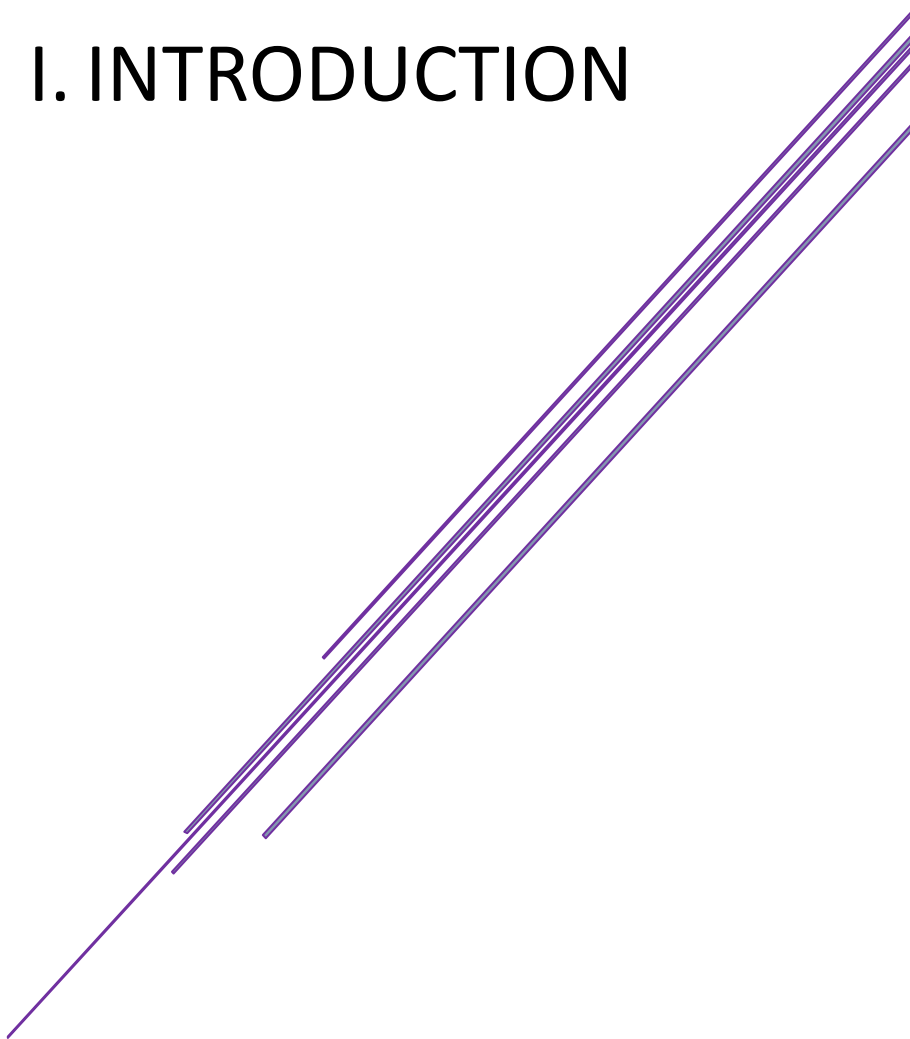
<b>I. INTRODUCTION</b> .....	<b>1</b>
1. Lipid bilayer.....	4
2. Transmembrane transport.....	6
2.1. Chloride transport in nature.....	8
2.2. Bicarbonate transport in nature.....	9
2.3. Transport of anions in vesicle models.....	10
2.3.1. Techniques employed to measure anion transport in vesicle models.....	14
2.3.1.1. Ion-selective electrode assays.....	14
2.3.1.2. Fluorescence based assays.....	14
2.3.1.3. NMR assays.....	16
3. Molecules with activity as transmembrane anion carriers.....	16
3.1. Anion recognition and coordination chemistry.....	16
3.2. Thermodynamic features of coordination chemistry.....	18
3.3. Transmembrane anion carriers.....	19
3.3.1. Transport mechanisms.....	19
3.3.2. Transmembrane anion transport mediated by mobile carriers.....	23
3.3.2.1. Hydrogen bonding interactions.....	23
3.3.2.2. Non-classical interactions.....	40
3.3.3. Transmembrane anion transport promoted by channels.....	42
4. Biological activity of anion transporters.....	45
5. Aims of the thesis.....	49
<b>II. DISCUSSION OF RESULTS</b> .....	<b>51</b>
1. Tambjamine-like transporters.....	53
1.1. Introduction.....	53
1.2. Synthesis.....	57

1.3. Pyrrole–pyrrole tambjamines.....	59
1.3.1. Crystal structures.....	59
1.3.2. Exploring the influence of substituents in the anion transport properties.....	60
1.3.2.1. Chloride binding constants.....	61
1.3.2.2. Anion transport assays.....	64
1.3.3. QSAR analysis.....	70
1.4. Indole–pyrrole tambjamines.....	80
1.4.1. Anion transport assays.....	81
1.4.2. <b>136</b> .HCl and <b>142</b> .HCl study.....	84
1.4.2.1. Crystal structures.....	84
1.4.2.2. Determination of apparent pKa values.....	85
1.4.2.3. Anion binding constants.....	86
1.4.2.4. Anion transport assays.....	88
2. Tetraheterocyclic transporters.....	95
2.1. Introduction.....	96
2.1.1. Prodiginines conformational analysis.....	99
2.1.2. Tetraheterocycles.....	99
2.2. Synthesis.....	101
2.2.1. Mechanism of synthesis.....	101
2.3. Crystal structure.....	101
2.4. Determination of apparent pKa values.....	102
2.5. Anion transport assays.....	103
2.6. BODIPY derivative from <b>158</b> .HCl.....	127
2.6.1. Introduction.....	127
2.6.2. Synthesis.....	128
2.6.3. Characterization of photophysical properties.....	129
2.6.3.1. Solvatochromism.....	131
2.6.4. Anion transport assays.....	135

3. Prodiginine inspired compounds.....	139
3.1. Introduction.....	139
3.2. Synthesis.....	145
3.3. Conformational analysis.....	147
3.3.1. Crystal structure.....	147
3.3.2. Relative conformations in solution.....	147
3.4. Determination of apparent pKa values.....	152
3.5. Binding constants assays.....	153
3.6. Anion transport assays.....	155
<b>III. CONCLUSIONS.....</b>	<b>169</b>
<b>IV. EXPERIMENTAL PART.....</b>	<b>173</b>
1. General remarks.....	175
1.1. Starting reagents and solvents.....	175
1.2. Cromatography.....	175
1.3. Instrumental techniques.....	175
2. Synthetic procedures.....	177
2.1. Tambjamine-like transporters synthesis.....	177
2.2. Tetraheterocyclic transporters synthesis.....	179
2.3. BODIPY synthesis.....	180
2.4. Prodiginine inspired compounds synthesis.....	181
3. Vesicles transport assays.....	183
3.1. Preparation of vesicles.....	184
3.2. Transport assays.....	185
3.2.1. Electrochemical transport assays. Chloride Selective Electrode assays and Hill plots.....	185
3.2.1.1. NO <sub>3</sub> <sup>-</sup> /Cl <sup>-</sup> exchange.....	186
3.2.1.2. SO <sub>4</sub> <sup>2-</sup> /Cl <sup>-</sup> exchange.....	186
3.2.1.3. HCO <sub>3</sub> <sup>-</sup> /Cl <sup>-</sup> , ClO <sub>4</sub> <sup>-</sup> /Cl <sup>-</sup> , AcO <sup>-</sup> /Cl <sup>-</sup> and NO <sub>3</sub> <sup>-</sup> /Cl <sup>-</sup> Exchange.....	187

3.2.1.4. Gluconate <sup>-</sup> /Cl <sup>-</sup> exchange.....	187
3.2.2. Photochemical transport assays. Fluorescence probes.....	188
3.2.2.1. Lucigenin based assays.....	188
3.2.2.2. 5(6)-Carboxyfluorescein based assays.....	189
3.2.2.3. HPTS based assays.....	190
3.2.2.4. Safranin O based assays.....	191
4. Titration and job-plot analysis.....	191
5. Calculation of Lucigenin Stern Volmer constants.....	192
6. pKa measurements.....	193

# I. INTRODUCTION





Ion gradients control the osmotic balance, maintenance of cell homeostasis, synapse or nerves and muscles excitations at the biological level. Transmembrane protein channels or ion channels are responsible of creating and maintaining these concentration gradients on either sides of the lipid bilayer.<sup>1</sup> The ion channels dysfunction implies the lack of a correct ionic transport across the cell membranes. These defects can lead to pathologies such as hyper or hypotension, deafness, osteopetrosis or cystic fibrosis for instance.<sup>2, 3, 4</sup> Supramolecular chemists have been involved in the development of small molecules with activity as transmembrane ion carriers, which can replace protein channel defects.<sup>5, 6, 7, 8, 9, 10</sup>

Supramolecular chemistry studies non covalent interactions. It is a highly interdisciplinary area, which intersects from physics to biology, crystallography or medicine. The Nobel Prize in Chemistry (1987), Jean Marie Lehn, defines it as “*the designed chemistry of the intermolecular bond just as molecular chemistry is that of the covalent bond*”.<sup>11</sup> It is based on non-covalent forces such as ion-ion interactions, ion-dipole interactions, dipole-dipole interactions, hydrogen bonding, cation- $\pi$  interactions, anion- $\pi$  interactions,  $\pi$ - $\pi$  interactions, Van der Waals forces or closed shell interactions.<sup>12</sup> It should not be overlooked that the strength or weakness of the non-covalent forces involved in coordination chemistry are completely dependent of the solvent.

Three different branches could be differentiated in the development of this discipline: molecular recognition, self-assembly and self-organization, and

---

<sup>1</sup> B. Hille, *Ion Channels of Excitable Membranes*, Sinauer, Sunderland, 2001.

<sup>2</sup> T. J. Jentsch, T. Maritzen and A. A. Zdebik, *J. Clin. Invest.*, 2005, **115**, 2039–2046.

<sup>3</sup> F. M. Ashcroft, *Nature*, 2006, **440**, 440–447.

<sup>4</sup> F. M. Ashcroft, *Ion Channels and Disease*, Academic Press, San Diego and London, 2000.

<sup>5</sup> H. Li, H. Valkenier, L. W. Judd, P. R. Brotherhood, S. Hussain, J. A. Cooper, O. Jurček, H. A. Sparkes, D. N. Sheppard and A. P. Davis, *Nat. Chem.*, 2016, **8**, 24–32.

<sup>6</sup> N. Busschaert and P. A. Gale, *Angew. Chem. Int. Ed.*, 2013, **52**, 1374–1382.

<sup>7</sup> P. A. Gale, R. Pérez-Tomás and R. Quesada, *Acc. Chem. Res.*, 2013, **46**, 2801–2813.

<sup>8</sup> S. Matile, A. Vargas-Jentzsch, J. Montenegro and A. Fin, *Chem. Soc. Rev.*, 2011, **40**, 2453–2474.

<sup>9</sup> J. T. Davis, O. Okunola and R. Quesada, *Chem. Soc. Rev.*, 2010, **39**, 3843–3862.

<sup>10</sup> A. Vargas-Jentzsch, A. Hennig, J. Mareda and S. Matile, *Acc. Chem. Res.*, 2013, **46**, 2791–2800.

<sup>11</sup> J. M. Lehn, *Angew. Int. Ed. Engl.*, 1990, 1304–1319.

<sup>12</sup> J. W. Steed and J. L. Atwood, *Supramolecular Chemistry*, John Wiley & Sons, Ltd., United Kingdom, 2nd ed, 2009, ch. 1, pp. 27–36.

adaptation and evolution.<sup>13</sup> Emil Fischer described the first one, molecular recognition, in 1894. He used the analogy of a lock–key interaction. Years later, in 1948, H. M. Powell defined the host–guest concept. The host is the larger molecule, which has a central hole or cavity where the guest, a simple ion or maybe a more sophisticated molecule such as a hormone or neurotransmitter, is nested.<sup>14</sup> The affinity of this supramolecular structure, in solution at a given temperature, is measured by the binding constant, *K*. The larger the constant the more stable is the complex. There are a variety of techniques, such as potentiometric titrations, NMR titrations, fluorescence or UV-Vis titrations, or colorimetric titrations, which give information about the chemical equilibrium between the free host and guest and the complex concentration.<sup>15</sup>

Very recently, this discipline has been awarded again with a Nobel Prize (2016) to J. P. Sauvage (University of Strasbourg, France), J. F. Stoddart (University of Northwestern, USA) and B. L. Feringa (University of Groningen, Netherlands) because of their work in the development of molecular machines.

## 1. LIPID BILAYER

Cells are the building blocks of living organisms. They are defined by phospholipid membranes, which are involved in controlling the fluxes of matter (water, oxygen, ions, glucose, etc.) from and to the exterior of the cell. The interior of eukaryote cells is partitioned again into organelles, defined by membranes. The function of this cellular envelope is to separate the internal and external environments, avoiding the free flow of matter from one side to the other, and allowing the creation of gradients. The *Fluid–Mosaic Membrane Model* for the membrane structure was postulated in 1972 by S. J. Singer and G. L. Nicolson and the concepts described in it are still applicable.<sup>16, 17</sup>

Cellular bilayers are composed mainly of proteins and lipids. Their relative amount can vary depending on the type of cell, from 75% of proteins in the internal

---

<sup>13</sup> J. M. Lehn, *Prod. Natl. Acad. Sci. U.S.A.*, 2002, **99**, 4763–4768.

<sup>14</sup> E. P. Kyba, R. C. Helgeson, K. Madan, G. W. Gokel, T. L. Tarnowski, S. S. Moore and D. J. Cram, *J. Am. Chem. Soc.*, 1977, **99**, 2564–2571.

<sup>15</sup> P. Thordarson, *Chem. Soc. Rev.*, 2011, **40**, 1305–1323.

<sup>16</sup> S. J. Singer and G. L. Nicolson, *Science*, 1972, **175**, 720–731.

<sup>17</sup> G. L. Nicolson, *Biochim. Biophys. Acta*, 2014, **1838**, 1451–1466.

membrane of mitochondria to 25% in myelin membranes from nerve cells.<sup>18</sup> The proportion and characteristics of them will determine the bilayer properties. It should be outlined its amphiphilic features due to the bilayer structure. The hydrophobic fatty acid chains are oriented to the internal side of the membrane creating a nonpolar core, whereas the hydrophilic polar head groups are directed to the external side (Figure 1.1).

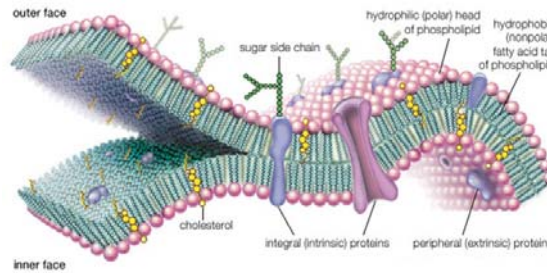


Figure 1.1. Phospholipid membrane<sup>19</sup>

There are five principles that govern the physicochemical cellular membrane properties: fluidity, semi-permeability, asymmetry, reparation and renovation. The fluidity varies as a function of external conditions (e.g. temperature) or chemical composition (e.g. the higher the number of unsaturated bonds the more fluent it is). The semi-permeability comes from the hydrophobic interior, which allows only the simple diffusion of small molecules without net charge. The asymmetric distribution of its components among both sides of the bilayer starts in the membrane synthetic pathway and has important functional consequences.<sup>20</sup> Some biological processes involve fission of membranes followed by fusion between two lipid bilayers giving a single one, and it also has the ability of been repaired when it have been damaged.

Eukaryote cell bilayers are dynamic. Membrane components display two different movements, lateral diffusion (in plane) and transverse diffusion or “flip-

<sup>18</sup> Alberts B, Johnson A, Lewis J, et al. *Molecular Biology of the Cell*. 4th edition. New York: Garland Science; 2002. Membrane Proteins. Available from: <https://www.ncbi.nlm.nih.gov/books/NBK26878/>

<sup>19</sup> <https://global.britannica.com/science/cell-biology/Intercellular-communication> (accessed March 2017)

<sup>20</sup> D. L. Daleke, *J. Biol. Chem.*, 2007, **282**, 821–825.

flop" movement used for jumping from one monolayer to the other. The second one takes longer times and has been observed only for lipids (Figure 1.2).<sup>21</sup>

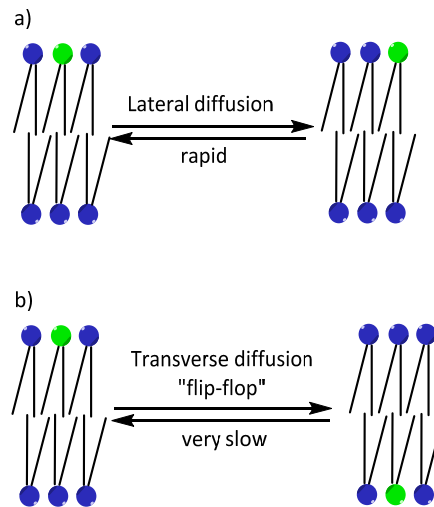


Figure 1.2. a) Lateral diffusion movement; b) Transverse diffusion movement

## 2. TRANSMEMBRANE TRANSPORT

Transmembrane transport can take place as both active or passive processes. The first one implies transport against an electrochemical gradient and requires energy. Passive transport is based on simple diffusion down an electrochemical gradient. The membrane selective permeability leads to osmotic processes (movements of water) and electrochemical gradients. These differences in charge concentrations between both sides of the membrane are known as membrane potential.

The electrochemical gradients are essential to maintain the proper functioning of cells. They are involved in driving metabolic processes, controlling electrical signalling in nerves, muscle contractions or synapsis. Their origin and maintenance are the result from the action of transmembrane proteins. There are three different types of structures responsible for promoting ions and charged molecules to cross the lipid bilayer.

---

<sup>21</sup> J. M. Berg, J. L. Tymoczko, L. Stryer, in *Biochemistry*, ed. W H Freeman, New York, 5th edn, 2002, ch. 12, pp. 477–480

- Pumps: are transmembrane proteins able to facilitate transport against concentration gradients by using energy. Active transport (chloride-transporting ATPase)
- Channels: are transmembrane proteins that communicate both sides of the membrane through a hydrophilic hollow space. They allow the movement of ions down a concentration gradient. Passive transport (e.g. the transmembrane conductance regulator, CFTR)
- Carriers/transporters: are transmembrane proteins, which enable the transport of substances by facilitated diffusion. The transport event relies in the binding between the protein and the ion or molecule. Passive transport. Ejem.

Table 1.1. Differences between channels and carriers in the transport of ions<sup>22</sup>

Carriers	Channels
High selectivity	Low selectivity
Transport rate below limit of diffusion	Transport rate approaches limit of diffusion ( $10^7$ – $10^8$ ion $s^{-1}$ )
Usually monomeric	Usually oligomers of identical subunits
Transport activity not gated	Transport activity often gated in response to cellular events

Possible mechanisms for transmembrane transport, as a function of transport direction and stoichiometry are described in Figure 1.3:

- Uniport: a single molecule or ion is transported in one direction.
- Cotransport: two different molecules or anions are transported at the same time.<sup>23</sup>
  - Symport: both molecules or ions are moved in the same direction. NBCe1  $Na^+/HCO_3^-$  is responsible of renal sodium ions and bicarbonate reabsorption.
  - Antiport: the two molecules or ions are moving in opposite direction. The natural AE protein acts as a  $Cl^-/HCO_3^-$  antiporter. This protein is involved in

<sup>22</sup> J. T. Davis, O. Okunola and R. Quesada, *Chem. Soc. Rev.*, 2010, **39**, 3843–3862.

<sup>23</sup> E. Cordat and J. R. Casey, *Biochem. J.*, 2009, **417**, 423–439.

the cellular respiration process, enabling the transport of  $\text{CO}_2$  in the form  $\text{HCO}_3^-$ .

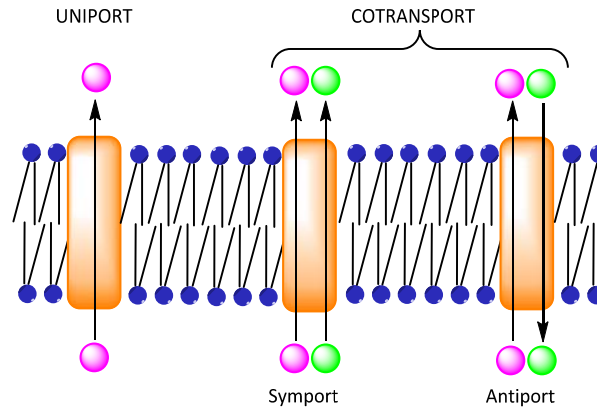


Figure 1.3: Schematic representation of the mechanisms for transmembrane transport

In the case of neutral small molecules, such as water,  $\text{O}_2$  or  $\text{CO}_2$ , the transport mechanism is simple solubility–diffusion.

## 2.1. Chloride transport in nature

The average extra- and intra-cellular concentrations of chloride are 110 mM and 5–15 mM, respectively. Chloride transport in cells is carried out by anion exchangers, cation-dependent chloride transporters and chloride channels.<sup>24</sup> CIC proteins are a family of chloride channels/transporters that control Chloride gradients in organism from eubacteria to animals. They are homodimers and their mechanism of transport consists in the translocation of one ion per subunit. The different members of this family are found widespread all over the body in mammals and their dysfunctions could be responsible for diseases such as Dent's disease or Bartter syndrome.<sup>25</sup>

ABC (ATP Binding Cassette) transporters are members of another important family of integral membrane proteins. Their structure is based on two membrane-spanning domains (MSD) and two nucleotide-binding domains (NBD). 48 ABC transporters have been identified in the human genome, of which 17 are related to genetic diseases such as Stargardt disease (ABCA4), Dubin-Johnson syndrome (ABCC2), or cystic fibrosis (ABCC7). This last arises by a mutation in the epithelial

<sup>24</sup> A. P. Davis, D. N. Sheppard and B. D. Smith, *Chem. Soc. Rev.*, 2007, **36**, 348–357.

<sup>25</sup> T. J. Jentsch, *J. Physiol.*, 2015, **18**, 4091–4109.

cAMP-dependent chloride channel, the transmembrane conductance regulator (CFTR). This channel is able to move  $10^6$ – $10^7$   $\text{Cl}^-$  /s and the symptoms associated to its dysfunction go from lung diseases to male infertility or intestinal blockage.<sup>26</sup> Its operation is based on a passive diffusion mechanism, although other members of the ABC family are active transporters.

## 2.2. Bicarbonate transport in nature

Bicarbonate plays an essential role in biology. It is associated to respiration and is a natural pH buffer system, being involved in several pH equilibria (Figure 1.4). Its highest concentration is located in the pancreatic fluids with a value around 140 mM.

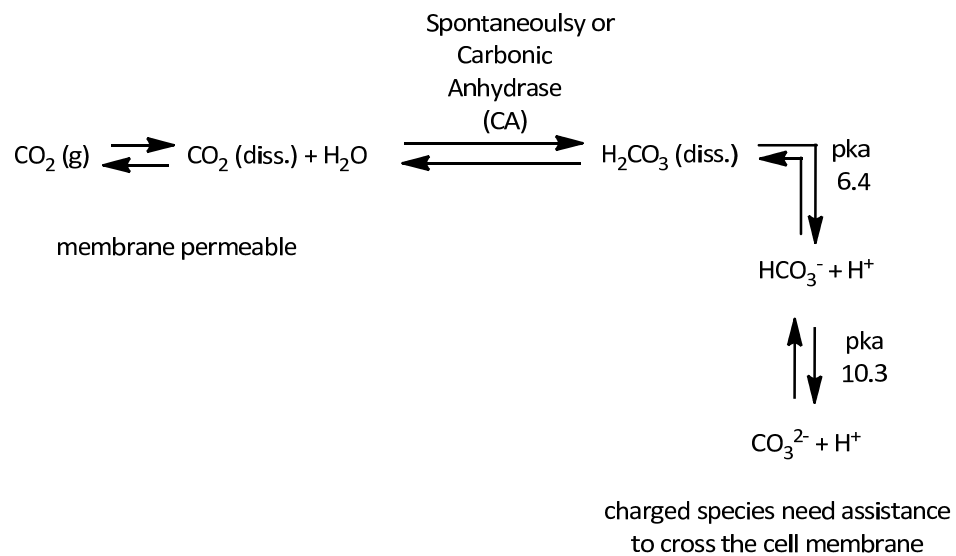


Figure 1.4. Bicarbonate equilibria in nature

Proteins responsible for bicarbonate transmembrane transport are divided into 3 classes. The AE (anion exchanger) family which members (AE1, AE2 and AE3) are found spread all over the body and work as  $\text{Cl}^-/\text{HCO}_3^-$  exchangers, the  $\text{Na}^+/\text{HCO}_3^-$  from the NBC family and the SLC26 family. Their functions are bicarbonate metabolism and excretion, pH regulation and readjusting cell volume. Bicarbonate

<sup>26</sup> T.-Y. Chen and T.-C. Hwang, *Physiol. Rev.*, 2008, **88**, 351–387.

transport proteins are expressed over the whole body and some diseases such as deafness or blindness appear as a consequence of their dysfunctions.<sup>27, 28</sup>

### 2.3. Transport of anions in vesicle models

Phospholipids are amphiphilic molecules. The hydrophobic portion is a hydrocarbon tail and they tend to self-assemble in aqueous solution giving rise to different structures. Liposomes are one of the most important among them.

Lipid membranes could be found in different phases depending on their structural properties such as length of hydrocarbon tails, charge, head groups, insaturations, as well as on temperature, pressure or the degree of hydration. The transition of one phase into the other does not imply important molecular rearrangements. Nevertheless, there are found different properties in each of them.

The low-temperature phase, known as subgel phase ( $L_c$ ), displays highly hydrocarbon ordered chains, which present a tilt with the bilayer plain. As temperature increases this phase is transformed to a gel phase characterised by higher hydration and still large order, but to a lesser extent than  $L_c$  phase. Hydrocarbon chains are fully extended and almost perpendicular to the internal plane, giving rise to a maximum bilayer thickness with the minimum effective cross-sectional area. Movements are highly restricted leading to a highly impermeable barrier. Depending on the structural properties of the lipids, there are found  $L_\beta$  or  $L_\beta'$ . Upon heating these phases over the phase transition temperature ( $T_m$ ) it is obtained the  $L_\alpha$  phase, also known as liquid crystalline or fluid phase. Under these conditions the bilayer structure is conserved meanwhile, the hydrocarbon chains present higher freedom of movements without any tilt. Consequently, the bilayer thickness decreases and the effective cross-sectional area increases as well as its permeability (Figure 1.5).<sup>29, 30, 31</sup>

$T_m$  is affected by the length of hydrocarbon tails, charge, head groups, insaturations, etc. Longer hydrocarbons chains make Van der Waals interactions stronger and consequently the transition temperature increases, *cis*- insaturations have the opposite effect.

---

<sup>27</sup> J. R. Casey, *Biochem. Cell Biol.*, 2006, **84**, 930–939.

<sup>28</sup> K. Alka and J. R. Casey, *IUBMB Life*, 2014, **66**, 596–615.

<sup>29</sup> M. Kranenburg and B. Smit, *J. Phys. Chem. B*, 2005, **109**, 6553–6563.

<sup>30</sup> M. O. Eze, *Biochem. Educ.*, 1991, **19**, 204–208.

<sup>31</sup> <https://avantlipids.com/tech-support/faqs/transition-temperature/> (accessed March 2017).

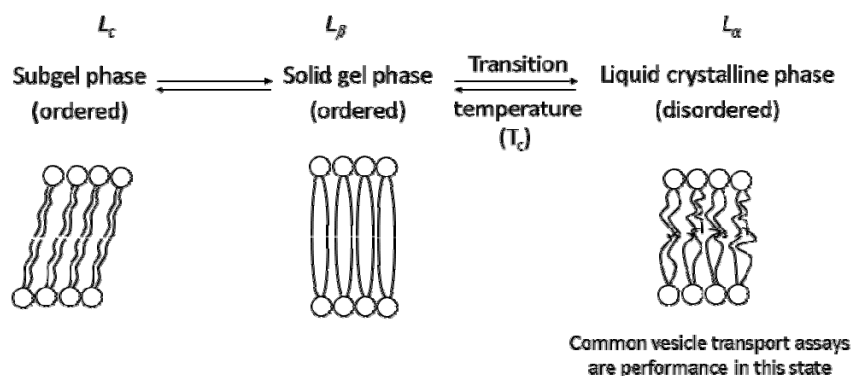


Figure 1.5. Phase transition temperature of lipids

These structures allow to work under a huge variety of conditions. The wide range of synthetic and commercially available lipids enable to obtain vesicles with different physicochemical properties. The composition of their internal and external solutions could be geared to the needs. The nature of the internal medium is determined by the solution used for treating the lipids. The external one corresponds to the composition of the solution in which they are suspended. Their diameter can be modulated as well as the number of lamellae. The non-encapsulated material is easily removed by dialysis or size exclusion chromatography.<sup>32</sup> Application of these methods allow obtaining vesicles with well-defined characteristics, in a reproducible manner.

The most common liposomes used in transmembrane transport studies are large unilamellar vesicles (LUVs; 100–200 nm) composed of one or two different kind of lipids such as POPC (1-*palmitoyl*-2-oleoyl-sn-glycero-3-phosphatidylcholine), EYPC (egg yolk phosphatidylcholine) and cholesterol. In Figure 1.6 there are shown some of the common lipids used in preparing synthetic vesicles.

- Phosphatidylcholine lipids (PC): characterised by a choline head group and total neutral charge in the head-group region.
  - POPC: ( $T_m = 3\text{ }^{\circ}\text{C}$ ) one insaturation.
  - DOPC: ( $T_m = -20\text{ }^{\circ}\text{C}$ ) two insaturations.

<sup>32</sup> V. P. Torchilin and V. Weissig, in *Liposomes*, Oxford University Press, 2nd edn, 2003.

- DPPC: ( $T_m = 41\text{ }^\circ\text{C}$ ) fully saturated. At room temperature is going to be in the gel phase. It is used in mobility assays to determine if an ionophore follows a mobile carrier mechanism or a membrane-spanning pathway.
- DMPC: ( $T_m = 23\text{ }^\circ\text{C}$ ) fully saturated.
- EYPC : ( $T_m = -15 - -7\text{ }^\circ\text{C}$ ) is a mixture of phosphatidylcholines.<sup>33</sup>
- Phosphatidylethanolamine lipids (PE): characterised by an ethanolamine head group and neutral charge in the head-group region, at physiological pH.
  - POPE: it does not form vesicles on its own. It could be used as POPE:POPC (3:1).
- Phosphatidylglycerol lipids (PG): characterised by a glycerol head group and an overall negative charge in the head-group region.
  - POPG: ( $T_m = -2\text{ }^\circ\text{C}$ ) one insaturation
- Cholesterol: is a rigid and planar non polar lipid. It is able to moderate the membrane viscosity thanks to its ability of fitting into the leaflets with the -OH group oriented to outside of the bilayer. The presence of cholesterol in vesicles will diminish the acyl chain rotation and thus the fluidity and permeability of the membrane will decrease. This lipid does not form vesicles on its own. It is usually used in mixtures with phospholipids (7:3).<sup>34</sup>

---

<sup>33</sup> L. Beney, J.-M. Perrier-Cornet, M. Hayert and P. Gervais, *Biophys. J.*, 1997, **72**, 1258–1263.

<sup>34</sup> Biochemistry Online, An Approach Based on Chemical Logic, [https://employees.csbsju.edu/hjakubowski/classes/ch331/lipidstruct/LS\\_1C4\\_Lipid\\_Conformational\\_Transitions.html](https://employees.csbsju.edu/hjakubowski/classes/ch331/lipidstruct/LS_1C4_Lipid_Conformational_Transitions.html) (accessed January 2017).

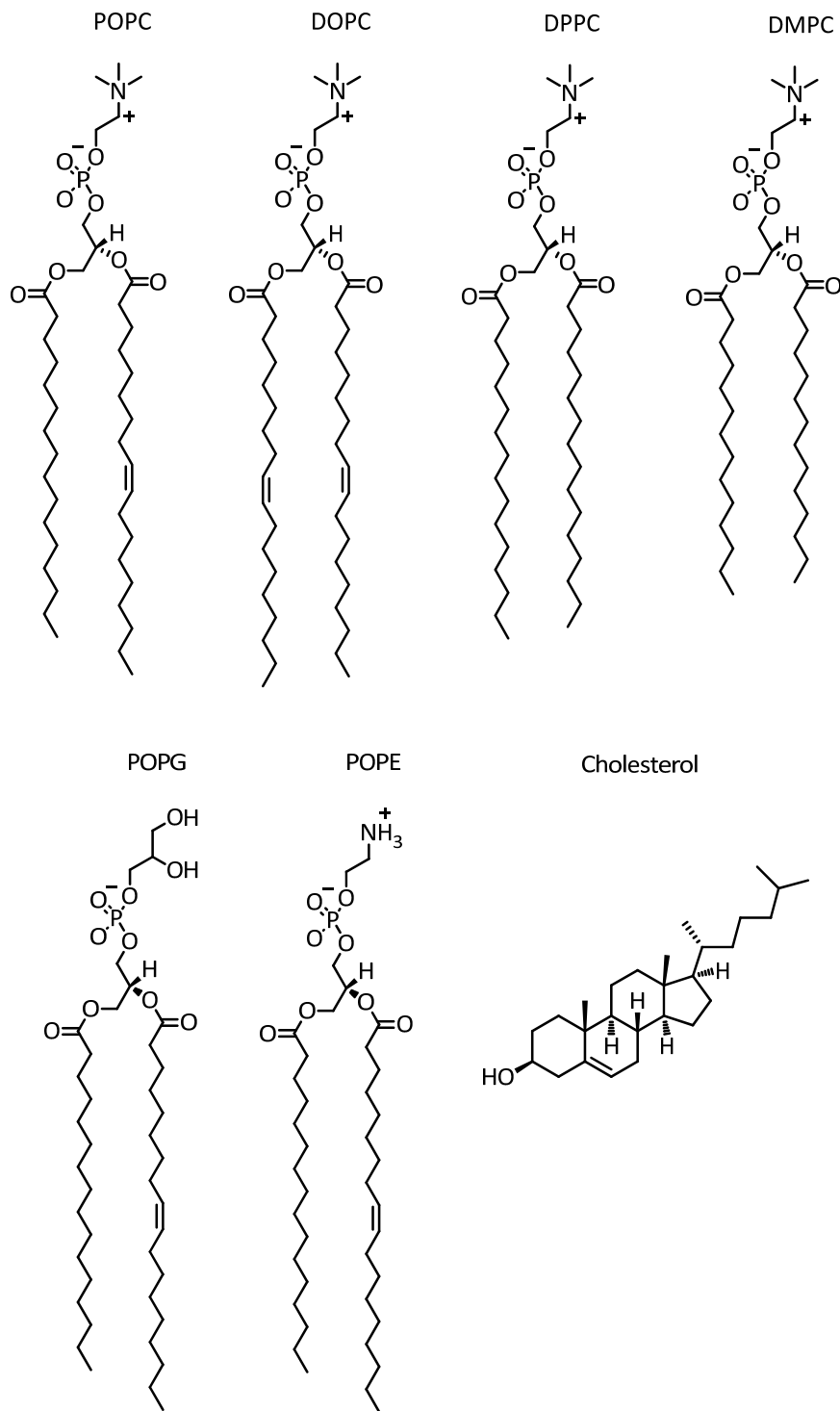


Figure 1.6. Common lipids used in vesicles preparation

In Table 1.2 there is shown an approximation of different cell membranes composition.

Table 1.2. Approximate lipid composition of different cell membranes, expressed as % of total lipids by weight <sup>35</sup>

Lipid	Liver cell plasma membrane	Red blood cell plasma membrane	Myelin	Mitochondrion (inner and outer membranes)	<i>E. Coli</i> Bacterium
Cholesterol	17	23	22	3	0
PE	7	18	15	28	70
PS	4	7	9	2	trace
PC	24	17	10	44	0
SPH	19	18	8	0	0
Glycolipids	7	3	28	trace	0
Others	22	14	8	23	30

### 2.3.1. Techniques employed to measure anion transport in vesicle models

Different methodologies are used to study the trafficking of anions across membranes in vesicles.

#### 2.3.1.1. Ion-selective electrode assays

The use of ion selective electrodes allows to quantify ion fluxes directly. Its potential lies on the fact that internal components of the liposomes are not visible for the electrode. On the other hand, they are readily detected when released to the external medium. Most common ISE assays involved chloride loaded vesicles, therefore a chloride selective electrode is used for monitoring the chloride efflux.

#### 2.3.1.2. Fluorescence based assays

Fluorescence quenching was first detected by Stokes (1869), when he realised that the fluorescence emission of quinine, in a sulphuric acid solution, was reduced on addition of chloride anions.<sup>36</sup>

Different fluorescence probes, with different potential applications are found in the literature (Figure 1.7). These dyes can be encapsulated or added in the

<sup>35</sup> B. Alberts, A. Johnson, J. Lewis, M. Raff, K. Roberts, P. Walter, in *Molecular Biology of Cell*, ed. Garland Science, Taylor & Francis Group, LLC, New York, 5th edn, 2008, ch. 10, pp. 617–650.

<sup>36</sup> K. Bowman-James, A. Bianchi, E. García-España, in *Anion Coordination Chemistry*, ed. Wiley-VCH Verlag & Co. KGaA, Weinheim, 1st edn, 2012, ch. 9, pp. 521–551.

extravesicular medium depending on the assay. In most cases they are entrapped inside the vesicles.

These techniques are based on monitoring fluorescence changes corresponding to the selected dye as a function of variations in different parameters such as pH, alterations of the membrane potential, concentration of the fluorescence probe, etc.

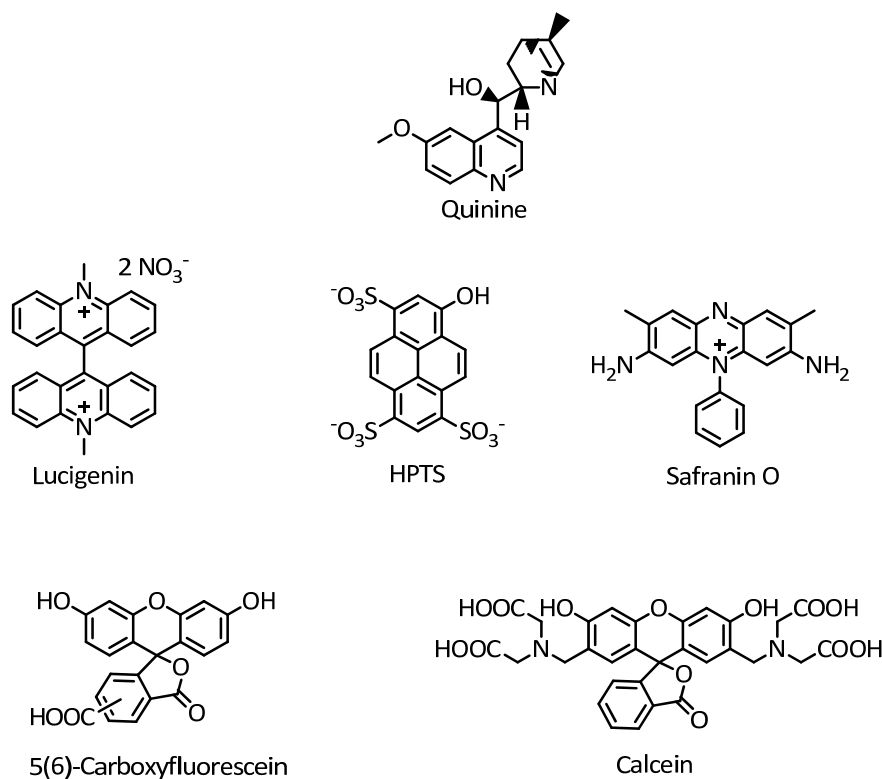


Figure 1.7. Fluorescence probes

Lucigenin is a bisacridinium salt. Its fluorescence emission is not altered by nitrate, sulfate or phosphate. Nevertheless, it is quenched by halides ( $K_{sv, Cl^-} = 390 \text{ M}^{-1}$ ).<sup>37, 38</sup> Based on these properties, lucigenin could be employed to monitor the chloride transport inside vesicles at 503 nm, after exciting at 372 nm.

The 8-hydroxy-1,3,6-pyrenetrisulfonate HPTS, is sensitive to pH changes. Its protonated and non-protonated forms have different excitation wavelengths (403

<sup>37</sup> J. Biwersi, B. Tulk and A. S. Verkman, *Anal. Biochem.*, 1994, **219**, 139–143.

<sup>38</sup> C. Huber, K. Fährnich, C. Krause and T. Werner, *J. Photochem. Photobiol.*, 1999, **128**, 111–120.

nm and 460 nm), meanwhile both emit in the same position of the electromagnetic spectrum (510 nm). Once encapsulated, it is a reliable indicator of pH changes inside the vesicles. Alterations in the internal pH could be a consequence of anion transport *via* OH<sup>-</sup>/Cl<sup>-</sup> antiport or H<sup>+</sup>/Cl<sup>-</sup> symport.

The unidirectional movement of anions across lipid membranes could give rise to the creation of transmembrane potentials. This alteration can be detected with the fluorescence dye safranin O.<sup>39</sup>

Carboxyfluorescein and calcein are large molecules which fluorescence is self-quenched at high concentrations. These compounds have been widely used for detecting the formation of membrane pores or defects.

### 2.3.1.3. NMR assays

In order to be useful in these assays, one of the species involved in the transport process should be NMR active. Often, paramagnetic agents are encapsulated or added in the extravesicular medium with the aim of obtaining differences in the signals from the NMR active specie such as shift and/or line-width, depending on if it is found in- or outside vesicles. This technique has been used to study bicarbonate (<sup>13</sup>C), chloride (<sup>35</sup>Cl) or sulphate (<sup>33</sup>S).<sup>40, 41</sup>

## 3. MOLECULES WITH ACTIVITY AS TRANSMEMBRANE ANION CARRIERS

### 3.1. Anion recognition and coordination chemistry

The first example of synthetic halide receptors, *katapinands* **1** (Figure 1.8), was published by Park and Simmons in 1967.<sup>42</sup> Years later, their structures were confirmed by diffraction studies.

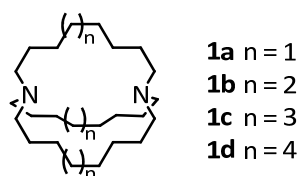
---

<sup>39</sup> V. Sidorov, F. W. Kotch, J. L. Kuebler, Y. F. Lam and J. T. Davis, *J. Am. Chem. Soc.*, 2003, **125**, 2840–2841.

<sup>40</sup> J. T. Davis, P. A. Gale, O. A. Okunola, P. Prados, J. C. Iglesias-Sánchez, T. Torroba and R. Quesada, *Nat. Chem.*, 2009, **1**, 138–144.

<sup>41</sup> A. V. Koulov, J. M. Mahoney and B. D. Smith, *Org. Biomol. Chem.*, 2003, **1**, 27–29.

<sup>42</sup> C. H. Park and H. E. Simmons, *J. Am. Chem. Soc.*, 1968, **90**, 2431–2432.

Figure 1.8. Cage-type receptors *katapinands*

Anions display a wide range of geometries (spherical, linear, tetrahedral, etc.) Thus a high level of design is needed to obtain selective receptors. Hydrophobicity (or lipophilicity) also plays an important role in the anion-binding process. It is based on the Hofmeister series, which is originally based on the effect of salts over the solubility of proteins. Recent studies propose that these behaviours should be understood from the point of view of interactions between ions and macromolecules.<sup>43</sup> Figure 1.9 shows the Hofmeister series in which anions are ordered by increasing lipophilicity.<sup>44</sup>

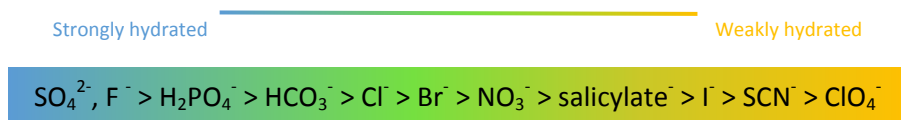


Figure 1.9. Hofmeister series

Non-covalent forces such as hydrogen bonding, anion- $\pi$  or electrostatic interactions address the anion recognition process following the well established principles of chelate cooperativity, complementary, preorganization and macrocyclic effect.<sup>45</sup> Small changes in the receptor could also change its coordination tendency because parameter such as dimension, hydrophobicity, charge, contribution of Van der Waals interactions, etc. have been altered.

Nature of solvent will play an important role in the anion recognition and coordination chemistry. For example, the anion binding of a neutral receptor which binding ability is based solely on hydrogen bonds, will be more effective in aprotic organic solvents, since the anion will interact with the solvent to a lesser extent. On the contrary, a charged receptor will be able to compete with polar protic solvents

<sup>43</sup> Y. Zhang and P. S. Cremer, *Curr. Opin. Chem. Biol.*, 2006, **10**, 658–663.

<sup>44</sup> J. L. Sessler, P. A. Gale, W.-S. Cho, in *Anion Receptor Chemistry*, ed. Royal Society of Chemistry, Cambridge, 1st edn, 2006, ch. 1, pp. 1–22.

<sup>45</sup> K. Bowman-James, A. Bianchi and E. Garcia-España, in *Anion Coordination Chemistry*, ed. Wiley-VCH Verlag & Co. KGaA, Weinheim, 1st edn, 2012, ch.2, pp. 76–93.

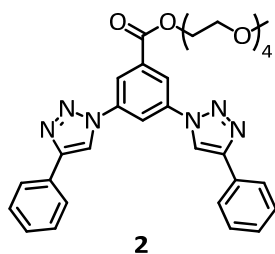
aid by the electrostatic effects. It is important to note that anions are conjugated bases from protic acids. Therefore, depending on their basicity constants they could experience protonation what implies that their coordination chemistry is going to be determined by the pH of the working conditions.

Anions have Lewis base character. For this reason molecules with Lewis acid centres, should play an important role in the anion coordination chemistry. Among these possible receptors are boron, phosphorus, aluminium, tin, silicon, indium, antimony, germanium or mercury species.<sup>46</sup>

### 3.2. Thermodynamic features of the coordination chemistry

The thermodynamic stability of a supramolecular complex is quantified by the binding constant (K), also known as stability constant, association constant or formation constant. It allows to compare the selectivity of two coordination processes, as long as, they have the same stoichiometry, the resulting complexes coexist in the same experimental conditions and there are no competitive reactions.

Most of coordination chemistry is carried out in solution, so two aspects should be taken into account. The studied compounds should be soluble in the chosen study medium and the solvated grade of both, host and guest, must be considered. If ionic species such as anions are present in the process, the desolvation penalties could be very important, especially in protic solvents. As example, in Table 1.3 it is shown how the calculated binding constants of compound **2** with chloride ( $\text{Bu}_4\text{N}^+\text{Cl}^-$ ) change as a function of solvents.<sup>47</sup>



<sup>46</sup> A. S. Wendji, C. Dietz, S. Kihn, M. Lutter, D. Schollmeyer, W. Hiller and K. Jurkschat, *Chem. Eur. J.*, 2016, **22**, 404–416

<sup>47</sup> H. Juwarker, J. M. Lenhardt, J. C. Castillo, E. Zhao, S. Krishnamurthy, R. M. Jamiolkowski, K.-H. Kim and S. L. Craig, *J. Org. Chem.*, 2009, **74**, 8924–8934.

Table 1.3. Effect of solvent in the chloride binding ability of **2**

Acetone	1260
DMSO	5.1
CD <sub>2</sub> Cl <sub>2</sub>	34
CDCl <sub>3</sub>	18

### 3.3. Transmembrane anion carriers

The present thesis is focused on compounds with the ability of coordinating anions and transporting them through lipid bilayers, known as anionophores. Below is given a summary of some of the natural and synthetic anion carriers described in the literature in the last years.

#### 3.3.1. Transport mechanism

Two big groups could be made in the field of transmembrane anion transport based on their mechanism of action, *mobile carriers* and *channels*. The action of mobile carriers is based on binding the anion on one side of the membrane, forming a supramolecular complex that is able to diffuse through the lipid bilayer and release it on the other side. On the contrary, channel transporters are relatively immobile structures, based on their ability to span the membrane creating a polar hole/pore through which the polar guests are able to pass (Figure 1.10).

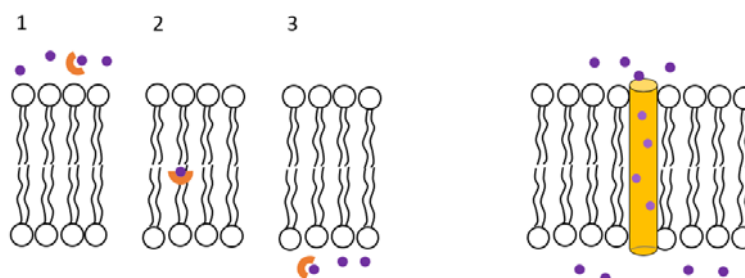


Figure 1.10. Left) Mobile carrier mechanism; Right) Channel mechanism

Other relevant synthetic transport systems displaying other mechanism include the urea appended phospholipid derivative **3**. This compound, developed by B. D. Smith and *co-workers*, is proposed to facilitate a “*relay*” transport process (Figure

1.11). The ionophore (R) located at the end of the lipid tail, is able to bind an anion on one side of the membrane, and pass it to another carrier located on the other leaflet, finally releasing it on the other side of the membrane.<sup>48</sup>

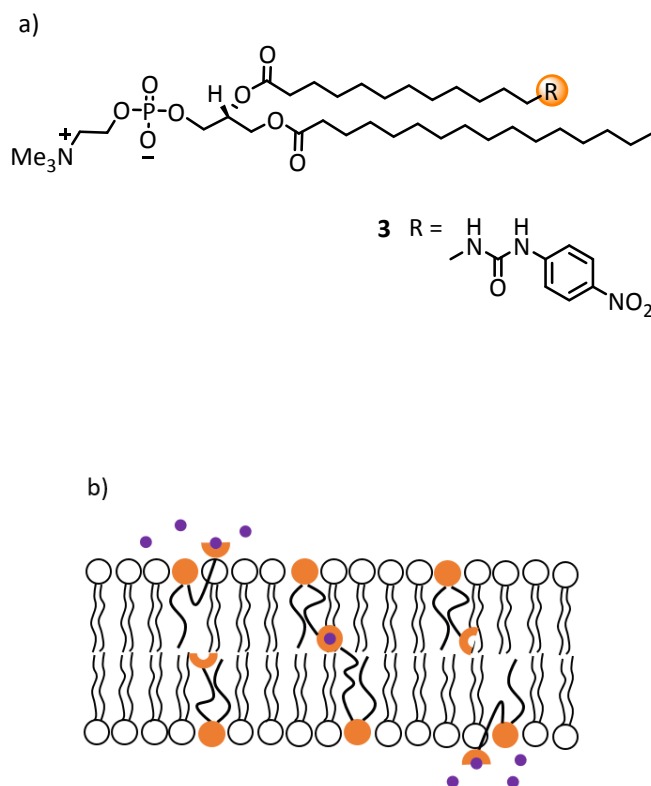


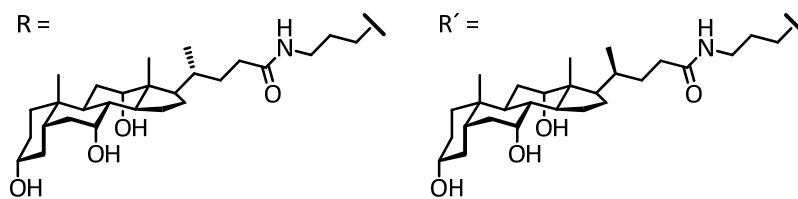
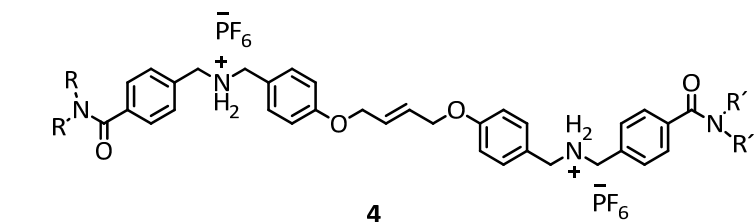
Figure 1.11. a) Phospholipid derivative carrier structure; b) Representation of relay mechanism

Schmitzer (e.g. **4**) or Regen applied the concept “*molecular umbrellas*” (Figure 1.12) to describe the way by which some of their synthetic molecules transport anions through lipid bilayers. It involved structures consisting of a central hydrophilic scaffold coupled with two or more facially amphiphilic units. While they are immersed in a polar environment, they display an *open* conformation, which enhanced the interaction between the core and the polar side of the amphiphilic units with the medium. In apolar conditions, such as the lipid membrane, they adopt

<sup>48</sup> B. A. McNally, E. J. O’Neil, A. Nguyen and B. D. Smith, *J. Am. Chem. Soc.*, 2008, **130**, 17274–17275.

a shielded conformation minimizing the interactions between the core and the bilayer and, in turn, masking the guest hydrophilicity.<sup>49, 50</sup>

a)



b)

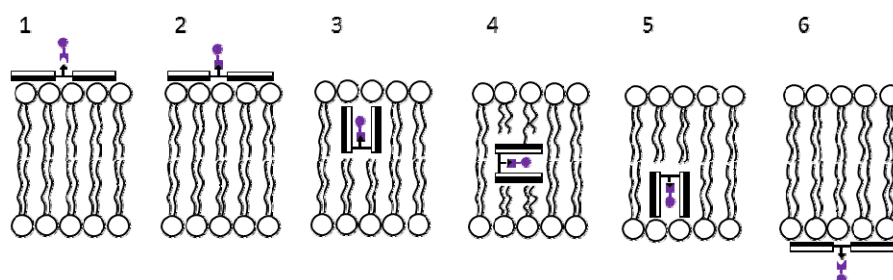


Figure 1.12. a) Molecular umbrella carrier; b) Representation of molecular umbrella approach

An approach in which two independent molecules are combined in the transport assay is known as “*dual-host*”. One of the members carries the positive charge (cationophore) and the other the negative one (anionophore). In Figure 1.13 it is

<sup>49</sup> J. Kempf and A. Schmitzer, *RCS. Adv.*, 2016, **6**, 42713–42719.

<sup>50</sup> V. Janout, B. Jing, I. V. Staina and S. L. Regen, *J. Am. Chem. Soc.*, 2003, **125**, 4436–4437.

shown an example formed by valinomycin **5**, a selective  $K^+$  carrier, and calix[4]pyrrole **6** a chloride transporter. The overall result is an enhanced rate of anion transport through  $K^+/Cl^-$  symport.<sup>51, 52</sup>

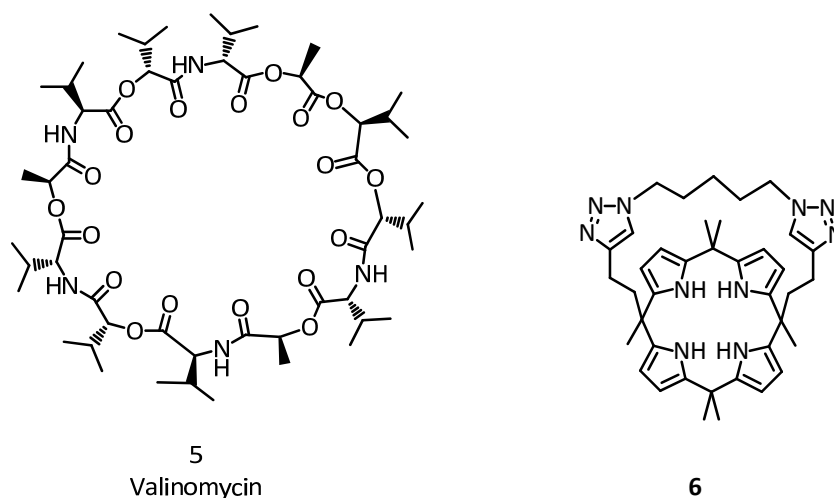


Figure 1.13. Example of compounds involved in a dual-host transport mechanism

Matile and co-workers described the “Jacobs-ladder” approach (Figure 1.14). Oligoureia/amide macrocycle **7** is able to form transmembrane parallel nanotubes established by water bridged. Anions interact to the positive side of this supramolecular structure through four hydrogen bonds. Continuing rotations of consecutive macrocycles allow anions to move from one side of the membrane to the other.<sup>53</sup>

<sup>51</sup> S.-K. Ko, S. K. Kim, A. Share, V. M. Lynch, J. Park, W. Namkung, W. V. Rossom, N. Busschaert, P. A. Gale, J. L. Sessler and I. Shin, *Nat. Chem.*, 2014, **6**, 885–892.

<sup>52</sup> S. J. Moore, M. G. Fisher, M. Yano, C. C. Tong and P. A. Gale, *Chem. Commun.*, 2011, **47**, 689–691.

<sup>53</sup> A. Hennig, L. Fischer, G. Guichard and S. Matile, *J. Am. Chem. Soc.*, 2009, **131**, 16889–16895.

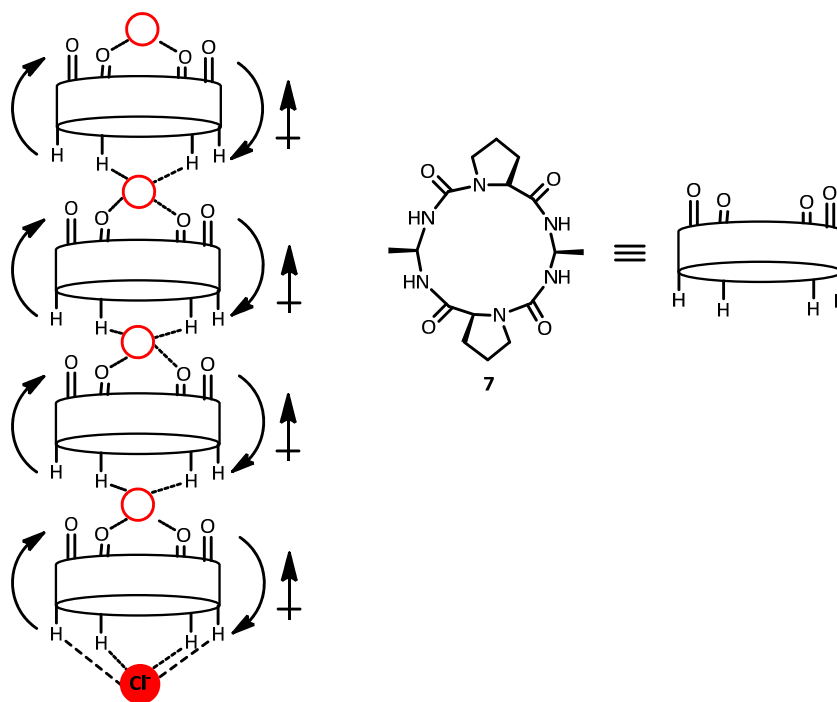


Figure 1.14. Schematic representation of Jacobs-Ladder transport mechanism

### 3.3.2. Transmembrane anion transport mediated by mobile carriers

Transmembrane anion carriers could be classified in different manners. Below there is shown a description of the most relevant molecules described in the last ten years, based on the interactions employed to coordinate anions.

#### 3.3.2.1. Hydrogen bonding interactions

Some mobile carriers are based on the structure of natural products. For example, prodiginines are a tripyrrolic family of red pigments that were isolated for the first time in 1930s.<sup>54, 55</sup> The most representative example of this set is prodigiosin **8**, a natural product generated by microorganisms such as *Serratia marcescens* and *Streptomyces*. In 1977, Fullan and co-workers first showed its antitumor properties.<sup>56</sup> Two approaches of its mechanism of action were postulated. Manderville, Melvin and co-workers suggested that it is related to copper-mediated cleavage of duplex

<sup>54</sup> F. Wrede, *Z. Physiol. Chem.*, 1932, **210**, 125–128.

<sup>55</sup> A. Fürstner, *Angew. Chem. Int. Ed.*, 2003, **42**, 3582–3603.

<sup>56</sup> N. P. Fullan, D. L. Lynch and D. H. Ostrow, *Microbiol. Lett.*, 1977, **5**, 157–161.

DNA.<sup>57</sup> Alternatively, Ohkuma, Wasserman and *co-workers* proposed that it comes from its  $H^+/Cl^-$  symport activity.<sup>58</sup> In 2005, related with its ionophoric activity, J. T. Davis *et al* demonstrated with Lucigenin and HPTS fluorescence probes in vesicles assays, that they act as mobile carriers and, even more important that they can work as symporters ( $H^+/Cl^-$ ) or anion exchangers ( $Cl^-/NO_3^-$ ) depending on the assay conditions.<sup>59</sup>

Studies about how A, B or C ring substituents affect their ionophoric activities have been made. Transmembrane transport assays of synthetic analogs in which have been varied substituents in B ring show, that is possible modulate their ionophoric activity by tuning the pKa of its skeleton (pKa around 7). The most basic compounds (**9d** and **9e**) display better  $Cl^-/NO_3^-$  exchange rate. Probably because at physiological pH a larger proportion of the compound is protonated.<sup>60</sup> Related to C ring, the introduction of an extra-methyl group does not affect the anion carrier activity of the prodiginine. However, the addition of an ester instead of the  $-C_5H_{11}$  aliphatic chain, results in a decreased of the exchange rate, although they are still potent anion carriers compared with most of the compounds described in the literature. The presence of the ester substituent was checked varying the length of aliphatic substituents **10**. Results demonstrated that the effect on the transport efficiency is governed by the lipophilicity.<sup>61</sup>



**8**

---

<sup>57</sup> M. S. Melvin, J. T. Tomlinson, G. Park, C. S. Day, G. R. Saluta, G. L. Kucera and R. A. Manderville, *Chem. Res. Toxicol.*, 2002, **15**, 734-741.

<sup>58</sup> T. Sato, H. Konno, Y. Tanaka, T. Kataoka, K. Nagai, H. H. Wasserman and S. Ohkuma, *J. Biol. Chem.*, 1998, **273**, 21455-21462.

<sup>59</sup> J. L. Seganish and J. T. Davis, *Chem. Commun.*, 2005, 5781-5783.

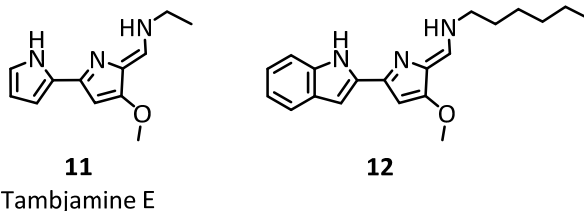
<sup>60</sup> E. Marchal, S. Rastogi, A. Thompson and J. T. Davis, *Org. Biomol. Chem.*, 2014, **12**, 7515-7522.

<sup>61</sup> S. Rastogi, E. Marchal, I. Uddin, B. Groves, J. Colpitts, S. A. McFarland, J. T. Davis and A. Thompson, *Org. Biomol. Chem.*, 2013, **11**, 3834-3845.



<b>9a</b>	R <sup>1</sup> = Bn	<b>9e</b>	R <sup>1</sup> = <i>p</i> -NMe <sub>2</sub> -Ph	<b>10a</b>	R <sup>2</sup> = Methyl	<b>10e</b>	R <sup>2</sup> = phenyl
<b>9b</b>	R <sup>1</sup> = Ph	<b>9f</b>	R <sup>1</sup> = <i>p</i> -CF <sub>3</sub> -Ph	<b>10b</b>	R <sup>2</sup> = <i>i</i> -propyl	<b>10f</b>	R <sup>2</sup> = octyl
<b>9c</b>	R <sup>1</sup> = <i>p</i> -Me-Ph	<b>9g</b>	R <sup>1</sup> = <i>p</i> -Me(CO)-Ph	<b>10c</b>	R <sup>2</sup> = butyl	<b>10g</b>	R <sup>2</sup> = C <sub>13</sub> H <sub>27</sub>
<b>9d</b>	R <sup>1</sup> = <i>p</i> -OMe-Ph	<b>9h</b>	R <sup>1</sup> = <i>p</i> -Cl-Ph	<b>10d</b>	R <sup>2</sup> = pentyl	<b>10h</b>	R <sup>2</sup> = C <sub>16</sub> H <sub>33</sub>

Another family of natural anion carriers are the marine alkaloid tambjamins (e.g. **11**, tambjamine E and **12**).<sup>62</sup> They are characterised by a 4-methoxy bipyrrrole unit with an enamine substituent. Tambjamins (pKa around 10) are more basic than prodigiosenes, so at physiological pH a higher rate of compound should be protonated. Anion binding studies with TBACl (from tambjamins as ClO<sub>4</sub><sup>-</sup> salt) show that proton signals from NH groups are shifted downfield (10–14 ppm), consistent with a strong interaction with chloride through hydrogen bonds. Transmembrane transport assays showed that they promote both NO<sub>3</sub><sup>-</sup>/Cl<sup>-</sup> and HCO<sub>3</sub><sup>-</sup>/Cl<sup>-</sup> exchange.<sup>63</sup> Biological studies on a set of tambjamins bearing aromatic groups in the enamine motif have shown their antitumor ability in different cancer cell lines.

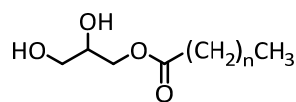


Other backbones based on natural products are the monoacylglycerides, studied by J. T. Davis and co-workers. Their ability to bind anions lies on the 1,2-diol group. Compounds **13** display Cl<sup>-</sup>/NO<sub>3</sub><sup>-</sup> antiporter activity at 1 mol% carrier to lipid,

<sup>62</sup> V. Saggiomo, S. Otto, I. Marques, V. Félix, T. Torroba and R. Quesada, *Chem. Commun.*, 2012, **48**, 5274–5276

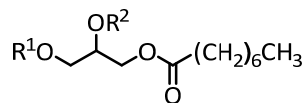
<sup>63</sup> P. Iglesias-Hernández, D. Moreno, A. Araujo-Javier, T. Torroba, R. Pérez-Tomás and R. Quesada, *Chem. Commun.*, 2012, **48**, 1556–1558.

meanwhile their analogs without this binding site available **14** seem to be no active transmembrane carriers.<sup>64</sup>



**13a** n = 6

**13b** n = 16



**14a** R<sup>1</sup> = H, R<sup>2</sup> = C(O)(CH<sub>2</sub>)<sub>16</sub>CH<sub>3</sub>

**14b** R<sup>1</sup> = R<sup>2</sup> = C(O)(CH<sub>2</sub>)<sub>16</sub>CH<sub>3</sub>

Regarding to synthetic anionophores, Schmitzer and *co-workers* have shown with lucigenin based assays how imidazolium salts, protonated independently of pH, can exchange Cl<sup>-</sup>/NO<sub>3</sub><sup>-</sup> through charge-assisted hydrogen bonding. Moreover, they have demonstrated by <sup>1</sup>H NMR and UV spectroscopy, the ability **15a** to form inclusion complexes with α-CD (α-cyclodextrin) or CB-7 (cucurbit[7]uril). The addition of these two water-soluble compounds in the transport assay implies that the inclusion complex increases the distribution of **15a** in the aqueous phase, and consequently the inhibition of the anion transport. It means α-CD or CB-7 work as supramolecular switches.<sup>65, 66</sup>

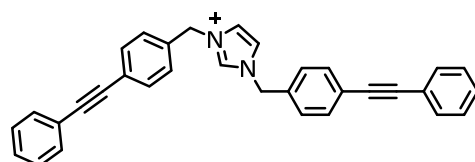
The substitution of the imidazolium moiety by a benzimidazolium one **16a–16d**, increases their chloride transport ability (EC<sub>50</sub> (**15d**) = 5.74 %, EC<sub>50</sub> (**16d**) = 2.99 %). These authors have revealed the importance of the nature of the counter-anion in the chloride transport efficiency. The bromide anion displays the higher tendency to interact with water molecules, among these four anions (Br<sup>-</sup>, BF<sub>4</sub><sup>-</sup>, PF<sub>6</sub><sup>-</sup> and NTf<sub>2</sub><sup>-</sup>). Therefore, **16a** is less predisposed to self-aggregate and to interact with the bilayer. On the contrary, less hydrated salts penetrate easily in the membrane and consequently are better transporters (**16a** < **16b** < **16c** < **16d**). These salts seem to be able to transport Ca<sup>2+</sup>, in a symport Ca<sup>2+</sup>/2Cl<sup>-</sup> way, in *E. coli*.<sup>67</sup>

<sup>64</sup> S. Bahmanjah, N. Zhang and J. T. Davis, *Chem. Commun.*, 2012, **48**, 4432–4434.

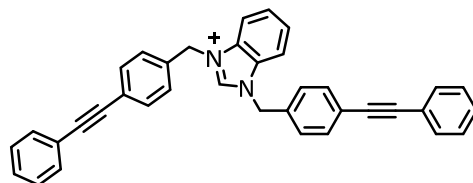
<sup>65</sup> C.-R. Elie, N. Noujeim, C. Pardin and A. R. Schmitzer, *Chem. Commun.*, 2011, **47**, 1788–1790.

<sup>66</sup> C.-R. Elie, M. Charbonneau and A. R. Schmitzer, *Med. Chem. Commun.*, 2012, **3**, 1231–1234.

<sup>67</sup> C.-R. Elie, A. Hébert, M. Charbonneau, A. Haiun and A. R. Schmitzer, *Org. Biomol. Chem.*, 2013, **11**, 923–928.

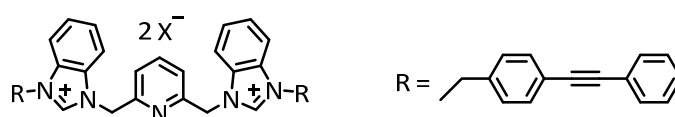


- 15a** Br<sup>-</sup>  
**15b** BF<sub>4</sub><sup>-</sup>  
**15c** PF<sub>6</sub><sup>-</sup>  
**15d** NTf<sub>2</sub><sup>-</sup>



- 16a** Br<sup>-</sup>  
**16b** BF<sub>4</sub><sup>-</sup>  
**16c** PF<sub>6</sub><sup>-</sup>  
**16d** NTf<sub>2</sub><sup>-</sup>

Lucigenin vesicle assays applied to a new family of benzoimidazolium salts **17a–17c** demonstrated that their anionophoric properties depends, again, on the nature of the counter-anion. U-tube experiments exhibit that **17c** acts as a mobile carrier, meanwhile **17a** and **17b** seem to form channels, which could be related with the tendency of the anions to be solvated. **17c** was found to be active against some *Gram-positive* and *Gram-negative* bacterium because of its ability to disrupt their membrane potential.<sup>68</sup>

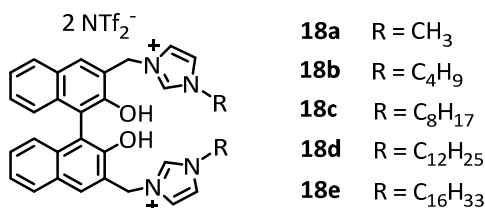


- 17a** X = Br<sup>-</sup>  
**17b** X = NTf<sub>2</sub><sup>-</sup>  
**17c** X = OTf<sup>-</sup>

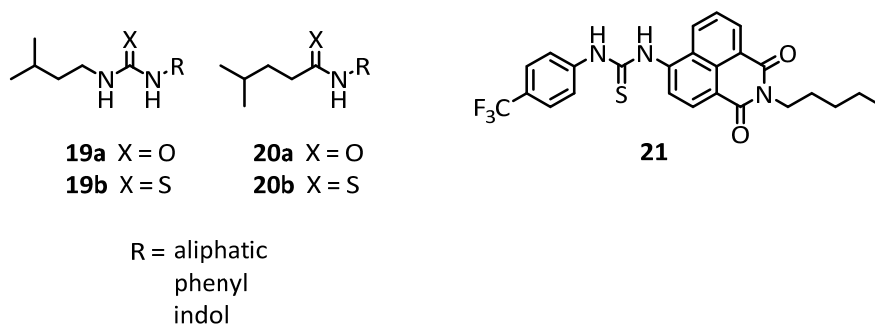
The same authors described a set of anion carriers based on the 2, 2'-binaphthol scaffold with alkyl-imidazolium chains **18a–18e**. Their study in vesicles loaded with HPTS show that both, antiport Cl<sup>-</sup>/NO<sub>3</sub><sup>-</sup> and symport H<sup>+</sup>/Cl<sup>-</sup> processes seem to be present and reveal the importance of the length of the aliphatic chain in the mechanism of action. Longer aliphatic chains favour the insertion of the host in the membrane and span it. **18a** and **18b** present a mobile carrier mechanism, meanwhile

<sup>68</sup> C.-R. Elie, G. David and A. R. Schmitzer, *J. Med. Chem.*, 2015, **58**, 2358–2366.

**18d** and **18e** form channels. Compound **18c**, the most active one, seems to act in both ways, simultaneously.<sup>69, 70</sup>



Gale and *co-workers* are focused on preparing small and simple anion carriers. They started checking the anionophoric ability, via Cl<sup>-</sup>/NO<sub>3</sub><sup>-</sup> and Cl<sup>-</sup>/HCO<sub>3</sub><sup>-</sup> exchange in vesicle models, of a simple family of ureas and thioureas (**19a** and **19b**). Chloride selective electrode assays show the superiority of thioureas vs ureas, probably because of the higher acidity and lipophilicity of thioureas. Their amides and thioamides analogs (**20a** and **20b**) display low activity, indicating the importance of the thio(urea) scaffold.<sup>71</sup> Related to biological activity, it has been elucidated with fluorescent thio(ureas) (e.g. **21**) that localization of the carrier inside the cell plays an important role in its toxicity. Those located in specific organelles are non-toxic toward cancer cell lines, meanwhile those localised widespread throughout the cytoplasm display activity against cancerous cells.<sup>72</sup>



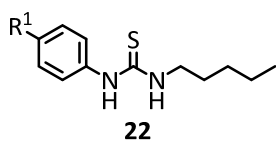
<sup>69</sup> M. Vidal, C.-R. Elie, S. Campbell, A. Claing and A. R. Schmitzer, *Med. Chem. Commun.*, 2014, **5**, 436–440.

<sup>70</sup> M. Vidal and A. Schmitzer, *Chem. Eur. J.*, 2014, **20**, 9998–10004.

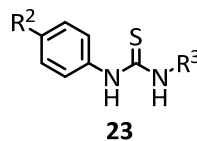
<sup>71</sup> N. J. Andrews, C. J. E. Haynes, M. E. Light, S. J. Moore, C. C. Tong, J. T. Davis, W. A. Harrell Jr. and P. A. Gale, *Chem. Sci.*, 2011, **2**, 256–260.

<sup>72</sup> S. N. Berry, V. Soto-Cerrato, E. N. W. Howe, H. J. Clarke, I. Mistry, A. Tavassoli, Y.-T. Chang, R. Pérez-Tomás and P. A. Gale, *Chem. Sci.*, 2016, **7**, 5069–5077.

QSAR is a useful tool for determining which factors affect the anion transport of a set of compounds, with similar structure. Gale and *co-workers* prepared 22 easy to make 1-hexyl-3-phenylthioureas, of general structure **22**, for which it was varied 4-phenyl position ( $R^1$ ) with different electron-donor and electron-withdrawing groups. The most relevant effect was found to be the lipophilicity of the substituents, followed by molecular size and hydrogen bond acidity. Based on the importance of the first factor, Davis and Gale studied it on a series of thioureas, **23**. As a conclusion, they introduced the concept of “lipophilicity balance”, which implies that the anion carrier activity is increased when the lipophilic substituents are distributed in a balanced way on both sides on the binding site. The initial rate is also affected by lipophilicity. Compounds with similar chloride efflux ability at 270 s, could present different profiles of transport as a function of lipophilicity, because highly lipophilic compounds take more time to partitioning in the lipid bilayer. This inconvenient could be solved by preincorporating highly lipophilic compounds in the vesicles membrane.<sup>73, 74, 75</sup> The influence of the lipid composition membrane was studied in a set of phenyl thioureas which lipophilicity ranges from 2.19–8.68.  $\text{NO}_3^-/\text{Cl}^-$  ISE assays with POPC, POPG, POPE:POPC (3:1) and DPPC were carried out. It was concluded that diffusion through the core region of the membrane was not the rate-determinant stage. Moreover, different environment had influenced on the rate of chloride efflux but the optimum  $\text{Log } P$  remained unaltered. It means that the optimum lipophilicity is an endogenous property of each family of carriers.<sup>76</sup>



$R^1$  electron donor and electron withdrawing groups



$R^2, R^3$  aliphatic chains of different length

The same authors have designed a family of *ortho*-phenylenediamine based bisureas, **24**, and have compared their ionophoric activity with some of the

<sup>73</sup> N. Busschaert, S. J. Bradberry, M. Wenzel, C. J. E. Haynes, J. R. Hiscock, I. L. Kirby, L. E. Karagiannidis, S. J. Moore, N. J. Wells, J. Herniman, G. J. Langley, P. N. Horton, M. E. Light, I. Marques, P. J. Costa, V. Félix, J. G. Frey and P. A. Gale, *Chem. Sci.*, 2013, **4**, 3036–3045

<sup>74</sup> H. Valkenier, C. J. E. Haynes, J. Herniman, P. A. Gale and A. P. Davis, *Chem. Sci.*, 2014, **5**, 1128–1134.

<sup>75</sup> C. J. E. Haynes, S. J. Moore, J. R. Hiscock, I. Marques, P. J. Costa, V. Félix and P. A. Gale, *Chem. Sci.*, 2012, **3**, 1436–1444.

<sup>76</sup> M. J. Spooner and P. A. Gale, *Chem. Commun.*, 2015, **51**, 4883–4886.

corresponding mono-ureas analogs.  $^1\text{H}$  NMR titrations of this new set of compounds, showed that they present better ability to bind anions. The  $\text{Cl}^-/\text{NO}_3^-$  and  $\text{Cl}^-/\text{HCO}_3^-$  exchanges were increased with the presence of the bisurea scaffold, and even  $\text{Cl}^-/\text{R-COO}^-$  was observed. Biological studies showed that the most active compounds are those with better ability as anion carriers. It has been demonstrated that highly fluorinated compounds such as **25** enhance the transport properties of this family of molecules. Moreover, this molecule is more active in  $\text{Cl}^-/\text{HCO}_3^-$  antiport, than the natural ionophore, prodigiosine.<sup>77, 78</sup> Anion carrier assays on a set of bisamide (e.g. **26**) have shown that they exchange  $\text{Cl}^-/\text{NO}_3^-$  better than  $\text{Cl}^-/\text{HCO}_3^-$  and both are worse than the corresponding values obtained for bis(ureas).<sup>79</sup> Jeong *et al* have demonstrated that bis(ureas) based on *cis*- or *trans*-amide linkage display really different ionophoric activity as a function on the amide conformation. *Trans*-amide conformation is nearly no active. On the contrary, *cis*-amides (e.g. **27**) are potent anion carriers due to the formation of an internal cavity and the decrease in the contact between the carrier and lipids, favour by the adopted geometry.<sup>80</sup> Following with tris(ureas) (e.g. **28**), it was observed that, apart from anions antiport, cation cotransport is involved in their ionophoric activity, in a lesser extent. Compared to bisureas, trisureas showed a slightly better ionophoric activity and one order of magnitude lower binding constants.<sup>81</sup>

---

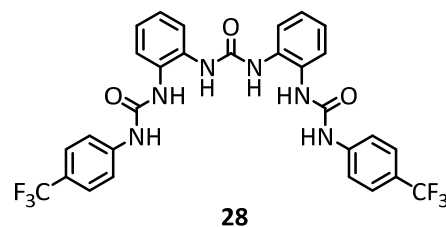
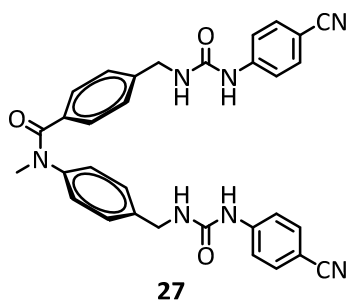
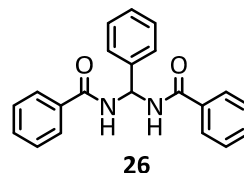
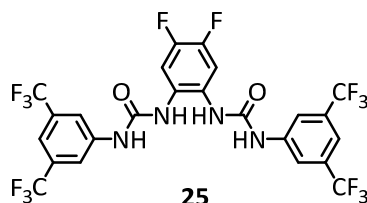
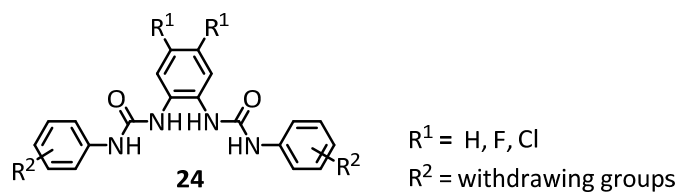
<sup>77</sup> S. J. Moore, C. J. E. Haynes, J. González, J. L. Sutton, S. J. Brooks, M. E. Light, J. Herniman, G. J. Langley, V. Soto-Cerrato, R. Pérez-Tomás, I. Marques, P. J. Costa, V. Félix and P. A. Gale, *Chem. Sci.*, 2013, **4**, 103–117.

<sup>78</sup> L. E. Karagiannidis, C. J. E. Haynes, K. J. Holder, I. L. Kirby, S. J. Moore, N. J. Wells and P. A. Gale, *Chem. Commun.*, 2014, **50**, 12050–12053.

<sup>79</sup> H. J. Clarke, W. V. Rossom, P. N. Horton, M. E. Light and P. A. Gale, *Supramol. Chem.*, 2016, **28**, 10–17.

<sup>80</sup> E. B. Park and K.-S. Jeong, *Chem. Commun.*, 2015, **51**, 9197–9200.

<sup>81</sup> M. Olivari, R. Montis, S. N. Berry, L. E. Karagiannidis, S. J. Coles, P. N. Horton, L. K. Mapp, P. A. Gale and C. Caltagirone, *Dalton Trans.*, 2016, **45**, 11892–11897.

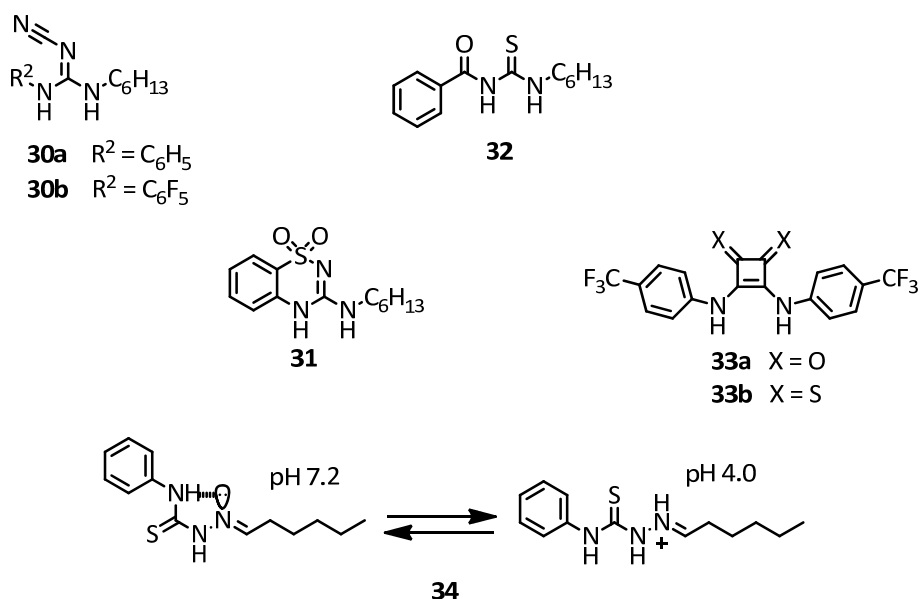


Tris-(thio)ureas based on the tris(2-aminoethyl) amine scaffold (“TREN”) have been investigated (e.g. **29a** and **29b**) as anionophores. This family of anion carriers present high selectivity binding for sulfate in solution, however the tendency of anion transport is  $\text{Cl}^- > \text{HCO}_3^- > \text{SO}_4^{2-}$ , suggesting that their ionophoric activity is governed by the lipophilicity of the anions and not by the binding affinity. As in previous examples, thioureas are better ionophores than ureas and fluorinated compounds display better anion carrier activity and seems to be more cytotoxic in cancer cell lines.<sup>82</sup>

<sup>82</sup> N. Busschaert, M. Wenzel, M. E. Light, P. Iglesias-Hernández, R. Pérez-Tomás and P. A. Gale, *J. Am. Chem. Soc.*, 2011, **133**, 14136–14148.



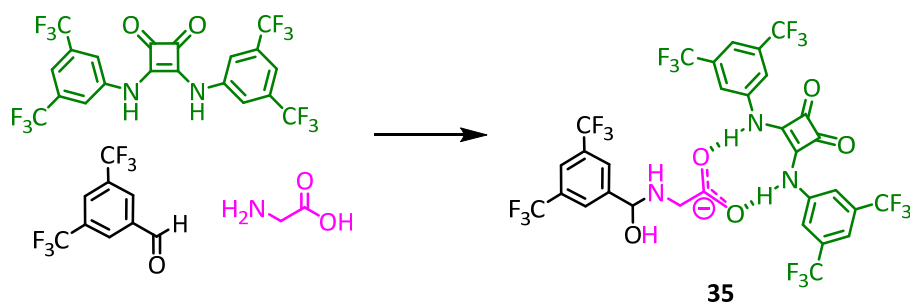
Phenylthiosemicarbazones (e.g. **34**) also display this behaviour with higher anionophoric properties than the thio/squaramides previously described. Their transport ability change up to 640-fold from working at pH 7.2 to 4.0.<sup>87</sup>



Squaramides has been used in a novel approach to transport amino acids through lipid bilayers. This study is based on the formation of a three components supramolecular structure that includes a non-covalent interaction between the squaramide and the glycine carboxylate through hydrogen bonds and a hemiaminal/imine linkage between the Glycine NH and a lipophilic and highly electrophile aldehyde (e.g. **35**). The anionophoric activity of this system has been checked applying two innovative  $^{13}\text{C}$  NMR and fluorescence techniques. The first one consist of measuring the glycine (Gly-1- $^{13}\text{C}$ ) influx into sulphate loaded vesicles, monitoring the amount of Gly-1- $^{13}\text{C}$  in the intra/extravesicular medium, by addition of paramagnetic  $\text{Mn}^{2+}$  to the exterior of the vesicles. The second one, based on the ability of  $\text{Cu}^{2+}$  to quench calcein, was proposed because of the long times required in  $^{13}\text{C}$  NMR assays. These fluorescence vesicle assays show the synergic effect among squaramide and aldehydes, in the glycine efflux.<sup>88</sup>

<sup>87</sup> E. N. W. Howe, N. Busschaert, X. Wu, S. N. Berry, J. Ho, M. E. Light, D. D. Czech, H. A. Klein, J. A. Kitchen and P. A. Gale, *J. Am. Chem. Soc.*, 2016, **138**, 8301–8308.

<sup>88</sup> X. Wu, N. Busschaert, N. J. Wells, Y.-B. Jiang and P. A. Gale, *J. Am. Chem. Soc.*, 2015, **137**, 1476–1484.

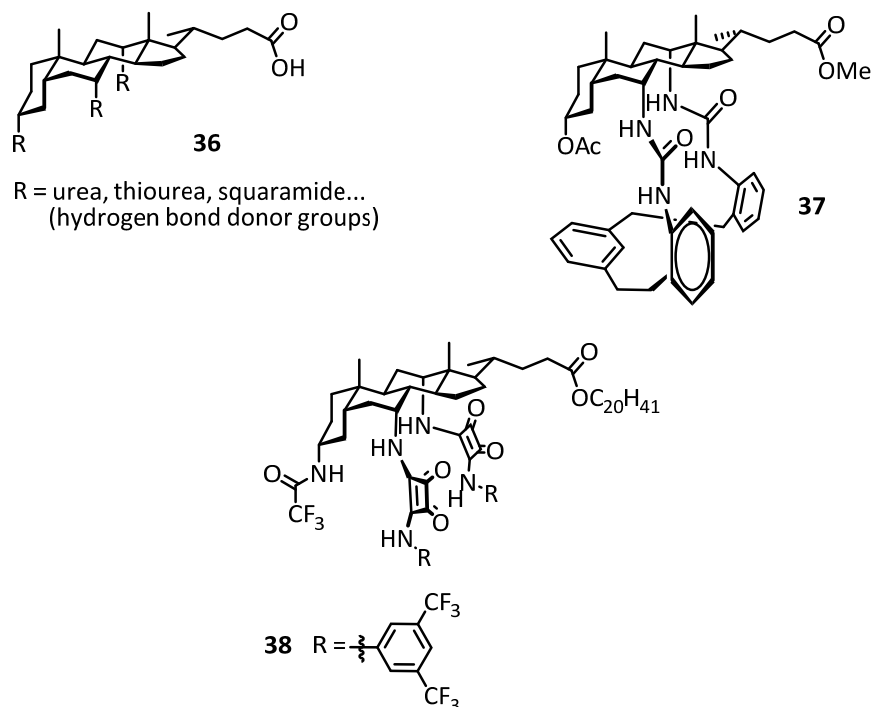


One of the first scaffolds used in the design of small anion carriers was the cholic acid **36**. Its steroidal framework provides lipophilicity and a preorganised structure to be used in the development of synthetic anionophores able to interact with anions through hydrogen bonds. A. P. Davis and *co-workers* showed the high association constants that these derivatives present in solution ( $> 10^7 \text{ M}^{-1}$ ) and their ability to exchange  $\text{Cl}^-/\text{NO}_3^-$  in POPC:cholesterol (7:3) vesicles under ISE assay conditions with moderate results. Both, the binding constants and the anionophoric activity of these compounds are correlated showing the importance of hydrogen bonds strength.<sup>89</sup> In order to improve the ionophoric activity of this kind of molecules, cholaphane cyclic analogs (e.g. **37**) were designed. This steric shielding structure had not relevant influence in the binding affinities. Nevertheless, the anion carrier activity was increased significantly.<sup>90</sup> Gale and Davis have shown the exceptional anion binding affinities (in the order of  $10^{14} \text{ M}^{-1}$ ) of these steroid based receptors with squaramides in axial positions (e.g. **38**), related to the high acidity of the squaramide motif combined with an excellent binding geometry. On the contrary, this strong interaction is not directly related to an enhancement in their ionophoric activity. Maybe because strong supramolecular complexes do not decomplex.<sup>91</sup>

<sup>89</sup> A. V. Koulov, T. N. Lambert, R. Shukla, M. Jain, J. M. Boon, B. D. Smith, H. Li, D. N. Sheppard, J.-B. Joos, J. P. Clare and A. P. Davis, *Angew. Chem. Int. Ed.*, 2003, **42**, 4931–4933.

<sup>90</sup> L. W. Judd and A. P. Davis, *Chem. Commun.*, 2010, **46**, 2227–2229.

<sup>91</sup> S. J. Edwards, H. Valkenier, N. Busschaert, P. A. Gale and A. P. Davis, *Angew. Chem. Int. Ed.*, 2015, **54**, 4592–4596.



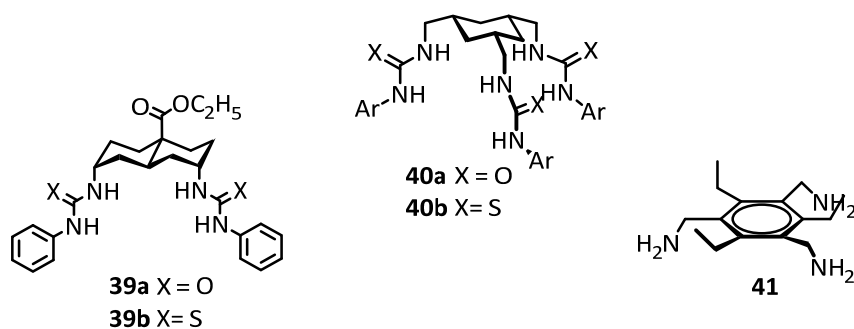
The cholapod architecture presents some drawbacks such as high molecular weight and high lipophilicity. In an attempt to avoid these disadvantages, the steroid scaffold was substituted by a simple diureido decalin system (e.g. **39**). This new family maintains good ionophoric activity at very low loadings of anion carrier, with smaller lipophilicity.<sup>92</sup> Moreover, the cholapod could be substituted by a cyclohexane structure with three pendant thio/ureas **40** or even by the directly accessible tris-amine **41** because it does not imply a decrease in chloride efflux.<sup>93, 94</sup> This means that the steroid structure is not essential to reach the membrane interior. The  $\text{Cl}^-/\text{NO}_3^-$  activity of some of these compounds has been studied using Giant Unilamellar Vesicles (GUVs).<sup>95</sup>

<sup>92</sup> S. Hussain, P. R. Brotherhood, L. W. Judd and A. P. Davis, *J. Am. Chem. Soc.*, 2011, **133**, 1614–1617.

<sup>93</sup> H. Valkenier, L. W. Judd, H. Li, S. Hussain, D. N. Sheppard and A. P. Davis, *J. Am. Chem. Soc.*, 2014, **136**, 12507–12512.

<sup>94</sup> H. Valkenier, C. M. Dias, K. L. P. Goff, O. Jurcek, R. Puttreddy, K. Rissanen and A. P. Davis, *Chem. Commun.*, 2015, **51**, 14235–14238.

<sup>95</sup> H. Valkenier, N. L. Mora, A. Kros and A. P. Davis, *Angew. Chem. Int. Ed.*, 2015, **54**, 2137–2141.



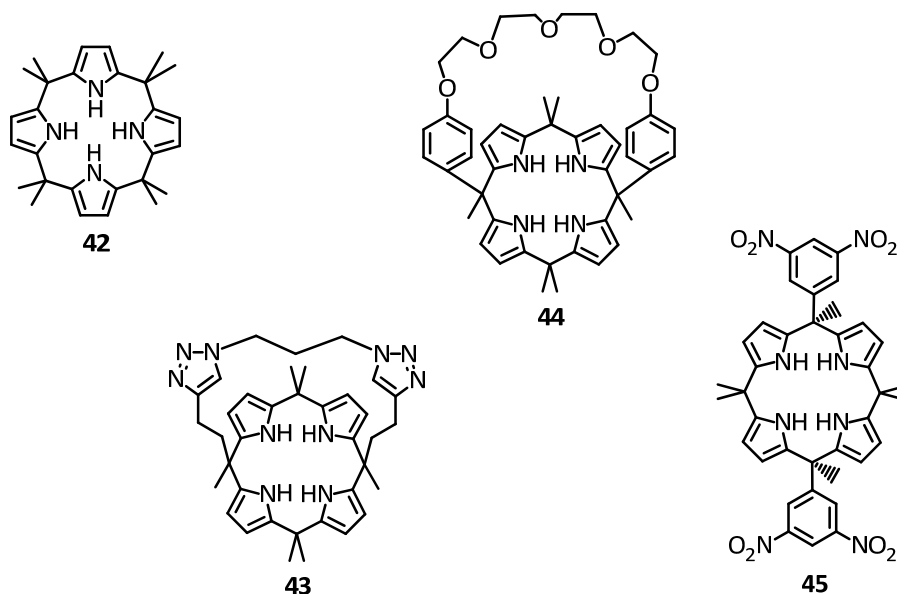
Calix[4]pyrrole, a macrocycle known since 19<sup>th</sup> century, is another neutral scaffold that displays anionophoric properties. In the past years, its anion recognition properties have been studied in detail. More recently, its ability as transmembrane anion carrier has been examined by Gale, Sessler and Quesada.<sup>96</sup> The octamethylcalix[4]pyrrole **42** co-transport Cs<sup>+</sup>/Cl<sup>-</sup> in a selective way. The symport mechanism is based on the binding of chloride through four hydrogen bonds to the pyrrolic N-H groups and the complexation of caesium through  $\pi$ -cation interactions in the cup defined by the macrocycle. Gale and *co-workers* design a set of strapped calix[4]pyrroles with additional hydrogen bond donors in the linker chain (e.g. **43**). The most important factor involved in their anionophoric properties seems to be the linker length. For these compounds, the longer the chain the more active and the higher tendency to function as antiporters (Cl<sup>-</sup>/NO<sub>3</sub><sup>-</sup>) instead of symporters.<sup>97</sup> By introducing an oligoether chain **44** is possible to coordinate alkali metals through this motif and anions through the calix[4]pyrrole moiety, and consequently a modest M<sup>+</sup>/Cl<sup>-</sup> is observed.<sup>98</sup> Matile and *co-workers* designed a set of “two aromatic wall”  $\alpha,\alpha$ -calix[4]pyrroles **45** bearing two opposite *meso*-carbons with aryl groups which mechanism of action is based on  $\pi$  interactions between the  $\pi$ -acidic aromatic substituents in  $\alpha$  positions and anions. They display moderate ionophoric activity with high NO<sub>3</sub><sup>-</sup> selectivity probably because of the complementary geometry between this oxoanion and the “two wall”  $\alpha,\alpha$ -calix[4]pyrrole binding site.<sup>99</sup>

<sup>96</sup> C. C. Tong, R. Quesada, J. L. Sessler and P. A. Gale, *Chem. Commun.*, 2008, 6321–6323.

<sup>97</sup> M. Yano, C. C. Tong, M. E. Light, F. P. Schmidtchen and P. A. Gale, *Org. Biomol. Chem.*, 2010, **8**, 4356–4363.

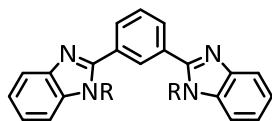
<sup>98</sup> I.-W. Park, J. Yoo, B. Kim, S. Adhikari, S. K. Kim, Y. Yeon, C. J. E. Haynes, J. L. Sutton, C. C. Tong, V. M. Lynch, J. L. Sessler, P. A. Gale and C.-H. Lee, *Chem. Eur. J.*, 2012, **18**, 2514–2523.

<sup>99</sup> L. Adriaenssens, C. Estarellas, A. Vargas Jentzsch, M. Martinez-Belmonte, S. Matile and P. Ballester, *J. Am. Chem. Soc.*, 2013, **135**, 8324–8330.



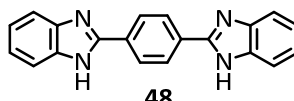
Chen and *co-workers* have been working on the development of anion carriers based on neutral benzimidazol benzene derivatives. The importance of benzimidazolyl–NH fragments, their relative position and number were studied with **46–49**. To evaluate these variables their ability to compensate pH gradients and to transport anions were measured in EYPC vesicles with the fluorescence probe pyranine and the chloride-sensitive fluorescence dye lucigenin, respectively, (at 5 mol% carrier to lipid). It was concluded that the three factors play an important role in the transport process because only **46a** presents good activity. Symport  $M^+/Cl^-$  was discarded as possible way of transport, since assays varying the metal anion ( $M = Li^+, Na^+, K^+, Rb^+$  and  $Cs^+$ ) resulted in similar rates of activity. The finding that chloride transport was dramatically suppressed when sulfate ( $Cl^-/SO_4^{2-}$ ) was used instead of nitrate ( $Cl^-/NO_3^-$ ), implies that these compounds act as anion antiporters. Six derivatives of **46a** with electron withdrawing groups in *para* position were studied (**50a–50f**). Compound **50f**, with the  $-NO_2$  substituent and a lipophilicity value of 4.03, is three orders of magnitude more active than **46a**. With respect to **51a** and **51b**, the tendency is the same as between **46a** and **46b**. The N-methylated compound presented no activity as anion carrier because it has lost the ability of establishing hydrogen bondings, which is observed experimentally, in the binding association constants with different anions. Values for **51a** are one order of magnitude higher than those obtained for **51b** ( $8710 M^{-1}$  and  $400 M^{-1}$  respectively;

obtained by spectrophotometric titrations of the compounds with TBACl in a mixture  $\text{CH}_3\text{CN}:\text{H}_2\text{O}$  1:2, v/v).<sup>100, 101</sup>

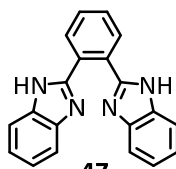


**46a** R = H

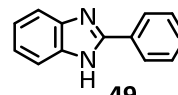
**46b** R = Me



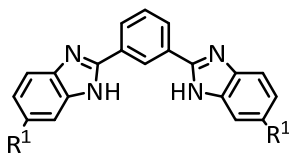
**48**



**47**



**49**



**50a** R<sup>1</sup> = Me

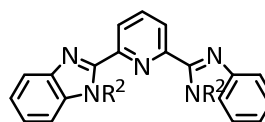
**50b** R<sup>1</sup> = F

**50c** R<sup>1</sup> = Cl

**50d** R<sup>1</sup> = Br

**50e** R<sup>1</sup> = CF<sub>3</sub>

**50f** R<sup>1</sup> = NO<sub>2</sub>



**51a** R<sup>2</sup> = H

**51b** R<sup>2</sup> = Me

A variety of novel designs of anion carriers, mainly based on hydrogen bonds, have been introduced in the last couple of years. Gale and *co-workers* have synthesised macrocyclic 2,6-bis-(1,2,3-triazo-lyl)-pyridine receptors (e.g. **52**) with moderate chloride affinity constants and antiport  $\text{NO}_3^-/\text{Cl}^-$  behaviour together with  $\text{H}^+/\text{Cl}^-$  to a lesser extent.<sup>102</sup> They have also worked, in the design of the perenosins (e.g. **53**). Benzimidazole and indazole based perinosins show poor activity. On the contrary, indole-based ones are good  $\text{Cl}^-/\text{NO}_3^-$  antiporters.<sup>103</sup> This family of compounds exhibits some similarities with prodiginines and tambjamines such as comparable pka values to prodiginines, low lipophilicity values, a flat X-ray structure

<sup>100</sup> C.-C. Peng, M.-J. Zhang, X.-X. Sun, X.-J. Cai, Y. Chen and W.-H. Chen, *Org. Biomol. Chem.*, 2016, **14**, 8232–8236.

<sup>101</sup> C.-C. Peng, Z. Li, L.-Q. Deng, Z.-F. Ke, W. H. Chen, *Bioorg. Med. Chem. Lett.*, 2016, **26**, 2442–2445.

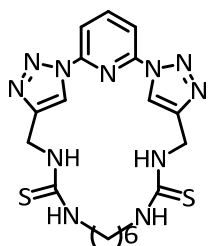
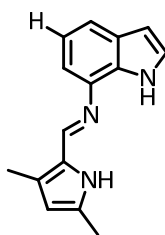
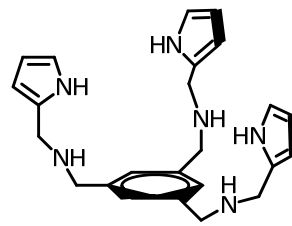
<sup>102</sup> T. Merckx, C. J. E. Haynes, L. E. Karagiannidis, H. J. Clarke, K. Holder, A. Kelly, G. J. Tizzard, S. J. Coles, P. Verwilst, P. A. Gale and W. Dehaen, *Org. Biomol. Chem.*, 2015, **13**, 1654–1661.

<sup>103</sup> W. V. Rossom, D. J. Asby, A. Tavassoli and P. A. Gale, *Org. Biomol. Chem.*, 2016, **14**, 2645–2650.

in the protonated state with three hydrogen bonds interacting with the anion and a similar mechanism of transport in which only the protonated specie is active.

These authors have also been involved in the development of a series of amino pyrrolic receptors anchored to benzene or naphthalene rings (e.g. **54**). Their predominant mechanism of action is  $M^+/Cl^-$  symport, which seems to play a significant role in their antibiotic activity against *S. aureus*, (gram-positive bacteria).<sup>104</sup> Biotin[6]uril hexaesters (e.g. **55**), have an internal cavity that displays 12 CH groups available to interact with anions through hydrogen bonds ( $C-H \cdots anion$ ), as confirmed by X-ray analysis. The binding affinities in solution seem to be related with the anion shape,  $Cl^- > NO_3^- \sim HCO_3^- \gg SO_4^{2-}$ . Their anionophoric properties studied in lucigenin based assays under  $NO_3^-/Cl^-$  exchange conditions depends on the side chain. The higher the chain the better the activity.<sup>105</sup>

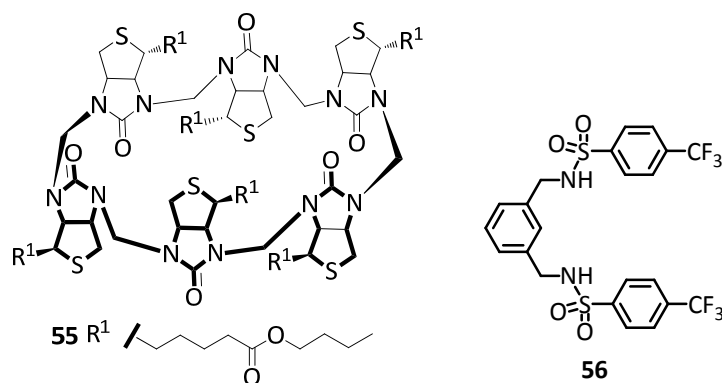
P. Talukdar *et al* have used the sulphonamide as anion carrier motif (e.g. **56**). Its NH proton acidity and chloride binding are higher than the corresponding amides. They observed that the ionophoric activity of these kind of compounds, is favoured by the presence of electron-withdrawing substituents and governed by lipophilicity with  $EC_{50}$  values in the  $\mu M$  range. U-tube assays were used to confirm their carrier mechanism of action.<sup>106</sup>

**52****53****54**

<sup>104</sup> A. I. Share, K. Patel, C. Nativi, E. J. Cho, O. Francesconi, N. Busschaert, P. A. Gale, S. Roelens and J. L. Sessler, *Chem. Commun.*, 2016, **52**, 7560-7563.

<sup>105</sup> M. Lisbjerg, H. Valkenier, B. M. Jessen, H. Al-Kerdi, A. P. Davis and M. Pittelkow, *J. Am. Chem. Soc.*, 2015, **137**, 4948-4951.

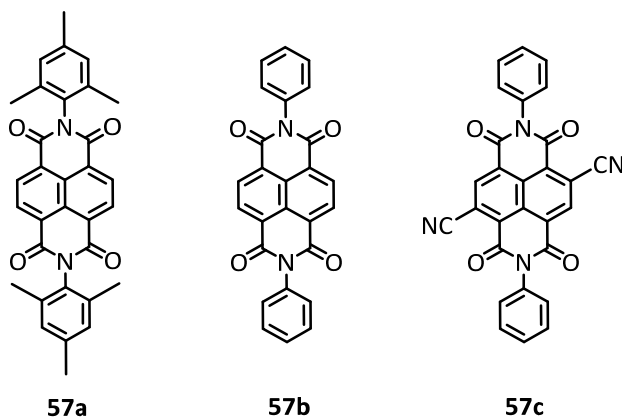
<sup>106</sup> T. Saha, M. S. Hossain, D. Saha, M. Lahiri and P. Talukdar, *J. Am. Chem. Soc.*, 2016, **138**, 7558-7567.



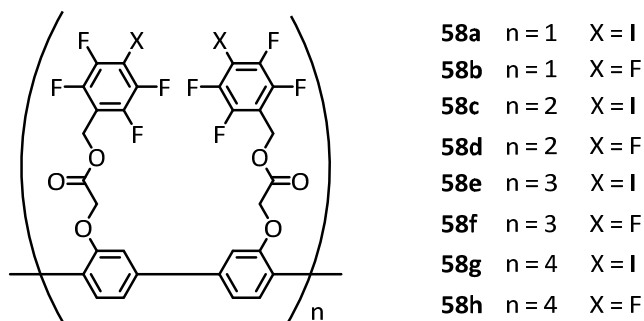
### 3.3.2.2. Non-classical interactions

Anion- $\pi$  interactions are based on interactions between anions and  $\pi$ -acidic aromatic surfaces. These interactions are weak and techniques such as electrospray ionization Fourier-transform ion cyclotron resonance tandem mass spectrometry (ESI-FTICR-MS-MS) are appropriate for their study. Matile and co-workers postulated that naphthalenediimides (NDI) based on rigid rods are able to catalyze anion transport across lipid membranes through this kind of interactions. ESI-FTICR-MS-MS experiments showed that the anion affinity enhancements when  $\pi$ -acidity increases and the  $\pi$ -binding site is less crowded. HPTS and lucigenin assays demonstrated that the selectivity was governed by  $\pi$ -acidity and decrowded active site. In order to demonstrate that these non-classical interactions were the responsible of the transport process three simpler NDI models **57a–57c** were synthesised. The anionophoric activity of these three compounds was tested in HPTS loaded vesicles. **57c**, with the most acidic  $\pi$  system, was found to be the best anion carrier with an  $EC_{50}$  value in the nM range (330 nM). Therefore, these results were found to be consistent with the hypothesis that anion- $\pi$  interactions are the driving forces involved in the anionophoric activity of these compounds.<sup>107</sup>

<sup>107</sup> R. E. Dawson, A. Hennig, D. P. Weimann, D. Emery, V. Ravikumar, J. Montenegro, T. Takeuchi, S. Gabutti, M. Mayor, J. Mareda, C. A. Schalley and S. Matile, *Nat. Chem.*, 2010, **2**, 533–538.



Another type of non-classical interaction is the halogen bond which is based on non-covalent interactions between a Lewis base and an electrophilic region associated with a halogen atom in a molecule (so-called  $\sigma$  hole). The strength of this interaction varied from 10 to 200 KJ/mol and the distance is shorter than the sum of the Van der Waals radius of both atoms involved in the interaction.<sup>108</sup> Matile *et al* have studied the ability of halogen bond interactions to transport anions using a set of eight rigid rods (e.g. **58**). Vesicles loaded with HPTS were used to test the capacity of this family of compounds to compensate pH gradients. Compounds with iodine in the structure were found to be more active than their analogs with fluorine with a difference of one order of magnitude in the EC<sub>50</sub> values.<sup>109</sup>

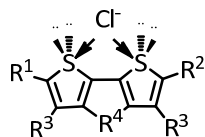


Matile and *co-workers* have used chalcogen bonds in an innovative family of carriers, the electron deficient dithieno [3,2-b;2',3'-d] thiophenes (DTTs) **59a–59j**. This non-classical interaction comes from the ability of the Lewis acidic  $\sigma$  holes from

<sup>108</sup> A. Brown and P. D. Beer, *Chem. Commun.*, 2016, **52**, 8645–8658.

<sup>109</sup> A. V. Jentzsch and S. Matile, *J. Am. Chem. Soc.*, 2013, **135**, 5302–5303.

two sulfur atoms located in a preorganised way, to interact with negative density charge. Among members of this family, compound **59g** which  $\sigma$  holes acidity is enhanced by the electron withdrawing substituents, was found to be the most active carrier in HPTS EYPC vesicle assays, with an  $EC_{50}$  value of 1.9  $\mu$ M.<sup>110</sup>



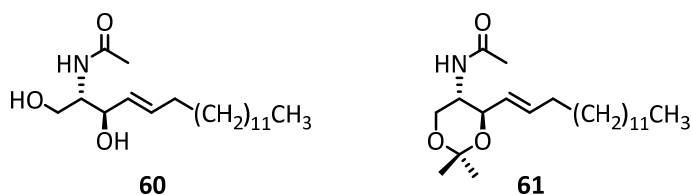
<b>59a</b>	R <sup>1</sup> = H	R <sup>2</sup> = H	R <sup>3</sup> = <i>i</i> -Bu	R <sup>4</sup> = S
<b>59b</b>	R <sup>1</sup> = CHO	R <sup>2</sup> = CHO	R <sup>3</sup> = <i>i</i> -Bu	R <sup>4</sup> = S
<b>59c</b>	R <sup>1</sup> = H	R <sup>2</sup> = H	R <sup>3</sup> = <i>i</i> -Bu	R <sup>4</sup> = SO
<b>59d</b>	R <sup>1</sup> = CN	R <sup>2</sup> = H	R <sup>3</sup> = <i>i</i> -Bu	R <sup>4</sup> = SO
<b>59e</b>	R <sup>1</sup> = H	R <sup>2</sup> = H	R <sup>3</sup> = <i>i</i> -Bu	R <sup>4</sup> = SO <sub>2</sub>
<b>59f</b>	R <sup>1</sup> = CN	R <sup>2</sup> = H	R <sup>3</sup> = <i>i</i> -Bu	R <sup>4</sup> = SO <sub>2</sub>
<b>59g</b>	R <sup>1</sup> = CN	R <sup>2</sup> = CN	R <sup>3</sup> = <i>i</i> -Bu	R <sup>4</sup> = SO <sub>2</sub>
<b>59h</b>	R <sup>1</sup> = CHO	R <sup>2</sup> = CHO	R <sup>3</sup> = <i>i</i> -Bu	R <sup>4</sup> = SO <sub>2</sub>
<b>59i</b>	R <sup>1</sup> = SO <sub>2</sub> Et	R <sup>2</sup> = H	R <sup>3</sup> = Me	R <sup>4</sup> = SO <sub>2</sub>
<b>59j</b>	R <sup>1</sup> = SO <sub>2</sub> Et	R <sup>2</sup> = SO <sub>2</sub> Et	R <sup>3</sup> = Me	R <sup>4</sup> = SO <sub>2</sub>

### 3.3.3. Transmembrane anion transport promoted by channels

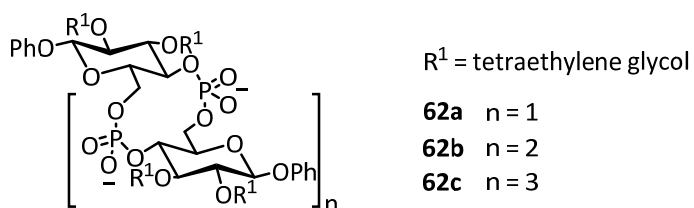
J. T. Davis and co-workers have reported how natural products such as sphingolipid ceramide **60**, which is able to bind anions through hydrogen bonds, can transport chloride and bicarbonate across lipid bilayers. Its mechanism of action is borderlined between mobile carriers and channels. EYPC vesicles loaded with NaCl and the fluorescence probe lucigenin were suspended over nitrate, bicarbonate and sulphate solutions. The addition of **60** and **61** (at 1 mol% carrier to lipid) demonstrated that only **60**, with free OH groups available to form hydrogen bonds, was active. Moreover, it was observed that the transport efficiency was dictated by the extravascular anion ( $NO_3^- > HCO_3^- \gg SO_4^{2-}$ ). In order to better understand the mechanism of transport followed by **60** at this concentration, vesicle loaded with the fluorescence dye carboxyfluorescein were used to demonstrate that it is a mobile carrier. At higher concentrations (50 mol% carrier to lipid) the leakage of CF indicated the formation of channels or pores.<sup>111</sup>

<sup>110</sup> S. Benz, M. Macchione, Q. Verolet, J. Mareda, N. Sakai and S. Matile, *J. Am. Chem. Soc.*, 2016, **138**, 9093–9096.

<sup>111</sup> W. A. Harrell, Jr., M. L. Bergmeyer, P. Y. Zavalij and J. T. Davis, *Chem. Commun.*, 2010, **46**, 3950–3952.



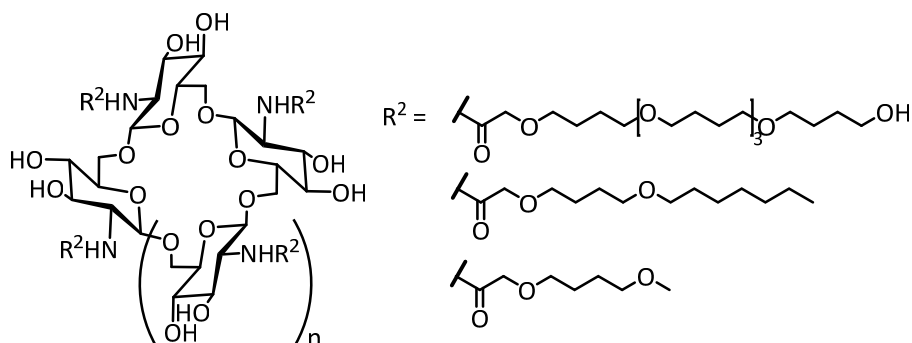
Another class of natural molecules such as carbohydrates has been studied as anionophoric platforms. Montesarchio and *co-workers* have been investigating the ability of CyPLOS (cyclic phosphate-linked oligosaccharide) scaffold **62** to destabilise the membrane and consequently allow the transport of small ions, in a nonspecific way.<sup>112</sup>



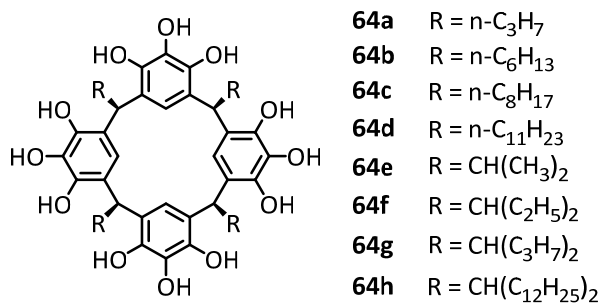
P. Talukdar and *co-workers* have developed a family of macrocyclic anion carriers based on cyclic oligo-(1-6)- $\beta$ -D-glucosamine functionalised with different length tails **63**. Both the number of oligomers that form the macrocycle and the tail length affect the ion transport activity.<sup>113</sup> As the number of oligomers increases, the pore size is increasing and, with it, the transport activity (**63a** < **63b** < **63c** < **63d**). When medium size chains are linked to the skeleton, the active supramolecular specie is a dimer. On the other hand, when long chains are present in the structure the formation of pores is promoted by a monomer. Short-tail analogs are used as negative control in transport studies because of the poor anionophoric activity. The total number of tails also displays an important role in the transport activity since the movement of anions decreases when fewer chains are connected to the central scaffold.

<sup>112</sup> E. Busi, G. Vitiello, M. Niccoli, R. Basosi, D. Montesarchio, G. D'Errico, *Biochim. Biophys. Acta*, 2013, **1828**, 2074–2082.

<sup>113</sup> A. Roy, T. Saha, M. L. Gening, D. V. Titov, A. G. Gerbst, Y. E. Tsvetkov, N. E. Nifantiev and P. Talukdar, *Chem. Eur. J.*, 2015, **21**, 17445–17452.

**63a**  $n = 2$ **63b**  $n = 3$ **63c**  $n = 4$ **63d**  $n = 5$ 

The anionophoric properties of a set of pyrogallol[4]arenes (Pgs) **64** with side chains of different lengths in the position R were studied by Gokel and *co-workers*. Voltage-clamp and ISE assays were applied and it was concluded that all of them form channels in the bilayer. Among compounds with lineal chain **64a–64d**, longer chains make them less active chloride carriers. With respect to branched chains, Pgs **64e–64h**, compound **64e** shows the higher conductance and the best chloride transport activity. These results are consistent with the ability of **64e** to form a hexameric unit **64e<sub>6</sub>**, that link together giving as a result a nanotube (**64e<sub>6</sub>**)<sub>n</sub> with an internal network of hydrogen bonds. They postulate that this species is the responsible of the chloride transport trough the bilayer.<sup>114</sup>



<sup>114</sup> S. Negin, R. Li, O. V. Kulikov, M. M. Daschbach and G. W. Gokel, *Inorg. Chim. Acta*, 2014, **417**, 177–185.

#### 4. BIOLOGICAL ACTIVITY OF ANION TRANSPORTERS

Molecules with the ability to transport anions through lipid membranes are able to alter the ion homeostasis of cells, which implies that they display the capacity to impact over multiple cellular processes. These biological alterations could be used to explore the connections between chemistry and medicine, giving rise to the development of the *supramolecular medicinal chemistry* field, still in an early stage.<sup>115</sup>

Homeostasis changes promoted by anionophores give rise to cellular stress in such a way that could damage the cell, triggering its death. This response presents applications in regulating uncontrolled cell growth and elimination of damaged cells, for example in chemotherapy. Natural systems such as tambjamins and prodiginines are excellent anion carriers. It is known that they present antimicrobial, antimalarial and immunosuppressive properties.<sup>116, 117</sup> Members of these families display apoptotic effects in both, *in vitro* and *in vivo* assays. The cytotoxicity of obatoclax **65** and some synthetic analogs **66–68** was tested in a small-cell lung carcinoma cell line (GLC4) and it was found that active  $\text{Cl}^-/\text{NO}_3^-$  and  $\text{Cl}^-/\text{HCO}_3^-$  anionophores **65** and **66** present cytotoxic properties, meanwhile those with poor properties as anion carriers, such as **67** and **68** were found to be non cytotoxic.<sup>118</sup> Applying the acridine orange staining assay in a set of tambjamins (i.e. **11** or **69**), it was demonstrated that only those with good properties as anion carriers such as **69** were able to deacidified acidic organelles in GLC4 cancer cells.<sup>119</sup> These breakthroughs evidence that although these compounds can be working as BH3 mimetics,<sup>120</sup> their anionophoric activity plays an important role in their antitumor properties.

---

<sup>115</sup> D. K. Smith, *J. Chem. Educ.*, 2005, **82**, 393–400.

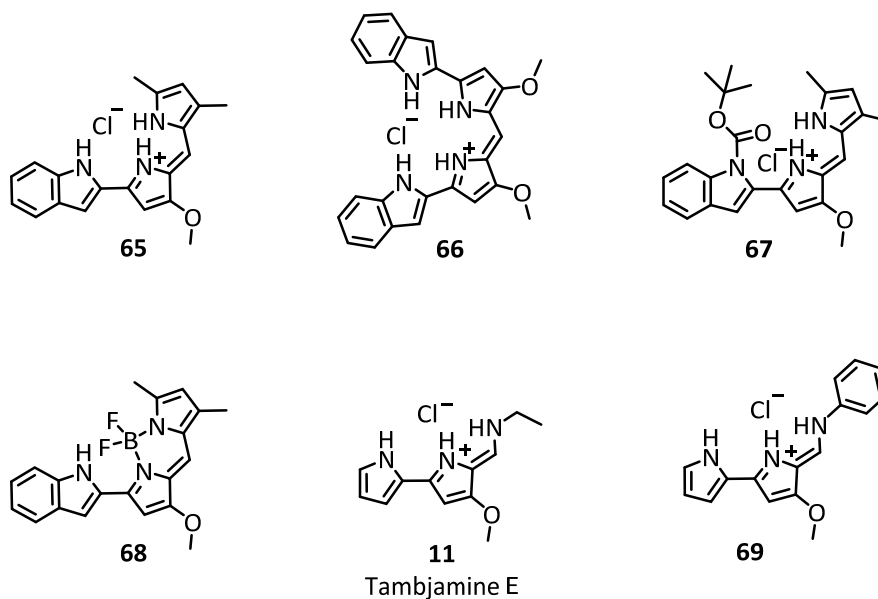
<sup>116</sup> B. C. Cavalcanti, H. V. N. Júnior, M. H. R. Selegim, R. G. S. Berlinck, G. M.A. Cunha, M. O. Moraes, C. Pessoa, *Chem.-Biol. Interact.*, 2008, **174**, 155–162.

<sup>117</sup> P. Kancharla, J. X. Kelly and K. A. Reynolds, *J. Med. Chem.*, 2015, **58**, 7286–7309.

<sup>118</sup> B. Díaz de Greñu, P. Iglesias-Hernández, M. Espona, D. Quiñonero, M. E. Light, T. Torroba, R. Pérez-Tomás and R. Quesada, *Chem. Eur. J.* 2011, **17**, 14074–14083.

<sup>119</sup> P. Iglesias-Hernández, D. Moreno, A. Araujo-Javier, T. Torroba, R. Pérez-Tomás and R. Quesada, *Chem. Commun.*, 2012, **48**, 1556–1558.

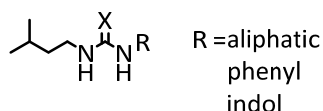
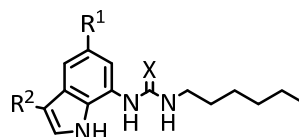
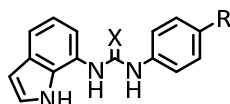
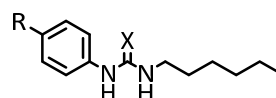
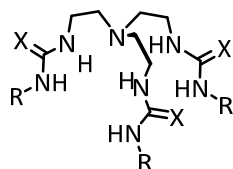
<sup>120</sup> A. Hosseini, M. Espona-Fiedler, V. Soto-Cerrato, R. Quesada, R. Pérez-Tomás, V. Guallar, *PLoS ONE*, 2013, **8**, e57562.



In the view of synthetic small ureas and thioureas **19** were good anion carriers, the relationship between anionophoric activity and cytotoxicity was also tested in similar ureas and thioureas with and without the presence of trifluoromethyl substituents **70–72**. In general, thioureas displayed greater anionophoric activity than ureas and those with fluorinated groups were found to be more potent anion carriers than their unfluorinated analogs. A viability study of these compounds in different human cancer cell lines demonstrated that the most active carriers were able to induce cell death, with significant lower  $IC_{50}$  values in cancerous cells than those found in the non-cancerous cell line MCF10A.<sup>121</sup> Similar results were observed in the case of tripodal, tren-based, tris(thio)ureas **73** and **74**. Only compounds with good anionophoric properties such as **73c–d** and **74b–d** display the ability to alter the internal cellular pH in acridine orange assays and trigger cell death in cancerous cell lines.<sup>122</sup>

<sup>121</sup> S. J. Moore, M. Wenzel, M. E. Light, R. Morley, S. J. Bradberry, P. Gómez-Iglesias, V. Soto-Cerrato, R. Pérez-Tomás and P. A. Gale, *Chem. Sci.*, 2012, **3**, 2501–2509.

<sup>122</sup> N. Busschaert, M. Wenzel, M. E. Light, P. Iglesias-Hernández, R. Pérez-Tomás and P. A. Gale, *J. Am. Chem. Soc.*, 2011, **133**, 14136–14148.

**19a** X = O**19b** X = S**70a** X = O; R<sup>1</sup> = H; R<sup>2</sup> = H**70b** X = S; R<sup>1</sup> = H; R<sup>2</sup> = H**70c** X = O; R<sup>1</sup> = CF<sub>3</sub>; R<sup>2</sup> = nBu**70d** X = S; R<sup>1</sup> = CF<sub>3</sub>; R<sup>2</sup> = nBu**71a** X = O; R = H**71b** X = S; R = H**71c** X = O; R = CF<sub>3</sub>**71d** X = S; R = CF<sub>3</sub>**72a** X = O; R = H**72b** X = S; R = H**72c** X = O; R = CF<sub>3</sub>**72d** X = S; R = CF<sub>3</sub>**73a** X = O R = *p*-C<sub>6</sub>H<sub>4</sub>F**73b** X = O R = C<sub>6</sub>F<sub>5</sub>**73c** X = O R = *p*-C<sub>6</sub>H<sub>4</sub>(CF<sub>3</sub>)**73d** X = O R = **74a** X = S R = *p*-C<sub>6</sub>H<sub>4</sub>F**74b** X = S R = C<sub>6</sub>F<sub>5</sub>**74c** X = S R = *p*-C<sub>6</sub>H<sub>4</sub>(CF<sub>3</sub>)**74d** X = S R = 

As it has been shown in the previous section, the malfunction of natural ion carrier systems is linked to a huge variety of diseases. The development of synthetic low molecular weight lipid membrane anion carriers with potential use in channel replacement therapy is a field of intensive interest.<sup>123, 124, 125, 126, 127</sup> Thus, an approach that can be attributed to these compounds could be replacing the function of faulty proteins in living organisms and consequently substitute this proteins behaviour may lead to a therapy to combat these “channelopathies”. In this way, Yang and *co-workers* tested, in both liposomes and cells, the ability of isophtalamide

<sup>123</sup> H. Li, H. Valkenier, L. W. Judd, P. R. Brotherhood, S. Hussain, J. A. Cooper, O. Jurček, H. A. Sparkes, D. N. Sheppard and A. P. Davis, *Nat. Chem.*, 2016, **8**, 24–32.

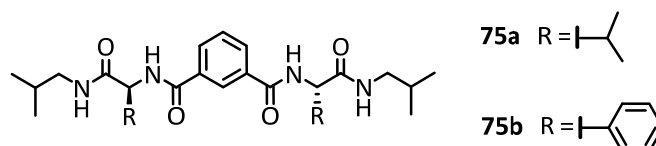
<sup>124</sup> N. Busschaert and P. A. Gale, *Angew. Chem. Int. Ed.*, 2013, **52**, 1374–1382.

<sup>125</sup> P. A. Gale, R. Pérez-Tomás and R. Quesada, *Acc. Chem. Res.*, 2013, **46**, 2801–2813.

<sup>126</sup> S. Matile, A. V. Jentzsch, J. Montenegro and A. Fin, *Chem. Soc. Rev.*, 2011, **40**, 2453–2474.

<sup>127</sup> J. T. Davis, O. Okunola and R. Quesada, *Chem. Soc. Rev.*, 2010, **39**, 3843–3862.

**75a** to modulate membrane potential by transporting chloride in a selective way through channels formation.<sup>128, 129</sup> The measurement of whole cell currents for bronchial epithelia cells of CF patients after being treated with **75a** demonstrated that it was able to increase the chloride permeability. The isophthalamide scaffold linked to two  $\alpha$ -phenylalanine **75b** gave as a result a more efficient chloride carrier than **75a**. Vesicle-based  $\text{H}^{13}\text{CO}_3^-$  NMR assays evidenced the ability of **75b** to promote  $\text{Cl}^-/\text{HCO}_3^-$  exchange, which could be applied to treat channelopathies such as cystic fibrosis as well as cancer.<sup>130</sup>



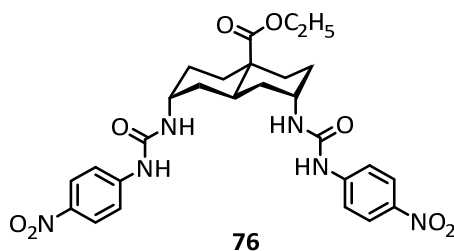
At the same time, A. P. Davis and *co-workers* tested the biological activity of an extensive series of anionophores in Fischer rat thyroid (FRT) cells expressing the halide sensor YFP-H148Q/I152L. This method allows monitoring iodine transport based on the ability of this variant Yellow Fluorescence Proteins (YFP) to be quenched by iodide more strongly than chloride. Over FRT-YFP cells submerged in a chloride buffer and treated with the anion carriers, was added NaI. A decrease in fluorescence was observed when the anionophores were able to transport iodide under these conditions. Among all studied compounds, the bis-ureidodecalin **76** was found to be highly active iodide carrier at dosages which do not present cytotoxicity. Electrophysiological studies demonstrated that at a concentration of 2  $\mu\text{M}$  the transport rate promoted by this compound is closed to the expressed by CFTR channels.<sup>131</sup>

<sup>128</sup> X. Li, B. Shen, X. -Q. Yao and D. Yang, *J. Am. Chem. Soc.*, 2009, **131**, 13676–13680.

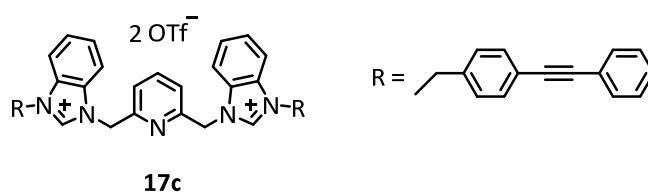
<sup>129</sup> B. Shen., X. Li., F. Wang, X. Yao and D. Yang, *PLoS ONE*, 2012, **7**, e34694.

<sup>130</sup> P. -Y. Liu, S. -T. Li, F. -F. Shen, W. -H. Ko, X. -Q. Yao and D. Yang, *Chem. Commun.*, 2016, **52**, 7380–7383.

<sup>131</sup> H. Li, H. Valkenier, L. W. Judd, P. R. Brotherhood, S. Hussain, J. A. Cooper, O. Jurček, H. A. Sparkes, D. N. Sheppard and A. P. Davis, *Nat. Chem.*, 2016, **8**, 24–32.



Some anionophores, such as **74a–74d** were found to inhibit bacteria growth *in vitro*, with MIC values in the low micromolar range for the Mu50 *S. aureus*.<sup>132</sup> The benzoimidazolium salt **17c** reported by Schmitzer and *co-workers*, which present good anionophoric properties, also displays antimicrobial activity against *E. coli* and *B. thuringiensis* strains.<sup>133</sup>



## 5. AIMS OF THE THESIS

The present thesis is focused on developing new transmembrane anion carriers based on naturally occurring structures, with potential applications in biomedicine. In order to address this challenge several different families of compounds have been developed.

We aim to understand the parameters that govern the anionophoric activity of these compounds with the purpose of developing more potent anionophores. To accomplish it, we pinpoint several targets:

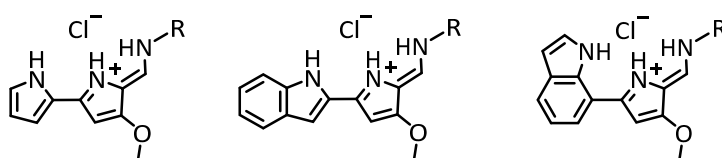
- To generate a large family of naturally occurring and synthetic **tambjamine-like transporters** bearing different substituents in the enamine motif, as well as alkoxy groups in order to cover a broad range of lipophilicities, functionalities and transport activities.

<sup>132</sup> A. I. Share, K. Patel, C. Nativi, E. J. Cho, O. Francesconi, N. Busschaert, P. A. Gale, S. Roelens and J. L. Sessler, *Chem. Commun.*, 2016, **52**, 7560–7563.

<sup>133</sup> C.-R. Elie, G. David and A. R. Schmitzer, *J. Med. Chem.*, 2015, **58**, 2358–2366.

- To study the ability of these tambjamine analogs to transport anions in POPC vesicle models, using chloride selective electrodes and fluorescence based assays.
- To perform QSAR studies, modelling the anionophoric activity of these compounds against a wide variety of theoretical and experimental descriptors, calculated for each of the studied molecules.

In order to gain insights about the role of the binding pocket in the anion transport event of tambjamins, we decided to modify the tambjamine backbone introducing indole groups connected in different manners to the enamine moiety (Figure 1.15), to study the binding properties of this set of compounds through <sup>1</sup>H NMR titrations and their anionophoric properties using chloride selective electrodes.



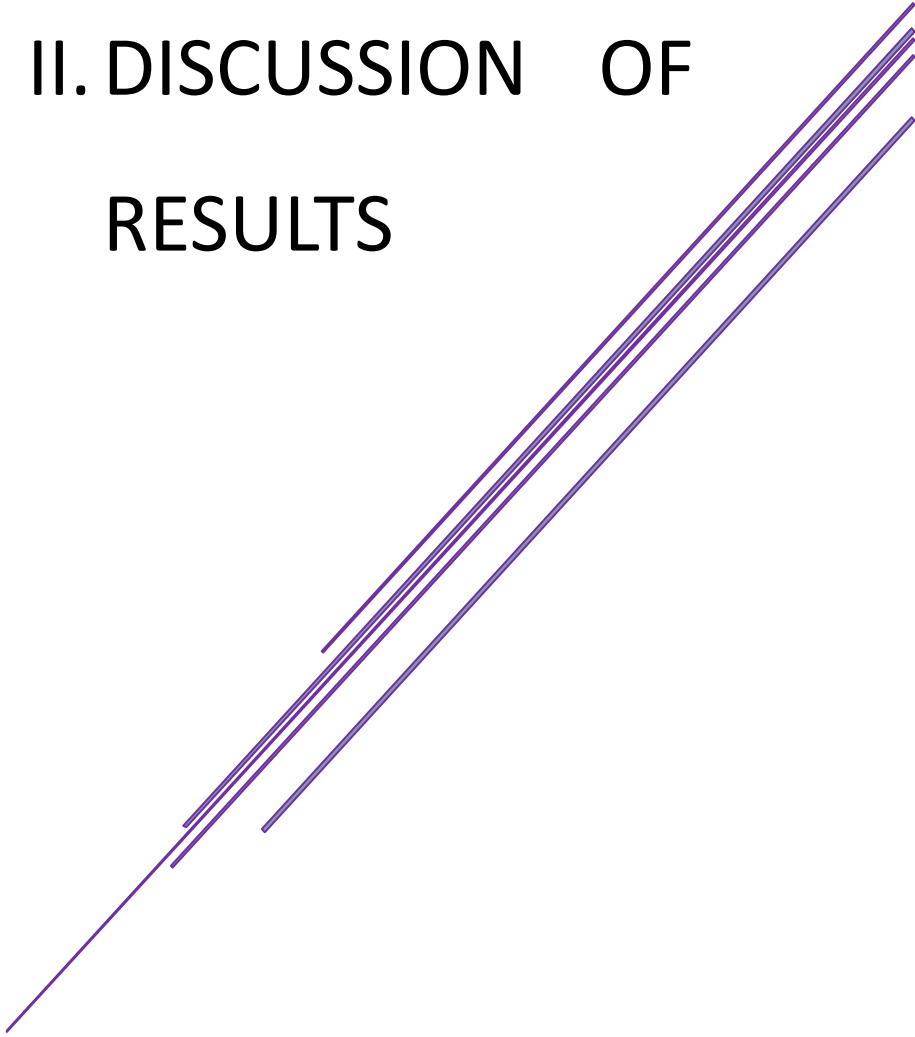
R = aliphatic or aromatic

Figure 1.15. Synthetic tambjamine analogs

We aim to develop a family of **tetraheterocyclic compounds** and to characterised their behaviour as anion carriers using both ISE assays and spectroscopic experiments with a variety of fluorescence probes, such as lucigenin, carboxyfluorescein or HPTS. We planned to design a fluorescent anion carrier, based on one of the tetraheterocycles, by synthesizing a **BODIPY** analog, and to study its anionophoric behaviour applying chloride selective electrode assays and fluorescence experiments.

Inspired in the structure of the natural product prodiginines, we design anion carriers with hydrogen bond donor less polarised and different affinities for anions compared to tambjamins or prodiginines. In order to carry out this goal the A ring of the prodiginines structure was replaced by a 1,2,3-triazole moiety. To better understand the behaviour of these **prodiginine-inspired compounds**, the ability of these compounds to promoted chloride efflux in the presence of different external anions, such as bicarbonate, perchlorate, sulphate, etc., using a chloride selective electrode and different fluorescence probes was studied.

## II. DISCUSSION OF RESULTS





# 1. TAMBAMINE-LIKE TRANSPORTERS

## 1.1. Introduction

For many years, natural products and medicine have been closely linked due to the use of traditional remedies and natural poisons. One of the key pillars of the drug discovery field has been the understanding of secondary metabolites. These small molecules are not indispensable for life but their presence provide advantages to the producer organism. Their pathway of synthesis is characteristic of each group of organism, thus they display a huge structural variability, accompanied by a broad spectrum of biological activities. Nowadays, the use of secondary metabolites in medical therapies accounts for one third of all commercialised drugs.<sup>134</sup>

The tambjamines are secondary metabolites of marine origin. They were first isolated from bryozoans, nudibranchs and ascidians. It is believed that they function as a defence mechanism for the producing organisms. These marine alkaloids are characterised by a 4-methoxy-2,2'-bipyrrole unit where the B pyrrole (Figure 2.1a) possesses an exocyclic enamine substituent, which consists always in an aliphatic chain in the case of the natural members. Tambjamines isolated from bryozoans could contain or not a bromine atom in their structure. (Figure 2.1b)<sup>135, 136, 137, 138</sup>

The tambjamine scaffold consists on a bipyrrole unit. During the last 20–30 years, pyrrole has gained a position among the best known anion binding motifs. In the field of the anion coordination chemistry, pyrrole-based compounds present potential advantages over other N–H bond donors such as amides, ureas or amines. For instance, the absence of hydrogen–bond acceptors, thus avoiding possible competitive intra- or intermolecular hydrogen bonds. The pKa of pyrrole is around

<sup>134</sup> S. E. O'Connor, *Annu. Rev. Genet.*, 2015, **49**, 1–24.

<sup>135</sup> B. Carté and D. J. Faulkner, *J. Org. Chem.*, 1983, **48**, 2314–2318.

<sup>136</sup> N. Lindquist and W. Fenical, *Experientia*, 1991, **47**, 504–506.

<sup>137</sup> A. J. Blackman and C. Li, *Aust. J. Chem.*, 1994, **47**, 1625–1629.

<sup>138</sup> G. W. Gribble, *Chem. Soc. Rev.*, 1999, **28**, 335–346.

16–17. This value restricts the existence of protonation–deprotonation equilibria and allows its use under a wide range of pH and in a variety of solvents.<sup>139</sup>

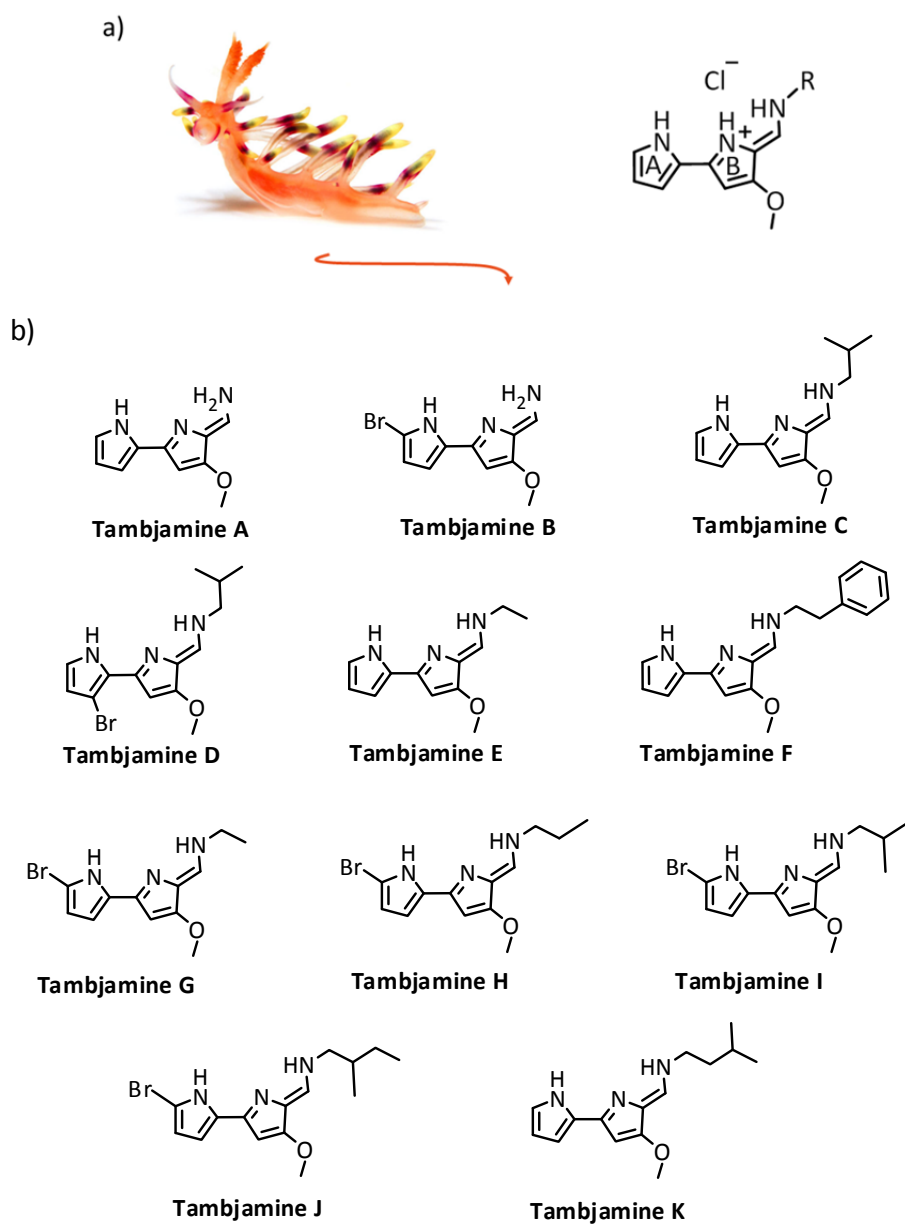


Figure 2.1. a) nudibranch.<sup>140</sup> b) natural tambjamine derivatives

<sup>139</sup> J. L. Sessler, N. M. Barkey, G. D. Pantos and V. M. Lynch, *New J. Chem.*, 2007, **31**, 646–654.

The solid state structure of the hydrochloric salt of two members of this family determined by single crystal X-ray diffraction, were published by Quesada *et al* (Figure 2.2).<sup>141</sup> On the left, it is shown the natural product tambjamine E and on the right a synthetic analog. The bipyrrrole-enamine core displays an essentially planar disposition with the chloride anion interacting with the N-H units through hydrogen bonds. It should be noticed that pyrrole A, in tambjamine E, is rotated 180 ° in relation to the central ring.

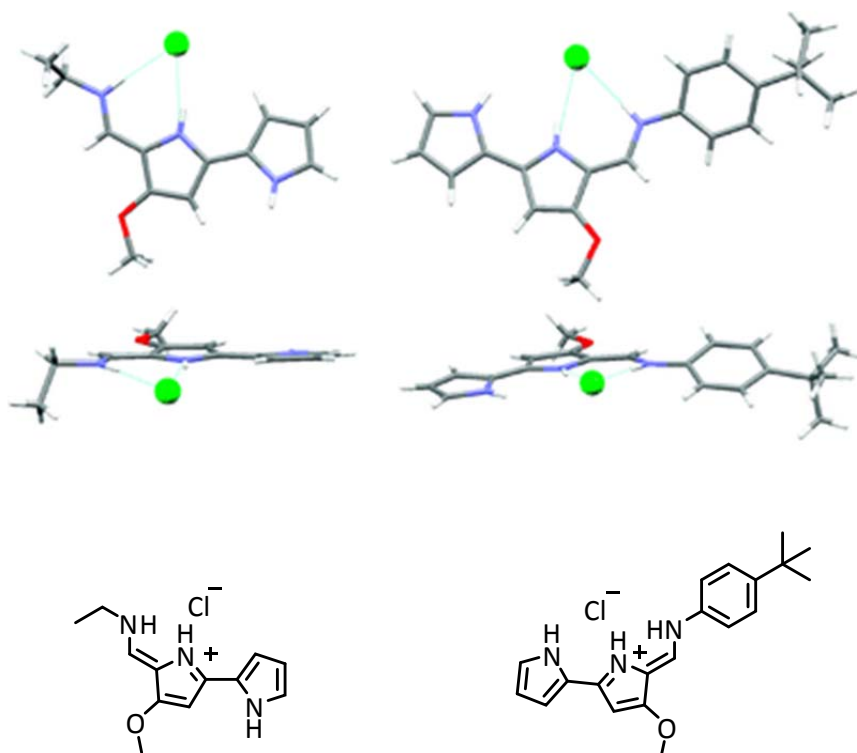


Figure 2.2. Left: tambjamine E. Right: tambjamine synthetic analog

The intriguing biological activity exhibited by tambjamins seems to be associated with defence mechanisms against unfavourable ecological niche, displayed by producing microorganisms (such as *Tambja Eliora*, *T. Abdere* or *Roboastra tigris*). Although, the exact mechanism of action of these compounds is

<sup>140</sup> <http://ngm.nationalgeographic.com/2008/06/nudibranchs/doublet-photography> (accessed April 2017)

<sup>141</sup> P. Iglesias-Hernández, D. Moreno, A. Araujo-Javier, T. Torroba, R. Pérez-Tomás and R. Quesada, *Chem. Commun.*, 2012, **48**, 1556–1558.

yet unknown, there is a growing body of evidence linking their anionophoric properties with their bioactivity. Tambjamines A–D display activity against *E. coli*, *S. aureus* and *V. anguillarum*.<sup>142</sup> The last alkaloid of this set also presents antifungal properties against *Candida albicans* and antibacterial activity against *B. subtilis*.<sup>143</sup> Some members of this family have been found to offer protection and curative activity in a malaria infected mouse model at doses of 80 mg/kg,<sup>144</sup> antitumor properties against different cell lines are also known to be displayed by several of these compounds. Certain tambjamines, such as tambjamine E has been observed to bind DNA in the presence of copper<sup>II</sup>.<sup>145, 146</sup>

In 2012, our group decided to study the anionophoric properties of these compounds, both natural and synthetic analogs, demonstrating that they are potent anion carriers capable of effecting  $\text{Cl}^-/\text{HCO}_3^-$  and  $\text{Cl}^-/\text{NO}_3^-$  exchange in POPC vesicle models at low concentrations. Compounds identified as the most active carriers in liposome experiments were found to be the most active in biological assays on small lung cancer cells (GLC4).<sup>147</sup>

Based on these precedents, different tambjamine analogs were developed in order to achieve the aims of this section.

- To examine the effect of replacing the methoxy substituent in B ring (Figure 2.1a) by a benzyloxy group, on the transport rate.
- To study the influence of the enamine substituent on the anionophoric properties of the tambjamine analogs.
- To evaluate the influence of an indole as A ring instead of a pyrrole (Figure 2.1a), on the transport efficiency.
- To estimate the effect of modifying the geometry of the binding site connecting the indole motif to the B ring through different positions.

---

<sup>142</sup> B. Carté, D. J. Faulkner, *J. Org. Chem.*, 1983, **48**, 2314–2318.

<sup>143</sup> B. C. Cavalcanti, H. V. N. Júnior, M. H. R. Selegim, R. G. S. Berlinck, G. M. A. Cunha, M. O. Moraes, C. Pessoa, *Chem. Biol. Interact.*, 2008, **174**, 155–162.

<sup>144</sup> P. Kancharla, J. X. Kelly and K. A. Reynolds, *J. Med. Chem.*, 2015, **58**, 7286–7309.

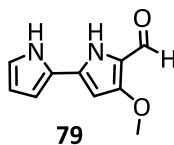
<sup>145</sup> R. A. Manderville, *Curr. Med. Chem., Anticancer Agents*, 2001, **1**, 195–218.

<sup>146</sup> D. M. Pinkerton, M. G. Banwell, M. J. Garson, N. Kumar, M. Odorico de Moraes, B. C. Cavalcanti, F. W. A. Barros and C. Pessoa, *Chem. Biodivers.*, 2010, **7**, 1311–1324.

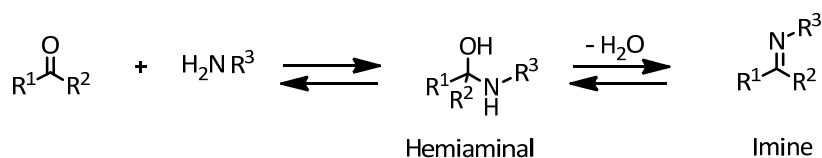
<sup>147</sup> P. Iglesias-Hernández, D. Moreno, A. Araujo-Javier, T. Torroba, R. Pérez-Tomás and R. Quesada, *Chem. Commun.*, 2012, **48**, 1556–1558.

## 1.2. Synthesis

In 2007 Banwell *et al* established the total synthesis of some members of this family,<sup>148</sup> based on the previously reported protocol of Lavallée and *co-workers* to synthesise the bipyrrrole aldehyde **79** and react this compound with different amines.<sup>149</sup>



Tambjamins are Schiff bases (imines). The Schiff base motif is easily obtained from the nucleophilic addition of an amine to an aldehyde or ketone, with the elimination of water, under mild acid conditions (Scheme 2.1). This procedure tolerates a broad variety of substituents ( $R^1$  and  $R^2$ ). The determinant step is the elimination of water since the hemiaminal formation is reversible.<sup>150</sup>



$R^1, R^2, R^3$  = aliphatic or aromatic groups

Scheme 2.1. Imine synthesis

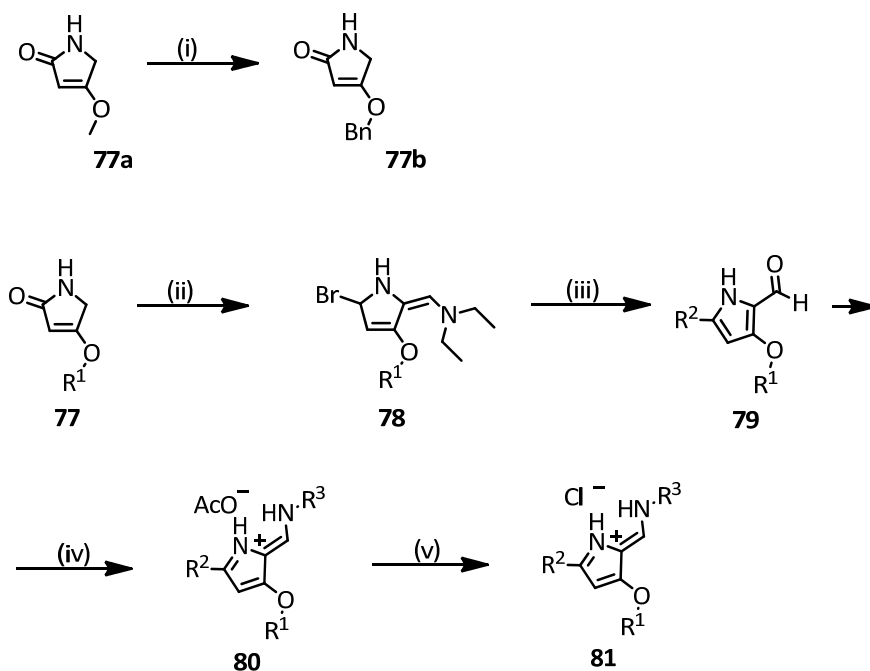
All tambjamins inspired derivatives described in this thesis were synthesised as described in Scheme 2.2. The synthetic route started from 4-methoxy or benzyloxy-3-pyrrolin-2-one. The benzyloxy- one was synthesised from commercially available methoxy-3-pyrrolin-2-one and benzyl alcohol. Pyrrolin-2-one was subjected to a Vilsmeier-Haack reaction to yield the corresponding bromoenamine. This bromoenamine was reacted with the convenient boronic acid under Suzuki-Miyaura coupling conditions. Finally, the corresponding carbaldehyde was reacted with a variety of amines to yield a library of tambjamins in good to excellent yields. The

<sup>148</sup> D. M. Pinkerton, M. G. Banwell and A. C. Willis, *Org. Lett.*, 2007, **9**, 5127–5130.

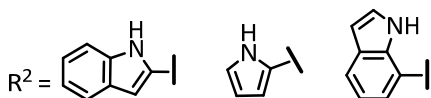
<sup>149</sup> K. Dairi, S. Tripathy, G. Attardo and J.-F. Lavallée, *Tetrahedron Lett.*, 2006, **47**, 2605–2606.

<sup>150</sup> R. D. Patil and S. Adimurthy, *Asian J. Org. Chem.*, 2013, **2**, 726–744.

compounds were generally obtained as hydrochloride salts in the form of yellow to orange solids.



$R^1 = \text{Me, Bn}$



$R^3 = \text{Aromatic or aliphatic substituent}$

Scheme 2.2. Reagents and conditions: (i) 9.3 eq. benzyl alcohol. 0.12 eq.  $\text{MeSO}_3\text{H}$ , reflux, 1.5–2 h; (ii) DCM, 3 eq.  $\text{POBr}_3$ , 3 eq. DEF, reflux, 5 h.; (iii) Boronic precursor (1.1 equiv),  $\text{Pd}(\text{PPh}_3)_4$ , dioxane,  $\text{H}_2\text{O}$ ,  $\text{Na}_2\text{CO}_3$ , reflux, overnight and water, MW (if necessary); (iv)  $\text{CHCl}_3$  or DCE, 1.3–5 eq. amine, 60–80 °C, 40  $\mu\text{L}$  AcOH, Hexane:AcOEt (1:1); (v) dissolve in DCM and wash x3 HCl (1M)

### 1.3. Pyrrole–pyrrole tambjamines

#### 1.3.1. Crystal structures

The solid-state structures of several pyrrole-pyrrole tambjamines were determined by single crystal X-ray diffraction. Crystals were obtained from slow evaporation under different mixtures of solvents. Then, it is shown the analysis of their properties. The atoms of the tambjamine scaffold are labelled in Figure 2.3.

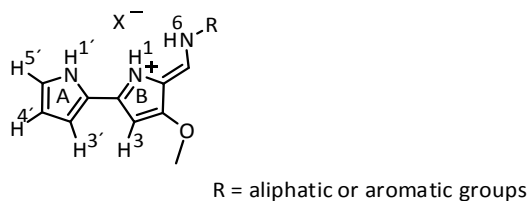


Figure 2.3. Numbering of the backbone of tambjamines

Crystals of the natural product **82**.HCl (Tambjamine F), were obtained by slow evaporation of a mixture of DCM:hexane (1:1). The bipyrrrole enamine unit displays an almost flat disposition with the phenethyl group out of this plane. All NH groups are interacting with the chloride anion through hydrogen bonds and all carbon-carbon bonds display intermediate distances between simple (1.54 Å) and double bond (1.34 Å) (Figure 2.4).

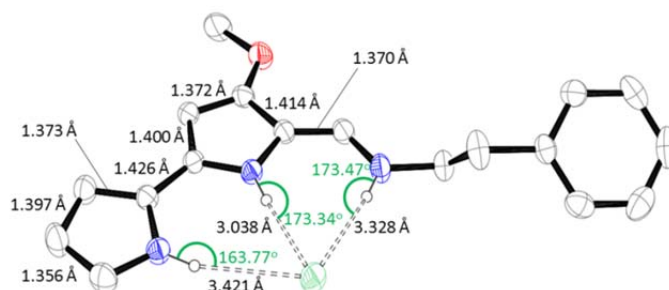


Figure 2.4. X-ray solid structure of **82**.HCl

**83**.HCl is an example of tambjamine with an aromatic enamine substituent, a *p*-nitro phenyl group. It adopts a conformation (Figure 2.5), with the bipyrrrole unit and the enamine motif essentially coplanar, displaying a flat disposition. The  $\pi$ -conjugated system is extended along all aromatic system including the enamine

substituent, giving rise to carbon-carbon bond distances between simple and double bonds. The chloride anion is found interacting with all NHs through hydrogen bonds.

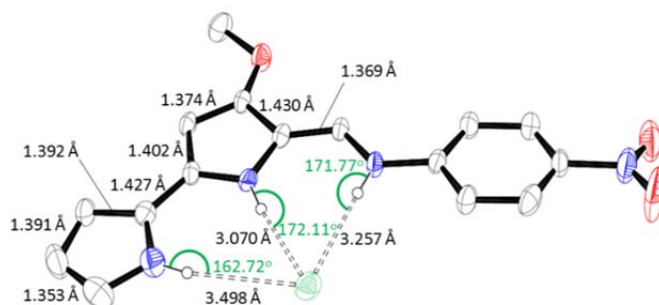


Figure 2.5. X-ray solid structure of **83**.HCl

In Figure 2.6 it is shown a tambjamine with an aliphatic enamine substituent. The three nitrogen units of **84**.HCl are located in the same plane with the cyclohexyl motif out of it. It should be noticed that the A ring is rotated 180° which implies a smaller N–H⋯Cl hydrogen bonding angle. H<sup>3+</sup> as well as NHs from B ring and enamine are hydrogen bonded to the chloride anion. The NH from the A pyrrole is also hydrogen bonded to another chloride anion.

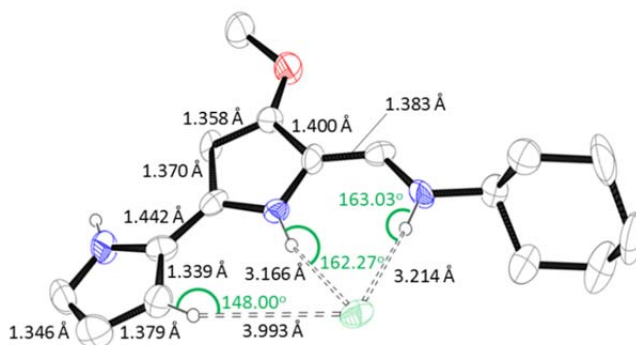


Figure 2.6. X-ray solid structure of **84**.HCl

### 1.3.2. Exploring the influence of substituents in the anion transport properties

In a previous study, our group proved that tambjamine derivatives with both aliphatic chains and aromatic groups as enamine substituents were highly active transmembrane anion carriers in vesicle models. By that time, only naturally occurring tambjamines characterised by aliphatic chains as enamine substituent and

methoxy group in the central ring had been tested.<sup>151</sup> Based on the obtained results, we decided to explore the possible influence of the substitution of both enamine and alkoxy substituents in the transport properties of these compounds. Thus, we prepared a small library of synthetic tambjamins bearing aromatic and heteroaromatic enamine substituents with different electronic character. We also prepared compounds bearing a benzyloxy instead of the characteristic methoxy group found in natural derivatives.

The compounds discussed in this section are shown in Figure 2.7.

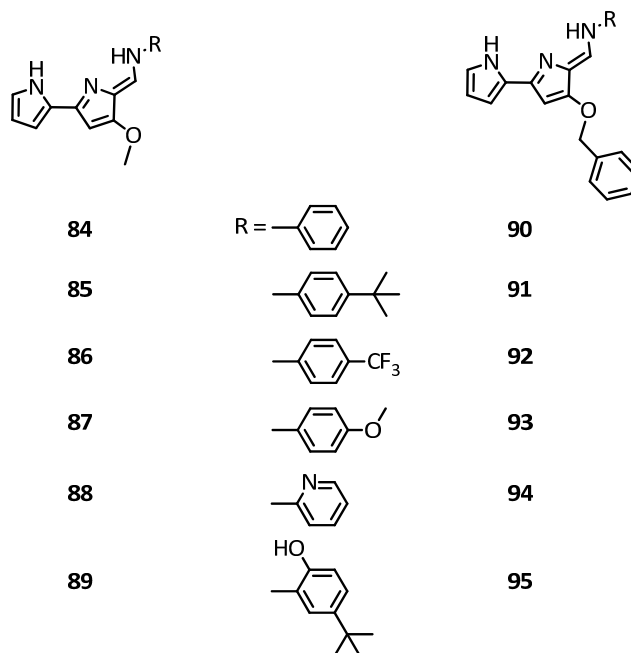


Figure 2.7. Tambjamins discussed in this section.

### 1.3.2.1. Chloride binding constants

<sup>1</sup>H NMR spectra of these compounds (Figure 2.9) showed the strong interaction between the chloride anion and the bipyrrrole-enamine motif through hydrogen bonds (Figure 2.8).

<sup>151</sup> P. Iglesias-Hernández, D. Moreno, A. Araujo-Javier, T. Torroba, R. Pérez-Tomás and R. Quesada, *Chem. Commun.*, 2012, **48**, 1556–1558.

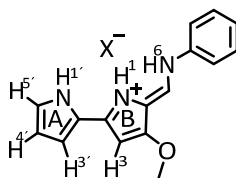


Figure 2.8. **84.HCl** (i.e.) with labelling protons

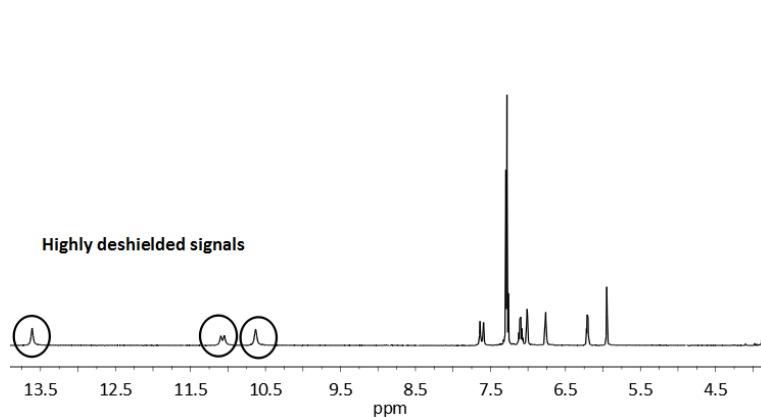


Figure 2.9.  $^1\text{H}$  NMR **84.HCl**. NH signals are rounded

The anion binding ability of these compounds was studied in solution ( $\text{DMSO-}d_6$  0.5%  $\text{H}_2\text{O}$ ) by  $^1\text{H}$  NMR titrations. Thus, perchlorate salts were first prepared and the replacement of perchlorate by chloride (added as TBACl) monitored. Consecutive additions of TBACl gave as a result the replacement of perchlorate anion by chloride. The chemical shift of  $\text{NH}^1$ ,  $\text{NH}^6$  and  $\text{CH}^3$  protons was affected by the addition of TBACl, but surprisingly the  $\text{NH}^1$  signal (Figure 2.8) seems to be only slightly altered during the titration.

The titrations were carried out for the twelve tambjamins. The obtained data were fitted with WinEQNMR2 software,<sup>152</sup> and the association constant ( $K_a$ ,  $\text{M}^{-1}$ ) for each molecule was calculated for the three protons affected by the titration (Table 2.1). In Figure 2.10 is shown the stack plot of the titration corresponding to **84.HClO<sub>4</sub>** with TBACl.

<sup>152</sup> M. J. Hynes, *J. Chem. Soc. Dalton Trans.*, 1993, 311–312.

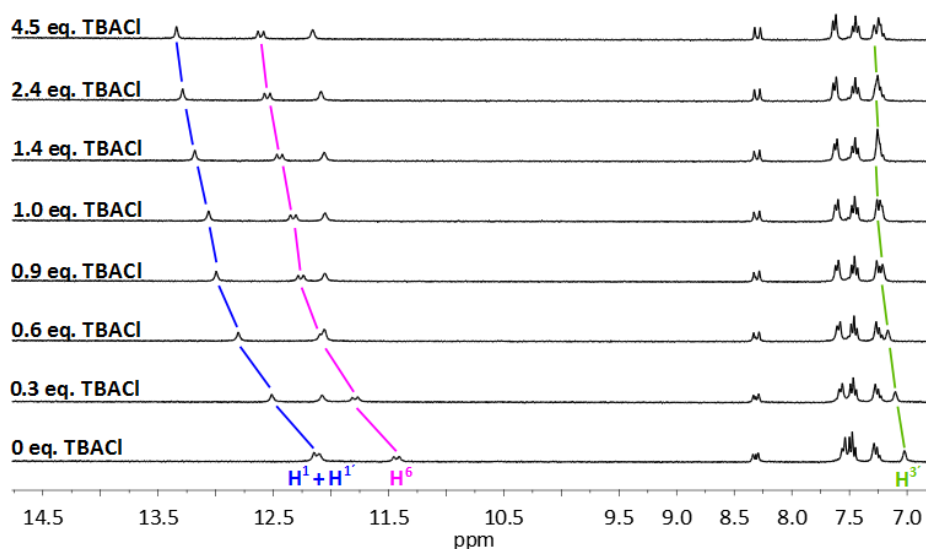


Figure 2.10. Partial stack plot of  $^1\text{H}$  NMR spectra of compound **84**. $\text{HClO}_4$  in  $\text{DMSO-}d_6$ -0.5%  $\text{H}_2\text{O}$  solution under the addition of increasing amounts of tetrabutylammonium chloride

Table 2.1. Binding constant ( $K_a$ ,  $\text{M}^{-1}$ ) calculated from  $\text{N}^1\text{H}$ ,  $\text{N}^6\text{H}$  and  $\text{C}^3\text{H}$  protons

	$K_{a, \text{N}^1\text{H}} (\text{M}^{-1})$	$K_{a, \text{N}^6\text{H}} (\text{M}^{-1})$	$K_{a, \text{C}^3\text{H}} (\text{M}^{-1})$
<b>84</b>	$1740 \pm 76$	$1592 \pm 25$	$1493 \pm 149$
<b>85</b>	$2208 \pm 245$	$1990 \pm 122$	$2047 \pm 370$
<b>86</b>	$2019 \pm 244$	$1789 \pm 222$	$2720 \pm 256$
<b>87</b>	$1721 \pm 50$	$1681 \pm 107$	$2164 \pm 278$
<b>88</b>	$1636 \pm 19$	$1510 \pm 157$	$1490 \pm 197$
<b>89</b>	$302 \pm 18$	$265 \pm 19$	$284 \pm 21$
<b>90</b>	$1566 \pm 35$	$1428 \pm 30$	$1620 \pm 121$
<b>91</b>	$1581 \pm 29$	$1498 \pm 48$	$1662 \pm 196$
<b>92</b>	$1673 \pm 46$	$1491 \pm 59$	$2134 \pm 205$
<b>93</b>	$1934 \pm 128$	$1836 \pm 114$	$2128 \pm 289$
<b>94</b>	$2109 \pm 200$	$1960 \pm 219$	$3688 \pm 435$
<b>95</b>	$429 \pm 36$	$397 \pm 3$	$352 \pm 3$

All binding constants were found to be quite similar. This could reflect that the nature of the enamine substituent already influenced the affinity for the perchlorate anion and thus, comparable binding constants for the replacement by chloride are experimentally measured. It should be noted that **89**. $\text{HCl}$  and **95**. $\text{HCl}$  display significantly lower binding constants. The presence of an additional  $-\text{OH}$  group in

this case appears to be detrimental for the binding process and a similar result was observed in the case of transport.

### 1.3.2.2. Anion transport assays

Transport assays were carried out using POPC vesicles. These vesicles are easily prepared with a good control of size and composition.

A stock solution of 1-palmitoyl-2-oleoyl-sn-glycero-3-phosphocholine (POPC) (Sigma-Aldrich) (20 mg/mL) in chloroform was prepared and kept in the freezer. The organic solvent was evaporated, *in vacuo*, using a rotary evaporator. The obtained lipid film was dried under high vacuum overnight. It was then rehydrated by careful vortexing with a sodium chloride solution (489 mM NaCl, ionic strength 500 mM and 5 mM phosphate buffer, pH 7.2 or 451 mM NaCl, ionic strength 500 mM and 20 mM phosphate buffer, pH 7.2), giving rise to a lipid suspension, composed of vesicles with different size and different number of lamellae. It was subjected to nine freeze-thaw cycles, in order to obtain unilamellar liposomes. For that, the flask was alternatively introduced in a liquid nitrogen bath to freeze the suspension, followed by a mild water bath in order to thaw it. Next, twenty nine extrusions were carried out through a 100 or 200 nm polycarbonate Nucleopore membrane using a LiposoFast Basic extruder (Aves tin, Inc.), in order to obtain vesicles with uniform size. The obtained unilamellar vesicles were dialysed against 500 mL (x 2) of NaNO<sub>3</sub> solution (489 mM NaNO<sub>3</sub>, ionic strength 500 mM and 5 mM phosphate buffer, pH 7.2) or Na<sub>2</sub>SO<sub>4</sub> (150 mM Na<sub>2</sub>SO<sub>4</sub> mM, ionic strength 500 mM and 20 mM phosphate buffer, pH 7.2) respectively, to remove the unencapsulated chloride. To finalize, the vesicles were diluted to a 10 mL with the NaNO<sub>3</sub> or Na<sub>2</sub>SO<sub>4</sub> solution, respectively. Details of how performing the experiments are described in Chapter IV.

The ability as transmembrane anion carriers of compounds **84.HCl**–**95.HCl** was tested in Ion (chloride) Selective Electrode (ISE) assays under Cl<sup>-</sup>/NO<sub>3</sub><sup>-</sup> and Cl<sup>-</sup>/HCO<sub>3</sub><sup>-</sup> conditions.

Related to Cl<sup>-</sup>/NO<sub>3</sub><sup>-</sup> assays, the activity of these twelve compounds was measured as described below. A 5 or 10 mM stock solution of each anion carrier was prepared in DMSO. A suspension of POPC vesicles loaded with 489 mM NaCl was added in 489 NaNO<sub>3</sub> mM, both buffered to pH 7.2 with NaH<sub>2</sub>PO<sub>4</sub> 5 mM, to give a final POPC concentration of 0.5 mM. A pulse of the corresponding anionophore in DMSO was incorporated and the chloride efflux out of the vesicles was monitored over time using a chloride selective electrode. After 300 s a pulse of detergent was

added in order to lyse the vesicles and release all chloride ions. This value was used as the 100% of chloride encapsulated and the rest of data were calculated as a function of it. Full details of how preparing and carrying out these experiments are described in Chapter IV.

In Figure 2.11 it is shown the activity of this set of tambjamins at 0.05 mol% anion carrier to lipid, in  $\text{Cl}^-/\text{NO}_3^-$  ISE assays. Although clear differences are appreciated in their anionophoric behaviour, all of them were found to be active  $\text{Cl}^-/\text{NO}_3^-$  antiporters.

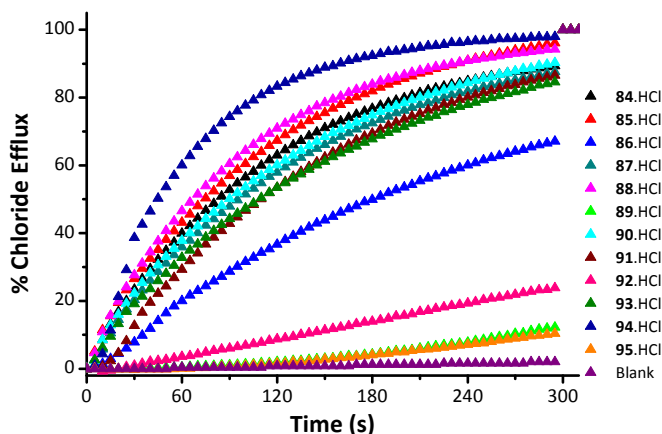


Figure 2.11. Chloride efflux upon addition of 84.HCl–95.HCl (0.25  $\mu\text{M}$ , 0.05 mol % carrier to lipid) to vesicles composed of POPC. The vesicles contained NaCl (489 mM NaCl and 5 mM phosphate buffer, pH 7.2) were immersed in  $\text{NaNO}_3$  (489 mM  $\text{NaNO}_3$  and 5 mM phosphate buffer, pH 7.2). At the end of the experiment, the vesicles were lysed with detergent to release all chloride ions and the resulting value was considered to represent 100% release and used as such. Each trace represents an average of at least three different experiments, done with at least two different batches of vesicles.

Their ability to transport bicarbonate was tested under the previously described conditions. A suspension of POPC vesicles loaded with 451 mM NaCl was added in 150 mM  $\text{Na}_2\text{SO}_4$ , to give a final lipid concentration of 0.5 mM. At the beginning of the experiment, a pulse of the corresponding anionophore in DMSO was incorporated. After one minute, a pulse of  $\text{NaHCO}_3$  was added to achieve a 40 mM concentration. The chloride efflux out of the vesicles was monitored over time using a chloride selective electrode. After 300 s, a pulse of detergent was added in order to lyse the vesicles and release all chloride ions. This value was used as the 100% of chloride encapsulated and the rest of data were calculated as a function of it. Full

details of how preparing and carrying out these experiments are described in Chapter IV.

In Figure 2.12 it is shown the activity of this set of tambjamines at 1 mol% anion carrier to lipid, in  $\text{Cl}^-/\text{HCO}_3^-$  ISE assays.

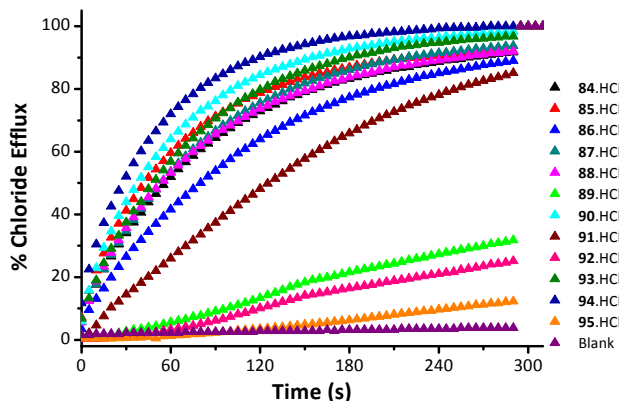


Figure 2.12. Chloride efflux upon addition of 84.HCl–95.HCl (5  $\mu\text{M}$ , 1 mol% carrier to lipid) to vesicles composed of POPC. The vesicles contained NaCl (451 mM NaCl and 20 mM phosphate buffer, pH 7.2) were immersed in  $\text{Na}_2\text{SO}_4$  (150 mM  $\text{Na}_2\text{SO}_4$ , 40 mM  $\text{HCO}_3^-$  and 20 mM phosphate buffer, pH 7.2). At the end of the experiment, the vesicles were lysed with detergent to release all chloride ions and the resulting value was considered to represent 100% release and used as such. Each trace represents an average of at least three different experiments, done with at least two different batches of vesicles.

### Hill plots

In order to quantify more precisely the anionophoric activity of these compounds and to get a series of values which allow us comparing activities among them and among other compounds described in the literature, the Hill analysis was employed (equation 2.1).

$$y = V_{\max} \cdot \frac{x^n}{(k)^n + x^n}$$

$$\% \text{ Chloride release} = 100 \cdot \frac{[\text{Cl}^-]^n}{(\text{EC}_{50})^n + [\text{Cl}^-]^n} \quad \text{Eq. 2.1}$$

Where:

- Y chloride efflux at 300 s (%)  
 x anion carrier concentration ( $\mu\text{M}$ , nM or mol% to lipid carrier)  
 $V_{\text{max}}$  maximum chloride efflux (100%)  
 n Hill coefficient  
 k anion carrier concentration needed to achieve  $V_{\text{max}}/2$  (when  $V_{\text{max}}$  is fixed to 100%, k equals  $\text{EC}_{50}$ )

The  $\text{EC}_{50}$  is the anion carrier concentration needed to achieve 50% release of the total of the chloride encapsulated under the defined conditions, in this case 300 s. It gives a useful value for a comparison of transport efficiencies.

The Hill coefficient  $n$ , is a measure of cooperativity. A Hill coefficient close to one indicates non-cooperativity. Values greater than one indicate cooperativity in the process.

The transport activity of each compound was measured at different concentrations and the chloride efflux at 300 s was plotted against these concentrations. As an example, the anionophoric activity of **90.HCl** at five different concentrations and its Hill analysis are shown in Figure 2.13 and 2.14 respectively.

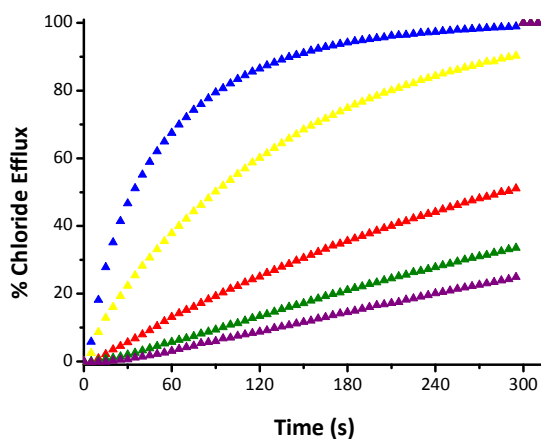
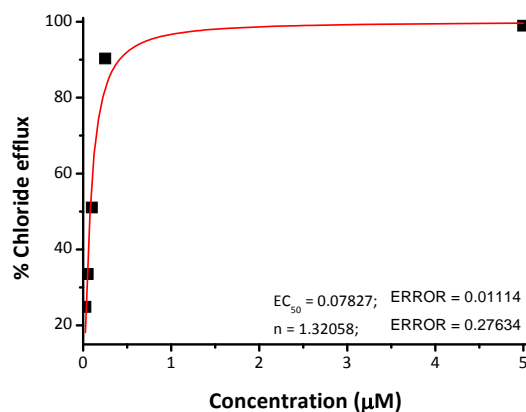


Figure 2.13. Anion transport activity of **90.HCl** in  $\text{Cl}^-/\text{NO}_3^-$  ISE experiment. 0.5 mM POPC. Vesicles loaded with 489 mM NaCl (phosphate buffer 5 mM, pH 7.2) where suspended in  $\text{NaNO}_3$  489 mM (phosphate buffer 5 mM, pH 7.2). At  $t = 300$  s a pulse of detergent was added in order to release all chloride anions. Each trace represents the average of at least three trials, done with at least two different batches of vesicles. Blue trace: 1 mol% = 5  $\mu\text{M}$ ; yellow trace: 0.05 mol% = 0.25  $\mu\text{M}$ ; red trace: 0.02 mol% = 0.1  $\mu\text{M}$ ; green trace 0.01 mol% = 0.05  $\mu\text{M}$  and purple trace: 0.005 mol% = 0.025  $\mu\text{M}$ .

Figure 2.14. Hill analysis of **90**.HCl transport results.

In Table 2.2, the  $EC_{50}$  and  $n$  values obtained from the Hill analysis of ISE assay data are shown.

Table 2.2. Summary of parameters recovered from ISE assays, and lipophilicity. **84**.HCl–**95**.HCl

	$EC_{50}$ (nM) $NO_3^-/Cl^-$ <sup>a</sup>	Hill parameter $n$ $NO_3^-/Cl^-$ <sup>a</sup>	$EC_{50}$ (nM) $HCO_3^-/Cl^-$ <sup>b</sup>	Hill parameter $n$ $HCO_3^-/Cl^-$ <sup>b</sup>	ALOGPs <sup>c</sup>
<b>84</b>	$38 \pm 2$	$1.17 \pm 0.09$	$459 \pm 66$	$0.89 \pm 0.13$	2.81
<b>85</b>	$51 \pm 11$ <sup>d</sup>	$1.30 \pm 0.01$ <sup>d</sup>	$241 \pm 36$	$1.19 \pm 0.23$	4.72
<b>86</b>	$141 \pm 6$	$1.18 \pm 0.07$	$893 \pm 83$	$1.04 \pm 0.09$	3.57
<b>87</b>	$98 \pm 24$ <sup>d</sup>	$1.29 \pm 0.15$ <sup>d</sup>	$456 \pm 56$	$0.90 \pm 0.11$	2.86
<b>88</b>	$21 \pm 9$	$0.92 \pm 0.29$	$263 \pm 26$	$1.05 \pm 0.08$	1.91
<b>89</b>	$3181 \pm 762$	$0.93 \pm 0.19$	$10703 \pm 3100$	$1.15 \pm 0.36$	4.25
<b>90</b>	$78 \pm 11$	$1.32 \pm 0.28$	$366 \pm 54$	$1.12 \pm 0.18$	4.40
<b>91</b>	$58 \pm 3$	$1.20 \pm 0.09$	$877 \pm 281$	$0.67 \pm 0.15$	5.94
<b>92</b>	$724 \pm 72$	$1.04 \pm 0.09$	$11923 \pm 1012$	$1.11 \pm 0.10$	5.11
<b>93</b>	$67 \pm 3$	$1.45 \pm 0.10$	$433 \pm 113$	$0.99 \pm 0.19$	4.38
<b>94</b>	$44 \pm 2$	$1.24 \pm 0.10$	$172 \pm 22$	$1.10 \pm 0.11$	3.30
<b>95</b>	$5587 \pm 1182$	$0.80 \pm 0.19$	$54164 \pm 7314$	$0.82 \pm 0.14$	5.61

<sup>a</sup> Liposomes loaded with 489 mM NaCl suspended in 489 mM NaNO<sub>3</sub> (5 mM phosphate buffer, pH 7.2).  $EC_{50}$  represents the average of three different Hill plots

<sup>b</sup> Liposomes loaded with 451 mM NaCl suspended in 150 mM Na<sub>2</sub>SO<sub>4</sub> (20 mM phosphate buffer, pH 7.2). After one minute addition of NaHCO<sub>3</sub> to achieve the extravesicular bicarbonate concentration 40 mM.

<sup>c</sup> One of the lipophilicities calculated using e-dragon

<sup>d</sup> Average of at least three Hill plot analysis

Data from Table 2.2 showed that all these compounds are active anionophores independently of the nature of the aromatic substituent in the enamine position.

Comparing the  $EC_{50}$  values with the % of chloride efflux obtained when a one independent concentration was studied (Figures 2.11 and 2.12; 0.05 mol% in  $Cl^-/NO_3^-$  and 1 mol% in  $Cl^-/HCO_3^-$  assays) the efficiency order is maintained. For all compounds, Hill parameter is close to one, supporting the lack of cooperativity or active self-assembled structures facilitating the transport.

It should be noticed that  $EC_{50}$  values are highly dependent on the extravesicular anion. Thus,  $EC_{50}$  values obtained in  $Cl^-/NO_3^-$  assays are one order of magnitude smaller than those obtained in  $Cl^-/HCO_3^-$  experiments. When there is just sulfate in the external solution and chloride in the internal one, the chloride outflow of the vesicles is negligible (Figure 2.15). The addition of a pulse of  $NaHCO_3$  switches on the flux of chloride ions from the vesicles. These results underscore the existence of a relation between the anion transport and the nature of the extravesicular solution. Nitrate, bicarbonate and sulfate display different permeability to the membrane. Nitrate is the most hydrophobic anion from this set ( $\Delta G_{hyd} = -300$  kJ/mol) follow by bicarbonate ( $\Delta G_{hyd} = -355$  kJ/mol) and sulfate ( $\Delta G_{hyd} = -1080$  kJ/mol). The anion transport induced by tambjamins follows the Hofmeister's sequence ( $NO_3^- > HCO_3^- > SO_4^{2-}$ ).

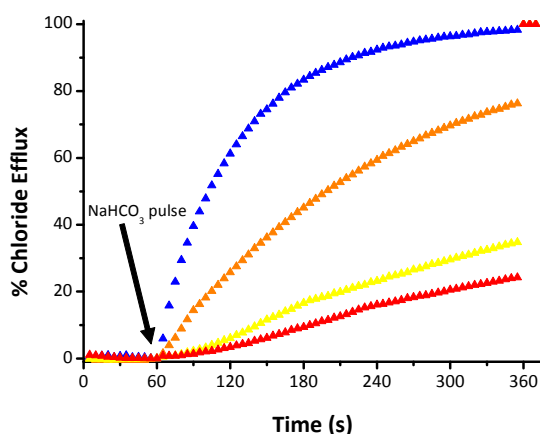


Figure 2.15. Anion transport activity of **90.HCl** in  $Cl^-/HCO_3^-$  ISE experiment. 0.5 mM POPC. Vesicles loaded with 451 mM NaCl (phosphate buffer 20 mM, pH 7.2) where suspended in  $Na_2SO_4$  150 mM (phosphate buffer 20 mM, pH 7.2). At  $t = 60$  s a pulse of  $NaHCO_3$  was added in order to obtain 40 mM in the experiment. At  $t = 360$  s a pulse of detergent was added in order to release all chloride anions. Each trace represents the average of at least three trials, done with at least two different batches of vesicles. Blue trace: 1 mol% = 5  $\mu$ M; orange trace: 0.2 mol% = 1  $\mu$ M; yellow trace: 0.05 mol% = 0.25  $\mu$ M and red trace: 0.02 mol% = 0.1  $\mu$ M.

Under  $\text{Cl}^-/\text{NO}_3^-$  conditions, tambjamins with the benzyloxy substituent were found to be slightly less active than their corresponding parent compounds with the methoxy group. In the case of  $\text{Cl}^-/\text{HCO}_3^-$  assays, no clear trends were found when the OMe/OBn pairs were considered.

Compounds **86.HCl** and **92.HCl**, bearing *p*-trifluoromethyl aromatic substituents showed comparatively low transport efficiency. It has been shown in other families of carriers such as ureas, thioureas or *ortho*-phenylenediamine-based bisureas that similar fluorinated substituents enhance the transport efficiencies of these compounds.<sup>153, 154</sup> The opposite is observed in our set of anionophores. This could be due to their low solubility. **92.HCl** was not totally soluble under the experimental conditions, and, probably, **86.HCl** lack solubility to a lesser degree.

### 1.3.3. QSAR analysis

In the last decade, computer-aided drug design methods emerged as a way to understand drugs behaviour and to help in the design of better candidates. Examples of these methods include Structure Activity Relationship (SARs), Quantitative Structure Activity Relationship (QSARs), pharmacophore mapping, ligand docking, etc. Two big categories could be differentiated: structure-based methods, which are focused on the structure of the target protein (i.e. ligand docking) and ligand-based methods, which are centered in building predictive models from libraries of active and inactive molecules with chemical similarities (i.e. QSAR). The application of these methodologies has helped researchers and companies to speed up the drug development processes.<sup>155</sup>

In the QSAR field, the first step consists in generating a library of molecules based on the scaffold of interest, bearing substituents in the desired position/s. Then, a large number of structural, physicochemical and experimental features of the molecules, known as descriptors or predictors are calculated, as well as, biological or physical activities. After that, the biological or physical response is modelled against all the calculated descriptors. Finally, the obtained model is validated in order to check if a robust equation has been obtained. This last step,

---

<sup>153</sup> N. Busschaert, M. Wenzel, M. E. Light, P. Iglesias-Hernández, R. Pérez-Tomás and P. A. Gale, *J. Am. Chem. Soc.*, 2011, **133**, 14136–14148.

<sup>154</sup> S. J. Moore, C. J. E. Haynes, J. González, J. L. Sutton, S. J. Brooks, M. E. Light, J. Herniman, G. J. Langley, V. Soto-Cerrato, R. Pérez-Tomás, I. Marques, P. J. Costa, V. Félix and P. A. Gale, *Chem. Sci.*, 2013, **4**, 103–117.

<sup>155</sup> G. Sliwoski, S. Kothiwale, J. Meiler and E. W. L. Jr., *Pharmacol. Rev.*, 2014, **66**, 334–395.

ignored in many instances, has a paramount importance in the development of useful QSAR models.<sup>156, 157, 158</sup>

Lipophilicity is a parameter of great importance in the pharmaceutical industry. In a previous study with a small data set carried out by our group, it was demonstrated that lipophilicity is a key descriptor in the anionophoric activity of tambjamines.<sup>159</sup>

These marine alkaloids are perfect candidates to create this kind of libraries mentioned above, because of their easy synthetic access.

Employing QSAR methods, in this thesis has been made an effort to provide clarity about which are the parameters that govern the anionophoric properties of tambjamines.

The majority of this research was developed during my stay in Southampton (UK) at Southampton University, working in the group of Professor Phil A. Gale. All tambjamines were synthesised in Burgos and their ionophoric activity, was tested in both institutions. The measurement of retentions times (RT), an indirect experimental data of lipophilicity, was carried out in Southampton using reverse phase HPLC, as well as, the first stage of the modelling process using the software JMP 9.0.0.<sup>160</sup> This investigation was completed in collaboration with Nicole K. Night, from the group of Computational Systems Chemistry at the University of Southampton (Professor Jeremy G. Frey).

Forty three tambjamines were included in this study (Figure 2.16). The effect of varying two different positions was examined, the substitution at the central azafulvene and the enamine. Some of them were used in the previous study and others have already been published by our group (113.HCl-125.HCl, 128.HCl, 129.HCl and 131.HCl).<sup>161</sup> In the enamine functional group there were introduced aliphatic chains, heteroaromatic and aromatic groups with electron donor and electron

<sup>156</sup> N. Busschaert, S. J. Bradberry, M. Wenzel, C. J. E. Haynes, J. R. Hiscock, I. L. Kirby, L. E. Karagiannidis, S. J. Moore, N. J. Wells, J. Herniman, G. J. Langley, P. N. Horton, M. E. Light, I. Marques, P. J. Costa, V. Félix, J. G. Frey and P. A. Gale, *Chem. Sci.*, 2013, **4**, 3036–3045.

<sup>157</sup> Y.-L. Wu, D.-L. Wang, E.-H. Guo, S. Song, J.-T. Feng, X. Zhang, *Bioorg. Med. Chem. Lett.*, 2017, **27**, 1284–1290.

<sup>158</sup> D. Sokolović, J. Ranković, V. Stanković, R. Stefanović, S. Karaleić, B. Mekić, V. Milenković, J. Kocić, A. M. Veselinović, *Med. Chem. Res.*, 2017, **26**, 796–804.

<sup>159</sup> V. Saggiomo, S. Otto, I. Marques, V. Félix, T. Torroba and R. Quesada, *Chem. Commun.*, 2012, **48**, 5274–5276.

<sup>160</sup> JMP®, version 9.0.0 single user, SAS Institute Inc., Cary, NC, 1989-2016

<sup>161</sup> V. Saggiomo, S. Otto, I. Marques, V. Félix, T. Torroba and R. Quesada, *Chem. Commun.*, 2012, **48**, 5274–5276.

withdrawing substituents. In the alkoxy position it was checked the impact of having a methoxy or a benzyloxy group. By this way, it was tried to cover a large range of lipophilicities, molecular sizes, electronic properties, as well as, transport activities.

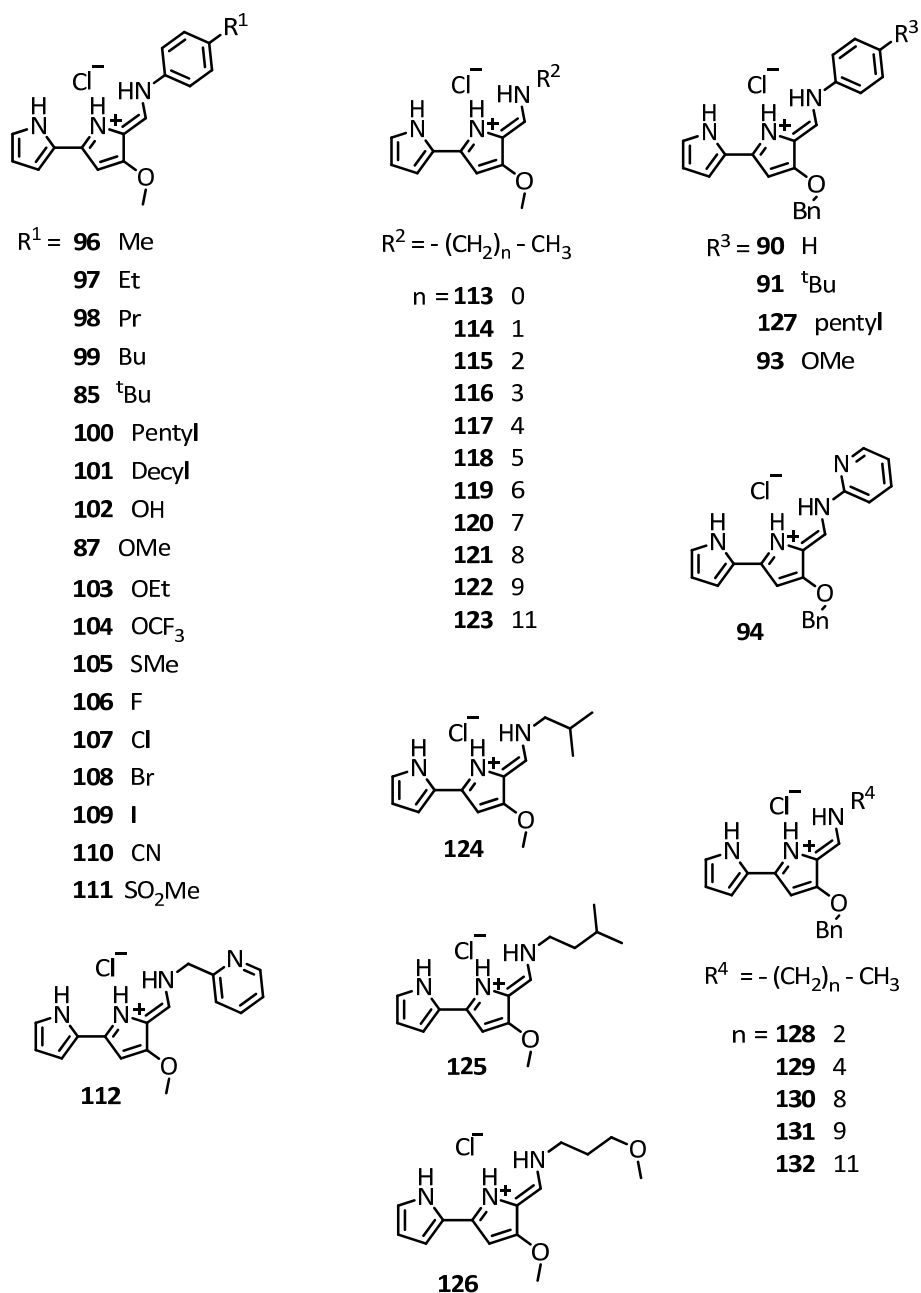


Figure 2.16. Tambjamines included in the QSAR analysis

A total of five hundred and six descriptors were calculated using a variety of softwares such as VCCLab and e-dragon 1.0,<sup>162, 163</sup> Chemicalize,<sup>164</sup> ACDiLabs 2.0,<sup>165</sup> TorchV10lite<sup>166</sup> and ChemBio-Draw 12.0 ultra-software.<sup>167</sup> Among the predictors, there were geometrical descriptors, charge descriptors, topological charge indices, WHIM descriptors, constitutional descriptors, molecular properties, number of H bond donor atoms, number H bond acceptor atoms, pKa, molecular weight, etc.

Retention time in phase reverse HPLC was used as an experimental measure of the lipophilicity of these derivatives. These values were plotted against all calculated Log *P* values. In all cases, R<sup>2</sup> values were higher than 0.89, indicating a good correlation between the theoretical (calculated) and experimental values. The best correlation was found with ALOGPs, calculated with ALOPGS 2.1 from e-dragon. Thus, this descriptor was used as lipophilicity value in the QSAR model design.

Anion transport ability was tested in ISE assays under conventional Cl<sup>-</sup>/NO<sub>3</sub><sup>-</sup> conditions. In Table 2.3 there are summarised the obtained results from these experiments, as well as, ALOGPs and RT for the forty three tambjamins.

Table 2.3. EC<sub>50</sub> values, Hill parameters, ALOGPs and retention times summary

Compound	EC <sub>50</sub> <sup>a</sup>	Hill parameter n	Log <i>P</i> <sup>b</sup>	Retention Time (min)
<b>96</b>	0.0072 <sup>d</sup>	1.19 <sup>d</sup>	3.08	10.4
<b>97</b>	0.0061 <sup>d</sup>	1.23 <sup>d</sup>	3.74	11.0
<b>98</b>	0.0070 <sup>d</sup>	1.25 <sup>d</sup>	4.17	11.6
<b>99</b>	0.0078 <sup>d</sup>	1.32 <sup>d</sup>	4.63	12.2
<b>85</b>	0.0104 <sup>d</sup>	1.29 <sup>d</sup>	4.72	11.9
<b>100</b>	0.0095 <sup>d</sup>	1.25 <sup>d</sup>	5.02	12.7
<b>101</b>	0.2884 <sup>d</sup>	0.96 <sup>d</sup>	7.11	14.5
<b>102</b>	0.0688 <sup>d</sup>	1.42 <sup>d</sup>	2.58	8.8
<b>87</b>	0.0197 <sup>d</sup>	1.29 <sup>d</sup>	2.86	9.8
<b>103</b>	0.0136 <sup>d</sup>	1.28 <sup>d</sup>	3.37	10.5
<b>104</b>	0.0231 <sup>d</sup>	1.31 <sup>d</sup>	3.76	11.0

<sup>162</sup> VCCLAB, Virtual Computational Chemistry Laboratory, *ALOGPS 2.1* and *e-Dragon 1.0*, <http://www.vcclab.org> (accessed August 2013)

<sup>163</sup> I. Tetko, J. Gasteiger, R. Todeschini, A. Mauri, D. Livingstone, P. Ertl, V. Palyulin, E. Radchenko, N. Zefirov, A. Makarenko, V. Tanchuk and V. Prokopenko, *J. Comput. Aid. Mol. Des.*, 2005, **19**, 453–463.

<sup>164</sup> *Chemicalize*, <http://www.chemicalize.org/> (accessed August 2013)

<sup>165</sup> *ACD/I-Lab 2.0*, <https://ilab.acdlabs.com/iLab2/> (accessed August 2013)

<sup>166</sup> *Fieldview*, version 2.0.2, Cresset BMD Ltd., Hertfordshire, UK, 2011.

<sup>167</sup> *Chemdraw Ultra*, 12.0, Cambridge SoftCorporation, Cambridge, USA, 1986-2010.

Chapter II: Discussion of results

<b>105</b>	0.0260 <sup>d</sup>	1.29 <sup>d</sup>	3.20	10.4
<b>106</b>	0.0208 <sup>d</sup>	1.18 <sup>d</sup>	2.92	9.6
<b>107</b>	0.0155 <sup>d</sup>	1.26 <sup>d</sup>	3.49	10.3
<b>108</b>	0.0236 <sup>d</sup>	1.37 <sup>d</sup>	3.62	10.5
<b>109</b>	0.0221 <sup>d</sup>	1.29 <sup>d</sup>	3.76	10.8
<b>110</b>	0.0167 <sup>d</sup>	1.48 <sup>d</sup>	2.68	9.0
<b>111</b>	0.0494 <sup>d</sup>	1.59 <sup>d</sup>	2.11	8.2
<b>112</b>	0.1965	0.85	1.88	– <sup>c</sup>
<b>113</b>	0.3459	1.30	1.03	7.0
<b>114</b>	0.0921	1.08	1.55	7.7
<b>115</b>	0.0274	1.03	2.03	8.5
<b>116</b>	0.0116	0.86	2.46	9.3
<b>117</b>	0.0065	1.18	2.99	10.2
<b>118</b>	0.0050	1.19	3.52	10.9
<b>119</b>	0.0045	1.51	4.02	11.5
<b>120</b>	0.0031	1.07	4.79	12.1
<b>121</b>	0.0038	1.10	5.10	12.6
<b>122</b>	0.0053	1.33	5.36	13.1
<b>123</b>	0.0073	1.15	6.14	13.8
<b>124</b>	0.0113	1.20	2.24	9.2
<b>125</b>	0.0067	1.05	2.84	10.0
<b>126</b>	0.0977	0.96	1.50	– <sup>c</sup>
<b>90</b>	0.0157	1.32	4.40	11.5
<b>91</b>	0.0116	1.20	5.94	13.1
<b>127</b>	0.0123	0.86	6.46	– <sup>c</sup>
<b>93</b>	0.0133	1.45	4.38	11.6
<b>94</b>	0.0089	1.24	3.30	11.3
<b>128</b>	0.0196	1.14	3.62	10.7
<b>129</b>	0.0097	1.74	4.49	11.9
<b>130</b>	0.0052	1.15	6.07	– <sup>c</sup>
<b>131</b>	0.0204	0.93	6.42	13.9
<b>132</b>	0.0744	0.26	7.14	– <sup>c</sup>

<sup>a</sup> mol % carrier to lipid concentration

<sup>b</sup> ALOGPs: lipophilicity calculated with e-dragon 2.1

<sup>c</sup> Retention time value not determined

<sup>d</sup> Average of at least three Hill plot analysis

The first data set examined was composed of thirty-eight compounds (**112.HCl**, **126.HCl**, **127.HCl**, **130.HCl** and **132.HCl** were not present in the original set). An attempt to find a simple correlation between lipophilicity and transport activity was carried out. A plot of the logarithm of the transport activity, expressed as  $\text{Log}(1/\text{EC}_{50})$ , vs ALOGPs was performed (Figure 2.17). From the graph, a parabolic dependence was detected but the majority of lipophilicity values were found between 2.5 and 5.5. In order to confirm the existence of a parabolic relationship, five new tambjamines which  $\text{Log } P$  values corresponded to the extremes of the parabolic curve were synthesised. The plot that included these new five compounds shows a parabolic function with a maximum activity for compounds having  $\text{Log } P$  values close to four (Figure 2.18). This result indicated that lipophilicity plays an important role in the transport activity of this family of compounds. The QSAR study will help to understand other relevant parameters that are involved in maximizing the transport activity.

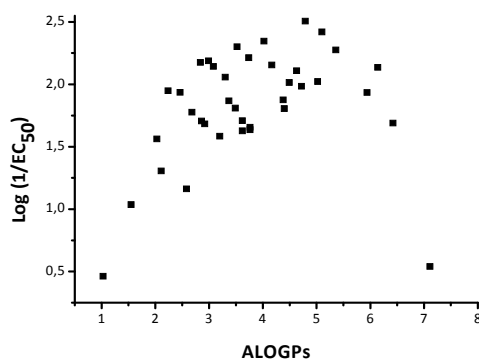


Figure 2.17. Thirty eight tambjamines:  $\text{Log}(1/\text{EC}_{50})$  vs ALOGPs.

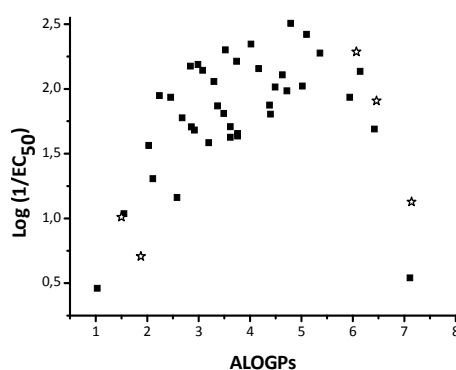


Figure 2.18. Forty three tambjamines:  $\text{Log}(1/\text{EC}_{50})$  vs ALOGPs, the five new compounds (**112.HCl**, **126.HCl**, **127.HCl**, **130.HCl** and **132.HCl**) are represented as stars.

Before starting the QSAR analysis, the data set was cured. A total of one hundred and seventy six descriptors were removed because the values corresponding to some molecules were not available, the variation of a predictor was negligible across the data set, some of them were recognised as non-numeric by JMP and others were repetitive. Two different representations of lipophilicity were maintained (ALOGPs and ALOGPs-sq).

The data set (forty three molecules) was divided into two groups. The training set, composed of thirty seven compounds, that was used for building the QSAR model/s and the test set, formed by the remaining six (**100.HCl**, **102.HCl**, **114.HCl**, **120.HCl**, **90.HCl** and **128.HCl**), which was used in the internal validation process of the obtained model/s.

Using JMP 9.0.0 and working with the training set,  $\text{Log}(1/\text{EC}_{50})$  was modelled against all descriptors, taking into account that only ALOGPs and ALOGPs-sq were used as a representation of lipophilicity. A stepwise multiple linear regression was executed, where the k-fold cross validation was set to two. All possible models with a maximum of three terms were calculated and subsequently ranked according to best fit (highest  $R^2$ ). The best model that contains two descriptors includes lipophilicity and squared lipophilicity. Regarding to results that contain three descriptors, most of them consist of extending the best two-descriptor model. There were found equations which extra parameter describes the size (AMW: average molecular weight or Mv: mean atomic Van der Waals volume), density, azafulvene pKa, etc. with no big differences in the goodness of fit ( $R^2$ ) (CD. Figure 530). Equations from 2.2 to 2.4 show three of the best obtained models. (JMP 13 (SW) analysis of equation 2.2: CD. Figure 531; JMP 13 (SW) analysis of equation 2.4: CD. Figure 532)

2 descriptors

( $R^2 = 0.65$ )

$$\text{Log}(1/\text{EC}_{50}) = -0.66 + 1.27 \cdot \text{ALOGPs} - 0.14 \cdot \text{ALOGPs-sq} \quad \text{Eq. 2.2}$$

3 descriptors

( $R^2 = 0.81$ )

$$\text{Log}(1/\text{EC}_{50}) = 0.68 + 1.40 \cdot \text{ALOGPs} - 0.16 \cdot \text{ALOGPs-sq} - 0.20 \cdot \text{AMW} \quad \text{Eq. 2.3}$$

3 descriptors

( $R^2 = 0.80$ )

$$\text{Log}(1/EC_{50}) = 3.18 + 1.42 \cdot \text{ALOGPs} - 0.16 \cdot \text{ALOGPs-sq} - 6.41 \cdot \text{Mv} \quad \text{Eq. 2.4}$$

Although the splitting into two groups (training and test set) was done taking into account the selection of representative compounds for the test set and maintaining a large training set, the validation process encountered problems. The origin of these obstacles lay in the parabolic dependence between  $\text{Log}(1/EC_{50})$  and lipophilicity, and consequently in the large leverage of molecules with low and high lipophilicity values.

To address this problem, the forty three tambjamines were used in the QSAR performance and a bootstrap method was used in the validation of the models, using the software R.<sup>168, 169</sup> This method consists in a data resampling technique which potential is based on a random sampling process using the dataset. Following the procedure described above for building the model, this time with the full set of tambjamines, a new modelling was done. The best equations obtained with two and three descriptors are shown below (equations 2.5 and 2.6). The results obtained with the thirty seven tambjamines training set (equations 2.2 and 2.4) and with the one that contains all of them (equations 2.5 and 2.6) are quite similar. (JMP 13 (SW) analysis of equation 2.5: CD. Figure 534; JMP 13 (SW) analysis of equation 2.6: CD. Figure 535)

2 descriptors

( $R^2 = 0.63$ )

$$\text{Log}(1/EC_{50}) = -0.60 + 1.21 \cdot \text{ALOGPs} - 0.13 \cdot \text{ALOGPs-sq} \quad \text{Eq. 2.5}$$

3 descriptors

( $R^2 = 0.79$ )

$$\text{Log}(1/EC_{50}) = 3.36 + 1.38 \cdot \text{ALOGPs} - 0.16 \cdot \text{ALOGPs-sq} - 6.65 \cdot \text{Mv} \quad \text{Eq. 2.6}$$

The obtained models were validated using the bootstrap method, applying a resampling of 999 times.

<sup>168</sup> R package version 1.3-17, Angelo Canty and Brian Ripley (2015), boot: Bootstrap R (S-Plus) Functions.

<sup>169</sup> A. C. Davison and D. V. Hinkley, *Bootstrap Methods and Their Applications*, Cambridge University Press, Cambridge, 1997.

In Table 2.4 there is summed up the validation of the obtained equations (2.5 and 2.6). The second column of this table is referred to the confidence intervals at which have been checked the models. Third and fourth columns correspond to the three (equation 2.5) and four descriptor (equation 2.6) models, respectively. The coefficients adopted by the intercept and the descriptors (ALOGPs, ALOGPs-sq, Mv), for each model are shown in color blue. In view of the goodness of fit ( $R^2$ ) and the good alignment between confidence intervals obtained in both, the least squares adjustment and the bootstrap, it was concluded that these two models are robust.

Table 2.4. Goodness of fit ( $R^2$ ) and confidence intervals for the best two (equation. 2.5) and three parameter (equation. 2.6) models

	Model parameters	ALOGPs, ALOGPs-sq	ALOGPs, ALOGPs-sq, Mv
<b>Coefficients</b>	$R^2$	0.6319	0.7928
<b>Linear fit</b>	Intercept	-0.596	3.364
	2.5 % C.I.	-1.183	1.842
	97.5 % C.I.	-0.009	4.887
<b>Bootstrap</b>	2.5 % C.I.	-1.108	2.159
	97.5 % C.I.	-0.086	4.419
<b>Linear fit</b>	ALOGPs	1.215	1.385
	2.5 % C.I.	0.914	1.148
	97.5 % C.I.	1.516	1.622
<b>Bootstrap</b>	2.5 % C.I.	0.904	1.126
	97.5 % C.I.	1.470	1.579
<b>Linear fit</b>	ALOGPs-sq	-0.135	-0.160
	2.5 % C.I.	-0.170	-0.188
	97.5 % C.I.	-0.099	-0.131
<b>Bootstrap</b>	2.5 % C.I.	-0.166	-0.190
	97.5 % C.I.	-0.093	-0.123
<b>Linear fit</b>	Mv		-6.648
	2.5 % C.I.		-9.091
	97.5 % C.I.		-4.205
<b>Bootstrap</b>	2.5 % C.I.		-8.432
	97.5 % C.I.		-4.473

A large number of descriptors seem to describe the anionophoric behaviour of this set of tambjamines without any advantage of one over the others. In an attempt to rationalise this result, the data set was divided into subsets as a function of the chemical groups and the position in different areas of the molecules. When the full data set was splitted into two groups considering the alkoxy substituent (Me, Bn) (Figure 2.19), the parabolic correlations between the ionophoric activity and lipophilicity did not improve. As the number of subsets increased (taking into account the substitution in the enamine position) and the compounds included in them were less and more similar structurally, the parabolic dependence between these two variables was found to be more marked (Figure 2.20). This result showed that the optimal Log *P* value is shifted into each series. From a global point of view, the parabolic behaviour is a property of the membrane.

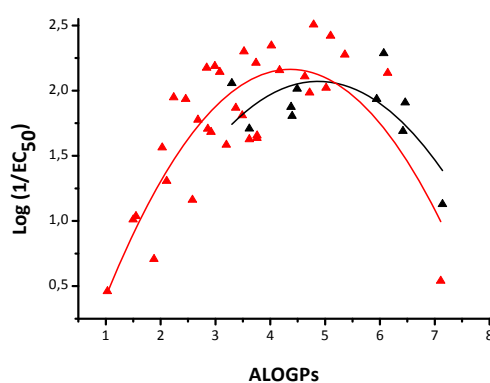


Figure 2.19. Forty three tambjamines splitted as a function of the alkoxy substituent: Me (red;  $R^2 = 0.65$ ) and Bn (black;  $R^2 = 0.28$ ).

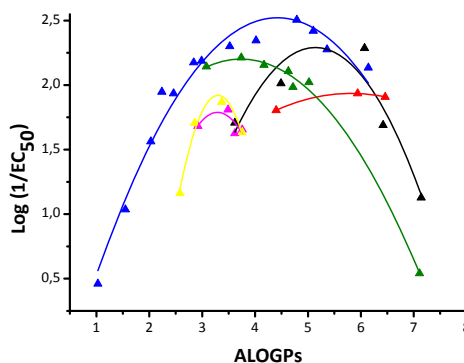


Figure 2.20. Thirty six tambjamines divided as OMe-NH-Ph-Alkyl (green;  $R^2 = 0.99$ ), OMe-NH-Ph-OR (yellow;  $R^2 = 0.93$ ), OMe-NH-Ph-Halogen (magenta;  $R^2 = -$ ), OMe-NH-Alkyl (blue;  $R^2 = 0.96$ ); OBn-NH-Ph-Alkyl (red;  $R^2 = -$ ), OBn-NH-Alkyl (black;  $R^2 = 0.71$ ), **105.HCl**, **110.HCl**, **111.HCl**, **112.HCl**, **126.HCl**, **93.HCl** and **94.HCl** have been excluded from this analysis.

This research highlighted the importance of lipophilicity in the anionophoric properties of tambjamines. When the full data set is splitted into subgroups different optimum Log P values are observed for each subset. This is consistent with the existence of specific interactions between the membrane and the tambjamine substituents.

#### 1.4. Indole–pyrrole tambjamines

In order to generate novel analogs inspired in the structure of the tambjamines we decided to introduce an indole group replacing one of the pyrrole groups. The indole presents good characteristic as hydrogen bond donor group and allows us to explore different conformations for the hydrogen bond cleft. Thus in these new synthetic tambjamines, the connection of the indole moiety to the pyrrole ring has been done through two different positions (positions 2 and 7; Figure 2.21).

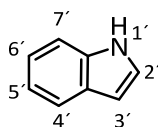


Figure 2.21. Indole positions labelled

In Figure 2.22 it is shown the series of tambjamines **85.HCl**, **133.HCl**–**143.HCl** synthesised to carry out this study. Aromatic and aliphatic substituents were chosen as substituents in the enamine position.

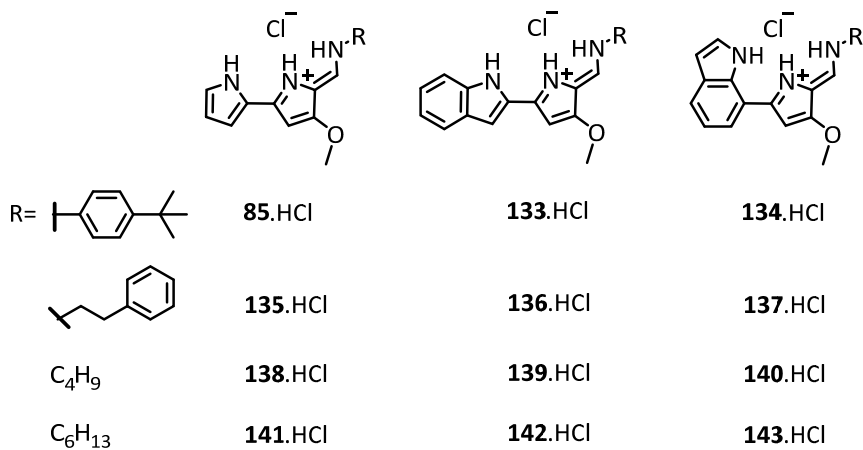


Figure 2.22. Tambjamine analogs design to study the effect of indole substituents

## 1.4.1. Anion transport assays

The chloride efflux from NaCl loaded POPC vesicles was studied under  $\text{Cl}^-/\text{NO}_3^-$  and  $\text{Cl}^-/\text{HCO}_3^-$  conditions, as previously described (detailed in Chapter IV). In Figure 2.23, there are shown the obtained results at 0.05 mol% carrier to lipid in  $\text{Cl}^-/\text{NO}_3^-$  experiments. Each graph contains the chloride efflux rates displayed by compounds with the same enamine substituent and a pyrrole, a 2-indole or a 7-indole unit at the A ring position.

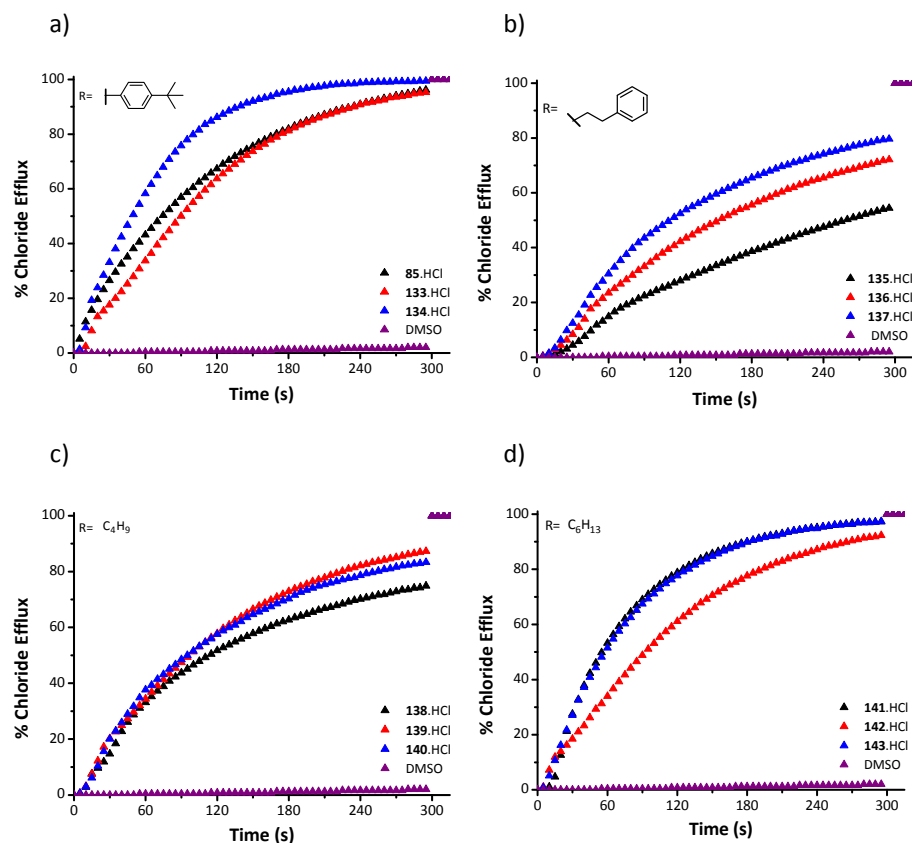


Figure 2.23. Chloride efflux upon addition of **85.HCl**, **133.HCl**–**143.HCl** (0.25  $\mu\text{M}$ , 0.05 mol% carrier to lipid) to vesicles composed of POPC. Vesicles contained NaCl (489 mM NaCl and 5 mM phosphate buffer, pH 7.2) were immersed in  $\text{NaNO}_3$  (489 mM  $\text{NaNO}_3$  and 5 mM phosphate buffer, pH 7.2). At the end of the experiment, the vesicles were lysed with detergent to release all chloride ions and the resulting value was considered to represent 100% release and used as such. Each trace represents an average of at least three different experiments, done with at least two different batches of vesicles. Black trace: pyrrole as A ring, red trace: 2-indole as A ring, blue trace: 7-indole as A ring and purple trace: blank. a) *p*-(*tert*-butyl)phenyl substituent, b) phenethyl substituent, c) butyl substituent and d) hexyl substituent.

The obtained results from  $\text{Cl}^-/\text{HCO}_3^-$  transport assays at 1 mol% carrier to lipid (Figure 2.24) were analysed in the same way as for  $\text{Cl}^-/\text{NO}_3^-$  transport data.

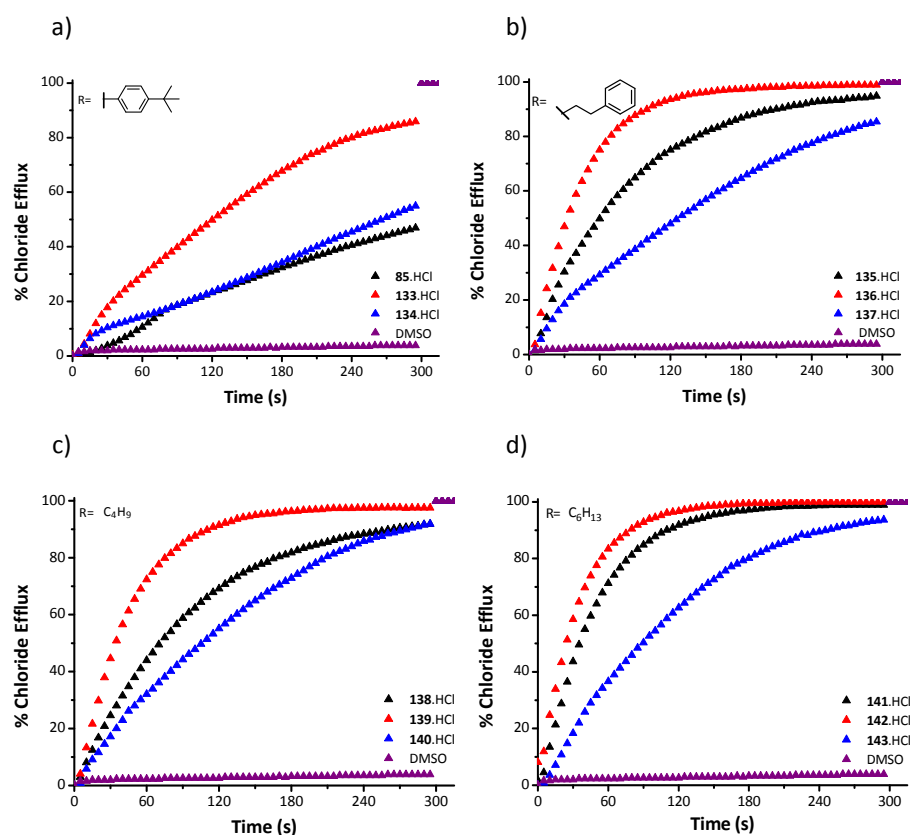


Figure 2.24. Chloride efflux upon addition of **85.HCl**, **133.HCl**–**143.HCl** (5  $\mu\text{M}$ , 1 mol% carrier to lipid) to vesicles composed of POPC. The vesicles contained NaCl (451 mM NaCl and 20 mM phosphate buffer, pH 7.2) were immersed in  $\text{Na}_2\text{SO}_4$  (150 mM  $\text{Na}_2\text{SO}_4$  and 20 mM phosphate buffer, pH 7.2). At the beginning of the experiment, a pulse of  $\text{NaHCO}_3$  was added in order to obtain a concentration of 40 mM. At the end of the experiment, the vesicles were lysed with detergent to release all chloride ions and the resulting value was considered to represent 100% release and used as such. Each trace represents an average of at least three different experiments. Black trace: pyrrole as A ring, red trace: 2-indole as A ring, blue trace: 7-indole as A ring and purple trace: blank. a) *p*-(*tert*-butyl)phenyl substituent, b) phenethyl substituent, c) butyl substituent and d) hexyl substituent.

In order to compare quantitatively their anionophoric activity, dose response curves were performed and the results fitted with the Hill equation. In Table 2.5, there are shown the obtained EC<sub>50</sub> and n values.

Table 2.5. Summary of parameters recovered from ISE assays and lipophilicity.

	EC <sub>50</sub> (nM) NO <sub>3</sub> <sup>-</sup> /Cl <sup>-</sup> <sup>a</sup>	Hill parameter n NO <sub>3</sub> <sup>-</sup> /Cl <sup>-</sup> <sup>a</sup>	EC <sub>50</sub> (nM) HCO <sub>3</sub> <sup>-</sup> /Cl <sup>-</sup> <sup>b</sup>	Hill parameter n HCO <sub>3</sub> <sup>-</sup> /Cl <sup>-</sup> <sup>b</sup>	ALOGPs <sup>c</sup>
<b>85</b>	46 ± 8	1.14 ± 0.28	241 ± 36	1.19 ± 0.23	4.72
<b>133</b>	38 ± 5	1.12 ± 0.19	467 ± 40	0.82 ± 0.08	5.70
<b>134</b>	31 ± 2	2.38 ± 0.28	2328 ± 412	0.54 ± 0.06	5.68
<b>135</b>	189 ± 13	1.11 ± 0.10	489 ± 64	1.04 ± 0.14	3.03
<b>136</b>	101 ± 7	1.12 ± 0.10	243 ± 23	1.16 ± 0.15	4.13
<b>137</b>	84 ± 1	1.30 ± 0.03	742 ± 211	0.82 ± 0.17	4.14
<b>138</b>	58 ± 4	0.86 ± 0.08	817 ± 71	1.06 ± 0.09	2.46
<b>139</b>	68 ± 4	1.26 ± 0.11	247 ± 30	0.99 ± 0.12	3.78
<b>140</b>	68 ± 3	1.17 ± 0.06	628 ± 86	0.97 ± 0.13	3.78
<b>141</b>	25 ± 14	1.19 ± 0.09	178 ± 3	1.38 ± 0.03	3.52
<b>142</b>	41 ± 3	1.17 ± 0.14	137 ± 4	1.49 ± 0.07	4.58
<b>143</b>	18 ± 6	0.80 ± 0.24	513 ± 41	0.96 ± 0.09	4.56

<sup>a</sup> Liposomes loaded with 489 mM NaCl suspended in 489 mM NaNO<sub>3</sub> (5 mM phosphate buffer, pH 7.2)

<sup>b</sup> Liposomes loaded with 451 mM NaCl suspended in 150 mM Na<sub>2</sub>SO<sub>4</sub> (20 mM phosphate buffer, pH 7.2). After one minute addition of NaHCO<sub>3</sub> to achieve the extravesicular bicarbonate concentration 40 mM.

<sup>c</sup> One of the lipophilicities calculated using e-dragon

Like in pyrrole-pyrrole tambjamine experiments, the observed EC<sub>50</sub> values in the nitrate exchange assays are smaller than those corresponding to the bicarbonate exchange experiments. This is probably due to the higher lipophilicity of nitrate compared with bicarbonate.

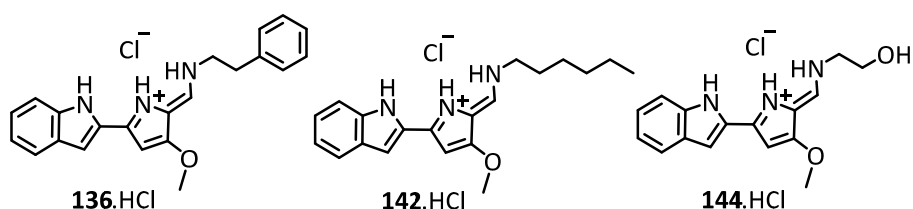
All these compounds were found to be potent anion carriers under both conditions. The nature of the enamine substituent seems to have little influence in the anionophoric properties of this set of tambjamins.

When the extravesicular anion was nitrate, the best activity was observed for those tambjamine analogs with the 7-indole moiety in A ring position (**134**.HCl, **137**.HCl, **140**.HCl and **143**.HCl), followed by 2-indole and pyrrole. On the contrary, these same compounds gave on average, the worst results when the external anion

was changed from nitrate to bicarbonate. These results underscored the importance of the binding cleft for these compounds. The selectivity towards transport of chloride against bicarbonate is greater than in the case of 7-indole analogs. The smaller bite angle of these compounds seems to favor the smaller chloride. On the other hand, the more open hydrogen bonding cleft of the pyrrole and 2-indole derivatives seems to be well suited to accommodate anions such as bicarbonate.

#### 1.4.2. 136.HCl and 142.HCl study

Indole containing tambjamine analogs were selected for further biological studies and compounds **136.HCl**, **142.HCl** and **144.HCl** were selected as candidates. These compounds were chosen because the calculated log *P* of **136** and **142** corresponds to the optimal log *P* range (ALOGPs 4.13 and 4.58 respectively) whereas **144** presents a much lower log *P* value (1.60), thus resulting as an appropriate control compound.



##### 1.4.2.1. Crystal structures

Crystals of **136.HCl** and **142.HCl** were grown from solutions in DCM:Hexane (1:1) by slow evaporation at room temperature. The X-ray diffraction analyses of the obtained structures (Figure 2.25 and 2.26) are detailed the CD. The solid state structure of both compounds is similar. Both tambjamins display an essentially planar indole-pyrrole-enamine core. The indole groups are rotated  $180^\circ$  with regard to pyrrole. The chloride anion is found interacting with the anion cleft defined by the pyrrole enamine moiety of one molecule as well as the rotated indole group from a second molecule.

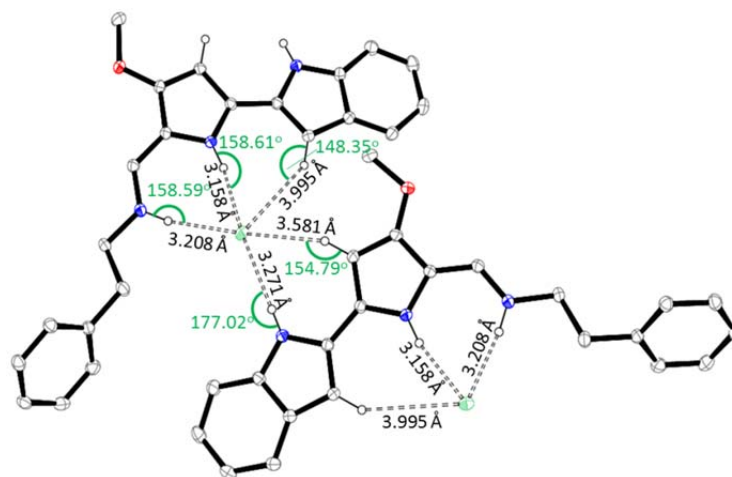


Figure 2.25. X-ray solid structure of **136.HCl**. It adopts a 1:1 stoichiometry. Hydrogen bonds are shown in dotted lines.

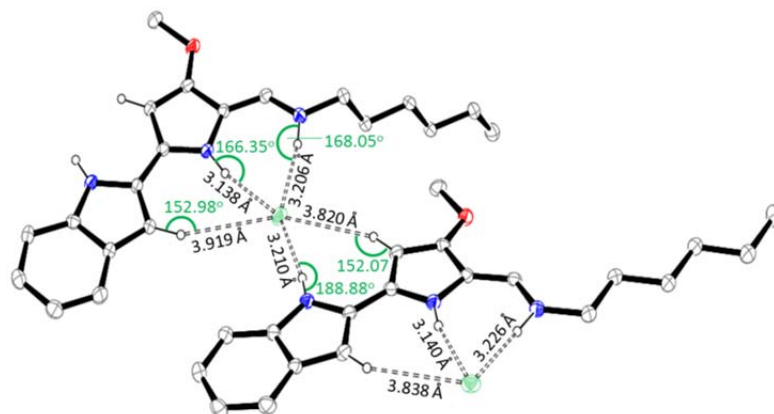


Figure 2.26. X-ray solid structure of **142.HCl**. It adopts a 1:1 stoichiometry. Hydrogen bonds are shown in dotted lines.

#### 1.4.2.2. Determination of apparent pKa values

The pKa of **136.HCl**, **142.HCl** and **144.HCl** was measured following a previously described spectrophotometric method.<sup>170</sup>

The methodology is based on monitoring absorbance changes as a function of pH. In a first attempt an  $8 \cdot 10^{-5}$  M solution was prepared in 250 mL of 1:1 DMSO–H<sub>2</sub>O

<sup>170</sup> G. S. Patterson, *J. Chem. Educ.*, 1999, **76**, 395–398.

(v/v) (0.1 M NaCl), at 25 °C. Using HCl 1M (in 0.1 M NaCl) the pH was adjusted to ~ 5. Consecutive aliquots of NaOH 1M (in 0.1 M NaCl) were added and the absorbance spectra were recorded after each one. pKa values were calculated using equation 2.7.

$$\text{Log} \left( \frac{A - A_{A^-}}{A_{AH} - A} \right) = -\text{pH} + \text{pKa} \quad \text{Eq. 2.7}$$

Where:

A is the absorbance at a time, (it was used  $\lambda_{\text{abs, max}}$  of protonated form)

$A_{A^-}$  is the absorbance of the neutral form, at its  $\lambda_{\text{abs, max}}$  of non protonated form

$A_{AH}$  is the absorbance of the protonated form, at its  $\lambda_{\text{abs, max}}$  of protonated form

The pKa values were calculated in 4:1 DMSO–H<sub>2</sub>O (v/v) (0.1 M NaCl) to avoid precipitation of compounds in all explored pH range. The obtained results are summarised in Table 2.6.

Table 2.6. Summary of pKa values. **136.HCl**, **142.HCl** and **144.HCl**

	pKa <sup>a</sup>
<b>136</b>	7.68
<b>142</b>	8.45
<b>144</b>	6.27

<sup>a</sup> 5·10<sup>-6</sup> M solution in 4:1 DMSO–H<sub>2</sub>O (v/v) (0.1 M NaCl), at 25 °C

#### 1.4.2.3. Anion binding constants

The anion binding properties of **136.HCl** (Figure 2.27) and **142.HCl** were studied by <sup>1</sup>H NMR titrations in DMSO-*d*<sub>6</sub> 0.5 % H<sub>2</sub>O. Both the perchlorate salts of each compound as well as their neutral forms were treated with different anions. Figure 2.28 shows the stack plot of the titration corresponding to **136.HClO<sub>4</sub>** with TBACl.

The obtained results are shown in Table 2.7.

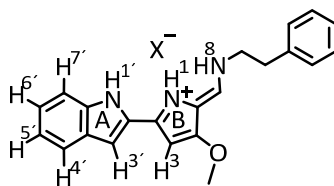


Figure 2.27. **136**.HCl with labelling protons

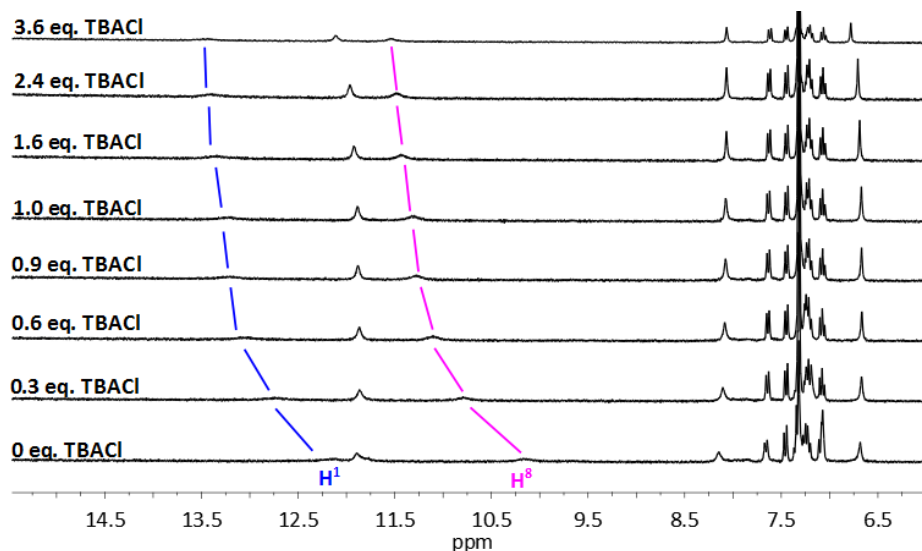
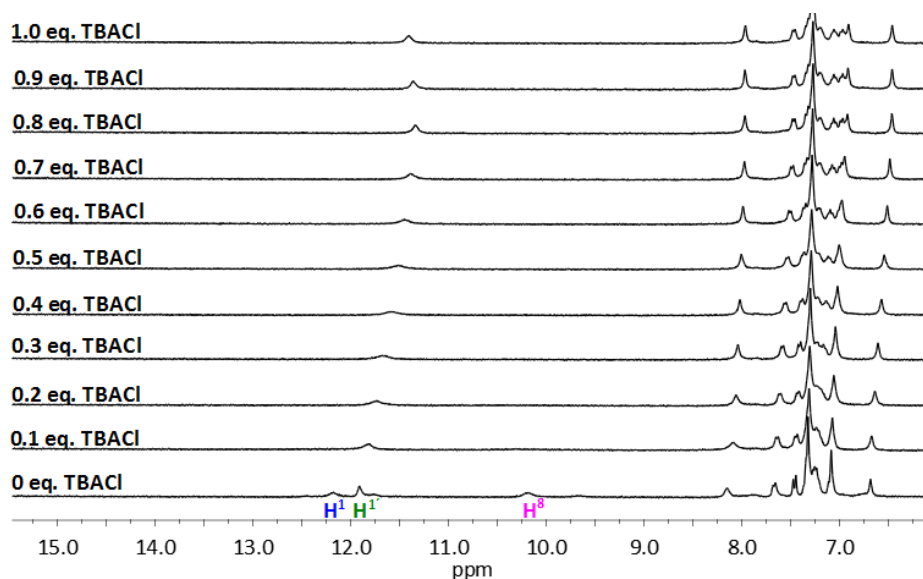


Figure 2.28. Partial stack plot of  $^1\text{H}$  NMR spectra of compound **136**.HClO<sub>4</sub> in DMSO-*d*<sub>6</sub> -0.5% H<sub>2</sub>O solution under the addition of increasing amounts of tetrabutylammonium chloride

The  $K_a$  value were calculated from fitting the drift of the chemical shift corresponding to affected protons as a function of the concentration of anion added. Calculated association constants with chloride (added as TBACl; Figure 2.28) were on average significantly higher than those calculated for the parent tambjamins (bipyrrole-enamine). Addition of nitrate anion (added as TBANO<sub>3</sub>) resulted in no changes, which seems to indicate that nitrate is not able to displace perchlorate. Addition of bicarbonate (added as TEAHCO<sub>3</sub>) resulted in deprotonation of the compounds (Figure 2.29) since the obtained  $^1\text{H}$  NMR are identical to the neutral ones. Neutral compounds are then able to weakly coordinate the anion. The compilation of these results is shown in Table 2.7.

Figure 2.29. **136.HClO<sub>4</sub>** treated with TEAHCO<sub>3</sub> resulted in deprotonation.Table 2.7. Binding constants ( $K_a$ ,  $M^{-1}$ ) calculated from NH<sup>1</sup>, NH<sup>8</sup> and CH<sup>3'</sup> protons

	$K_{a, NH1} (M^{-1})$	$K_{a, NH8} (M^{-1})$	$K_{a, CH3'} (M^{-1})$
<b>136.HClO<sub>4</sub></b> (+ TBACl)	3543 ± 417	3301 ± 375	4964 ± 225
<b>142.HClO<sub>4</sub></b> (+ TBACl)	2713 ± 426	3778 ± 442	— <sup>a</sup>
<b>136.HClO<sub>4</sub></b> (+TBAHNO <sub>3</sub> )	— <sup>b</sup>	— <sup>b</sup>	— <sup>b</sup>
<b>142.HClO<sub>4</sub></b> (+TBAHNO <sub>3</sub> )	— <sup>b</sup>	— <sup>b</sup>	— <sup>b</sup>
<b>136.HClO<sub>4</sub></b> (+ TEAHCO <sub>3</sub> )	— <sup>c</sup>	— <sup>c</sup>	— <sup>c</sup>
<b>142.HClO<sub>4</sub></b> (+ TEAHCO <sub>3</sub> )	— <sup>c</sup>	— <sup>c</sup>	— <sup>c</sup>
<b>136</b> (+TBACl)		2 ± 0	— <sup>b</sup>
<b>142</b> (+ TBACl)		1 ± 0	— <sup>b</sup>
<b>136</b> (+ TEAHCO <sub>3</sub> )		37 ± 4	— <sup>b</sup>
<b>142</b> (+ TEAHCO <sub>3</sub> )		24 ± 4	— <sup>b</sup>

<sup>a</sup> Error > 20%<sup>b</sup> Negligible changes in the proton shift<sup>c</sup> Deprotonation

#### 1.4.2.4. Anion transport assays

The anionophoric activity of these tambjamine analogs was studied with two different techniques. Potentiometric assays with the chloride selective electrode (ISE assays) and spectroscopic methods using fluorescent probes such as safranin O and carboxyfluorescein.

In Table 2.8 there are summed up the ISE experiment results (**136.HCl** and **142.HCl** were also included in Table 2.6).

The obtained results showed the differences in the level of activity between **144.HCl** and both **136.HCl** and **142.HCl**. **144.HCl** showed low activity in  $\text{Cl}^-/\text{NO}_3^-$  experiments and nearly inactive in  $\text{Cl}^-/\text{HCO}_3^-$  assays, meanwhile **136.HCl** and **142.HCl**, as already indicated, display very good anionophoric properties.

Table 2.8. Summary of parameters recovered from ISE assays and lipophilicity. **136.HCl**, **142.HCl** and **144.HCl**

	$\text{EC}_{50}$ (nM) $\text{NO}_3^-/\text{Cl}^-^{\text{a}}$	Hill parameter $n \text{ NO}_3^-/\text{Cl}^-$	$\text{EC}_{50}$ (nM) $\text{HCO}_3^-/\text{Cl}^-^{\text{b}}$	Hill parameter $n$ $\text{HCO}_3^-/\text{Cl}^-$	ALOGPs <sup>c</sup>
<b>136</b>	$101 \pm 7$	$1.12 \pm 0.10$	$243 \pm 23$	$1.16 \pm 0.15$	4.13
<b>142</b>	$41 \pm 3$	$1.17 \pm 0.14$	$137 \pm 4$	$1.49 \pm 0.07$	4.58
<b>144</b>	$17212 \pm 1172$	$1.13 \pm 0.10$	– <sup>d</sup>	– <sup>d</sup>	1.60

<sup>a</sup> Liposomes loaded with 489 mM NaCl suspended in 489 mM  $\text{NaNO}_3$  (5 mM phosphate buffer, pH 7.2)

<sup>b</sup> Liposomes loaded with 451 mM NaCl suspended in 150 mM  $\text{Na}_2\text{SO}_4$  (20 mM phosphate buffer, pH 7.2). After one minute addition of  $\text{NaHCO}_3$  to achieve the extravesicular bicarbonate concentration 40 mM.

<sup>c</sup> One of the lipophilicities calculated using e-dragon

<sup>d</sup> Not determined. Carrier concentrations over 5 mol% do not achieve 50% release of chloride anions

In order to rule out the influence of the metal cation in the transport process, some experiments in which the sodium salts were replaced by potassium, rubidium or caesium salts were carried out. Three different sets of vesicles were prepared. They were loaded with KCl, RbCl and CsCl (489 mM, I.S. 500 mM, buffered to pH 7.2 with 5 mM of  $\text{NaH}_2\text{PO}_4$ ) and suspended in a  $\text{NaNO}_3$  solution (489 mM, I.S. 500 mM, buffered to pH 7.2 with 5 mM of  $\text{NaH}_2\text{PO}_4$ ) or  $\text{KNO}_3$  (489 mM, I.S. 500 mM, buffered to pH 7.2 with 5 mM of  $\text{NaH}_2\text{PO}_4$ ) in the case of KCl. The obtained results showed that  $\text{M}^+/\text{Cl}^-$  symport could be discarded because no differences were found in chloride rates when the metal cation was changed (Figure 2.30. **136.HCl**).

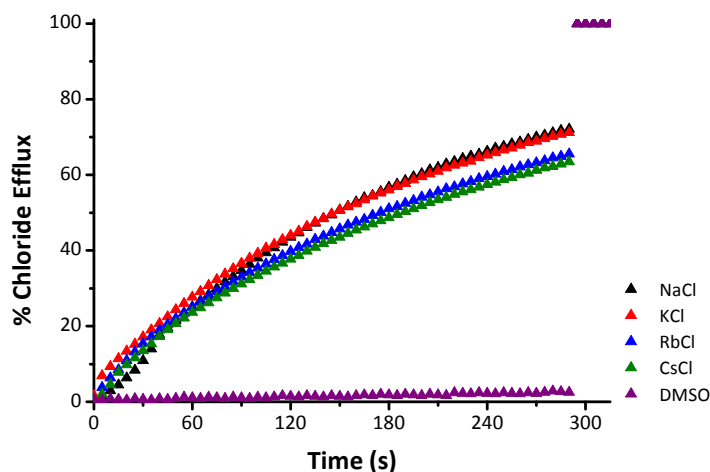


Figure 2.30. Chloride efflux upon addition of **136**.HCl (0.25  $\mu$ M, 0.05 mol%); purple: control, 10  $\mu$ L DMSO to POPC vesicles, 0.5 mM. Vesicles contained NaCl (black symbols, 489 mM NaCl, 5 mM NaH<sub>2</sub>PO<sub>4</sub> buffer, pH 7.2, 500 mM ionic strength), RbCl (blue symbols, 489 mM RbCl, 5 mM NaH<sub>2</sub>PO<sub>4</sub> buffer, pH 7.2, 500 mM ionic strength) or CsCl (green symbols, 489 mM CsCl, 5 mM NaH<sub>2</sub>PO<sub>4</sub> buffer, pH 7.2, 500 mM ionic strength) and were suspended in NaNO<sub>3</sub> (489 mM NaNO<sub>3</sub>, 5 mM NaH<sub>2</sub>PO<sub>4</sub> buffer pH 7.2, 500 mM ionic strength). KCl vesicles (red symbols, 489 mM KCl, 5 mM KH<sub>2</sub>PO<sub>4</sub> buffer, pH 7.2, 500 mM ionic strength) were suspended in KNO<sub>3</sub> (489 mM KNO<sub>3</sub>, 5 mM KH<sub>2</sub>PO<sub>4</sub> buffer, pH 7.2, 500 mM ionic strength). Each trace represents the average of at least three different trials, done with at least two different batches of vesicles.

Carboxyfluorescein leakage assays (Figure 1.7; Chapter I), detailed in Chapter IV, were performed. Vesicles loaded with NaCl (451 mM, buffered with NaH<sub>2</sub>PO<sub>4</sub> 20 mM to pH 7.2, I.S. 500 mM and 50 mM CF) were suspended in an external Na<sub>2</sub>SO<sub>4</sub> solution (150 mM, buffered with NaH<sub>2</sub>PO<sub>4</sub> 20 mM to pH 7.2, I.S. 500 mM) to give a final lipid concentration of 0.25 mM. After one minute, the tambjamine analog was incorporated to the assay (1 mol% carrier to lipid) and the fluorescence changes were monitored over time during five minutes. At six minutes, a pulse of detergent was added in order to lyse the vesicles and release all carboxyfluorescein. Consequently, it was diluted in the total volume of the experiment and its fluorescence increased. The obtained results shown that the enhancement of fluorescence was only observed when the detergent was added. Thus, the formation of large non-selective pores could be ruled out (Figure 2.31). Full details of how preparing and carrying out these experiments are described in Chapter IV.

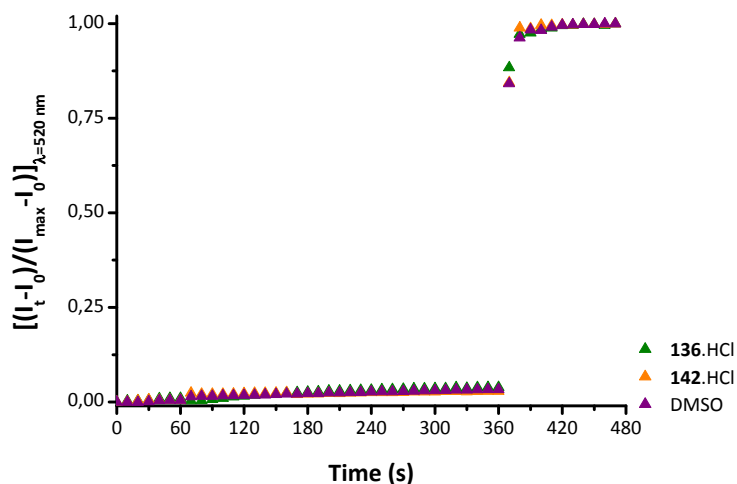


Figure 2.31. Carboxyfluorescein leakage upon addition of **136.HCl** and **142.HCl** to POPC vesicles, 0.25 mM. Vesicles contained NaCl (451 mM, buffered with NaH<sub>2</sub>PO<sub>4</sub> 20 mM to pH 7.2, I.S. 500 mM and 50 mM CF) were suspended in Na<sub>2</sub>SO<sub>4</sub> (150 mM, buffered with NaH<sub>2</sub>PO<sub>4</sub> 20 mM to pH 7.2, I.S. 500 mM). At t = 60 s addition of the anion carrier (1 mol% carrier to lipid). At t = 360 s addition of 20  $\mu$ L of detergent. Green trace: 136.HCl, orange trace: 142.HCl and purple trace: blank (10  $\mu$ L DMSO). Each trace represents the average of at least three different trials, done with at least two different batches of vesicles.

Once the mechanism of action was established, we aimed to determine the ability of these three tambjamine alkaloids to polarize the phospholipid membrane in vesicle assays.

The membrane potential ( $V_m$ ) is the difference of voltage between both sides of the membrane. It is determined by the concentration of ionic species in the intracellular and extracellular solutions in living systems. Ion channels and carriers located in the membrane are responsible of maintaining a regulated membrane potential. The imbalance of electrical charges, achieved when the ion driving forces are in equilibrium is known as resting membrane potential. It is found from -10 to -90 mV in some cell types.  $V_m$  varies when the conductance of at least one ion is altered. It is related to proliferation and differentiation events. Those cells that display highly polarised membranes such as somatic cells (hyperpolarised: the interior more negative) exhibit low tendency to proliferate, by contrast depolarised cells (the interior is less negative) like stem cells, regenerating systems or the rapidly proliferating cancerous cells are mitotically active.<sup>171, 172</sup>

<sup>171</sup> S. Sundelacruz, M. Levin and D. L. Kaplan, *Stem Cell Rev. and Rep.*, 2009, **5**, 231–246.

<sup>172</sup> M. Yang and W. J. Brackenbury, *Front. Physiol.*, 2013, **4**, 185–194.

Cancer Stem Cells (CSCs) are a subpopulation of cells present in tumours, which display a similar behaviour to SCs. They are characterised by their ability of self-renewal in serial transplantation assays, to act as tumour-initiating cells and remaining in an undifferentiated stage. There is a large number of evidences that CSCs contribute to chemotherapy resistance. Therefore, identifying them as a therapeutic target could yield promising results in the battle against cancer.<sup>173</sup>

In order to determine if our set of indole-pyrrole tambjamines was able to alter the membrane polarization, new vesicles assays were carried out. The fluorescent probe safranin O (Figure 1.7; Chapter I), detailed in Chapter IV, sensitive to changes in membrane polarization was used.

It is a lipophilic cationic dye. In vesicle assays, independently of working with it in the intra- or extravesicular medium, it is going to be located in the bilayer during the transport experiment. Its fluorescence intensity increases as long as the membrane potential increases. The direction in which this variation takes place depends on how the charges are distributed at the end of the experiment, which depends on how the experiment was designed. A schematic example is shown in Figure 2.32. On the left is shown how vesicles loaded with chloride are suspended in a sulfate solution. When an active carrier is added, the membrane is negative charged in the outer layer and a decrease in fluorescence is going to be observed. By contrast, on the right it is drawn the inverse situation. When a pulse of an active carrier is added the membrane is polarised in the opposite way and an enhancement of safranin O fluorescence is going to be detected.

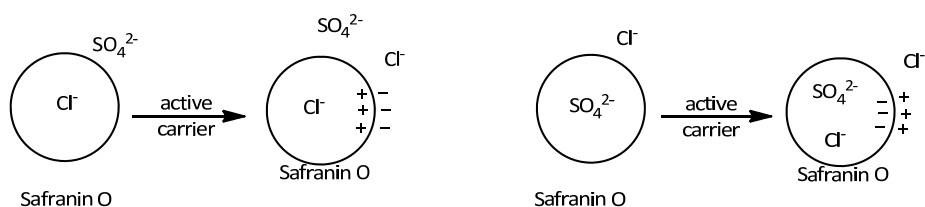


Figure 2.32. Left: vesicles loaded with chloride are suspended in a sulfate solution. After adding and active carrier the outer layer is negatively charged; right: vesicles loaded with sulfate are suspended in a chloride solution. After adding and active carrier the outer layer is positively charged.

<sup>173</sup> P. Valent, D. Bonnet, R. De Maria, T. Lapidot, M. Copland, J. V. Melo, C. Chomienne, F. Ishikawa, J. J. Schuringa, G. Stassi, B. Huntly, H. Herrmann, J. Soulier, A. Roesch, G. J. Schuurhuis, S. Wöhrer, M. Arock, J. Zuber, S. Cerny-Reiterer, H. E. Johnsen, M. Andreeff and C. Eaves, *Nat. Rev. Cancer*, 2012, **12**, 767–775.

In order to carry out these experiments, vesicles loaded with NaCl (28.8 mM, buffered with NaH<sub>2</sub>PO<sub>4</sub> 5 mM to pH 7.2, I.S. 40 mM) where suspended over a Na<sub>2</sub>SO<sub>4</sub> solution (9.6 mM, buffered with NaH<sub>2</sub>PO<sub>4</sub> 5 mM to pH 7.2, I.S. 40 mM, 0.2 μM safranin O) for a final lipid concentration of 0.25 mM. After two minutes, a pulse of the corresponding tambjamine was added in DMSO solution (0.1 mol% carrier to lipid). The fluorescence changes were monitored over time (Figure 2.33). Results obtained from these assays demonstrated that only the two active tambjamines in antiport ISE assays were able to polarize the membrane.

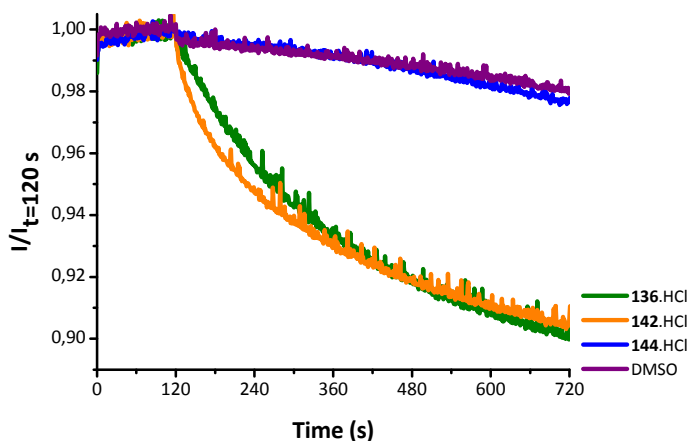


Figure 2.33. Membrane polarization upon addition of 136.HCl, 142.HCl and 144.HCl to POPC vesicles, 0.25 mM. Vesicles contained NaCl (28.8 mM, buffered with NaH<sub>2</sub>PO<sub>4</sub> 5 mM to pH 7.2, I.S. 40 mM) were suspended in Na<sub>2</sub>SO<sub>4</sub> (9.6 mM, buffered with NaH<sub>2</sub>PO<sub>4</sub> 5 mM to pH 7.2, I.S. 40 mM, and 0.2 μM S.O). At t = 120 s addition of the anion carrier (0.1 mol% carrier to lipid). Green trace: 136.HCl, orange trace: 142.HCl, blue trace: 144.HCl and purple trace: blank (10 μL DMSO). Each trace represents the average of at least three different trials, done with at least two different batches of vesicles.

A second set of safranin O experiments was carried out. It was used as a negative control because under these new experimental conditions, no membrane potential could be generated. Vesicles loaded with NaCl (28.8 mM, buffered with NaH<sub>2</sub>PO<sub>4</sub> 5 mM to pH 7.2, I.S. 40 mM) where suspended over a NaCl solution (28.8 mM, buffered with NaH<sub>2</sub>PO<sub>4</sub> 5 mM to pH 7.2, I.S. 40 mM, 0.2 μM safranin O) for a final lipid concentration of 0.25 mM. After two minutes, a pulse of the corresponding tambjamine was added in DMSO solution (0.1 mol % carrier to lipid) and no changes in the safranin O fluorescence were detected, as it was expected (Figure 2.34).

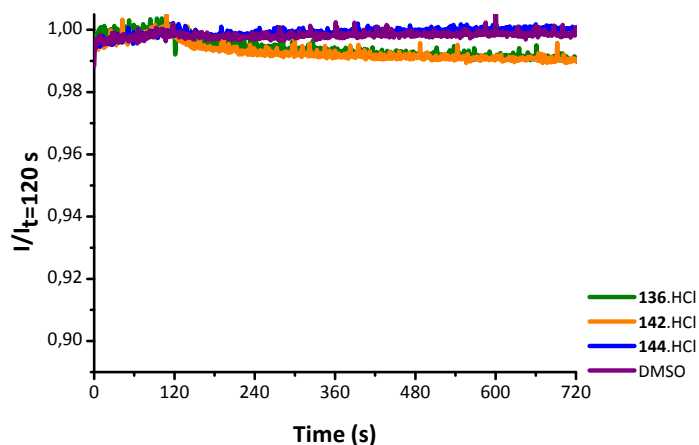


Figure 2.34. Membrane polarization upon addition of **136.HCl**, **142.HCl** and **144.HCl** to POPC vesicles, 0.25 mM. Vesicles contained NaCl (28.8 mM, buffered with  $\text{NaH}_2\text{PO}_4$  5 mM to pH 7.2, I.S. 40 mM) were suspended in NaCl (28.8 mM, buffered with  $\text{NaH}_2\text{PO}_4$  5 mM to pH 7.2, I.S. 40 mM, and 0.2  $\mu\text{M}$  S.O). At  $t = 120$  s addition of the anion carrier (0.1 mol % carrier to lipid). Green trace: **136.HCl**, orange trace: **142.HCl**, blue trace: **144.HCl** and purple trace: blank (10  $\mu\text{L}$  DMSO). Each trace represents the average of at least three different trials, done with at least two different batches of vesicles.

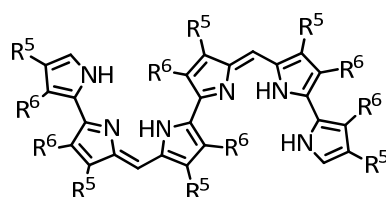
The polarization as a result of the facilitated anion transport was also observed in living cells. The induced hyperpolarization resulted in differentiation and elimination of cancer stem cells (CSC). Only active transporters (**136.HCl** and **144.HCl**) were able to modulate intracellular pH ( $\text{pHi}$ ) of A549 cells, stained with acridine orange. Membrane potential measurements, done in the same cell line, demonstrated that only the two active alkaloids had the ability to alter it. These two *in vitro* results are consistent with the behaviour of tambjamins in vesicles assays.

These experiments were carried out in the University of Barcelona, University of Valencia, Research Centre Príncipe Felipe and Imperial College from London. Therefore, the results are not detailed in this thesis.

## 2. TETRAHETEROCYCLIC TRANSPORTERS

### 2.1. Introduction

As it was shown in the previous section, the pyrrole unit plays an important role in the anion transport event. It is possible to find a huge variety of systems that contain the pyrrole motif such as macrocycles like porphyrin systems characterised by a high level of preorganization or open-chain oligopyrroles such as dipyrromethenes (i.e. prodiginines). The protonation of these systems makes them suitable structures to interact with anion through hydrogen bondings. A couple of linear hexapyrins **145** were tested as anion receptors under the same conditions and it was observed that the deprotonated form is able to bind, strongly, two chloride anions (**145b**,  $K_{a1} = 1.2 \cdot 10^6 \text{ M}^{-1}$ ,  $K_{a2} = 3.2 \cdot 10^4 \text{ M}^{-1}$ ). **145a**.HCl X-ray crystal analysis shows a flat diprotonated system, which is found binding two chloride anions through two sets of three well-defined hydrogen bonds (Figure 2.35).<sup>174</sup>



- 145**    a  $R^5 = C_3H_7$ ,  $R^6 = H$   
           b  $R^5 = R^6 = C_2H_5$

<sup>174</sup> J. L. Sessler, P. A. Gale and W.-S. Cho, in *Anion Receptor Chemistry*, The Royal Society of Chemistry, Cambridge, 1st ed, 2006, ch. 3, pp. 133–170.

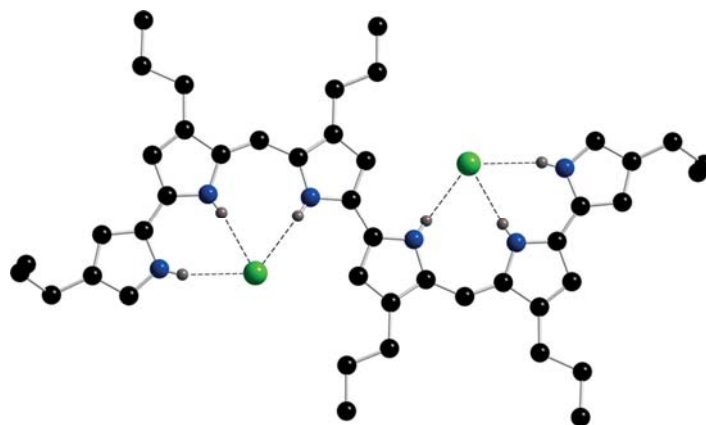


Figure 2.35. X-Ray solid structure of **145a.HCl**

Prodigiosin **8** and their synthetic analogs display a wide range of biological activity. From antimalarial, antifungal or antibiotic properties to ability to permeabilize cell membranes, modify intracellular pH and trigger apoptosis in cells.<sup>175</sup> The natural product prodigiosin **8** has been found to be too cytotoxic for healthy cells, therefore the pursuit of synthetic derivatives which cytotoxicity were selective to cancerous cells is a key objective in the drug development process. Obatoclax **65**, a synthetic prodiginine analog has completed pre-clinical and clinical trials with promising results in different cancer cell lines.<sup>176</sup>

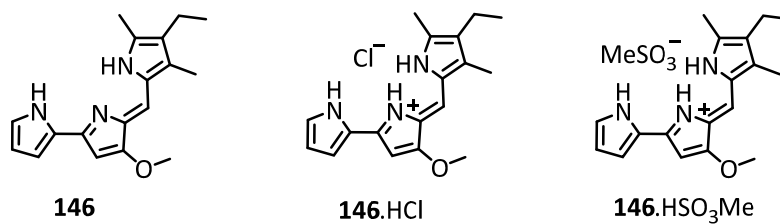
### 2.1.1. Prodiginines conformational analysis

Although prodiginines present a simple structure, they display rotameric forms and are involved in acid/base and tautomeric equilibria. Depending on the protonation state, the solvent and the counteranion, different conformations could be found. These different spatial distributions have an impact on the binding affinities toward each substrate. A conformational analysis of **146** as chloride and mesilate salts, carried out by our group, is listed below.

---

<sup>175</sup> S. Rastogi, E. Marchal, I. Uddin, B. Groves, J. Colpitts, S. A. McFarland, J. T. Davis and A. Thompson, *Org. Biomol. Chem.*, 2013, **11**, 3834–3845.

<sup>176</sup> M. García-Valverde, I. Alfonso, D. Quiñonero and R. Quesada, *J. Org. Chem.*, 2012, **77**, 6538–6544.



In relation to their tautomeric equilibria, the feasible tautomers corresponding to neutral **146** are pointed out in Figure 2.36.

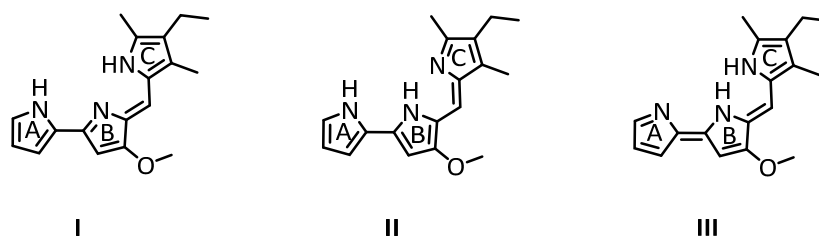


Figure 2.36. Possible tautomers of tambjamine **146**

Four possible conformations and some plausible interactions (signalled with dots), referred to protonated tautomer **I**, are indicated in Figure 2.37.

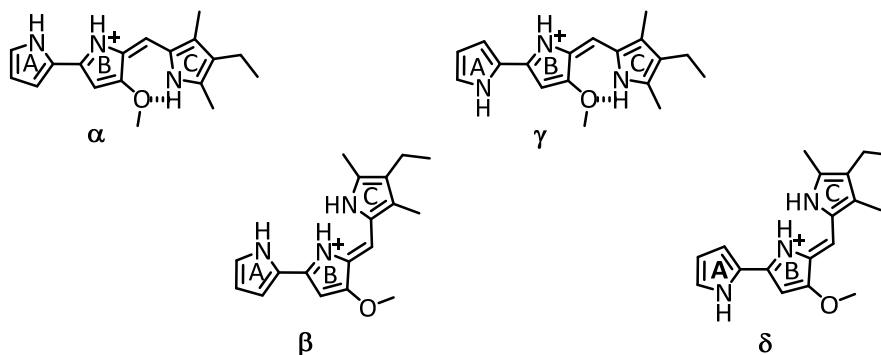


Figure 2.37. Prodiginine conformations

The solid-state structures determined by X-ray diffraction (Figure 2.38) showed that the protonated anion receptor **146** adopts a  $\beta$  conformation with the three NH groups oriented toward to the anion and interacting with it through hydrogen bonds. The tripyrrolic scaffold shows an essentially flat disposition with all C–C

methine distances quite similar (1.38 Å on average) and a shorter distance than a single C–C bond between the two pyrrole units of the bipyrrrole motif.

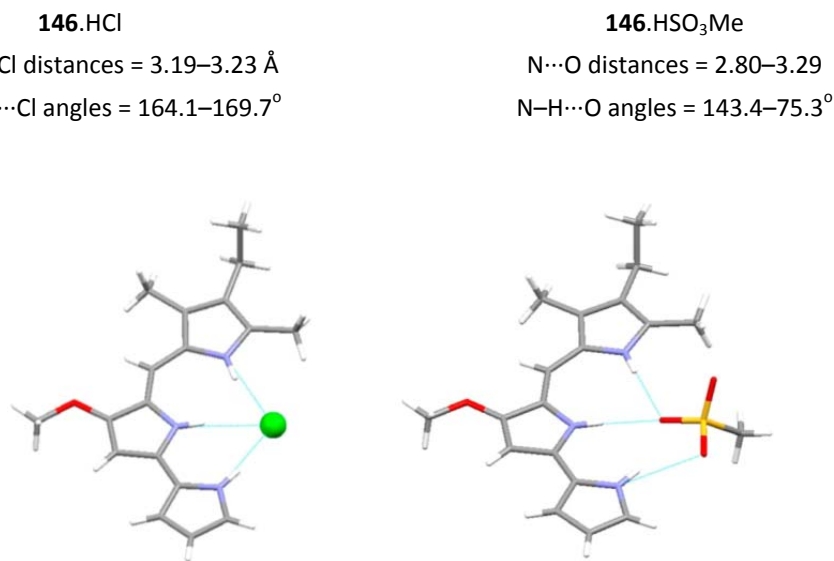


Figure 2.38. Left: **146.HCl** X-ray solid structure. Right: **146.HSO<sub>3</sub>Me**

NMR analysis by <sup>1</sup>H, <sup>13</sup>C, COSY, NOESY, HMBC and HMQC experiments were made, in CDCl<sub>3</sub> and DMSO-*d*<sub>6</sub>, in order to determine the relative conformations adopted in solution by the neutral form and chloride and mesilate salts of **146**.

**146.HCl** presents β conformation in both, CDCl<sub>3</sub> and DMSO-*d*<sub>6</sub>. When the same study was done for the mesylate salt, again β conformation was found in CDCl<sub>3</sub>. However, two different isomers were observed in the DMSO-*d*<sub>6</sub> <sup>1</sup>H NMR. The most abundant displays β disposition and the other one presents an intramolecular hydrogen bond between the OMe and NH from the C pyrrole ring, so it corresponds to the α isomer.

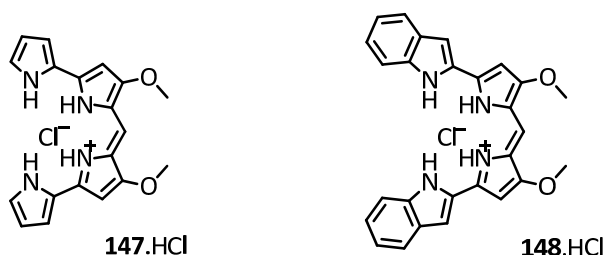
Neutral **146** adopts β conformation in both, CDCl<sub>3</sub> and DMSO-*d*<sub>6</sub>. Moreover, at high concentrations, in CDCl<sub>3</sub>, the NOESY and DOSY spectra show the formation of a homodimer **146**<sub>2</sub>. DFT studies also supported that the most favourable conformation corresponds to tautomer **I** in β disposition (**Iβ**).<sup>177</sup>

<sup>177</sup> M. García-Valverde, I. Alfonso, D. Quiñonero and R. Quesada, *J. Org. Chem.* 2012, **77**, 6538–6544.

### 2.1.2. Tetraheterocycles

The importance of natural products, extracted from soil or sea water microorganisms, has already been mentioned in this thesis. The dipyrrolyl-dipyrromethene **147.HCl** was first isolated from a mutant strain of *Serratia Marcescens*.<sup>178</sup> It has also been found in the blue-green mucus exuded by marine nudibranchs, along with tambjamines.<sup>179</sup> This tetraheterocycle derivative presents a conjugated  $\pi$ -system based on two pyrrolic rings connected by a methine linkage, resulting in an intense blue characteristic colour. It displays antibacterial activity against both Gram-Positive and Gram-Negative bacteria.<sup>180</sup> This compound presents an array of NH groups in adequate disposition to interact with anions through hydrogen bonds. Previously, our group described a synthetic analog in which two of the pyrrole had been substituted by indoles **148.HCl**.<sup>181</sup> Its anionophoric activity was tested in  $\text{Cl}^-/\text{NO}_3^-$  and  $\text{Cl}^-/\text{HCO}_3^-$  ISE vesicle assays and was shown to be an excellent anion carrier.

All these precedents prompted us to explore in detail the synthesis and properties of these tetraheterocycle compounds.



### 2.2. Synthesis

The common synthetic pathway for these structures is the Mac Donald coupling. It consists on an acid catalysed condensation between a 2-formylpyrrole and the free  $\alpha$ -position of pyrrole (Scheme 2.3a). Often, it is observed the formation of the symmetric product from the self-condensation of two carbaldehyde molecules (Scheme 2.3b). This second route is favoured when  $\text{R}^2$  is an electron withdrawing group which decreases the nucleophilicity of the  $\alpha$  position.

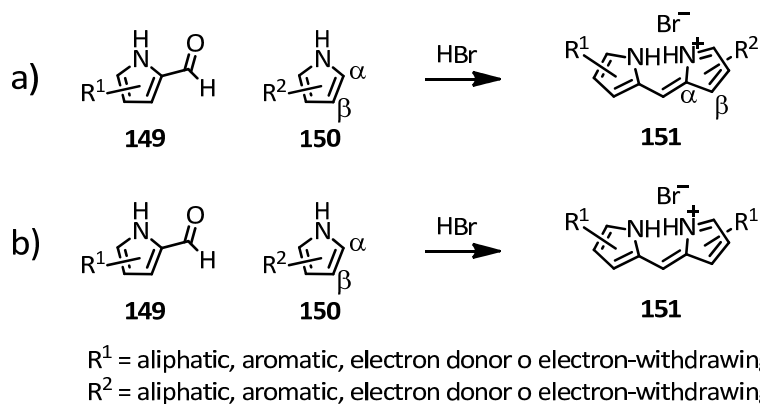
<sup>178</sup> H. H. Wasserman, D. J. Friedland and D. A. Morrison, *Tetrahedron Lett.*, 1968, **9**, 641–644.

<sup>179</sup> N. Lindquist and W. Fenical, *Experientia*, 1991, **47**, 504–506.

<sup>180</sup> J. H. Sharp, M. K. Winson and J. S. Porter, *Nat. Prod. Rep.*, 2007, **24**, 659–673.

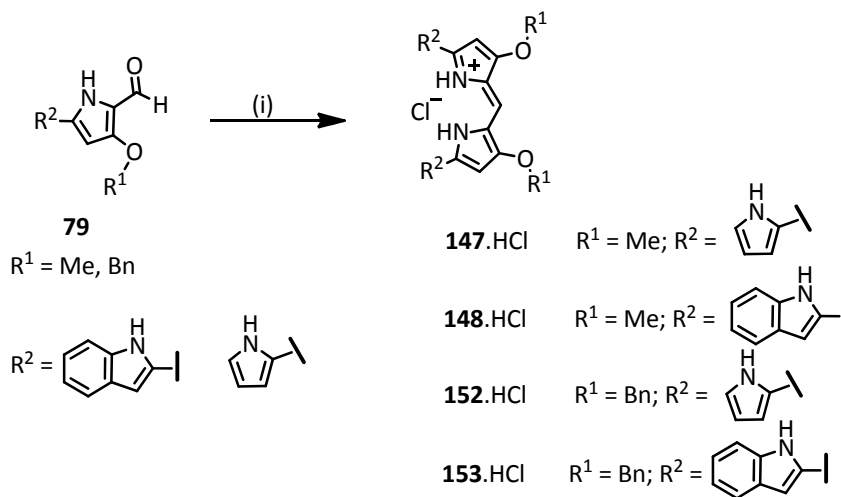
<sup>181</sup> B. Díaz de Greñu, P. Iglesias-Hernández, M. Espona, D. Quiñonero, M. E. Light, T. Torroba, R. Pérez-Tomás and R. Quesada, *Chem. Eur. J.*, 2011, **17**, 14074–14083.

When the desired compound is the tetraheterocycle the typical routes are combining two free  $\alpha$ -position pyrrole molecules in the presence of formic acid, reacting two equivalents of pyrrole 2-carboxylate in presence of formic acid or the Mac Donald coupling in which both species present the same substitution.<sup>182</sup>



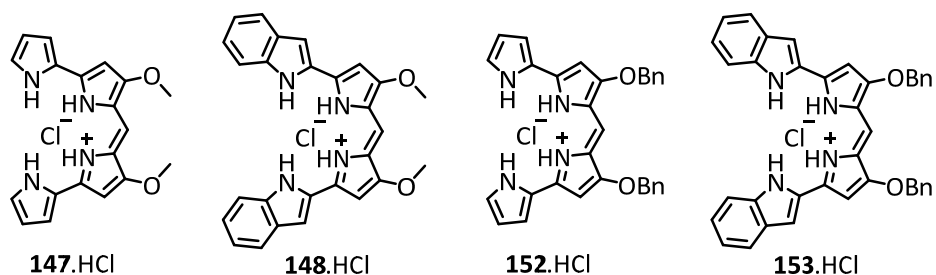
Scheme 2.3. a) Acid-Catalysed condensation. b) self-condensation of two carbaldehyde molecules.

Tetraheterocycles studied in this thesis were synthesised as described in Scheme 2.4. Carbaldehydes, prepared as described in the synthesis of tambjamines (Section 1.2), were treated under acidic conditions to yield the corresponding tetraheterocycle in good to excellent yields.



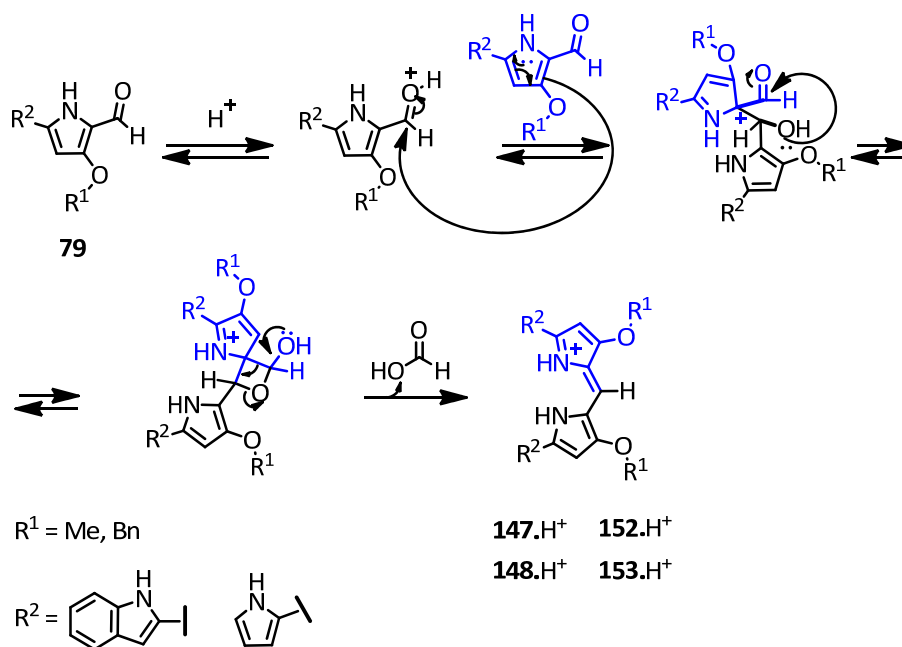
Scheme 2.4. Reagents and conditions: (i) MeOH, 3.5 eq. AcOH, 60 °C, Hexane:AcOEt (1:1).

<sup>182</sup> K. A. R. Lund and A. Thompson, *Synlett.*, 2014, **25**, 1142–1144.



### 2.2.1. Mechanism of synthesis

Based on a report published by K. Burgess *et al*, in which it is described the synthesis of tetraheterocycles, our proposal for the mechanism is shown below (Scheme 2.5).<sup>183</sup>



Scheme 2.5. Mechanism of tetraheterocycles synthesis.

### 2.3. Crystal structure

A suitable crystal for X-ray diffraction of compound **152.HCl** was grown from solution in  $\text{CCl}_4$ , by slow evaporation at room temperature. Its solid-state structure

<sup>183</sup> L. Wu and K. Burgess, *Chem. Commun.*, 2008, 4933–4935.

determined by single crystal X-ray diffraction is shown in Figure 2.39. This tetraheterocycle displays an essentially planar skeleton. All carbon–carbon distances were found to be shorter than a single bond but larger than a double one, what highlights the  $\pi$ -electron delocalization in the molecule. All NH atoms were found interacting with the chloride anion through hydrogen bonds (N–H $\cdots$ Cl distances 3.18–3.21 Å), with N–H–Cl angles close to the linearity ( $\sim 165^\circ$ ). X-ray diffraction analyses is detailed in the CD.

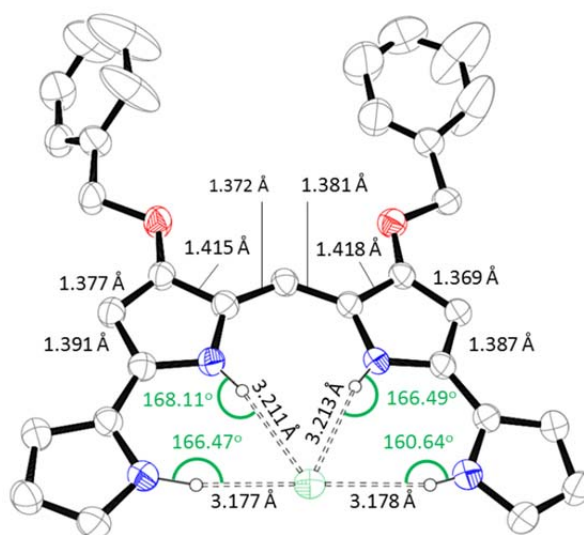


Figure 2.39. X-ray solid structure of **152**.HCl

#### 2.4. Determination of apparent pKa values

Following the procedure applied for tambjamins **136**.HCl, **142**.HCl and **144**.HCl (Section 1.4.2.2), the pKa values of the tetraheterocycles were calculated. 4:1 DMSO–H<sub>2</sub>O (v/v) (0.1 M NaCl) was used as solvent for these assays. Results are summarised in Table 2.9. Prodigiosin **8** and obatoclax **65** pKa values were also included for comparison purposes.

Table 2.9. Summary of pKa values. **147**, **148**, **152**, **153**, **8** and **65**

	pKa <sup>a</sup>
<b>147</b>	8.11
<b>148</b>	6.26
<b>152</b>	7.94
<b>153</b>	6.53
<b>8</b>	6.67
<b>65</b>	5.38

<sup>a</sup>  $5 \cdot 10^{-6}$  M solution in 4:1 DMSO–H<sub>2</sub>O (v/v) (0.1 M NaCl), at 25 °C

## 2.5. Anion transport assays

The ionophoric activity of these four tetraheterocycle compounds was tested in both, ISE and fluorescence vesicle based assays. The data for prodigiosin **8** and obatoclax **65** are also summarised along with those calculated for this new family for comparison purpose.

Their ability to exchange Cl<sup>-</sup>/NO<sub>3</sub><sup>-</sup>, Cl<sup>-</sup>/HCO<sub>3</sub><sup>-</sup>, Cl<sup>-</sup>/SO<sub>4</sub><sup>2-</sup> and Cl<sup>-</sup>/gluconate<sup>-</sup> was studied using the chloride selective electrode. Vesicles loaded with NaCl were suspended in isotonic solutions of different anions (for detailed procedures see Chapter IV). This set of tetraheterocycles presents similar trend to tambjamins regarding anion transport selectivity. The chloride rate decreases as a function of decreasing the lipophilicity of the external anion (NO<sub>3</sub><sup>-</sup> > HCO<sub>3</sub><sup>-</sup> > SO<sub>4</sub><sup>2-</sup> > gluconate<sup>-</sup>).

Interestingly, the chloride efflux when the external anion is sulfate or gluconate is not negligible for the most active compounds such as **147**.HCl. In Figure 2.40 and 2.41 it is shown the chloride efflux when 1 mol% (5 μM) carrier to POPC of **147**.HCl (above) and prodigiosin **8**.HCl (below) are added in aqueous solutions of NaCl loaded vesicles and different extravascular anions. With the obtained results, it seems that this tetraheterocycle displays better activity as anion carrier than the natural product prodigiosin **8**.HCl.

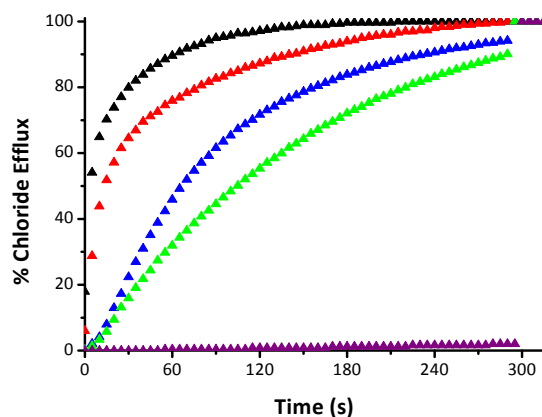


Figure 2.40. Chloride efflux upon addition of **147.HCl** (5  $\mu\text{M}$ , 1 mol%). Black trace:  $\text{NO}_3^-$  (NaCl loaded vesicles suspended in  $\text{NaNO}_3$ , both 489 mM, 5 mM  $\text{NaH}_2\text{PO}_4$  buffer, pH 7.2), red trace:  $\text{HCO}_3^-$  (NaCl 451 mM loaded vesicles suspended in  $\text{Na}_2\text{SO}_4$  150 mM with 40 mM  $\text{NaHCO}_3$  solution, both 20 mM  $\text{NaH}_2\text{PO}_4$  buffer, pH 7.2), blue trace:  $\text{SO}_4^{2-}$  (NaCl 451 mM loaded vesicles suspended in  $\text{Na}_2\text{SO}_4$  150 mM solution, both 20 mM  $\text{NaH}_2\text{PO}_4$  buffer, pH 7.2), green trace: gluconate $^-$  (NaCl 489 mM loaded vesicles suspended in NaGluconate 489 mM, both 5 mM  $\text{NaH}_2\text{PO}_4$  buffer, pH 7.2) and purple trace (blank, 10  $\mu\text{L}$  DMSO). Each trace represents the average of at least three different trials, done with at least two different batches of vesicles.

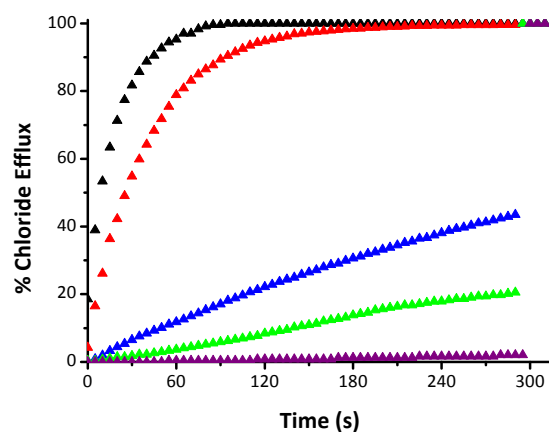


Figure 2.41. Chloride efflux upon addition of prodigiosin **8.HCl**. Black trace:  $\text{NO}_3^-$  (NaCl loaded vesicles suspended in  $\text{NaNO}_3$ , both 489 mM, 5 mM  $\text{NaH}_2\text{PO}_4$  buffer, pH 7.2), red trace:  $\text{HCO}_3^-$  (NaCl 451 mM loaded vesicles suspended in  $\text{Na}_2\text{SO}_4$  150 mM with 40 mM  $\text{NaHCO}_3$  solution, both 20 mM  $\text{NaH}_2\text{PO}_4$  buffer, pH 7.2), blue trace:  $\text{SO}_4^{2-}$  (NaCl 451 mM loaded vesicles suspended in  $\text{Na}_2\text{SO}_4$  150 mM solution, both 20 mM  $\text{NaH}_2\text{PO}_4$  buffer, pH 7.2), green trace: gluconate (NaCl 489 mM loaded vesicles suspended in NaGluconate 489 mM, both 5 mM  $\text{NaH}_2\text{PO}_4$  buffer, pH 7.2) and purple trace (blank, 10  $\mu\text{L}$  DMSO). Each trace represents the average of at least three different trials, done with at least two different batches of vesicles.

EC<sub>50</sub> values corresponding to the four tetraheterocycles were calculated with NaCl loaded vesicles and different anions in the external solution, with the chloride selective electrode. The obtained results are summarised in Table 2.10. Compound **153.HCl** were found to be a bad anion carrier due to its high lipophilicity value. **147.HCl**, **148.HCl**, **152.HCl** and **153.HCl** present excellent properties as anionophores, they display better activity than the natural product prodigiosin or its synthetic analog obatoclax in HCO<sub>3</sub><sup>-</sup>/Cl<sup>-</sup> assays. In the case of **147.HCl**, EC<sub>50</sub> values could be calculated even when the extravesicular anions were the highly hydrophilic sulfate and the large gluconate.

It could be concluded that the anion transport efficiency promoted by these compounds follow the Hofmeister series (NO<sub>3</sub><sup>-</sup> > HCO<sub>3</sub><sup>-</sup> > SO<sub>4</sub><sup>2-</sup> > gluconate) (Table 2.11).

Table 2.10. Summary of parameters recovered from ISE assays and lipophilicity. **147.HCl**, **148.HCl**, **152.HCl** and **153.HCl**

	EC <sub>50</sub> (nM) NO <sub>3</sub> <sup>-</sup> /Cl <sup>-</sup> <sup>a</sup>	EC <sub>50</sub> (nM) HCO <sub>3</sub> <sup>-</sup> /Cl <sup>-</sup> <sup>b</sup>	EC <sub>50</sub> (nM) SO <sub>4</sub> <sup>2-</sup> /Cl <sup>-</sup> <sup>c</sup>	EC <sub>50</sub> (nM) Gluconate <sup>-</sup> /Cl <sup>-</sup> <sup>d</sup>	ALOGPs <sup>e</sup>
<b>147.HCl</b>	1 ± 1	7 ± 1	605 ± 67	2415 ± 271	3.26
<b>148.HCl</b>	7 ± 1	109 ± 5	– <sup>f</sup>	– <sup>f</sup>	4.94
<b>152.HCl</b>	3 ± 1	44 ± 4	– <sup>f</sup>	– <sup>f</sup>	5.42
<b>153.HCl</b>	– <sup>f</sup>	– <sup>f</sup>	– <sup>f</sup>	– <sup>f</sup>	6.96
<b>65.HCl</b>	10 ± 1	448 ± 37	– <sup>g</sup>	– <sup>g</sup>	4.15
<b>8.HCl</b>	2 ± 1	58 ± 3	– <sup>g</sup>	– <sup>g</sup>	4.65

<sup>a</sup> Liposomes loaded with 489 mM NaCl suspended in 489 mM NaNO<sub>3</sub> (5 mM phosphate buffer, pH 7.2)

<sup>b</sup> Liposomes loaded with 451 mM NaCl suspended in 150 mM Na<sub>2</sub>SO<sub>4</sub> (20 mM phosphate buffer, pH 7.2). At t = 50 s addition of the anion carrier. At t = 60 s addition of a pulse of NaHCO<sub>3</sub> to achieve an extravesicular concentration of 40 mM.

<sup>c</sup> Liposomes loaded with 451 mM NaCl suspended in 150 mM Na<sub>2</sub>SO<sub>4</sub> (20 mM phosphate buffer, pH 7.2). At t = 60 s the anion carrier was added.

<sup>d</sup> Liposomes loaded with 489 mM NaCl suspended in 489 mM NaGluc. (5 mM phosphate buffer, pH 7.2)

<sup>e</sup> One of the lipophilicities calculated using e-dragon

<sup>f</sup> not determined because it could not be calculated

<sup>g</sup> not determined. It was not tried

Table 2.11. Gibbs free energy ( $\Delta G$ ) of some anions

	$\Delta G$ (KJ/mol) <sup>184</sup>
Chloride	-340
Bicarbonate	-355
Nitrate	-300
Sulfate	-1080
Gluconate <sup>a</sup>	–

<sup>a</sup> Value not found. It is highly hydrophilic and large

The ability of tetraheterocycles to form pores or channels in the lipid membrane could be a possible explanation for the high ionophoric activity displayed by some of them. This possibility was ruled out applying two different approaches.

The analysis of these compounds, with chloride selective electrode assays, in vesicles composed of 30% of cholesterol and 70% of POPC, showed a decrease in the transport activity, which is less pronounced for the most active compounds (Figure 2.42). The only tetraheterocycle to which the chloride efflux is higher for vesicles prepared with cholesterol is **152.HCl**. The difference between both traces, with and without cholesterol, is within the error. Although this test is not conclusive for determining a mechanism of transport, from these assays it could be concluded that the presence of cholesterol in the lipid membrane gives rise to a reduction in the chloride rate, what is consistent with a mobile carrier mechanism of action.

<sup>184</sup> Y. Marcus, *J. Chem. Soc. Faraday Trans.*, 1991, **87**, 2995–2999.

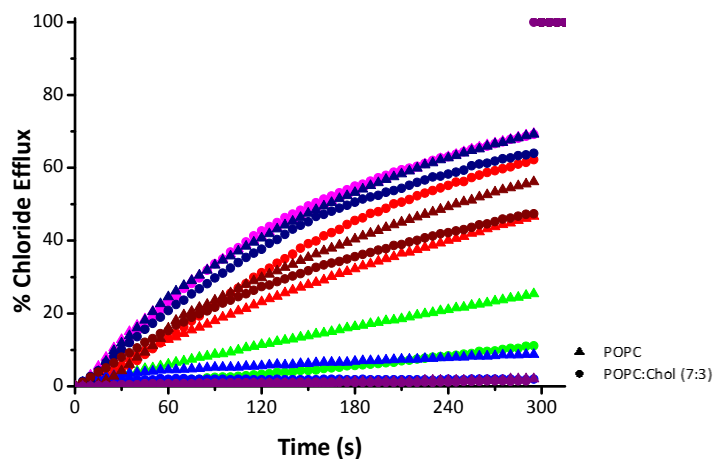


Figure 2.42. Chloride efflux upon addition of tetrahydrocyclohexene (**147**.HCl: 1.25 nM, 0.00025 mol%; **148**.HCl: 2.5 nM, 0.0005 mol%; **152**.HCl: 2.5 nM, 0.0005 mol%; **153**.HCl: 5  $\mu$ M, 1 mol%; prodigiosin **8**.HCl: 25 nM, 0.005 mol% and obatoclax **65**.HCl: 12.5 nM, 0.0025 mol% carrier to lipid) to vesicles composed of POPC (triangles) or POPC:cholesterol (7:3) (circles). Vesicles containing NaCl (489 mM NaCl and 5 mM phosphate buffer, pH 7.2) were immersed in NaNO<sub>3</sub> (489 mM NaNO<sub>3</sub> and 5 mM phosphate buffer, pH 7.2). At the end of the experiment, the vesicles were lysed with detergent to release all chloride ions and the resulting value was considered to represent 100% release and used as such. Each trace represents an average of at least three different experiments, done with at least two different batches of vesicles. Magenta trace: **147**.HCl, green trace: **148**.HCl, red trace: **152**.HCl, blue trace: **153**.HCl, navy trace: **8**.HCl, brown trace: **65**.HCl, purple trace: blank (10  $\mu$ L DMSO)

Regarding to the second approach, these four tetrahydrocyclohexene were subjected to the carboxyfluorescein leakage assay (full details of preparing and performing this assay in Chapter IV). None of them give rise to fluorescence changes until the moment in which a pulse of detergent was added ( $t = 360$  s) and consequently the carboxyfluorescein was released out the vesicles (Figure 2.43). This outcome supports the mobile carrier mechanism as the most plausible mechanism of transport.

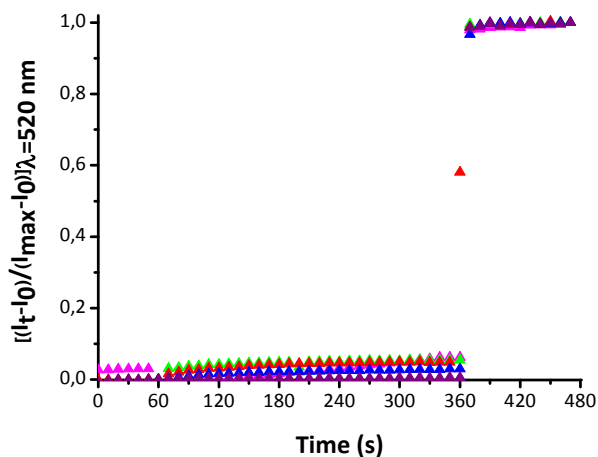


Figure 2.43. Carboxyfluorescein leakage upon addition of prodiginine inspired compounds to POPC vesicles, 0.05 mM. Vesicles contained NaCl (451 mM, buffered with  $\text{NaH}_2\text{PO}_4$  20 mM to pH 7.2, I.S. 500 mM and 50 mM CF) were suspended in  $\text{Na}_2\text{SO}_4$  (150 mM, buffered with  $\text{NaH}_2\text{PO}_4$  20 mM to pH 7.2, I.S. 500 mM). At  $t = 60$  s addition of the anion carrier (1 mol% carrier to lipid). At  $t = 360$  s addition of 20  $\mu\text{L}$  of detergent. Magenta trace: **147.HCl**, green trace: **148.HCl**, red trace: **152.HCl**, blue trace: **153.HCl**, purple trace: blank (10  $\mu\text{L}$  DMSO). Each trace represents the average of at least three different trials, done with at least two different batches of vesicles.

Chloride efflux to vesicles was also explored using the fluorescent probe lucigenin. This assay allows using small chloride gradients complementing the discussed ISE based experiments.

Lucigenin is a fluorescent probe which fluorescence emission is quenched selectively by halide ions (Figure 2.44. Left). When vesicles loaded with nitrate are suspended over a solution that contains chloride, the existence of a chloride influx could be measured as a function of time, by monitoring fluorescence quenching. A schematic representation of lucigenin assays is shown in (Figure 2.44. Right).

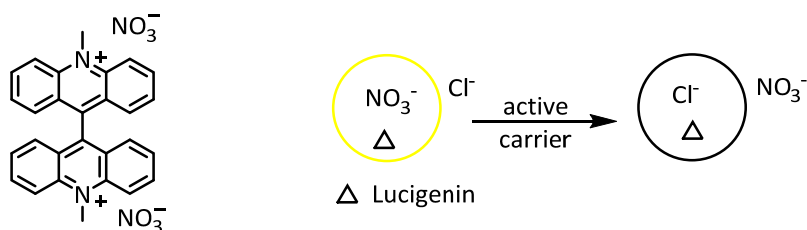


Figure 2.44. Left: lucigenin. Right: schematic representation of lucigenin transport assays

The fluorescence quenching of lucigenin follows a dynamic mechanism. The relationship between the quencher concentration and lucigenin fluorescence is described by the Stern-Volmer equation (equation 2.8).<sup>185</sup>

$$\frac{I_0}{I} = 1 + K_{SV} \cdot [Q] \quad \text{Eq. 2.8}$$

Where:

- $I_0$  is the maximum fluorescence (initial fluorescence, just before adding the anion carrier)
- $I$  is the quenched fluorescence (at each time)
- $K_{SV}$  is the Stern Volmer constant ( $M^{-1}$ )
- $[Q]$  is the quencher concentration (M); ( $Cl^-$  in this study)

The Stern Volmer constant was calculated for chloride under different experimental conditions (Table 2.12) (Experimental procedures are detailed in Chapter IV). Larger values of this constant imply higher ability of quenching the fluorescence. From data in Table 2.12, it could be concluded that lucigenin concentration does not affect the  $K_{SV}$  (Table 2.12. entry 1 compared to 2, 3 compared to 4 and 5 compared to 6). However, the ionic strength (I. S.) of the medium is determinant in the process of fluorescence quenching. At high concentration of electrolytes in solution, the fluorescence quenching efficiency becomes smaller because the probability of collision between the quencher and the dye decreases (Table 2.12; entries 5 and 6 compared to 1 and 2). This is why in lucigenin vesicles experiments the ionic strength is set to 150 mM (compared to 500 mM in ISE experiments).

<sup>185</sup> S. Jayaraman, A. S. Verkman, *Biophys. Chem.*, 2000, **85**, 49–57.

Table 2.12. Stern Volmer constant for chloride, calculated in different conditions

	$K_{SV} (M^{-1})$
1 <sup>a</sup>	184.0
2 <sup>b</sup>	190.2
3 <sup>c</sup>	217.1
4 <sup>d</sup>	206.5
5 <sup>e</sup>	81.8
6 <sup>f</sup>	78.0
7 <sup>186</sup>	174

<sup>a</sup> NaNO<sub>3</sub> 88.2 mM, phosphate buffer 5 mM, pH 7.2, I.S. 100 mM. Lucigenin 0.02 mM

<sup>b</sup> NaNO<sub>3</sub> 88.2 mM, phosphate buffer 5 mM, pH 7.2, I.S. 100 mM. Lucigenin 0.001 mM

<sup>c</sup> Na<sub>2</sub>SO<sub>4</sub> 17.6 mM, phosphate buffer 20 mM, pH 7.2, I.S. 100 mM. Lucigenin 0.02 mM

<sup>d</sup> Na<sub>2</sub>SO<sub>4</sub> 17.6 mM, phosphate buffer 20 mM, pH 7.2, I.S. 100 mM. Lucigenin 0.001 mM

<sup>e</sup> NaNO<sub>3</sub> 489 mM, phosphate buffer 5 mM, pH 7.2, I.S. 500 mM. Lucigenin 0.02 mM

<sup>f</sup> NaNO<sub>3</sub> 489 mM, phosphate buffer 5 mM, pH 7.2, I.S. 500 mM. Lucigenin 0.001 mM

Before performing lucigenin vesicle experiments, some considerations were taken into account. The stock solution of the anion carriers were prepared in MeOH instead of DMSO as done in the rest of assays, because DMSO quenches lucigenin fluorescence. The vesicles composition was changed to POPC:cholesterol (7:3) because measurements were found to be more robust than those carried out in pure POPC liposomes. To finish these experiments, some authors such as J. T. Davis and A. Schmitzer, add detergent at the end of the assay in order to determine the maximal chloride quenching of lucigenin.<sup>187, 188</sup> Others such as A. P. Davis, normalize the data to  $I_0/I$  or  $I/I_0$ .<sup>189</sup> In my opinion, adding detergent implies dilution of lucigenin. Therefore, the final fluorescence emission reading, independently of being more or less quenched, is going to introduce erroneous data.

POPC:cholesterol (7:3) vesicles were loaded with NaNO<sub>3</sub> (102.2 mM NaNO<sub>3</sub>, I.S. 150 mM, NaH<sub>2</sub>PO<sub>4</sub> 20 mM, pH 7.2; lucigenin 3 mM). The non-encapsulated solution was removed by size exclusion chromatography (SEC), using as mobile phase the nitrate solution. The obtained vesicles were suspended over NaNO<sub>3</sub> (102.2 mM NaNO<sub>3</sub>, I.S. 150 mM, NaH<sub>2</sub>PO<sub>4</sub> 20 mM, pH 7.2). At the beginning of the experiment, a

<sup>186</sup> C. Huber, K. Fährnich, C. Krause and T. Werner, *J. Photochem. Photobiol. A*, 1999, **128**, 111–120.

<sup>187</sup> S. Rastogi, E. Marchal, I. Uddin, B. Groves, J. Colpitts, S. A. McFarland, J. T. Davis and A. Thompson, *Org. Biomol. Chem.*, 2013, **11**, 3834–3845.

<sup>188</sup> M. Vidal and A. Schmitzer, *Chem. Eur. J.*, 2014, **20**, 9998–10004.

<sup>189</sup> P. R. Brotherhood and A. P. Davis, *Chem. Soc. Rev.*, 2010, **39**, 3633–3647.

pulse of NaCl was added in order to obtain a final concentration of 10 mM in the sample. After one minute the tetraheterocycle analog was added and the fluorescence decrease was monitored over time during five more minutes (vesicles preparation and experimental procedure are detailed in Chapter IV).

In the first stage of this research, it was found that when the anion carrier was added ( $t = 60$  s), sometimes, a decrease in fluorescence was observed even for no active compounds. Some experiments detailed in next section (Prodiginine inspired compounds) were carried out in order to shed light about the origin of this behaviour.

In order to figure out the origin of this quenching, the absorption and emission spectra of all compounds involved in these assays were measured using as a medium the nitrate solution 102.2 mM (Figure 2.45 and 2.46; prodiginosin and obatoclax spectra are shown in Figure 2.92). It was observed that the fluorescence emission spectrum of lucigenin (Figure 2.47) was overlapped with the absorption spectra of all carriers.

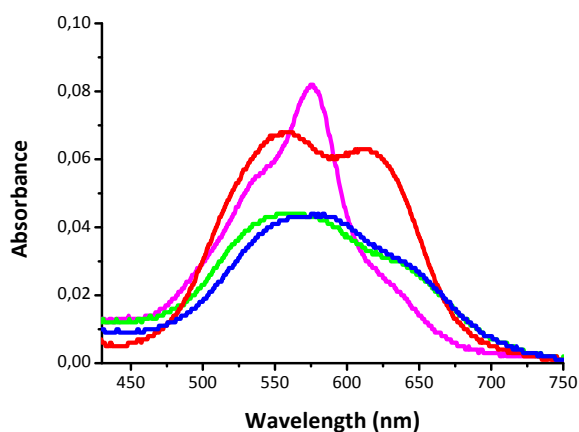


Figure 2.45. Absorption spectra of tetraheterocycles ( $1.2 \mu\text{M}$ ).  $\text{NaNO}_3$  (102.2 mM  $\text{NaNO}_3$ , I.S. 150 mM,  $\text{NaH}_2\text{PO}_4$  20 mM, pH 7.2). Magenta trace: **147.HCl**, green trace: **148.HCl**, red trace: **152.HCl**, blue trace: **153.HCl**.

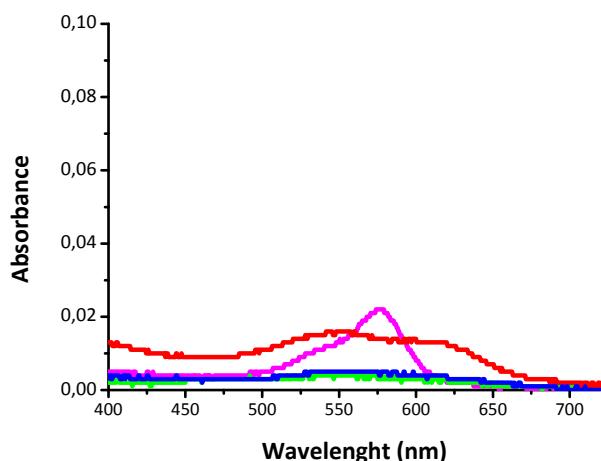


Figure 2.46. Absorption spectra of tetraheterocycles (250 nM).  $\text{NaNO}_3$  (102.2 mM  $\text{NaNO}_3$ , I.S. 150 mM,  $\text{NaH}_2\text{PO}_4$  20 mM, pH 7.2). Magenta trace: **147.HCl**, green trace: **148.HCl**, red trace: **152.HCl**, blue trace: **153.HCl**.

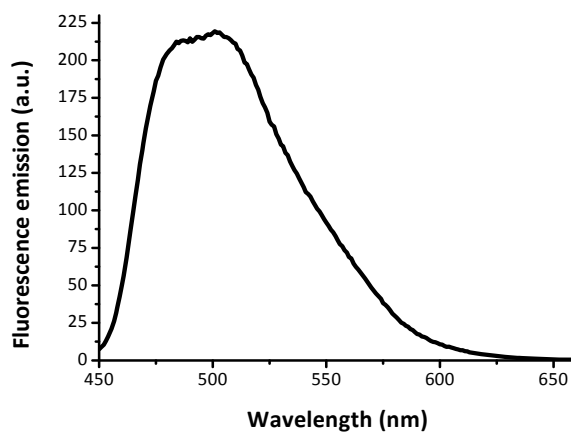


Figure 2.47. Lucigenin 0.002 mM emission spectrum.

Under these conditions, the compounds are able to partially absorb the fluorescence emitted by lucigenin. Consequently, a decrease in fluorescence non-related with anion transport was observed (the higher the anion carrier concentration, the larger the decrease in fluorescence observed) (Figure 2.48). This problem could be minimised by working at low concentrations of anion carriers so their absorbance were negligible. If needed, it is possible to work at higher carrier loadings by diminishing the total lipid concentration, thus the absolute concentration of anionophore studied remains in the appropriate range.

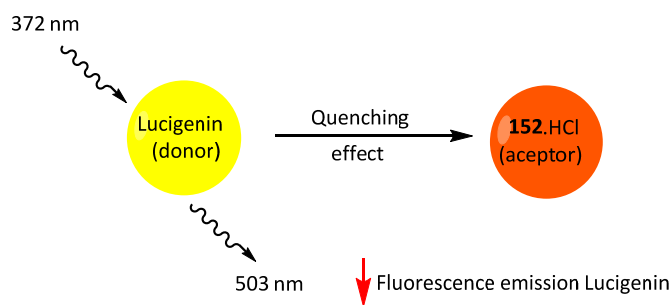


Figure 2.48. Schematic representation of the quenching effect.

Once the quenching problem was solved, lucigenin assays were performed at 0.014 mol% (50 nM) for all these compounds. The enhancement of the internal chloride concentration, quenched the lucigenin, thus it was observed as a decrease in fluorescence (Figure 2.49).

The obtained results were normalised to  $I_0/I$  and were plotted against time. These data were analysed to obtain initial rates ( $I$ ) and half-times ( $t_{1/2}$ ).

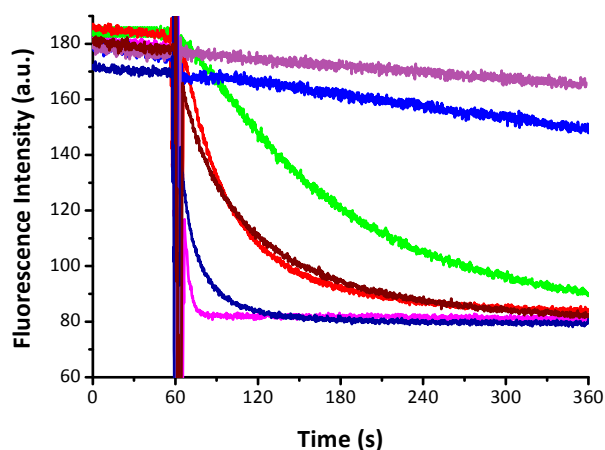


Figure 2.49. Crude fluorescence data of lucigenin assay upon addition of tetraheterocycles, prodigiosin and obatoclax to POPC:Cholesterol (7:3) vesicles, 0.35 mM POPC. Vesicles contained  $\text{NaNO}_3$  (102.2 mM  $\text{NaNO}_3$ , I.S. 150 mM,  $\text{NaH}_2\text{PO}_4$  20 mM, pH 7.2; lucigenin 3 mM) were suspended in  $\text{NaNO}_3$  (102.2 mM  $\text{NaNO}_3$ , I.S. 150 mM,  $\text{NaH}_2\text{PO}_4$  20 mM, pH 7.2). At  $t = 0$  s was added a pulse of  $\text{NaCl}$  to obtain a final concentration of 10 mM. At  $t = 60$  s the anion carrier was added (0.014 mol% carrier to lipid; 50 nM). Magenta trace: **147.HCl**, green trace: **148.HCl**, red trace: **152.HCl**, blue trace: **153.HCl**, navy trace: prodigiosin **8.HCl**, brown trace: obatoclax **65.HCl** and purple trace: blank (10  $\mu\text{L}$  MeOH). Each trace represents the average of at least three different trials, done with at least two different batches of vesicles.

The corresponding normalizations of chloride efflux or influx (% chloride efflux in ISE assays,  $I_0/I$  in lucigenin assays, etc.) traces present a growing exponential behaviour. In the literature, it is possible to find different exponential equations used for the quantification of initial rates of chloride. Equation 2.9 has been used by us to calculate the initial chloride efflux in a set of tambjamine analogs and it was also employed by Gale *et al* in a family of thioureas.<sup>190, 191</sup> Equations 2.11 and 2.12 were used by Gale and Davis to determine half-life times and initial rates respectively for other type of anion carriers.<sup>192, 193, 194</sup> They did not apply Equation 2.11 to figure out initial efflux, but is perfectly valid to this approach.

**Analysis of models used in bibliography for quantifying initial rates.**

$$y = a - b \cdot c^x \quad \text{Eq. 2.9}$$

$$y = 1 - e^{-k \cdot x} \quad \text{Eq. 2.10}$$

$$y = a - b \cdot e^{-c \cdot x} \quad \text{Eq. 2.11}$$

$$y = a - b \cdot e^{-c \cdot x} - d \cdot e^{-f \cdot x} \quad \text{Eq. 2.12}$$

The first derivative of a function at a point  $x$ , is the slope of the tangent line to the function at this point. Therefore, the initial rate is determined by the first derivative of each curve (equations 2.9–2.12) at  $x = 0$  (equations 2.13–2.16), where  $y$  is the chloride rate (%  $I_0/I$ , etc.) and  $x$  is the time (s).

$$y = a - b \cdot c^x$$

$$\frac{dy}{dx} = 0 - (0 \cdot c^x + b \cdot c^x \cdot \ln(c)) \quad \Rightarrow \quad \left( \frac{dy}{dx} \right)_{x=0} = -b \cdot \ln(c) \quad \text{Eq. 2.13}$$

<sup>190</sup> N. J. Knight, E. Hernando, C. J. E. Haynes, N. Busschaert, H. J. Clarke, K. Takimoto, M. García-Valverde, J. G. Frey, R. Quesada and P. A. Gale, *Chem. Sci.*, 2016, **7**, 1600–1608.

<sup>191</sup> N. Busschaert, S. J. Bradberry, M. Wenzel, C. J. E. Haynes, J. R. Hiscock, I. L. Kirby, L. E. Karagiannidis, S. J. Moore, N. J. Wells, J. Herniman, G. J. Langley, P. N. Horton, M. E. Light, I. Marques, P. J. Costa, V. Félix, J. G. Frey and P. A. Gale, *Chem. Sci.*, 2013, **4**, 3036–3045.

<sup>192</sup> H. Valkenier, L. W. Judd, H. Li, S. Hussain, D. N. Sheppard and A. P. Davis, *J. Am. Chem. Soc.*, 2014, **136**, 12507–12512.

<sup>193</sup> H. Valkenier, C. J. E. Haynes, J. Herniman, P. A. Gale and A. P. Davis, *Chem. Sci.*, 2014, **5**, 1128–1134.

<sup>194</sup> H. Valkenier, N. López-Mora, A. Kros and A. P. Davis, *Angew. Chem. Int. Ed.*, 2015, **54**, 2137–2141.

$$y = 1 - e^{-Kx}$$

$$\frac{dy}{dx} = 0 - (-K \cdot e^{-Kx}) \quad \Rightarrow \quad \left( \frac{dy}{dx} \right)_{x=0} = K \quad \text{Eq. 2.14}$$

$$y = a - b \cdot e^{-cx}$$

$$\frac{dy}{dx} = 0 - (0 \cdot e^{-cx} + b \cdot (-c) \cdot e^{-cx}) \quad \Rightarrow \quad \left( \frac{dy}{dx} \right)_{x=0} = b \cdot c \quad \text{Eq. 2.15}$$

$$y = a - b \cdot e^{-cx} - d \cdot e^{-fx}$$

$$\frac{dy}{dx} = 0 - (0 \cdot e^{-cx} + b \cdot (-c) \cdot e^{-cx}) - (0 \cdot e^{-fx} + d \cdot (-f) \cdot e^{-fx}) \quad \Rightarrow$$

$$\Rightarrow \left( \frac{dy}{dx} \right)_{x=0} = b \cdot c + d \cdot f \quad \text{Eq. 2.16}$$

Although, these equations (equations 2.9–2.12) fit the same curves, some differences could be observed in their form and in their first derivatives. The first three consist of two terms, meanwhile the last one consists of three. The base of the functions could be a natural number or the irrational number  $e$ . The exponent can be positive or negative and it could contain a constant or not. In order to figure out the meaning of each term, an analysis of these exponential equations has been carried out.

Starting with the simplest situation  $y = c^x$ ,  $c$  is the base. It never adopts negative values because otherwise the function is meaningless. If it is 0 the result will be 0 and if it is 1 the function is going to be constant. The values that give sense to this equation are:

- $0 < c < 1$ . This is a decreasing function (Figure 2.50. Black trace).
- $c > 1$ . This is an increasing function. (Figure 2.50. Red trace).

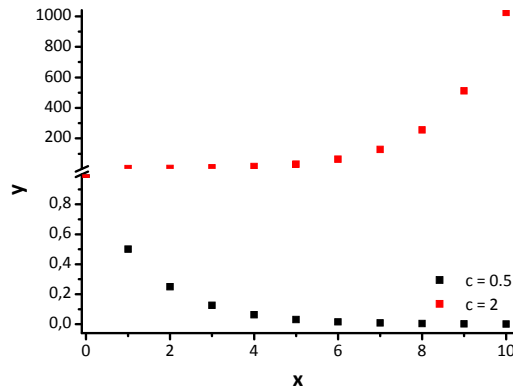


Figure 2.50. Simulation of  $y = c^x$ , where  $x$  (0–10) and  $c$  is fixed to 0.5 (black trace) or 2 (red trace)

The function can be enlarged by adding a parameter multiplying the base. It is expressed as  $y = b \cdot c^x$ , where  $b$  makes reference to the position at which the curve cuts the axis  $y$ .

- $b > 0$ . When  $b$  is higher than zero, for example 5, the plot cuts the axis  $y$  at 5. The growing or decreasing trend will depend on the value of  $c$  (Figure 2.51).
- $b < 0$ . On the contrary, if  $b$  is a negative number for example -5, the curve cuts the axis  $y$  at -5 and the tendency of the function is inverted by the presence of the negative sign (Figure 2.52). Taking into account that equations from 2.9 to 2.12 display this feature:

- If  $0 < c < 1$  the function will be growing. This function **presents the curve form displayed by our data** (Figure 2.52, black trace).
- If  $c > 1$  the function will be decreasing.

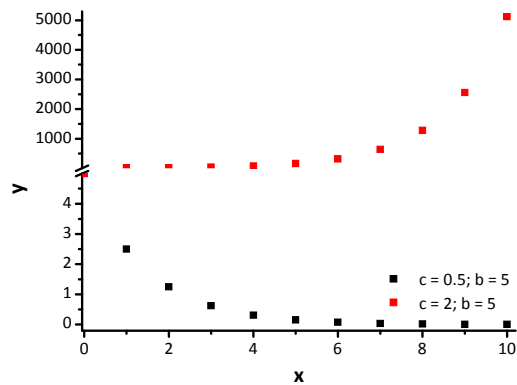


Figure 2.51. Simulation of  $y = b \cdot c^x$ , where  $x$  (0–10):  $b$  is fixed to 5 and  $c$  could be 0.5 (black trace) or 2 (red trace).

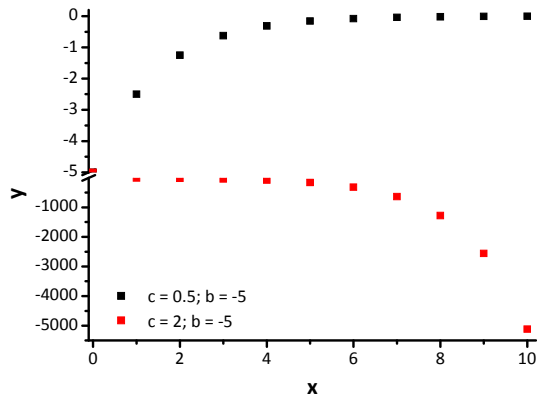


Figure 2.52. Simulation of  $y = b \cdot c^x$ , where  $x$  (0–10):  $b$  is fixed to  $-5$  and  $c$  could be  $0.5$  (black trace) or  $2$  (red trace).

Taking into account the magnitude of our transport data, from 0 to 100 in ISE assays or from 1 to  $\sim 2.2$  in lucigenin assays, the parameter  $b$  gives an indication of the amplitude of the data.

An extra parameter  $a$ , should be added to obtain equation 2.9. The values adopted by  $a$  are related to  $b$ . The purpose of this new term seems to be maintaining the amplitude of the data, but pointing the cut with the  $y$  axis at 0 for ISE obtained traces or at 1 for lucigenin assay data. A simulation of this function, with the same form as our transport data, is shown in Figure 2.53.

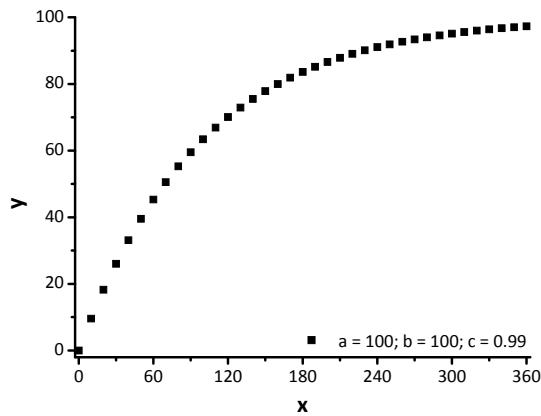


Figure 2.53. Simulation of  $y = a - b \cdot c^x$ , where  $x$  (0–360).  $a$  and  $b$  are fixed to 100 and  $c$  is fixed to 0.99

Extrapolating this analysis to models in which the base ( $c$ ) is the irrational number  $e$ , let a better understanding of equations 2.10–2.12. Equation 2.10 displays a similar form as equation 2.9 in which  $a = 1$ ,  $b = 1$  and the base  $c$  is the number  $e$ . The reasons why in the exponent of the new equation appears a constant,  $K$ , and a minus sign are related with the value of the base ( $e = 2.718281828$ ). Being a number higher than one, the tendency of the growth is reverted. In order to avoid this turning of the trend, a negative sign appears in the exponent. The existence of the constant  $K$  refers to the speed of the growing. In its absence ( $y = 1 - e^{-x}$ ), the function achieves its maximum value (1) when  $x$  is 5. Taking into account that our transport data present  $x$  values from 0 to 360 s, this model without  $K$  is not useful. This constant represents the initial rate ( $s^{-1}$ ).

This equation (equation 2.10) can be used when the transport is given from 0 to 1, otherwise it is not able to fit the data. In Figure 2.54 there are shown two simulations of equation 2.10 behaviour.

$$y = a - b \cdot c^x \quad \text{Eq. 2.9}$$

$$y = 1 - 1 \cdot e^{-Kx} \quad \text{Eq. 2.10}$$

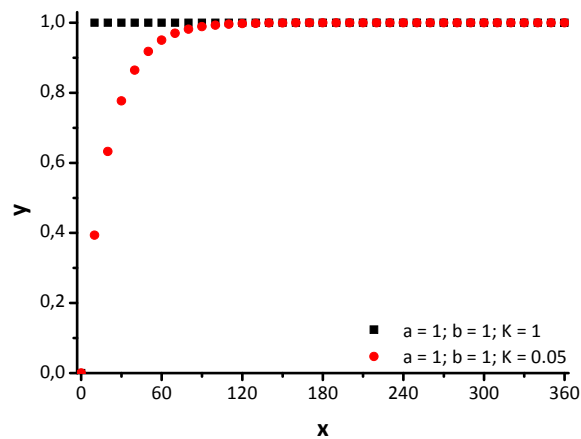


Figure 2.54. Simulation of  $y = 1 - e^{-Kx}$ , where  $x$  (0–360).  $a$  and  $b$  are 1 in this model. Black trace  $K = 1$ , red trace  $K = 0.05$ .

Equation 2.11 is the same as equation 2.10 with  $a$  and  $b$  free for iterating. During the fitting process, they both take similar values and in turn related with the asymptotic value. The advantage of equation 2.11 versus equation 2.10 comes from

the no restriction of  $a$  and  $b$ , therefore it could be applied when the chloride efflux is given from 0 to 1, from 0 to 100 or from 1 to 2.2 (lucigenin assays).

$$y = 1 - e^{-kx} \quad \text{Eq. 2.10}$$

$$y = a - b \cdot e^{-cx} \quad \text{Eq. 2.11}$$

Finally, the most complex model (equation 2.12) is an enlarged of equation 2.11. The third term refers to other decay processes that can take place during the transport assay such as intersystem crossing, collisional quenching, etc.<sup>195</sup> Due to its form, not all traces can be fitted when it is applied.

$$y = a - b \cdot e^{-cx} \quad \text{Eq. 2.11}$$

$$y = a - b \cdot e^{-cx} - d \cdot e^{-fx} \quad \text{Eq. 2.12}$$

Another parameter that can be determined by analysing transport traces is the half-time. Gale and Davis, have applied the single exponential decay model (equation 2.11) to quantify it. In order to do that it should be noticed that when  $x = x_{1/2}$ ,  $y = a - (1/2) \cdot b$ , where  $x$  is the time.<sup>196, 197</sup>

$$y = a - b \cdot e^{-cx} \quad \text{Eq. 2.11}$$

$$x = x_{1/2} \rightarrow y = a - \frac{b}{2}$$

$$x_{1/2} = \frac{\text{Ln}(2)}{c}$$

$$t_{1/2} = \frac{\text{Ln}(2)}{c} \quad \text{Eq. 2.17}$$

Once the assay was optimised to avoid the influence of the absorption of these derivatives the transport assays were carried out.

Obtained results were normalised to  $I_0/I$  and plotted against time (Figure 2.55). The initial rate and approximated half-times ( $t_{1/2}$ ) were quantified when possible (Table 2.13).

<sup>195</sup> <http://www.fluortools.com/software/decayfit/documentation/models> (accessed March 2017)

<sup>196</sup> M. Lisbjerg, H. Valkenier, B. M. Jessen, H. Al-Kerdi, A. P. Davis and M. Pittelkow, *J. Am. Chem. Soc.*, 2015, **137**, 4948–4951.

<sup>197</sup> H. Valkenier, C. J. E. Haynes, J. Herniman, P. A. Gale and A. P. Davis, *Chem. Sci.*, 2014, **5**, 1128–1134.

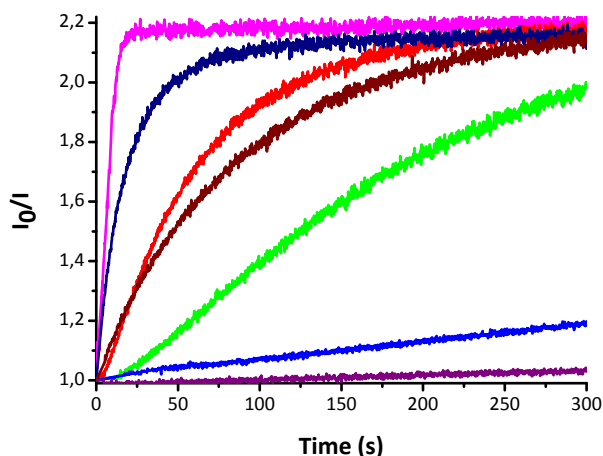


Figure 2.55.  $I_0/I$  normalization of lucigenin fluorescence emission upon addition of tetraheterocycles, prodigiosin and obatoclax to POPC:Cholesterol (7:3) vesicles, 0.35 mM POPC. Vesicles contained  $\text{NaNO}_3$  (102.2 mM  $\text{NaNO}_3$ , I.S. 150 mM,  $\text{NaH}_2\text{PO}_4$  20 mM, pH 7.2; lucigenin 3 mM) were suspended in  $\text{NaNO}_3$  (102.2 mM  $\text{NaNO}_3$ , I.S. 150 mM,  $\text{NaH}_2\text{PO}_4$  20 mM, pH 7.2). At  $t = 0$  s was added a pulse of NaCl to obtain a final concentration of 10 mM. At  $t = 60$  s the anion carrier was added (0.014 mol% carrier to lipid; 50 nM). Magenta trace: **147.HCl**, green trace: **148.HCl**, red trace: **152.HCl**, blue trace: **153.HCl**, navy trace: prodigiosin **8.HCl**, brown trace: obatoclax **65.HCl** and purple trace: blank (10  $\mu\text{L}$  MeOH). Each trace represents the average of at least three different trials, done with at least two different batches of vesicles.

Table 2.13. Obtained results from analysis of fluorescence decays, and lipophilicities. **147.HCl**, **148.HCl**, **152.HCl**, **153.HCl**, prodigiosin **8.HCl** and obatoclax **65.HCl**

	$t_{1/2}$ (s) <sup>a</sup>	$I$ ( $\text{s}^{-1}$ ) <sup>b</sup>	$I$ ( $\text{s}^{-1}$ ) <sup>c</sup>	$I$ ( $\text{s}^{-1}$ ) <sup>d</sup>	ALOGPs <sup>e</sup>
<b>147.HCl</b>	4.9	0.1941	0.1940	0.1963	3.26
<b>148.HCl</b>	218.0	0.0055	0.0055	0.0002	4.94
<b>152.HCl</b>	43.8	0.0198	0.0198	0.0202	5.42
<b>153.HCl</b>	3745.0	0.0006	0.0006	0.0020 <sup>f</sup>	6.96
<b>8.HCl</b>	15.4	0.0479	0.0479	0.0643	4.65
<b>65.HCl</b>	62.6	0.0128	0.0128	0.0156	4.15

<sup>a</sup> Eq. 2.17. Data fitted to eq. 2.11. Single exponential decay function

<sup>b</sup> Eq. 2.13. Data fitted to eq. 2.9. Asymptotic exponential function

<sup>c</sup> Eq. 2.15. Data fitted to eq. 2.11. Single exponential decay function

<sup>d</sup> Eq. 2.16. Data fitted to eq. 2.12. Double exponential decay function

<sup>e</sup> One of the lipophilicities calculated using e-dragon

<sup>f</sup> If it were fitted to a lineal function, the result is  $0.0006 \text{ s}^{-1}$ .

The obtained results are comparable with those obtained with the chloride selective electrode. It is detected again the impressive ionophoric activity of **147.HCl**. Its initial rates and half-life time are one order of magnitude better than the corresponding to prodigiosin, **8.HCl**. Even **152.HCl** presents better properties as anion carrier than this tripyrrolic red pigment. **153.HCl** displays the lower level of transport activity among the compounds belonging to this family, probably due to its large lipophilicity. With regard to the function applied for fitting the curves, results obtained from equations 2.13 and 2.15 differ from the calculated with equation 2.16. These differences are bigger for traces that represent a medium or low activity.

All these compounds were tested in vesicles assays with the fluorescent probe safranin O in order to check their ability to alter the membrane potential. The wavelength at which the fluorescence should be recorded is 580 nm. At this point, the tetraheterocycles absorbance is maximum (Figure 2.45).

The existence of quenching at 250 nM (0.1 mol%) was confirmed experimentally. The effect of adding **147.HCl**, **148.HCl**, **152.HCl** and **153.HCl** at 250 nM or 25 nM over a sample of safranin O 0.2  $\mu\text{M}$ , in absence of vesicles, was checked. The fluorescence was measured at 580 nm, after excitation at 520 nm during 720 s (Figure 2.56 and 2.57).

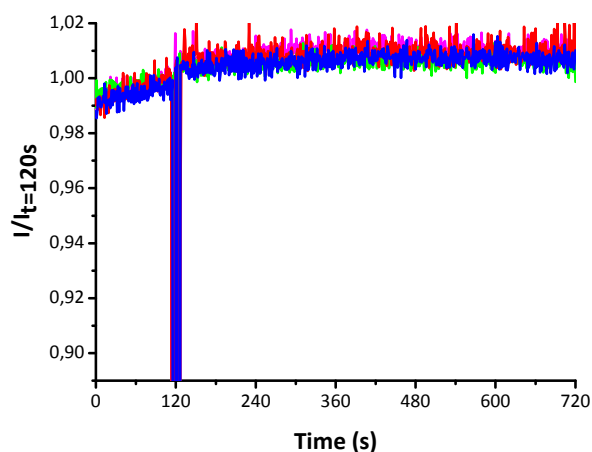


Figure 2.56. Effect of adding **147.HCl**, **148.HCl**, **152.HCl**, **153.HCl** (25 nM), at  $t = 60$  s, over 0.2  $\mu\text{M}$  of safranin O in  $\text{Na}_2\text{SO}_4$  (9.6 mM, buffered with  $\text{NaH}_2\text{PO}_4$ , 5 mM to pH 7.2, I.S. 40 mM). Magenta trace: **147.HCl**, green trace: **148.HCl**, red trace: **152.HCl** and blue trace: **153.HCl**. Each trace represents the average of at least three different trials.

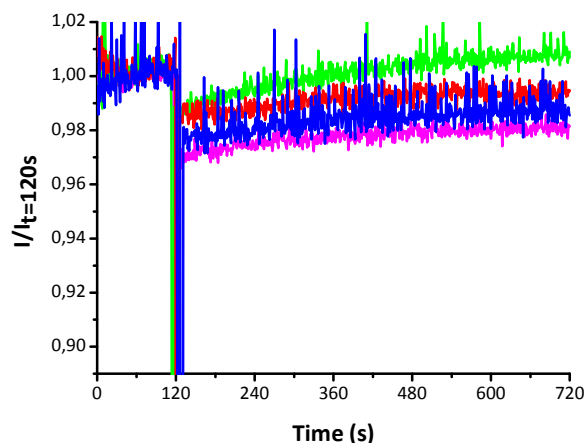


Figure 2.57. Effect of adding **147.HCl**, **148.HCl**, **152.HCl**, **153.HCl** (250 nM), at  $t = 60$  s, over  $0.2 \mu\text{M}$  of safranin O in  $\text{Na}_2\text{SO}_4$  (9.6 mM, buffered with  $\text{NaH}_2\text{PO}_4$ , 5 mM to pH 7.2, I.S. 40 mM). Magenta trace: **147.HCl**, green trace: **148.HCl**, red trace: **152.HCl** and blue trace: **153.HCl**. Each trace represents the average of at least three different trials.

After these considerations, the experiments were performed. Vesicles were loaded with NaCl (28.8 mM, buffered with  $\text{NaH}_2\text{PO}_4$  5 mM to pH 7.2, I.S. 40 mM) and suspended in a  $\text{Na}_2\text{SO}_4$  solution (9.6 mM, buffered with  $\text{NaH}_2\text{PO}_4$ , 5 mM to pH 7.2, I.S. 40 mM). A pulse of safranin O to achieve a concentration of  $0.2 \mu\text{M}$  in the assay was added. At  $t = 120$  s the anion carrier was incorporated and the fluorescence of the dye at 580 nm after excitation at 520 nm was recorded over time (full details of how performing these experiments are provided in Chapter IV).

Figure 2.58 shows the effect of adding these carriers at 0.01 mol%. The observed trend does not follow the order of ionophoric activity displayed in ISE or lucigenin assays. Now **152.HCl** is less active than **148.HCl**. Surprisingly, when these transporters were added at 0.1 mol% (Figure 2.59), the results were unexpected, it was observed an increase of fluorescence. For the less active compounds **148.HCl** and **153.HCl** the quenching of fluorescence, when they were added, could be detected. On the contrary, **147.HCl** and **152.HCl** display a faster response and the quenching was not detected. In ISE assays, was showed that these compounds seem to be able to exchange  $\text{Cl}^-/\text{SO}_4^{2-}$ .

It seems that **147.HCl** has achieved and asymptotic value, rather it is slightly decreasing. If the experiment were longer, maybe it was observed the same trend for **152.HCl** and even for **148.HCl**.

At this stage of the study, it is unclear the behaviour of this family of compounds under these conditions.

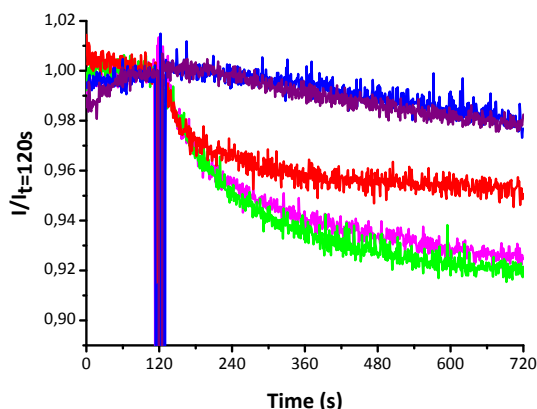


Figure 2.58. Membrane polarization upon addition of tetraheterocycles to POPC vesicles, 0.25 mM. Vesicles contained NaCl (28.8 mM, buffered with  $\text{NaH}_2\text{PO}_4$  5 mM to pH 7.2, I.S. 40 mM) were suspended in  $\text{Na}_2\text{SO}_4$  (9.6 mM, buffered with  $\text{NaH}_2\text{PO}_4$  5 mM to pH 7.2, I.S. 40 mM, and 0.2  $\mu\text{M}$  S.O). At  $t = 120$  s addition of the anion carrier (0.01 mol% carrier to lipid). Megenta trace: **147.HCl**, green trace: **148.HCl**, red trace: **152.HCl**, blue trace: **153.HCl** and purple trace: blank (10  $\mu\text{L}$  DMSO). Each trace represents the average of at least three different trials, done with at least two different batches of vesicles.

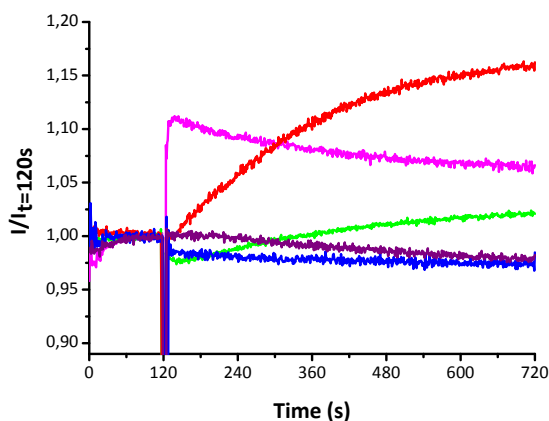


Figure 2.59. Membrane polarization upon addition of tetraheterocycles to POPC vesicles, 0.25 mM. Vesicles contained NaCl (28.8 mM, buffered with  $\text{NaH}_2\text{PO}_4$  5 mM to pH 7.2, I.S. 40 mM) were suspended in  $\text{Na}_2\text{SO}_4$  (9.6 mM, buffered with  $\text{NaH}_2\text{PO}_4$  5 mM to pH 7.2, I.S. 40 mM, and 0.2  $\mu\text{M}$  S.O). At  $t = 120$  s addition of the anion carrier (0.1 mol% carrier to lipid). Megenta trace: **147.HCl**, green trace: **148.HCl**, red trace: **152.HCl**, blue trace: **153.HCl** and purple trace: blank (10  $\mu\text{L}$  DMSO). Each trace represents the average of at least three different trials, done with at least two different batches of vesicles.

The HPTS fluorescence assay was also employed to explore the ability of these compounds to compensate pH gradients.

The protonated and deprotonated forms of this dye exhibit different absorption wavelengths, meanwhile both emit at the same position of the electromagnetic spectrum (Figure 2.60). Using a calibration, the relationship between the fluorescence intensity at 510 nm when the sample was excited at both 460 and 403 nm allows determining the internal pH, at a time.

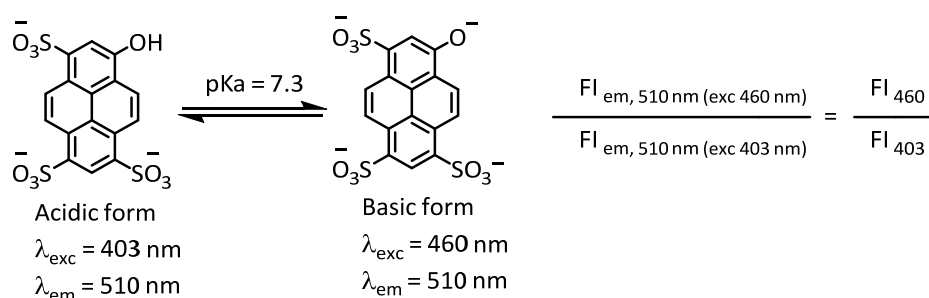


Figure 2.60. HPTS

The pH change promoted by addition of a NaOH pulse was first measured using a pHmeter under the experimental conditions. It was found to be from 7.22 to 8.17. The calibration of the dye was carried out using 15 nM HPTS and adding consecutive aliquots of NaOH 0.5 M to a solution so the pH is raised from 5.5 to 9.5. After each addition, the fluorescence rate was recorded.

Different calibrations can be found in the literature. Using a S-logistic model,<sup>198</sup> lineal equations<sup>199, 200</sup> or determining a rate  $[FI (\%) = (I - I_0)/(I_{total} - I_0) \times 100]$  from the initial  $I_0$  and final  $I_{total}$  fluorescence emissions.<sup>201</sup>

Performing a calibration applying a linear model, implies disregard pH data from 5.5 to 7.2 and 8.2 to 9.5. Thus, the information at the beginning and at the end of the experiment would be lost. Transforming the data into rates could be useful, but it does not exploit the HPTS potential of determining pH changes. We have decided to fit the data to an S-Logistic model (Figure 2.61) and a fifth polynomial grade

<sup>198</sup> N. Busschaert, P. A. Gale, C. J. E. Haynes, M. E. Light, S. J. Moore, C. C. Tong, J. T. Davis and W. A. Harrell, Jr., *Chem. Commun.*, 2010, **46**, 6252–6254.

<sup>199</sup> V. Sidorov, F. W. Kotch, G. Abdrakhmanova, R. Mizani, J. C. Fettinger and J. T. Davis, *J. Am. Chem. Soc.*, 2002, **124**, 2267–2278

<sup>200</sup> V. Sidorov, F. W. Kotch, J. L. Kuebler, Y.-F. Lam and J. T. Davis, *J. Am. Chem. Soc.*, 2003, **125**, 2840–2841.

<sup>201</sup> C.-C. Peng, M.-J. Zhang, X.-X. Sun, X.-J. Cai, Y. Chen and W.-H. Chen, *Org. Biomol. Chem.*, 2016, **14**, 8232–8236.

equation (Figure 2.62). Both adjustments display  $R^2 \text{ adj} > 0.99$ . The reason why the polynomial equation was used, is because at the beginning of the experiments, pH data obtained with this model are more similar to the pHmeter ones.

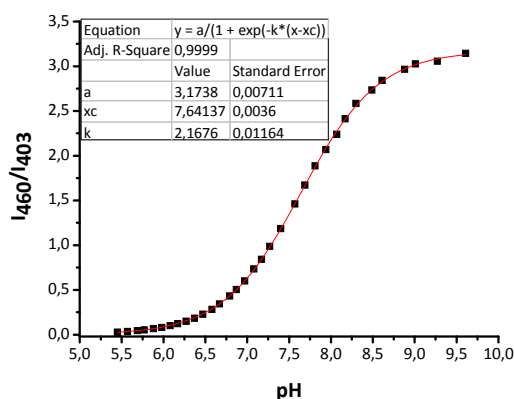


Figure 2.61. HPTS calibration. S-Logistic1 model.

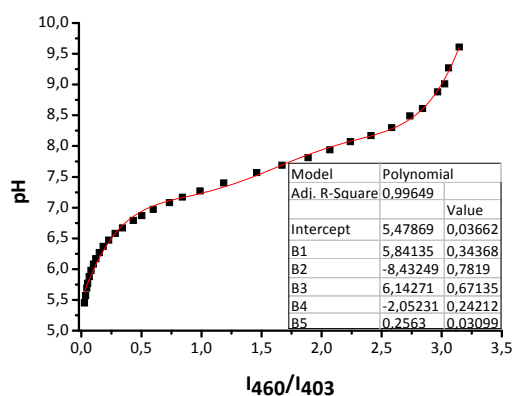


Figure 2.62. HPTS calibration. Fifth polynomial grade equation.

Regarding how to finish the assays, some authors such as A. Schmitzer<sup>202</sup> and W. H. Chen<sup>203</sup> add certain amount of detergent at the end of the experiments. Others such as P. A. Gale has reported both situations, adding detergent<sup>204</sup> or not.<sup>205</sup> In my opinion, the addition of detergent bias the results. I have observed that the final

<sup>202</sup> C.-R. Elie, M. Charbonneau and A. R. Schmitzer, *Med. Chem. Commun.*, 2012, **3**, 1231–1234.

<sup>203</sup> C.-C. Peng, Z. Li, L.-Q. Deng, Z. F. Ke, W.-H. Chen, *Bioorg. Med. Chem. Lett.*, 2016, **26**, 2442–2445.

<sup>204</sup> N. Busschaert, M. Wenzel, M. E. Light, P. Iglesias-Hernández, R. Pérez-Tomás and P. A. Gale, *J. Am. Chem. Soc.*, 2011, **133**, 14136–14148

<sup>205</sup> S. J. Moore, M. Wenzel, M. E. Light, R. Morley, S. J. Bradberry, P. Gómez-Iglesias, V. Soto-Cerrato, R. Pérez-Tomás, and P. A. Gale, *Chem. Sci.*, 2012, **3**, 2501-2509.

fluorescence after adding detergent varies randomly. For this reason, I did not add detergent at the end of the experiments.

After optimizing to avoid the influence from the absorption of these compounds at the working concentrations (0.01 mol% and 0.0001 mol%; Figures 2.63 and 2.64) the assays were performance. A mixture of POPC:cholesterol (7:3) was rehydrated with  $\text{NaNO}_3$  (126.25 mM  $\text{NaNO}_3$ , 10 mM buffer phosphate pH 7.2, I.S. 150 mM and 10  $\mu\text{M}$  HPTS). The non-encapsulated solution was removed by SEC using the  $\text{NaNO}_3$  solution (without HPTS) as mobile phase. The obtained vesicles were diluted in a known volume. Vesicles were suspended over  $\text{NaNO}_3$  (126.25 mM  $\text{NaNO}_3$ , 10 mM buffer phosphate pH 7.2 and I.S. 150 mM) for a final POPC concentration of 0.5 mM. At  $t = 30$  s it was added a pulse of the anion carrier in DMSO and at  $t = 60$  s, 11  $\mu\text{L}$  of  $\text{NaOH}$  0.5 M were incorporated to the exterior. Changes in the fluorescence relationship were measured over time (full details of how performing these experiments in Chapter IV). The conversion of fluorescence data in pH values was done with the S-Logistic1 model and the polynomial fifth grade (Figure 2.61 and 2.62 respectively). Tetraheterocycles were found to follow the same trend observed in ISE assays.

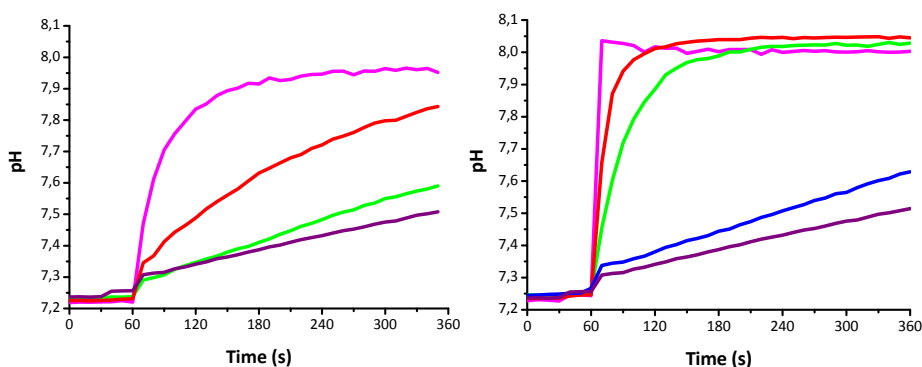


Figure 2.63. Variation of pH upon addition of tetraheterocycles to POPC:cholesterol (7:3) vesicles, 0.5 mM POPC. Vesicles contained  $\text{NaNO}_3$  (126.25 mM  $\text{NaNO}_3$ , 10 mM buffer phosphate pH 7.2, I.S. 150 mM and HPTS 10  $\mu\text{M}$ ) were suspended in  $\text{NaNO}_3$  (126.25 mM  $\text{NaNO}_3$ , 10 mM buffer phosphate pH 7.2 and I.S. 150 mM). At  $t = 30$  s addition of the anion carrier and at  $t = 60$  s addition of 11  $\mu\text{L}$   $\text{NaOH}$  0.5 M. Magenta trace: **147.HCl**, green trace: **148.HCl**, red trace: **152.HCl**, blue trace: **153.HCl** and purple trace: blank (10  $\mu\text{L}$  DMSO). Each trace represents the average of at least three different trials, done with at least two different batches of vesicles. Left: pH data obtained from the polynomial adjustment, 0.0001 mol% carrier to POPC. Right: pH data obtained from the polynomial adjustment, 0.01 mol% carrier to POPC.

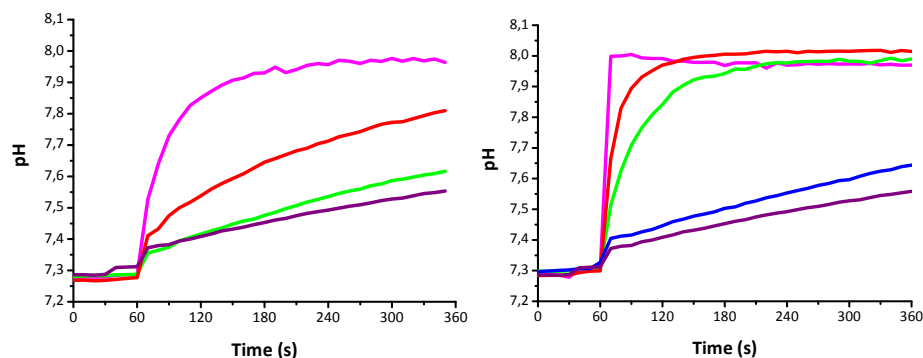


Figure 2.64. Variation of pH upon addition of tetraheterocycles to POPC:cholesterol (7:3) vesicles, 0.5 mM POPC. Vesicles contained  $\text{NaNO}_3$  (126.25 mM  $\text{NaNO}_3$ , 10 mM buffer phosphate pH 7.2, I.S. 150 mM and HPTS 10  $\mu\text{M}$ ) were suspended in  $\text{NaNO}_3$  (126.25 mM  $\text{NaNO}_3$ , 10 mM buffer phosphate pH 7.2 and I.S. 150 mM). At  $t = 30$  s addition of the anion carrier and at  $t = 60$  s addition of 11  $\mu\text{L}$  NaOH 0.5 M. Magenta trace: **147.HCl**, green trace: **148.HCl**, red trace: **152.HCl**, blue trace: **153.HCl** and purple trace: blank (10  $\mu\text{L}$  DMSO). Each trace represents the average of at least three different trials, done with at least two different batches of vesicles. Left: pH data obtained from the S-Logistic1 model, 0.0001 mol% carrier to POPC. Right: pH data obtained from the S-Logistic1 model, 0.01 mol% carrier to POPC.

After all these transport assays, it could be concluded that this tetraheterocycle scaffold constitutes an excellent motif to develop anion transporters. The most plausible mechanism of transport seems to be the antiport exchange of anions along with  $\text{H}^+/\text{X}^-$  symport, in a lesser extent.

## 2.6. BODIPY derivative from 147.HCl

### 2.6.1. Introduction

The tetraheterocyclic compounds described offer a good opportunity to develop fluorescent derivatives in the form of 4,4-difluoro-4-bora-3a,4a-diaza-s-indacene (BODIPY) compounds. BODIPYs are obtained from the complexation of a difluoroboryl unit to a dypirrin motif, giving as a result a tricyclic, planar structure with five resonating pairs of  $\pi$  electrons. 4,4-difluoro-4-bora-3a,4a-diaza-s-indacene (BODIPY) fluorescent dyes display interesting photophysical properties. This scaffold (Figure 2.65) was reported for the first time in 1968 by A. Treibs and F. H. Kreuzer,<sup>206</sup>

<sup>206</sup> A. Treibs and F.-H. Kreuzer, *Liebigs Ann. Chem.*, 1968, **718**, 208–223.

but it did not gain popularity until the nineties when Boyer and Pavlopoulos demonstrated their applications in lasers.<sup>207, 208</sup>

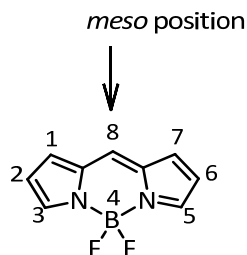


Figure 2.65. BODIPY scaffold

Its high fluorescent properties are related with their chromophoric unit. The difluoroboryl motif is not involved in the aromatic system, but plays an important role in the structure. It acts as a linkage between both nitrogen atoms, avoiding to any electron could leave the  $\pi$  system. Therefore, these compounds are classified as *quasi-aromatic* dyes.

BODIPYs are characterised by their low tendency to self-aggregate in solution, absorption and emission spectra in the visible range with narrow bandwidths, high molar absorption coefficients and quantum yields, as well as, stability against light and chemicals.<sup>209</sup>

They find a wide variety of applications, from fluorescent probes or chemical sensors in the field of biomedicine or biochemistry,<sup>210</sup> to materials that improve the performance of solar cells.<sup>211</sup>

### 2.6.2. Synthesis

Tetraheterocycle **147.HCl** was used as starting material of this reaction. The typical procedure consists on a one pot two step reaction consisting in the treatment

---

<sup>207</sup> T. G. Pavlopoulos, M. Shah and J. H. Boyer, *Appl. Opt.*, 1988, **27**, 4998–4999.

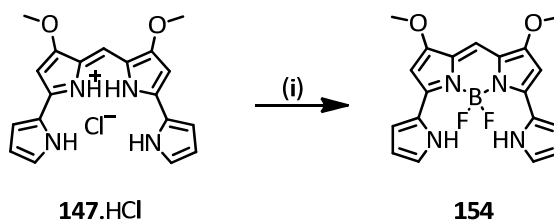
<sup>208</sup> M. Shah, K. Thangaraj, M.-L. Soong, L. T. Wolford and J. H. Boyer, I. R. Politzer and T. G. Pavlopoulos, *Heteroat. Chem.*, 1990, **1**, 389–399.

<sup>209</sup> N. Boens, V. Leen, W. Dehaen, L. Wang, K. Robeyns, W. Qin, X. Tang, D. Beljonne, C. Tonnelé, J. M. Paredes, M. J. Ruedas-Rama, A. Orte, L. Crovotto, E. M. Talavera and J. M. Alvarez-Pez, *J. Phys. Chem. A* 2012, **116**, 9621–9631.

<sup>210</sup> L. Mendive-Tapia, C. Zhao, A. R. Akram, S. Preciado, F. Albericio, M. Lee, A. Serrels, N. Kiehlund, N. D. Read, R. Lavilla and M. Vendrell, *Nat. Commun.*, 2016, **7**, 10940–10948.

<sup>211</sup> C. Y. Lee and J. T. Hupp, *Langmuir*, 2010, **26**, 3760–3765.

with  $\text{Et}_3\text{N}$ , in DCM or toluene, and fifteen minutes later adding  $\text{BF}_3\cdot\text{OEt}_2$ . This reaction is usually completed within two hours, with low yields (Scheme 2.6).<sup>212</sup>



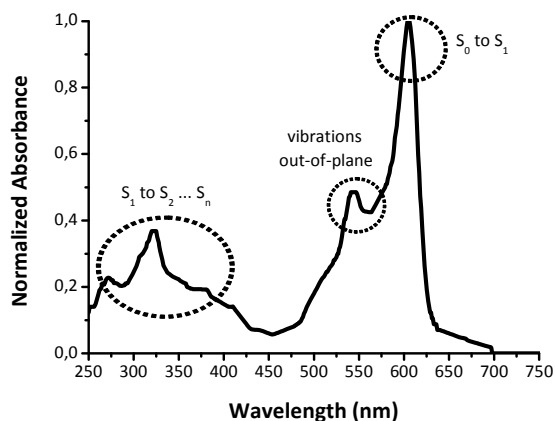
Scheme 2.6. Reagents and conditions: (i) 7.4 eq.  $\text{Et}_3\text{N}$ . After fifteen minutes, 7.4 eq.  $\text{BF}_3\text{OEt}_2$ ,  $25^\circ\text{C}$ , 2 h.

### 2.6.3. Characterization of photophysic properties

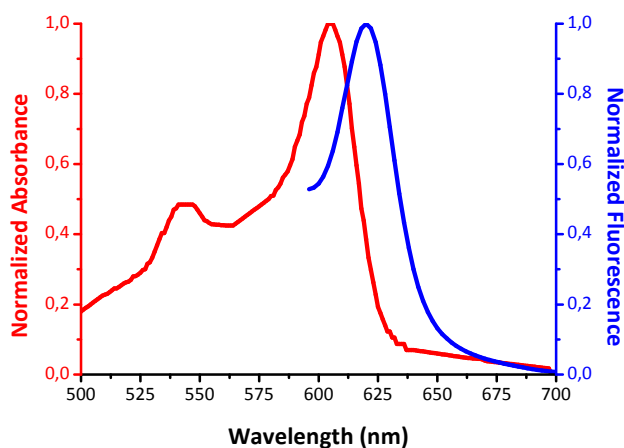
The UV/Vis absorption spectrum of **154** displays the characteristic bands of BODIPYs (Figure 2.66; spectrum in MeOH. All tested solvents give as a result a similar curve with different intensities). Three different absorption bands could be differentiated. The lowest energy one ( $\sim 600\text{ nm}$ ), corresponds to the electronic transition from the ground state to the first excited state ( $S_0 \rightarrow S_1$ ). This band presents the highest intensity among the three. Its shape is characterised by being concentration-independent. At a higher energy ( $\sim 540\text{ nm}$ ), it is observed a shoulder that is originated by vibrations out-of-plane of the aromatic structure. In the UV region, it appears another band. Transitions located in this area are less probable. The one observed for **154** could be attributed to a transition from the first excited state to higher excited states ( $S_2, S_3$ , etc.).<sup>213</sup>

<sup>212</sup> A. Loudet and K. Burgess, *Chem. Rev.*, 2007, **107**, 4891-4932.

<sup>213</sup> N. Boens, V. Leen, W. Dehaen, L. Wang, K. Robeyns, W. Qin, X. Tang, D. Beljonne, C. Tonnelé, J. M. Paredes, M. J. Ruedas-Rama, A. Orte, L. Crovetto, E. M. Talavera and J. M. Alvarez-Pez, *J. Phys. Chem. A* 2012, **116**, 9621-9631.

Figure 2.66. Absorption spectrum of **154** in MeOH (1  $\mu\text{M}$ )

The fluorescence emission spectrum of **154** shows the typical features of BODIPY dyes. Its fluorescence spectrum is almost the mirror image of  $S_0 \rightarrow S_1$  absorption band (Figure 2.67). This suggests that both electronic states,  $S_0$  and  $S_1$ , display similar vibrational levels. Therefore, the fluorescent band is characterised by small Stokes shift, in this particular case  $400 \text{ cm}^{-1}$ . The shape of the fluorescence band is independent of the excitation wavelength, which means that the emission takes place from the lowest vibrational level of the excited state  $S_1$ .

Figure 2.67. Absorption (red) and emission (blue) spectra of **154** 1  $\mu\text{M}$  in MeOH.  $\lambda_{\text{exc}} = 560 \text{ nm}$ .  $\lambda_{\text{abs, max}} = 605 \text{ nm}$ ,  $\lambda_{\text{em, max}} = 620 \text{ nm}$ . Stokes shift =  $400 \text{ cm}^{-1}$ .

### 2.6.3.1. Solvatochromism

A solvatochromism study of **154** was carried out. It consists on analyse photophysical properties as a function of solvents and interaction with other solutes.

Solvents with different polarities, from hexane to water were used. The maximum of absorption of **154** is shifted as a function of solvent, but there were not found the existence of a trend according to polarity. The band which maximum displays the highest energy is presented in water (dipolar moment 9.0) meanwhile the lowest energy maximum is exhibited in DMSO (dipolar moment 7.2).

When the fluorescence emission spectra of **154** different solvents is analysed it is observed a variation in the position of the maximum of luminiscence but no trend related with the protic or polarity properties of the solvent were found (Figure 2.68). The highest energy maximum were found in DMF solution and lowest in hexane.

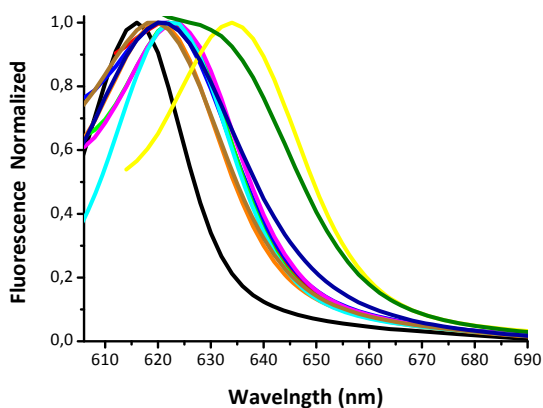


Figure 2.68: Normalised fluorescence emission spectra of **154** 1  $\mu\text{M}$ . ( $\lambda_{\text{exc}} = 560 \text{ nm}$ ) in hexane (black trace), toluene (red trace), DCM (blue trace), THF (light green),  $\text{CHCl}_3$  (magenta trace), MeOH (orange trace), acetone (cyan trace),  $\text{CH}_3\text{CN}$  (brown trace), DMF (yellow trace), DMSO (olive trace) and  $\text{H}_2\text{O}$  (navy trace).

Pictures of its fluorescence emission intensity, in the studied solvents, under 254 nm light (Figure 2.69. Left) and 366 nm light (Figure 2.69. Right) were took. With the exception of water (vial 11), **154** displays an intense fluorescence when is excited at 366 nm.

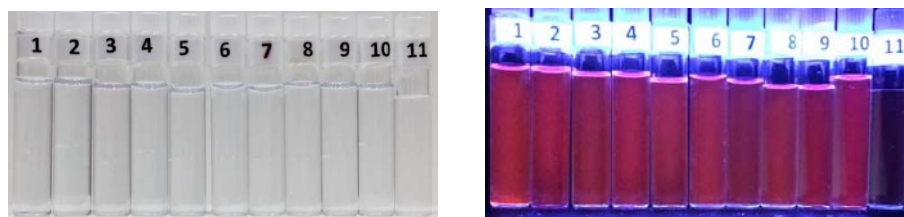


Figure 2.69. Solutions of **162** in 1: hexane; 2: toluene; 3: DCM; 4: THF; 5: CHCl<sub>3</sub>; 6: MeOH; 7: acetone; 8: CH<sub>3</sub>CN; 9: DMF; 10: DMSO and 11: H<sub>2</sub>O. Left: picture took under 254 nm light. Right: picture took under 366 nm light.

The quantum yield of **154** was measured in some of the previous solvents. Cresyl violet, in MeOH, was chosen as standard probe with a quantum yield,  $\phi$ , of 0.54.<sup>214</sup> The refraction index of MeOH,  $n$ , is 1.3288.<sup>215</sup> The followed procedure consisted in measuring the absorbance spectrum of **154** in all solvents in which the quantum yield was going to be calculated, adjusting the concentration in such a way that the absorbance maximum were around 0.08. Then, the emission spectra of these samples were recorded after exciting at 600 nm. Finally, it was applied equation 2.18. The obtained results a summarised in Table 2.14.

An attempt to calculate the quantum yields at a wavelength in which the emission band were found far from the Rayleigh diffraction band were carried out. In order to that, the samples were excited at 500 nm. The obtained results seem to be vague because a value of 0.37 for water (Table 2.14) makes little sense, since Figure 2.69. Right shows that **162** does not present fluorescence emission in water (vial 11).

---

<sup>214</sup> J. R. Lakowicz, in *Principle of Fluorescence Spectroscopy*. Baltimore, 3rd edn, 2006, ch. 2, pp. 54.

<sup>215</sup> J. E. Saunders, C. Sanders, H. Chen and H.-P. Loock, *Appl. Opt.*, **2016**, 55, 947–953.

$$\phi = \phi_{\text{ref}} \cdot \frac{I_{\text{F}}}{I_{\text{F, ref}}} \cdot \frac{I_{\text{Abs, ref}}}{I_{\text{Abs}}} \cdot \left( \frac{\eta}{\eta_{\text{ref}}} \right)^2 \quad \text{Eq. 2.18}$$

Where:

- $\phi_{\text{ref}}$  quantum yield of the standard in MeOH (0.54)  
 $I_{\text{F, ref}}$  area under the fluorescence curve of the standard in MeOH ( $\lambda_{\text{exc}} = 500 \text{ nm}$ ), integrated with Origin 8.0  
 $I_{\text{F}}$  area under the fluorescence curve of **154** in a solvent, integrated with Origin 8.0  
 $I_{\text{Abs, ref}}$  area under the absorption curve of the standard in MeOH, integrated with Origin 8.0  
 $I_{\text{Abs}}$  area under the absorption curve of **154** in a solvent, integrated with Origin 8.0  
 $\eta_{\text{ref}}$  refraction index of MeOH (1.3288)  
 $\eta$  refraction index of the corresponding solvent

Stokes shift ( $\text{cm}^{-1}$ ) were calculated as:

$$\text{Stoke shift} = \frac{1}{\lambda_{\text{em, max}}} - \frac{1}{\lambda_{\text{abs, max}}} \quad \text{Eq. 2.18}$$

Table 2.14. Summary of photophysical properties as a function of the solvent

Solvent	$\lambda_{\text{abs, max}}$ (nm)	$\lambda_{\text{em, max}}$ (nm)	Stoke shift ( $\text{cm}^{-1}$ )	Quantum Yield ( $\lambda_{\text{exc}} = 600 \text{ nm}$ )	Quantum Yield ( $\lambda_{\text{exc}} = 500 \text{ nm}$ )
Hexane	605	616	295	— <sup>a</sup>	— <sup>a</sup>
Toluene	611	622	289	$0.54 \pm 0.01$	$0.38 \pm 0.01$
DCM	605	620	400	— <sup>a</sup>	— <sup>a</sup>
THF	610	624	368	— <sup>a</sup>	— <sup>a</sup>
$\text{CHCl}_3$	608	624	422	$0.54 \pm 0.01$	$0.39 \pm 0.01$
MeOH	605	620	400	$0.57 \pm 0.01$	$0.43 \pm 0.03$
Acetone	607	622	397	$0.51 \pm 0.01$	$0.30 \pm 0.01$
$\text{CH}_3\text{CN}$	603	620	455	— <sup>a</sup>	— <sup>a</sup>
DMF	612	634	567	— <sup>a</sup>	— <sup>a</sup>
DMSO	617	626	233	$0.42 \pm 0.01$	$0.41 \pm 0.01$
$\text{H}_2\text{O}$	598	620	593	$0.11 \pm 0.01$	$0.37 \pm 0.02$

<sup>a</sup> Not determined

Many authors describe the solvent effect over the spectral shift analysing the photophysical data as a function of a single parameter (usually polarity).<sup>216, 217</sup> When it was tried with **154** no trend was observed. It is more appropriate apply a multiple parameter approach. Here, it has been followed a treatment in which the solvent effect is based on four empirical solvent scales (polarizability SP, dipolarity SdP, acidity SA and basicity SB).<sup>218, 219</sup>

In Table 2.15, there are shown the corresponding values of these parameters for each solvent, as well as the maximum frequency of absorption and emission spectra of **154** in the different solvents ( $\lambda_{\text{abs, max}}$  and  $\lambda_{\text{em, max}}$  where transformed into  $\sigma_{\text{abs, max}}$  and  $\sigma_{\text{em, max}}$  ( $\lambda = 1/\sigma$ ). Using JMP 13.0.0 some least square regressions were carried out in order to explain  $\sigma_{\text{abs, max}}$  and  $\sigma_{\text{em, max}}$  as a function of these solvent scales. Two and three descriptor models were performed.

Table 2.15. Photophysical properties as a function of the solvent, and SP, SdP, SB and SA solvent values

Solvent	SP	SdP	SB	SA	$\sigma_{\text{abs, max}}$ ( $\text{cm}^{-1}$ )	$\sigma_{\text{em, max}}$ ( $\text{cm}^{-1}$ )
Hexane	0.616	0	0.056	0	16528.9	16233.8
Toluene	0.782	0.284	0.128	0	16366.6	16077.2
DCM	0.761	0.769	0.178	0.040	16528.9	16129.0
THF	0.714	0.634	0.591	0	16393.4	16025.6
CHCl <sub>3</sub>	0.783	0.614	0.071	0.047	16447.4	16025.6
MeOH	0.608	0.904	0.545	0.605	16528.9	16129.0
Acetone	0.651	0.907	0.475	0	16474.5	16077.2
CH <sub>3</sub> CN	0.645	0.974	0.286	0.044	16583.7	16129.0
DMF	0.759	0.977	0.613	0.031	16339.9	15772.9
DMSO	0.830	1.000	0.647	0.072	16207.5	15974.4
H <sub>2</sub> O	0.681	0.997	0.025	1.062	16722.4	16129.0

<sup>216</sup> A. Filarowski, M. Lopatkova, P. Lipkowski, M. Van der Auweraer, V. Leen and W. Dehaen, *J. Phys. Chem. B*, 2015, **119**, 2576–2584.

<sup>217</sup> C. Caltagirone, M. Arca, A. M. Falchi, V. Lippolis, V. Meli, M. Monduzzi, T. Nylander, A. Rosa, J. Schmidt, Y. Talmon and S. Murgia, *RSC Adv.*, 2015, **5**, 23443–23449.

<sup>218</sup> N. Boens, V. Leen, W. Dehaen, L. Wang, K. Robeyns, W. Qin, X. Tang, D. Beljonne, C. Tonnelé, J. M. Paredes, M. J. Ruedas-Rama, A. Orte, L. Crovetto, E. M. Talavera and J. M. Alvarez-Pez, *J. Phys. Chem. A* 2012, **116**, 9621–9631.

<sup>219</sup> J. C. del Valle, F. García-Blanco and J. Catalán, *J. Phys. Chem. B*, 2015, **119**, 4683–4692.

In the case of the maximum absorption frequency shift, equations 2.19 (SP and SB) and 2.20 (SP, SdP and SB) with two and three terms respectively, are able to explain the absorption behaviour of **154** in the different environments. Its maximum emission frequency shift could be explained by the two terms equation 2.21 (SP and SB). Adding a third parameter does not improve the two terms equation, but gives as a result a no statistically valid model.

$$\begin{aligned} &2 \text{ descriptors; } \sigma_{\text{abs, max}} = 17367.65 - 1128.01 \cdot \text{SP} - 301.44 \cdot \text{SB} && \text{Eq. 2.19} \\ &(\text{R}^2 = 0.75) \end{aligned}$$

$$\begin{aligned} &3 \text{ descriptors; } \sigma_{\text{abs, max}} = 17284.65 - 1163.76 \cdot \text{SP} + 211.20 \cdot \text{SdP} - 442.63 \cdot \text{SB} && \text{Eq. 2.20} \\ &(\text{R}^2 = 0.94) \end{aligned}$$

$$\begin{aligned} &2 \text{ descriptors; } \sigma_{\text{em, max}} = 16745.54 - 837.12 \cdot \text{SP} - 261.00 \cdot \text{SB} && \text{Eq. 2.21} \\ &(\text{R}^2 = 0.64) \end{aligned}$$

3 descriptors;  $\sigma_{\text{em, max}}$   $\longrightarrow$  Not statistically valid

#### 2.6.4. Anion transport assays

The ionophoric properties of **154** were tested under the same experiments applied for the rest of compounds analysed in this thesis.

It presents an  $\text{EC}_{50}$  value of 24.8  $\mu\text{M}$  in  $\text{Cl}^-/\text{NO}_3^-$  assays (Figure 2.71), this result is below average, but still better than some of the studied compounds, such as the tetraheterocycle **153.HCl** or tambjamine **113.HCl**. The hill parameter,  $n$ , is close to one, consistent with a non-cooperative process. When the external nitrate was changed by the more hydrophilic bicarbonate the  $\text{EC}_{50}$  value could not be determined. This result supports anion antiport as the transport mechanism accounting by this compound.

Under  $\text{Cl}^-/\text{NO}_3^-$  assay conditions, the activity at 4 mol% was measured in 7:3 (POPC:cholesterol) vesicles. The chloride efflux was 42.9 % compared to 45.6 % obtained when vesicles were composed only by POPC.

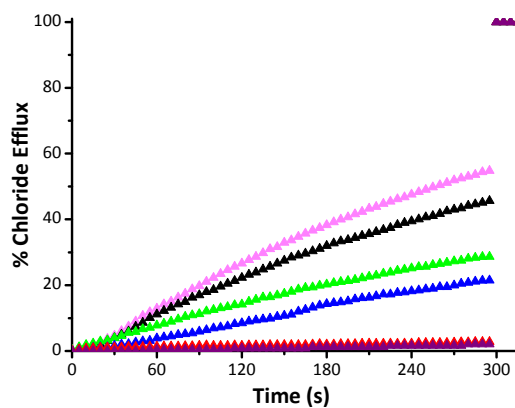


Figure 2.70. Anion transport activity of **154** in  $\text{Cl}^-/\text{NO}_3^-$  ISE experiment. 0.5 mM POPC. Vesicles loaded with 489 mM NaCl (phosphate buffer 5 mM, pH 7.2) where suspended in  $\text{NaNO}_3$  489 mM (phosphate buffer 5 mM, pH 7.2). At  $t = 300$  s a pulse of detergent was added in order to release all chloride anions. Each trace represents the average of at least three trials, done with at least two different batches of vesicles. Pink trace: 6 mol% = 30  $\mu\text{M}$ ; black trace: 4 mol% = 20  $\mu\text{M}$ ; green trace: 2 mol% = 10  $\mu\text{M}$ ; blue trace: 1 mol% = 5  $\mu\text{M}$ ; red trace: 0.02 mol% = 0.1  $\mu\text{M}$  and purple trace: blank (10  $\mu\text{L}$  DMSO).

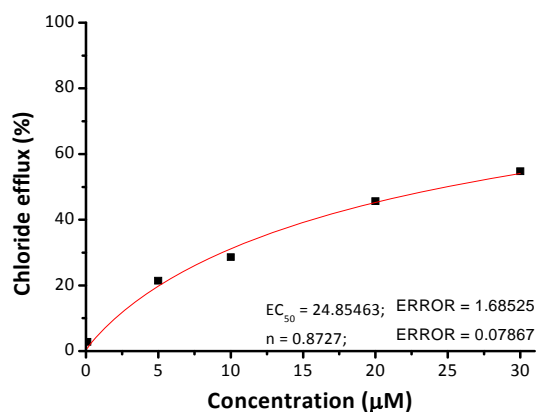


Figure 2.71. Hill analysis of **154** transport results.

To confirm that **154** does not disrupt the membrane, it was subjected to the carboxyfluorescein leakage assay. On the left of Figure 2.72, there is shown the normalised fluorescence of carboxyfluorescein from 450 to 650 nm. The emission band at 480 nm corresponds to the Rayleigh diffraction. At 520 nm the 0.2 (a.u.) emission band refers to traces collected before adding **154** and from its addition at 60 s to 360 s (0–360 s). Once the detergent was added, the carboxyfluorescein fluorescence increased to 1 (360–480 s). On the right there are shown the data at

520 nm, referred to the maximum, plotted against time. As all carriers tested in this thesis, the carboxyfluorescein fluorescence does not vary until the addition of detergent, meaning that **154** does not form large pores or disrupt the integrity of the membrane in the liposomes.

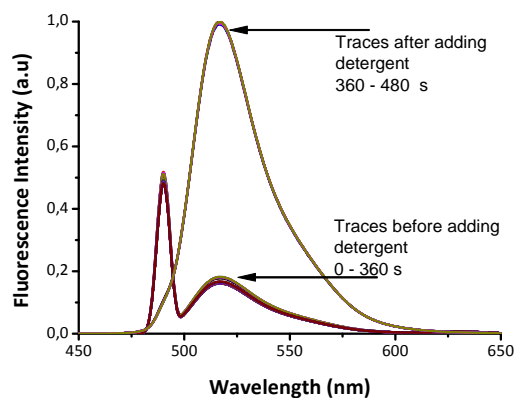


Figure 2.72. Carboxyfluorescein normalised fluorescence recorded from 450 to 650 nm upon addition of **154** to POPC vesicles, 0.05 mM. Vesicles contained NaCl (451 mM, buffered with  $\text{NaH}_2\text{PO}_4$  20 mM to pH 7.2, I.S. 500 mM and 50 mM CF) were suspended in  $\text{Na}_2\text{SO}_4$  (150 mM, buffered with  $\text{NaH}_2\text{PO}_4$  20 mM to pH 7.2, I.S. 500 mM). At  $t = 60$  s addition of the anion carrier (1 mol% carrier to lipid). Each trace represents the average of at least three different trials, done with at least two different batches of vesicles. At  $t = 360$  s addition of 20  $\mu\text{L}$  of detergent.

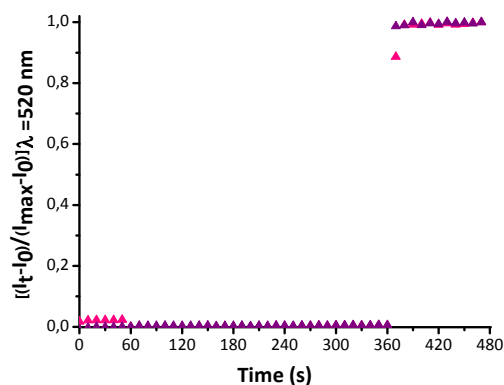


Figure 2.73. Carboxyfluorescein leakage upon addition of **154** to POPC vesicles, 0.05 mM. Vesicles contained NaCl (451 mM, buffered with  $\text{NaH}_2\text{PO}_4$  20 mM to pH 7.2, I.S. 500 mM and 50 mM CF) were suspended in  $\text{Na}_2\text{SO}_4$  (150 mM, buffered with  $\text{NaH}_2\text{PO}_4$  20 mM to pH 7.2, I.S. 500 mM). At  $t = 60$  s addition of the anion carrier (1 mol% carrier to lipid). At  $t = 360$  s addition of 20  $\mu\text{L}$  of detergent. Pink trace: **154** and purple trace: blank (10  $\mu\text{L}$  DMSO). Each trace represents the average of at least three different trials, done with at least two different batches of vesicles. Ratio of normalised data of carboxyfluorescein emission at 520 nm.

Their  $H^+/NO_3^-$  symport ability was checked in HPTS vesicle assays at 0.01 mol% carrier to lipid, the same working concentration applied for the rest ionophores of this thesis. In the above figure (Figure 2.74) there are shown the data obtained when the fluorescence ratio was converted into pH values applying the polynomial calibration. Below, it was applied the S-Logistic1 model.

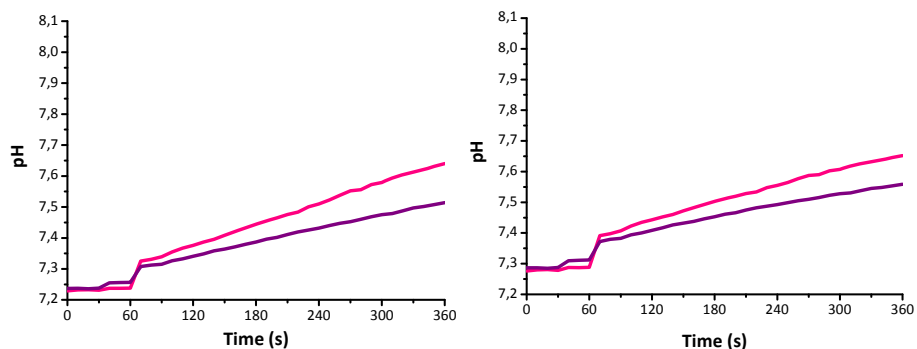


Figure 2.74. Variation of pH upon addition of **154** (0.01 mol% carrier to POPC) to (7:3) vesicles, 0.5 mM POPC. Vesicles contained  $NaNO_3$  (126.25 mM  $NaNO_3$ , 10 mM buffer phosphate pH 7.2, I.S. 150 mM and HPTS 10  $\mu$ M) were suspended in  $NaNO_3$  (126.25 mM  $NaNO_3$ , 10 mM buffer phosphate pH 7.2 and I.S. 150 mM). At  $t = 30$  s addition of the anion carrier and at  $t = 60$  s addition of 11  $\mu$ L NaOH 0.5 M. Pink trace: **154** and purple trace: blank (10  $\mu$ L DMSO). Each trace represents the average of at least three different trials, done with at least two different batches of vesicles. Left: pH data obtained from the polynomial adjustment. Right: S-Logistic1 model adjustment.



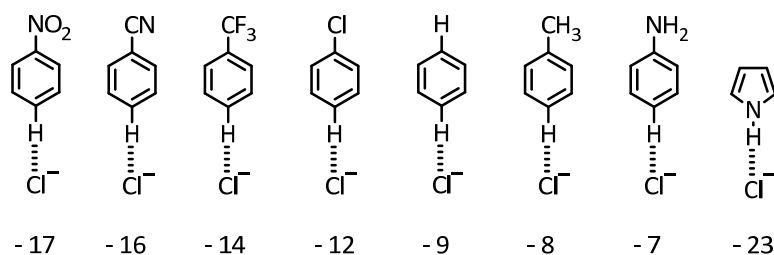


Figure 2.75. Computational data (MP2/aug-cc-pVDZ) of Hydrogen bond donor energies (Kcal/mol) of *p*-CH

The triazole motif presents a polarised C-H bond, which acts as a hydrogen bond donor (Figure 2.76). Two different regioisomers could be differentiated.

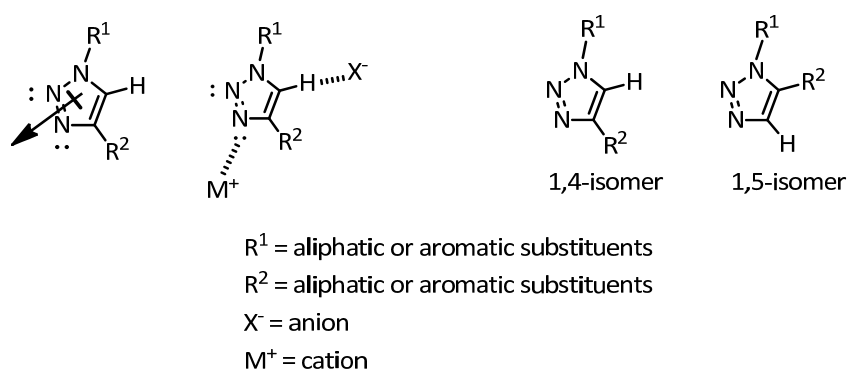


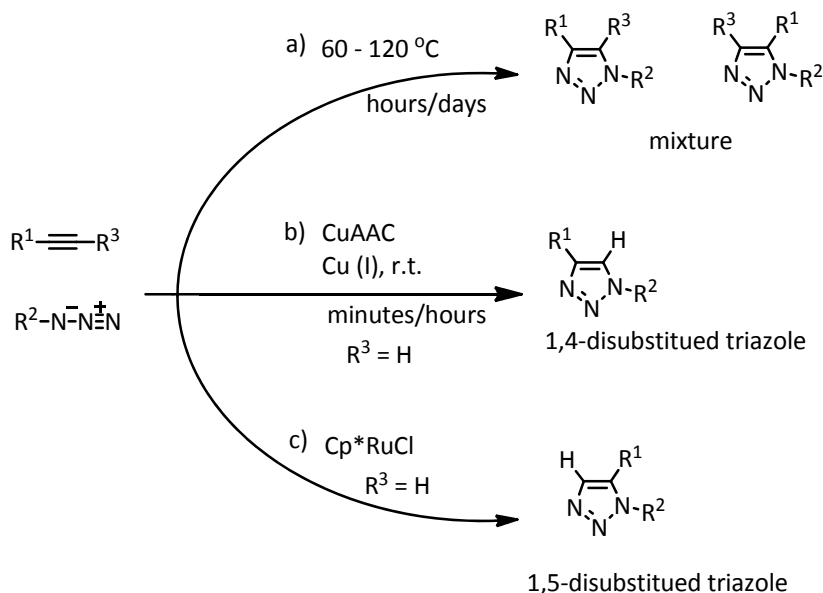
Figure 2.76. Left: triazole structure. Right: triazole regioisomers

The powerful properties as hydrogen bond donor of this motif come from the presence of three nitrogen atoms located on one side of the triazole scaffold, which increase the C-H proton acidity. In turn, the orientation of these three nitrogen atoms provides a 5-Debye dipole moment, which is almost collinear with the polarize C-H.<sup>223</sup>

1,3-dipolar cycloaddition among alkynes and azides, described by Huisgen in 1960, was a synthetic route to obtain 1,2,3-triazoles. This procedure presented some disadvantages such as the required long times, the needed high temperatures and the lack of selectivity between 1,4- and 1,5-regioisomers. In 2001, Sharpless, Fin and Kolb from US and Medal from Denmark reported simultaneously but independently,

<sup>223</sup> P. A. Gale and W. Dehaen, *Anion Recognition in Supramolecular Chemistry*, Springer Heidelberg Dordrecht, 2010, pp. 351–353.

the copper catalysed reaction (CuAAC) between terminal alkynes and azides, which yields selectively the 1,4-disubstituted triazoles. The rate of this modern procedure is  $10^7$  times faster to its relative thermal process. Other metals are known to catalyse this reaction, with worst results. It is interesting to point out the RuACC (*ruthenium-catalysed azide-alkyne cycloaddition*) that yields only the 1,5-disubstituted triazole regioisomer (Scheme 2.7.).<sup>224</sup>



Scheme 2.7. a) Huisgen 1,3-dipolar addition; b) CuAAC reaction; c) Ru catalysed reaction

CuAAC reactions are included in the so-called “click-chemistry” that consists on a methodology which allow to obtain C-X-C (X = heteroatom) under simple and widely reaction conditions (protic and aprotic solvents, even water), with low dependence on the reactive substituents (electron rich and deficient groups, aliphatic, aromatic, heteroaromatic, etc.), easy purification procedures, little or no byproducts and high yields.<sup>225</sup>

The copper (I) catalyst could be obtained from different sources. From coordination complexes such as  $[\text{Cu}(\text{CH}_3\text{CN})_4]\text{PF}_6$ , Cu (I) salts (CuI, CuBr, CuAOC, etc.), to be formed “*in situ*” by reduction of Cu (II) salts ( $\text{Cu}_2\text{SO}_4$ ) to small pieces of copper metal which give rise to the copper patina in the metal surface. Although this last

<sup>224</sup> J. E. Hein and V. V. Fokin, *Chem. Soc. Rev.*, 2010, **39**, 1302–1315.

<sup>225</sup> H. C. Kolb, M. G. Finn and K. B. Sharpless, *Angew. Chem. Int. Ed.*, 2001, **40**, 2004–2021.

option takes longer times, it displays low degree of copper contamination (such as homogeneous copper complexes).

Sodium ascorbate is usually added as reductant of copper (II) to copper (I) when the copper (I) source is  $\text{Cu}_2\text{SO}_4$ , as well as, when it comes from copper (I) salts since it transforms any oxidised Cu (II) back to copper (I).

The presence of ligands in the catalytic specie increases the reaction rate and contributes to maintain copper (I) in solution avoiding redox reactions, terminal alkynes coupling, etc.

The mechanism proposed by J. E. Hein and V. V. Fokin is represented in Scheme 2.8. In a first stage, the alkyne is coordinated to the copper (I) catalyst forming **156**. The acidity of the terminal hydrogen of the alkyne increases because of the  $\pi$ -coordination of the alkyne to copper. Under this situation, **156** could be deprotonated in water to yield an  $\sigma$ -acetylide **157**. The formation of polynuclear copper acetylides such as **158** must be avoided because it has negative consequences in the reaction rates. It could be achieved working with polar solvents (alcohols or water) that favour ligand exchange, over organic apolar solvents, which favour the formation of copper aggregates. The azide is coordinated to copper, through the nitrogen atom proximal to carbon, to give the intermediate **159**. The terminal nitrogen of the azide in **159** reacts with the C-2 carbon from the acetylide to generate an uncommon copper (III) metallacycle **160**, which is contracted to form the triazolyl-copper derivative **161**. Finally, it releases the triazole **162** by hydrolysis, completing the catalytic cycle. Under oxidative conditions, **161** can lead to formation of byproducts **163**.

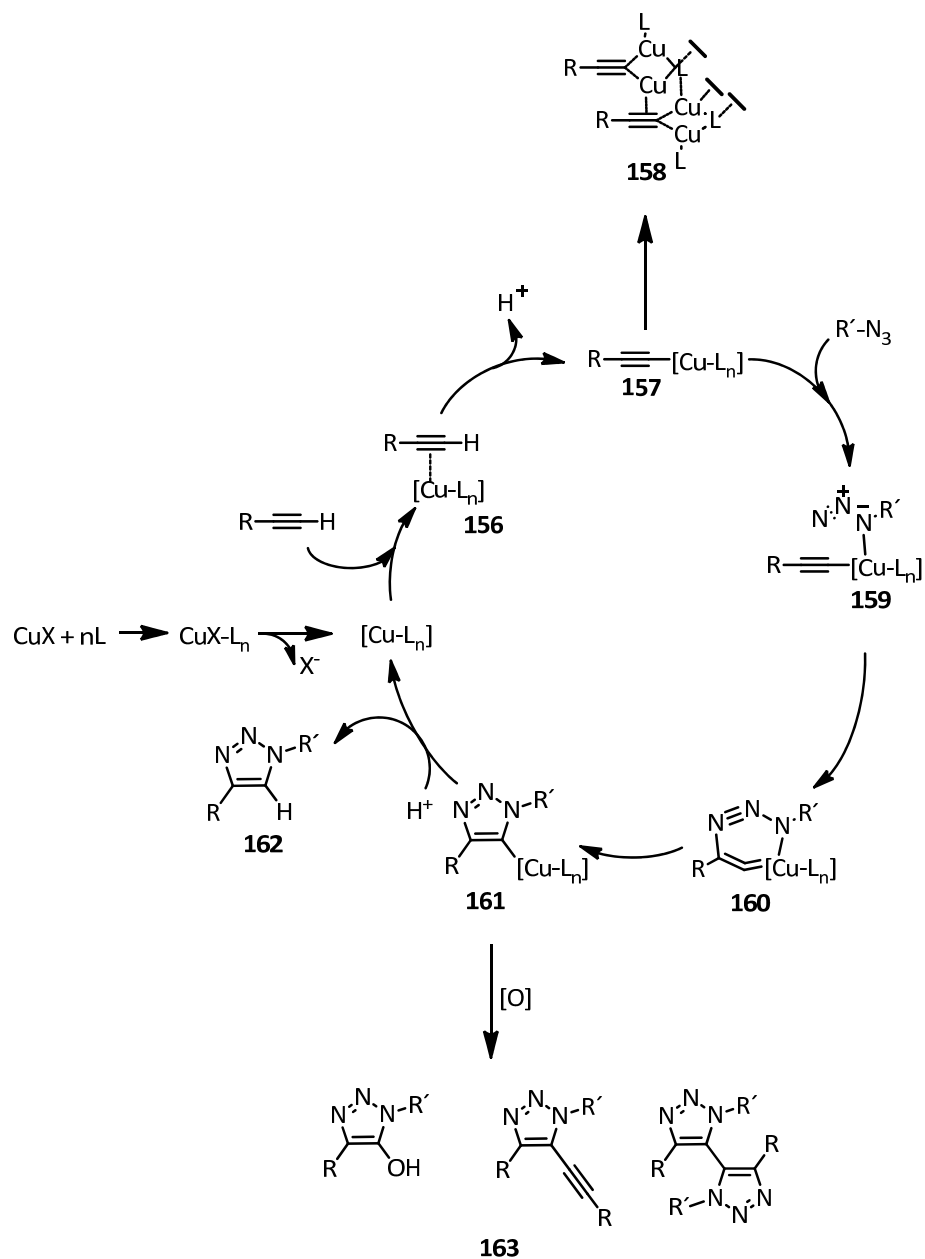
DFT calculations in aqueous medium demonstrated how the CuAAC reaction is accelerated over the non-catalysed, concerted cycloaddition.<sup>226, 227, 228</sup>

---

<sup>226</sup> S. Díez-González and S. P. Nolan, *Angew. Chem.*, 2008, **120**, 9013–9016.

<sup>227</sup> F. Himo, T. Lovell, R. Hilgraf, V. V. Rostovtsev, L. Noodleman, K. B. Sharpless and V. V. Fokin, *J. Am. Chem. Soc.*, 2005, **127**, 210–216.

<sup>228</sup> J. E. Hein and V. V. Fokin, *Chem. Soc. Rev.*, 2010, **39**, 1302–1315.

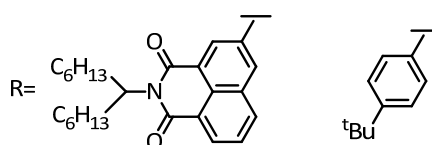
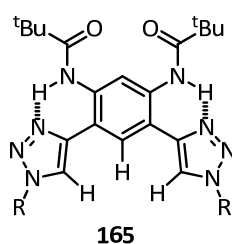
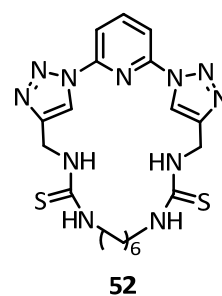
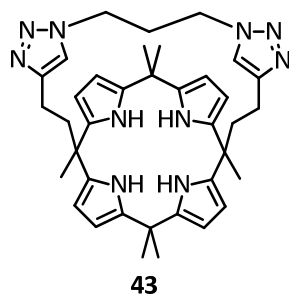


Scheme 2.8. Mechanism of triazoles synthesis proposed by E. Hein and V. V. Fokin

The breakthrough of copper (I) as an excellent catalyst to obtain 1,4-triazoles in an efficient and selective way, have opened a broad field of applications for this scaffold.

Flood *et al* designed a macrocyclic structure known as triazolophane **164** with eight CH H-bond donors. Four of them correspond to phenylene CH and the other

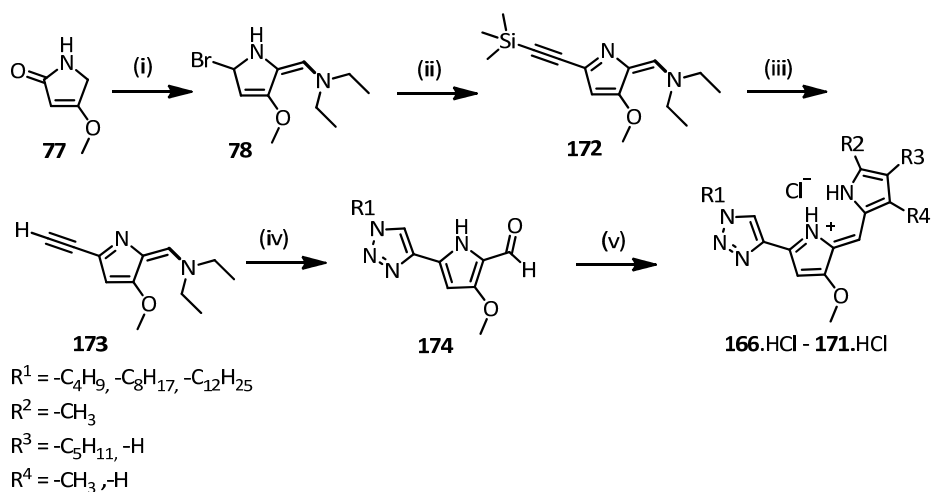




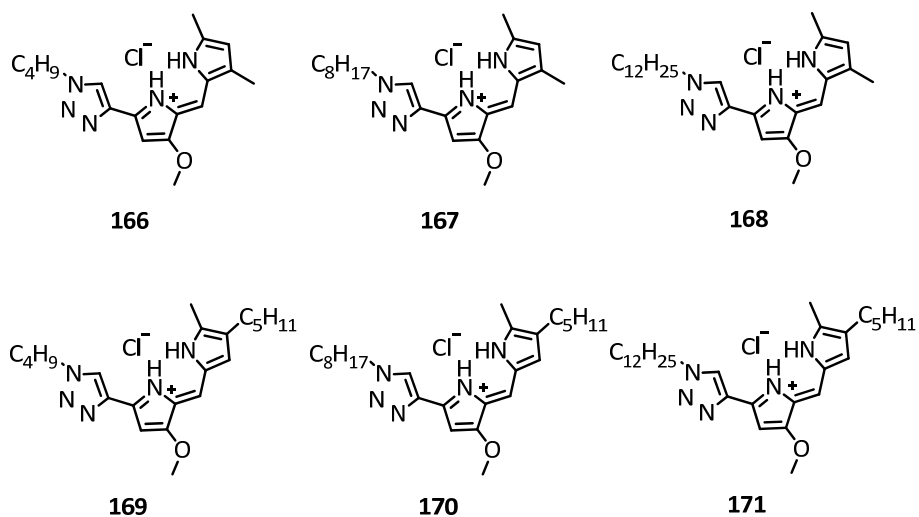
With these precedents we decided to replace one of the pyrrole groups in the backbone of the natural product prodiginines by a 1,2,3-triazole motif in order to develop a new family of anion carriers. With these modification we expected to obtain transporters which display a similar hydrogen bonding cleft to prodiginines but different properties such as lipophilicity.

### 3.2. Synthesis

Prodiginine inspired compounds were synthesised as described in Scheme 2.9. The azafulvene was prepared following the same method as for tambjamine synthetic analogs. Now, this intermediate is treated with ethynyltrimethylsilane under Suzuki-Miyaura coupling conditions to formish the alkyne derivative. Then, the trimethylsilyl group was removed with TBAF in THF. The obtained alkyne was subjected to a CuAAC reaction with alkyl azides to yield the corresponding triazole analogs. Finally, these products were reacted with pyrroles under acid catalytic conditions to obtain the prodiginine inspired compounds **166.HCl**–**171.HCl**.



Scheme 2.9. Reagents and conditions: (i) DCM, 3 eq.  $POBr_3$ , 3 eq. DEF, reflux, 5 h.; (ii) 2 eq. ethynyltrimethylsilane, 0.02 eq.  $Pd_2Cl_2(PPh_3)_2$ , 0.04 eq.  $CuI$ ,  $Et_2NH:Et_3N$  (1:1),  $80^\circ C$ ,  $N_2$  atmosphere, (Hexane:AcOEt 2:1); (iii) 1 eq. TBAF, THF, r.t., 3 h.; (iv) CuAAC conditions (see Chapter IV); (v) 2 eq. pyrrole, 2 eq. HCl (MeOH), MeOH, r.t.,  $N_2$  atmosphere, (Hexane:AcOEt 3:1)



### 3.3. Conformational analysis

A conformational analysis of the relative structure of these compounds have been performed in both, solid state and solution.

#### 3.3.1. Crystal structure

A suitable crystal for single crystal X-ray diffraction of compound **166**.HCl was grown of a Hexane:DCM solution, by slow evaporation at room temperature. The obtained structure is shown in Figure 2.77. X-ray diffraction analyses is detailed in the CD. The tris-heterocycle scaffold is essentially planar and adopts a  $\beta$  conformation (Figure 2.78). Both pyrrole rings are in relative *cis*-disposition around the methine bond, with their NHs interacting with the chloride anion through hydrogen bonds. The triazole C-H motif is orientated in the same direction as the NH groups, giving rise to another hydrogen bond with the halogen anion. Both NH-Cl bond distances are quite similar (3.096 and 3.133 Å), meanwhile the corresponding to the CH-Cl is slightly longer (3.472 Å) reflecting the poorer H-donor character of the C-H bond compared to N-H bonds.

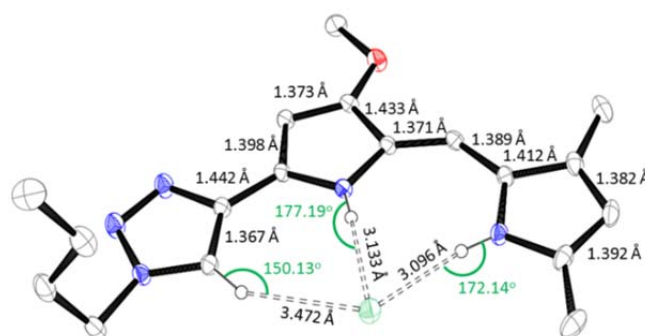


Figure 2.77. X-ray solid structure of **166**.HCl

#### 3.3.2. Relative conformations in solution

Based on previous conformational analysis performed by us (Section 2.1.1), Figure 2.78 shows four possible conformers for this family of molecules.

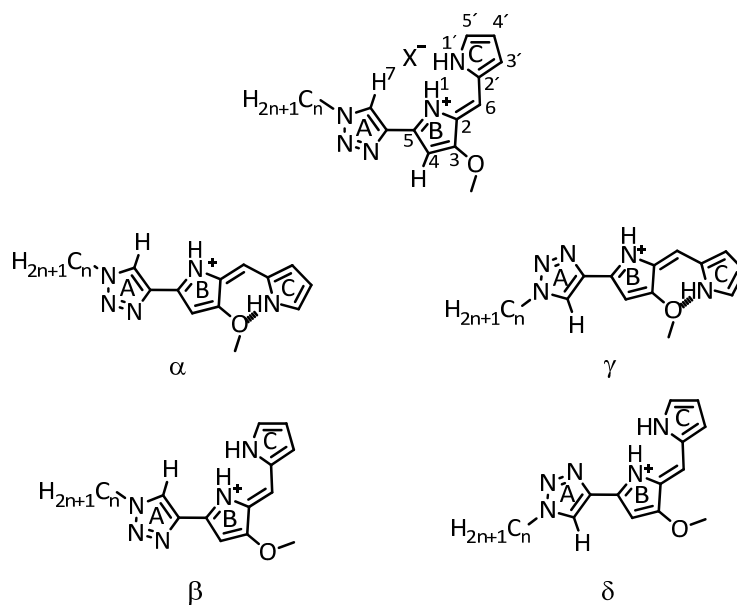
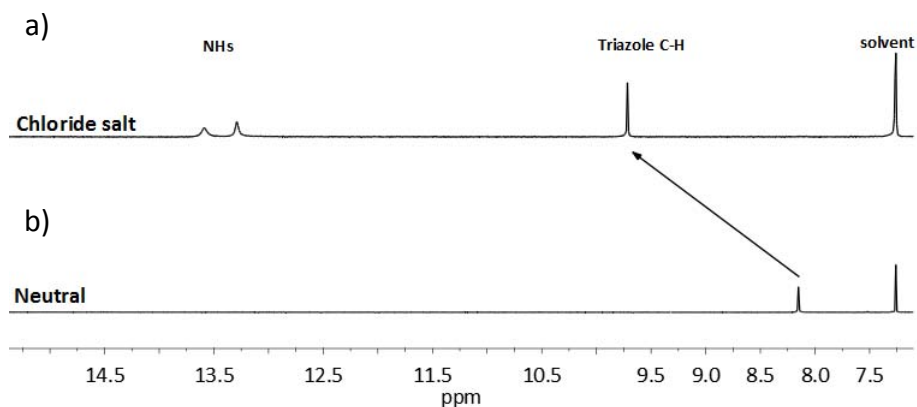


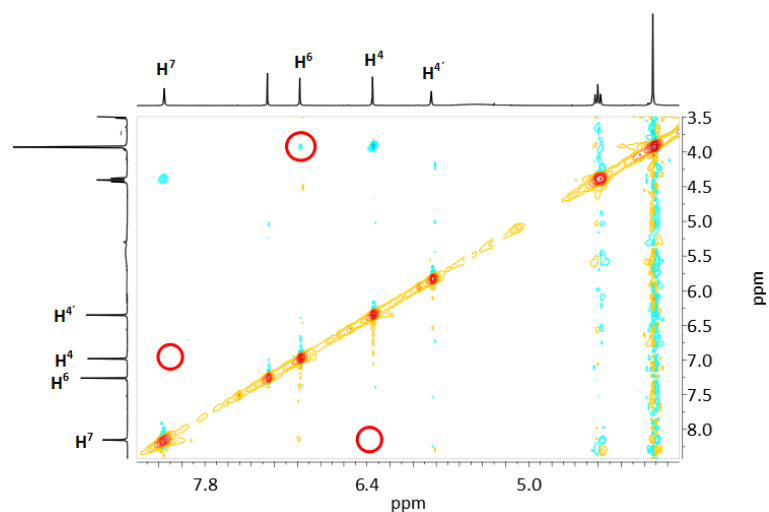
Figure 2.78. Prodiginine inspired compounds conformational analysis

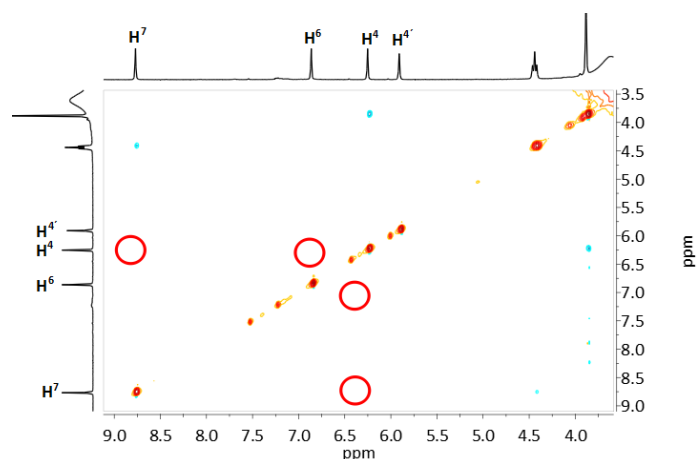
Using compound **166** as model, a study of the relative conformations of this compound in solution, as a function of the solvent and the counteranion was carried out.

**166.HCl** was synthesised as described in Scheme 2.9. Its neutral form was obtained by washing a DCM solution of the chloride salt with an aqueous solution of NaOH (1 M) (x 3). A  $^1\text{H}$  NMR analysis of both compounds demonstrated that the triazole moiety is taking part in the hydrogen bond with the anion because the C-H signal appears shifted downfield when the compound is found in the protonated state. In Figure 2.79b it is shown the  $^1\text{H}$  NMR deshielding region of neutral **152** and its chloride salt (Figure 2.79a) where it could be observed the different chemical shift of triazole C-H, under neutral and protonated conditions. Regarding to H-bond donors from NH units, it could be observed that they are absent in the neutral form (Figure 2.79b) because of their exchangeable nature, meanwhile they both appear interacting with the anion through well-defined hydrogen bonds in the protonated salt.

Figure 2.79. a)  $^1\text{H}$  NMR of **166.HCl**. b)  $^1\text{H}$  NMR of neutral **166**.

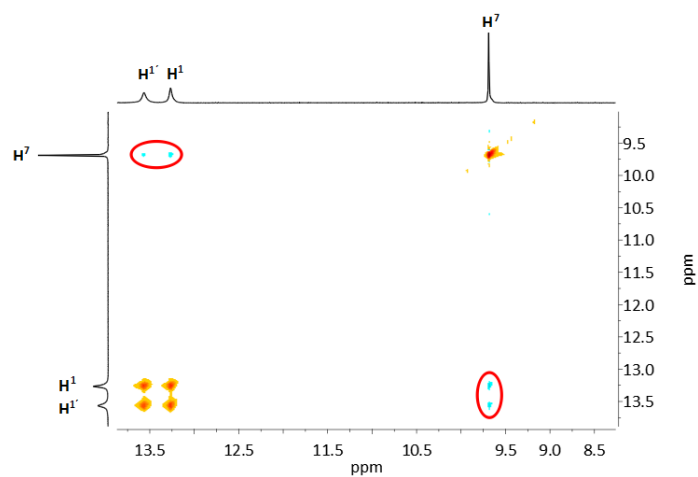
NOESY cross peaks between  $^6\text{H}$  and protons from the methoxy group (Figure 2.80) seem to indicate that neutral **152** displays a  $\beta$  conformation in  $\text{CDCl}_3$ , whereas the situation in  $\text{DMSO-}d_6$  solution is unclear. The most probable disposition is  $\alpha$  because no NOESY cross peaks are observed between  $^4\text{H}$  and  $^7\text{H}$ , neither  $^6\text{H}$  and protons from the methoxy group (Figure 2.81).

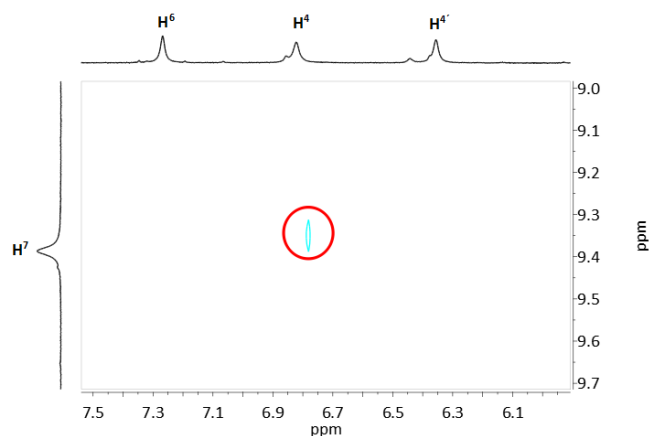
Figure 2.80. NOESY NMR **166** in  $\text{CDCl}_3$

Figure 2.81. NOESY NMR **166** in DMSO- $d_6$ .

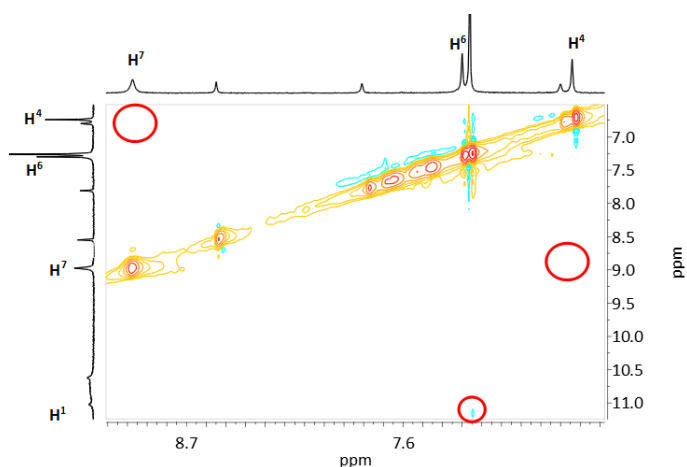
In order to evaluate the influence of the counteranion in the relative conformation of these compounds in solution, different salts **166.HX** ( $\text{BF}_4^-$ ,  $\text{ClO}_4^-$ ,  $\text{MeSO}_3^-$ , etc.) were prepared by washing a DCM solution of the neutral compound with aqueous solutions of the corresponding acid (1 M) (x 3). All NMR experiments are compiled in the CD.

The hydrochloride salt of **166** was found as  $\beta$  conformer in  $\text{CDCl}_3$  (Figure 2.82). In DMSO- $d_6$  the saturation is less clear. The A ring is known to be rotated because a NOESY interaction was found between the triazole CH ( $^7\text{H}$ ) and  $^4\text{H}$  (Figure 2.83), thus the plausible conformations would be  $\gamma$  or  $\delta$ . Lack of NOESY peaks between  $^6\text{H}$  and protons from the methoxy group seem to indicate that the most probable is  $\gamma$ .

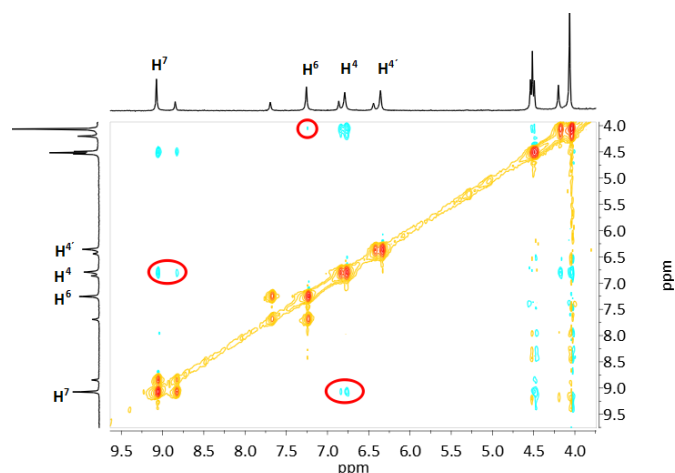
Figure 2.82. NOESY NMR **166.HCl** in  $\text{CDCl}_3$

Figure 2.83. NOESY NMR **166.HCl** in DMSO- $d_6$ .

When the tetrafluoroborate salt **166.HBF<sub>4</sub>** was studied in CDCl<sub>3</sub>, only the predominant conformation can be determined. A NOESY cross peak between <sup>1</sup>H and <sup>6</sup>H and the absence of <sup>4</sup>H and <sup>7</sup>H interaction suggest that it is the  $\alpha$  conformer (Figure 2.84). In DMSO- $d_6$  two conformations are also observed. The majority one presents cross peak between <sup>4</sup>H and <sup>7</sup>H atoms, and <sup>6</sup>H gives cross peak with protons from OCH<sub>3</sub> group, thus it is the  $\delta$ .

Figure 2.84. NOESY NMR **166.H BF<sub>4</sub>** in CDCl<sub>3</sub>

The mesilate salt **166.HMeSO<sub>3</sub>** in CDCl<sub>3</sub> presents a large majority conformation that corresponds to  $\beta$ . In DMSO- $d_6$  a NOESY cross peak was observed between <sup>4</sup>H and <sup>7</sup>H in both conformations. The majority one gives a cross peak between <sup>6</sup>H and the protons from OCH<sub>3</sub> group, thus it is the  $\delta$  (Figure 2.85).

Figure 2.85. NOESY NMR **166.HSO<sub>3</sub>Me** in DMSO-*d*<sub>6</sub>

The low solubility of the perchlorate salt **166.HClO<sub>4</sub>** in CDCl<sub>3</sub> did not allow its study by 2D experiments. Regarding to the sample in DMSO-*d*<sub>6</sub>, the most probable conformation is  $\gamma$  because a NOESY cross peak is observed between <sup>4</sup>H and <sup>7</sup>H, nevertheless no interaction appears among <sup>6</sup>H and protons from the methoxy group.

Table 2.16 shows a summary of the obtained results.  $\alpha$  and  $\beta$  conformations seem to be favoured in the less competitive solvent (CDCl<sub>3</sub>), meanwhile  $\gamma$  and  $\delta$  are predominant in DMSO-*d*<sub>6</sub>.

Table 2.16. Summary of relative conformations of **152** neutral and protonated in solution

	CDCl <sub>3</sub>	DMSO- <i>d</i> <sub>6</sub>
<b>166</b>	$\beta$	$\alpha^b$
<b>166.HCl</b>	$\beta^b$	$\gamma^b$
<b>166.HBF<sub>4</sub></b>	$\alpha^b$	$\delta^b + \gamma^c$
<b>166.MeSO<sub>3</sub>H</b>	$\beta^b$	$\delta^b + \gamma^c$
<b>166.HClO<sub>4</sub></b>	— <sup>a</sup>	$\gamma^b$

<sup>a</sup> Not determined because of the low solubility

<sup>b</sup> majority

<sup>c</sup> minority

<sup>d</sup> it was the neutral form

### 3.4. Determination of apparent pKa values

Following the procedure applied for tambjamins **136.HCl**, **142.HCl** and **144.HCl** (Section 1.4.2.2), the pKa values of the prodiginine inspired compounds (**166.HCl**–

**171.HCl**), as well prodigiosin (**8.HCl**) and obatoclax (**65.HCl**), were determined in of 4:1 DMSO–H<sub>2</sub>O (v/v) (0.1 M NaCl) solution.

The obtained results are summarised in Table 2.17.

Table 2.17. Summary of pKa values. **166–171**, **8** and **65**

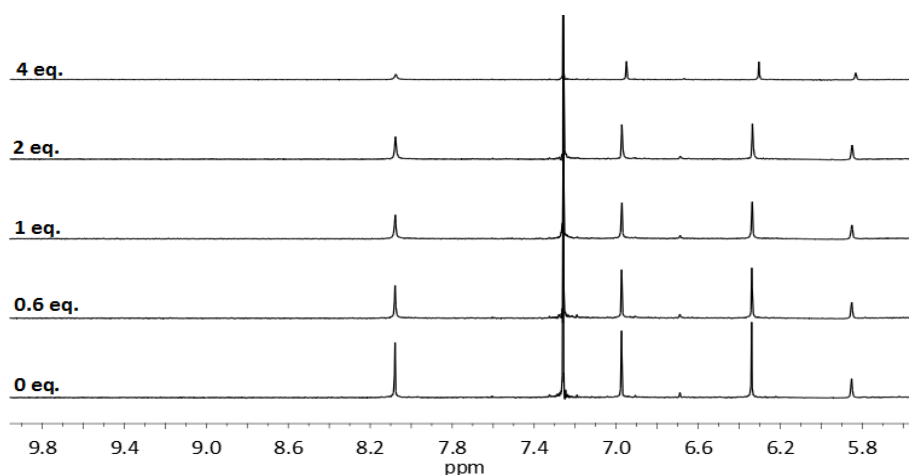
	pKa <sup>a</sup>
<b>166</b>	6.22
<b>167</b>	6.25
<b>168</b>	6.25
<b>169</b>	6.51
<b>170</b>	6.43
<b>171</b>	6.39
<b>8</b>	6.67
<b>65</b>	5.38

<sup>a</sup> 5·10<sup>-6</sup> M solution in 12 mL of 4:1 DMSO–H<sub>2</sub>O (v/v) (0.1 M NaCl), at 25 °C

All these compounds display similar pKa values what was expected, since the different substituents are alkylic chains which do not alter the NH acidity. The obtained values are more similar to the measured for the natural product prodigiosin **8**.

### 3.5. Binding constant assays

The only conditions in which this set of compounds are totally soluble and a single conformation is observed in <sup>1</sup>H NMR, correspond to the chloride salt in CDCl<sub>3</sub>. Thus, binding constants have not been calculated for this family of triazole analogs. Despite this, some titrations have been carried out in order to check how the proton signals are affected under different conditions. When TBACl, TBANO<sub>3</sub> or TEAHCO<sub>3</sub> were added over **166** in neutral state in CDCl<sub>3</sub>, no changes were detected in the proton chemical shifts of the prodiginine inspired compound (Figure 2.86). On the contrary, when AcOH was added, the proton chemical shift of the triazole moved ~1 ppm to downfield as a result of the formation of a hydrogen bonding. It means that the compound needs to be protonated in order to interact with anions (experimental pKa of these molecules are ~ 6.5).

Figure 2.86. Addition of TBACl over **166** in  $\text{CDCl}_3$ .

The addition of  $\text{TEAHCO}_3$  over **166.HCl** in  $\text{CDCl}_3$  gives as a result deprotonation.

The apparent  $K_a$ , was calculated with the shift of three different protons. The replacement of perchlorate by chloride was measured by a  $^1\text{H}$  NMR titration from **166.HClO<sub>4</sub>** with TBACl in  $\text{DMSO-}d_6$  (Figure 2.87). The value of the  $K_a$  obtained for the three different studied protons is shown in Table 2.17. It is said apparent because both salts, the starting (**166.HClO<sub>4</sub>**) and the final one (**166.HCl**), display two conformations in  $\text{DMSO-}d_6$  solution. Moreover, the perchlorate one is not totally soluble in this solvent (full details in Chapter IV; stack plots in the CD).

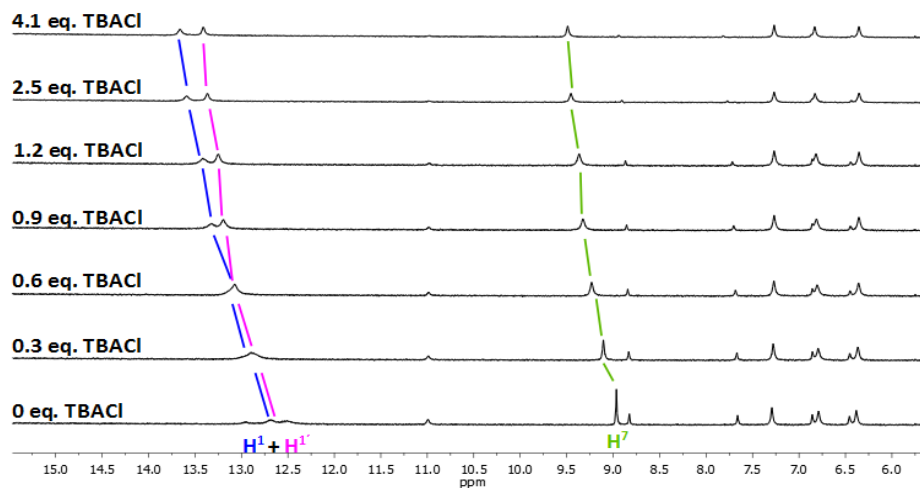
Figure 2.87. Partial stack plot of  $^1\text{H}$  NMR spectra of compound **166.HClO<sub>4</sub>** in  $\text{DMSO-}d_6$ -0.5%  $\text{H}_2\text{O}$  solution under the addition of increasing amounts of tetrabutylammonium chloride

Table 2.17. Binding constants ( $K_a, M^{-1}$ ) calculated from  $NH^1$ ,  $NH^{1'}$  and  $CH^7$  protons

	$K_{a, NH1} (M^{-1})$	$K_{a, NH1'} (M^{-1})$	$K_{a, CH7} (M^{-1})$
<b>166.HClO<sub>4</sub></b>	510±83	510±47	465±59

### 3.6. Anion transport assays

The ionophoric activity of these six compounds was studied with two different methods, potentiometric ISE experiments with the chloride selective electrode and experiments with lucigenin, carboxyfluorescein, HPTS and safranin O fluorescent probes. Alongside, prodigiosin **8.HCl** and obatoclax **65.HCl** were examined under the same conditions in order to obtain comparable results.

The  $Cl^-/AcO^-$ ,  $Cl^-/ClO_4^-$ ,  $Cl^-/NO_3^-$ ,  $Cl^-/HCO_3^-$ ,  $Cl^-/SO_4^{2-}$  and  $Cl^-/gluconate^-$  antiport activity of this set of eight compounds, was tested in vesicles models using the chloride selective electrode. Gluconate is a large hydrophilic anion, thus it is difficult to extract into lipid membranes by mobile carriers. Vesicles loaded with NaCl 451 mM were suspended in an isotonic solution of  $Na_2SO_4$ , to give a final concentration of 0.5 mM POPC. After fifty seconds, the carrier was incorporated in the assay and ten seconds later, a pulse of the extravascular anion salt was added to achieve a final concentration of 40 mM (full details in Chapter IV). Sulfate and gluconate transport is negligible under these conditions. The selectivity sequence followed by these compounds is acetate > perchlorate > nitrate >> bicarbonate. When the natural product, prodigiosin **8.HCl**, and its synthetic analog, obatoclax **65.HCl** were tested, it was observed a variation on the anion selectivity trend (acetate > nitrate > perchlorate > bicarbonate). The order established by the Hofmeister sequence for nitrate and perchlorate was inverted (Figure 2.88. a) **166.HCl**; b) **167.HCl**; c) obatoclax **65.HCl** and d) prodigiosin **8.HCl**).

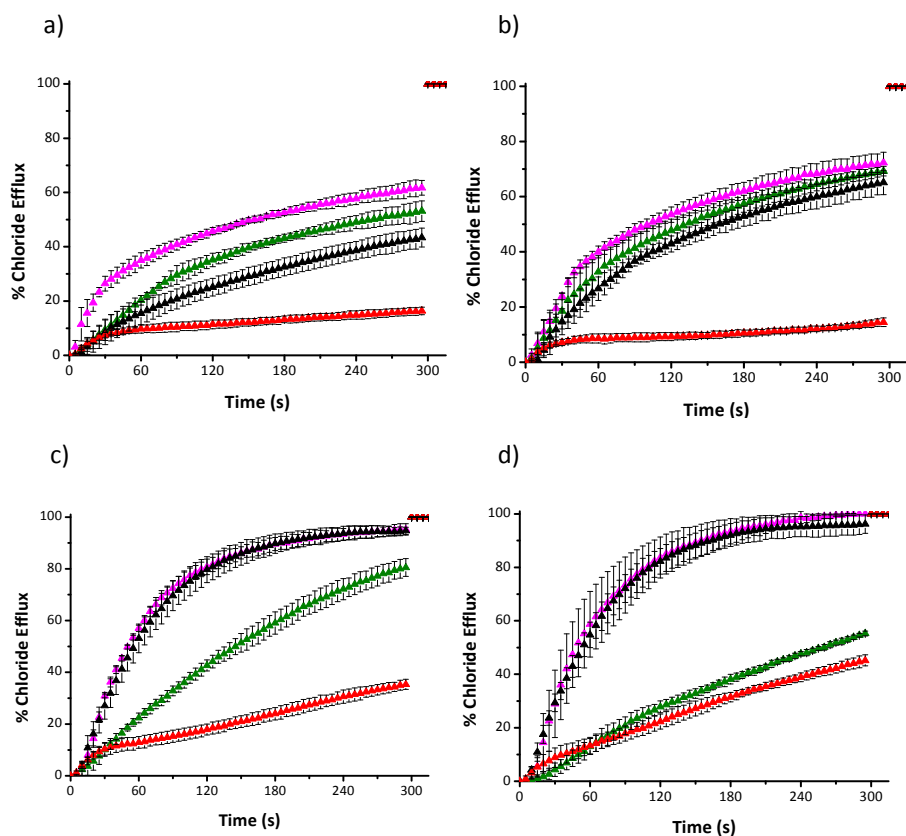


Figure 2.88. Chloride efflux upon addition of a) **166.HCl** 0.25  $\mu\text{M}$ , 0.05 mol%; b) **167.HCl** 0.25  $\mu\text{M}$ , 0.05 mol%; c) obatoclax **65.HCl** 0.25  $\mu\text{M}$ , 0.05 mol% and d) prodigiosin **8.HCl** 0.05  $\mu\text{M}$ , 0.01 mol%. Vesicles loaded with NaCl 451 mM (NaCl 451 mM, 20 mM  $\text{NaH}_2\text{PO}_4$  buffer, pH 7.2, 500 mM ionic strength) were suspended over  $\text{Na}_2\text{SO}_4$  150 mM ( $\text{Na}_2\text{SO}_4$  150 mM, 20 mM  $\text{NaH}_2\text{PO}_4$  buffer, pH 7.2, 500 mM ionic strength). At  $t = 50$  s a pulse of the anion carrier in DMSO, in the corresponding concentration, was added. At  $t = 60$  s a pulse of NaX solution ( $X = \text{AcO}^-$ ,  $\text{ClO}_4^-$ ,  $\text{NO}_3^-$ ,  $\text{HCO}_3^-$ ) to achieve a final concentration in the experiment of 40 mM was incorporated to the sample. Magenta trace:  $X = \text{AcO}^-$ , olive trace:  $X = \text{ClO}_4^-$ , black trace:  $X = \text{NO}_3^-$  and red trace:  $X = \text{HCO}_3^-$ . Each trace represents the average of at least three different trials, done with at least two different batches of vesicles.

After this selectivity analysis, the ionophoric activity of these compounds was measured at different carrier concentrations, under the typical conditions applied in this thesis for  $\text{Cl}^-/\text{NO}_3^-$ ,  $\text{Cl}^-/\text{HCO}_3^-$  assays. The obtained data were used to perform dose-response curves fitted with Hill equation (equation 2.1).  $\text{EC}_{50}$  values and  $n$  parameters were determined (transport figures are available in the CD). The obtained results are summarised in Table 2.18.

Table 2.18. Summary of parameters recovered from ISE assays and lipophilicity. **166.HCl–171.HCl**

	EC <sub>50</sub> (nM) NO <sub>3</sub> <sup>-</sup> /Cl <sup>-</sup> <sup>a</sup>	Hill parameter n NO <sub>3</sub> <sup>-</sup> /Cl <sup>-</sup> <sup>a</sup>	EC <sub>50</sub> (nM) HCO <sub>3</sub> <sup>-</sup> /Cl <sup>-</sup> <sup>b</sup>	Hill parameter n HCO <sub>3</sub> <sup>-</sup> /Cl <sup>-</sup> <sup>b</sup>	ALOGPs <sup>c</sup>
<b>166</b>	24 ± 1	1.39 ± 0.07	1911 ± 166	0.94 ± 0.09	3.38
<b>167</b>	18 ± 1	1.17 ± 0.08	1617 ± 166	0.65 ± 0.08	4.86
<b>168</b>	53 ± 10	0.71 ± 0.14	– <sup>d</sup>	– <sup>d</sup>	6.18
<b>169</b>	30 ± 1	1.27 ± 0.06	2609 ± 203	0.72 ± 0.06	4.93
<b>170</b>	50 ± 7	1.43 ± 0.28	42783 ± 6554	0.63 ± 0.10	6.24
<b>171</b>	641 ± 82	1.07 ± 0.12	– <sup>d</sup>	– <sup>d</sup>	7.41
<b>65</b>	10 ± 1	1.21 ± 0.06	448 ± 37	0.81 ± 0.06	4.15
<b>8</b>	2 ± 1	1.13 ± 0.11	58 ± 3	0.91 ± 0.06	4.65

<sup>a</sup> Liposomes loaded with 489 mM NaCl suspended in 489 mM NaNO<sub>3</sub> (5 mM phosphate buffer, pH 7.2)

<sup>b</sup> Liposomes loaded with 451 mM NaCl suspended in 150 mM Na<sub>2</sub>SO<sub>4</sub> (20 mM phosphate buffer, pH 7.2). After one minute addition of NaHCO<sub>3</sub> to achieve the extravesicular bicarbonate concentration 40 mM.

<sup>c</sup> One of the lipophilicities calculated using e-dragon

<sup>d</sup> not determined

For tambjamines, EC<sub>50</sub> values obtained in Cl<sup>-</sup>/NO<sub>3</sub><sup>-</sup> assays were, on average, one order or magnitude smaller than the corresponding to Cl<sup>-</sup>/HCO<sub>3</sub><sup>-</sup> experiments. In the case of this new family of compounds, the difference is much greater. With NO<sub>3</sub><sup>-</sup> as external anion, the obtained EC<sub>50</sub> values are two or even three orders of magnitude lower than in the case of bicarbonate. This result could be related to the modification of the hydrogen bonding cleft including a triazole C-H. This soft H-bond donor displays selectivity for lipophilic anions (i.e. NO<sub>3</sub><sup>-</sup>) over highly hydrated anions (i.e. HCO<sub>3</sub><sup>-</sup>).<sup>233</sup>

Two different approaches were conducted to confirm the behaviour as mobile carriers of this family of transporters. The first one consisted on testing Cl<sup>-</sup>/NO<sub>3</sub><sup>-</sup> exchange in vesicles composed of POPC:cholesterol (7:3). This methodology is based on the ability of cholesterol to increase the bilayer viscosity and, thus, on difficulting the diffusion of the supramolecular complex through the lipid bilayer. Figure 2.89 shows that the chloride efflux promoted by these prodiginine inspired compounds

<sup>233</sup> M. Lisbjerg, H. Valkenier, B. M. Jessen, H. Al-Kerdi, A. P. Davis and M. Pittelkow, *J. Am. Chem. Soc.*, 2015, **137**, 4948–4951.

tends to be smaller under these conditions, with the exception of the most active compound **167.HCl**, which remained constant (results for **8.HCl** and **65.HCl** display the same tendency. They have not been included in Figure 2.89 for clarity. They are included in Figure 2.42).

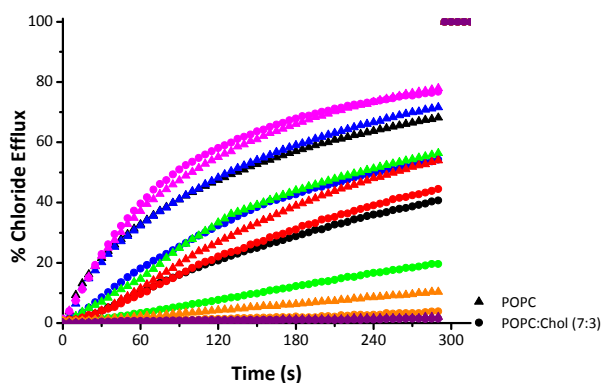


Figure 2.89. Chloride efflux upon addition of triazoles (0.05  $\mu\text{M}$ , 0.01 mol% carrier to lipid) to vesicles composed of POPC (triangles) or POPC:cholesterol (7:3) (circles). Vesicles containing NaCl (489 mM NaCl and 5 mM phosphate buffer, pH 7.2) were immersed in  $\text{NaNO}_3$  (489 mM  $\text{NaNO}_3$  and 5 mM phosphate buffer, pH 7.2). At the end of the experiment, the vesicles were lysed with detergent to release all chloride ions and the resulting value was considered to represent 100% release and used as such. Each trace represents an average of at least three different experiments, done with at least two different batches of vesicles. Black trace: **166.HCl**, magenta trace: **167.HCl**, red trace: **168.HCl**, blue trace: **169.HCl**, green trace: **170.HCl**, orange trace: **171.HCl**, purple trace: blank (10  $\mu\text{L}$  DMSO)

The second one is based on the carboxyfluorescein leakage assay. The use of this fluorescent probe has proved that prodigine-triazole analogs are not forming large non-selective pores in the membrane, as no leakage of carboxyfluorescein out of the vesicles was not detected (Figure 2.90). It means that they act *via* mobile carriers.

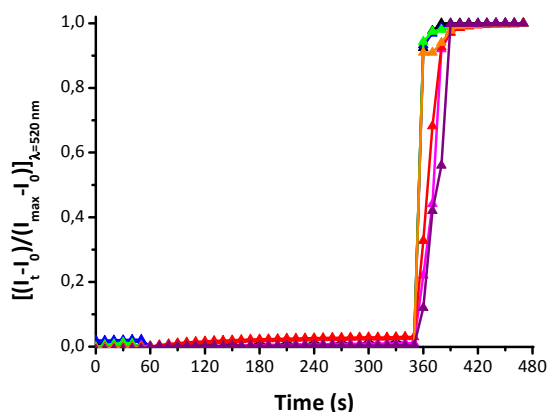


Figure 2.90. Carboxyfluorescein leakage upon addition of triazole-prodiginine analogs to POPC vesicles, 0.025 mM. Vesicles contained NaCl (451 mM, buffered with  $\text{NaH}_2\text{PO}_4$  20 mM to pH 7.2, I.S. 500 mM and 50 mM CF) were suspended in  $\text{Na}_2\text{SO}_4$  (150 mM, buffered with  $\text{NaH}_2\text{PO}_4$  20 mM to pH 7.2, I.S. 500 mM). At  $t = 60$  s addition of the anion carrier (1 mol% carrier to lipid). At  $t = 360$  s addition of 20  $\mu\text{L}$  of detergent. Black trace: **166.HCl**, magenta trace: **167.HCl**, red trace: **168.HCl**, blue trace: **169.HCl**, green trace: **170.HCl**, orange trace: **171.HCl** and purple trace: blank (10  $\mu\text{L}$  DMSO). Each trace represents the average of at least three different trials, done with at least two different batches of vesicles.

As it was mentioned in the tetraheterocycles section (Chapter II. Section 2), in the first stage of this lucigenin assays, it was found a decrease in fluorescence when the anion carrier was added ( $t = 60$  s), even for non active compounds, such as **171.HCl**.

The chloride added when the carrier is used as chloride salt was ruled out as the reason of this fluorescence quenching, by testing the anion carrier as nitrate salts (Figure 2.91).

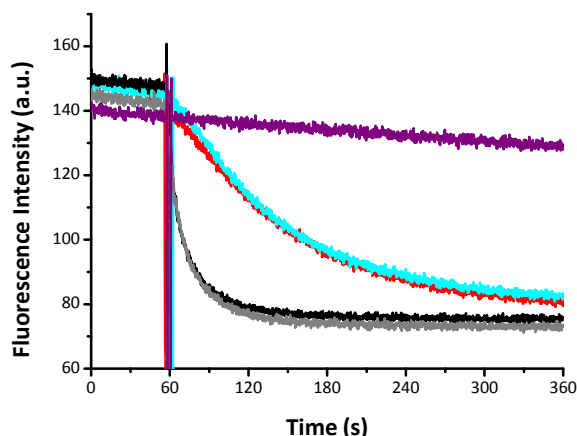


Figure 2.91. Lucigenin assay upon addition of **166.HX** and **168.HX** ( $X = \text{Cl}^-$  or  $\text{NO}_3^-$ ) to POPC:Cholesterol (7:3) vesicles, 0.35 mM POPC. Vesicles contained  $\text{NaNO}_3$  (102.2 mM  $\text{NaNO}_3$ , I.S. 150 mM,  $\text{NaH}_2\text{PO}_4$  20 mM, pH 7.2; lucigenin 3 mM) were suspended in  $\text{NaNO}_3$  (102.2 mM  $\text{NaNO}_3$ , I.S. 150 mM,  $\text{NaH}_2\text{PO}_4$  20 mM, pH 7.2). At  $t = 0$  s a pulse of NaCl was added to achieve a final concentration of 10 mM. At  $t = 60$  s the anion carrier was added (0.7 mol% carrier to lipid). Black trace: **166.HCl**, grey trace: **166.HNO<sub>3</sub>**, red trace: **168.HCl**, cyan trace: **168.HNO<sub>3</sub>** and purple trace: blank (10  $\mu\text{L}$  MeOH). Each trace represents the average of at least three different trials, done with at least two different batches of vesicles.

Experiments, in which no chloride (the quencher) was added to the extravesicular medium and the encapsulated solution contained only buffer, were carried out. After the analysis of these results, it was observed that this decrease in fluorescence emission was related with the concentration in which the anion carrier was added (Figure 2.92 and Figure 2.93). Above (Figure 2.92), all tested compounds were added at 0.14 mol% (500 nM) carrier to POPC (0.35 mM). After the addition of the anion carrier ( $t = 60$  s) the fluorescence remains constant. On the (Figure 2.93), the compounds were added at 0.7 mol% (2.5  $\mu\text{M}$ ) carrier to POPC (0.35 mM), this time it was observed a reduction in the fluorescence emission of lucigenin.

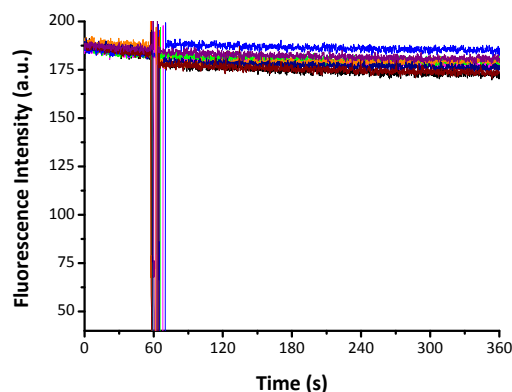


Figure 2.92. Lucigenin assay upon addition of prodiginine inspired compounds, prodigiosin and obatoclax to POPC:Cholesterol (7:3) vesicles, 0.35 mM POPC. Vesicles contained  $\text{NaNO}_3$  (102.2 mM  $\text{NaNO}_3$ , I.S. 150 mM,  $\text{NaH}_2\text{PO}_4$  20 mM, pH 7.2; lucigenin 3 mM) were suspended in  $\text{NaNO}_3$  (102.2 mM  $\text{NaNO}_3$ , I.S. 150 mM,  $\text{NaH}_2\text{PO}_4$  20 mM, pH 7.2). At  $t = 60$  s addition of the anion carrier (0.14 mol% carrier to lipid). Black trace: **166.HCl**, magenta trace: **167.HCl**, red trace: **168.HCl**, blue trace: **169.HCl**, green trace: **170.HCl**, orange trace: **171.HCl**, navy trace: prodigiosin; brown trace: obatoclax and purple trace: blank (10  $\mu\text{L}$  MeOH). Each trace represents the average of at least three different trials, done with at least two different batches of vesicles.

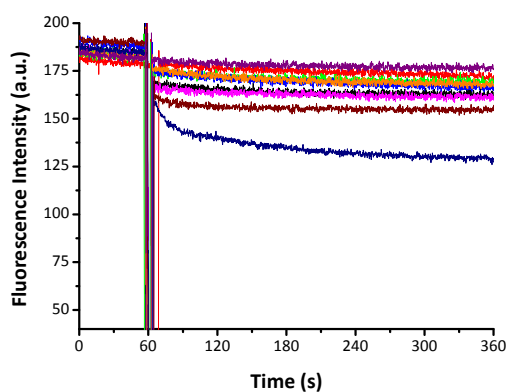


Figure 2.93. Lucigenin assay upon addition of prodiginine inspired compounds, prodigiosin and obatoclax to POPC:Cholesterol (7:3) vesicles, 0.35 mM POPC. Vesicles contained  $\text{NaNO}_3$  (102.2 mM  $\text{NaNO}_3$ , I.S. 150 mM,  $\text{NaH}_2\text{PO}_4$  20 mM, pH 7.2; lucigenin 3 mM) were suspended in  $\text{NaNO}_3$  (102.2 mM  $\text{NaNO}_3$ , I.S. 150 mM,  $\text{NaH}_2\text{PO}_4$  20 mM, pH 7.2). At  $t = 60$  s addition of the anion carrier (0.7 mol% carrier to lipid). Black trace: **166.HCl**, magenta trace: **167.HCl**, red trace: **168.HCl**, blue trace: **169.HCl**, green trace: **170.HCl**, orange trace: **171.HCl**, navy trace: prodigiosin; brown trace: obatoclax and purple trace: blank (10  $\mu\text{L}$  MeOH). Each trace represents the average of at least three different trials, done with at least two different batches of vesicles.

In order to shed light about the origin of this problem, the absorption and emission spectra of all compounds involved in these assays were measured using as a medium the nitrate solution 102.2 mM, as it was done in the case of tetraheterocycles. Again, it was noticed that the fluorescence emission spectrum of lucigenin was overlapped with the absorption spectra of prodiginine inspired compounds (Figure 2.94). Thus the fluorescence emitted by lucigenin (Figure 2.47) was been partially absorbed by the carriers (the higher the anion carrier concentration, the larger the decrease in fluorescence observed).

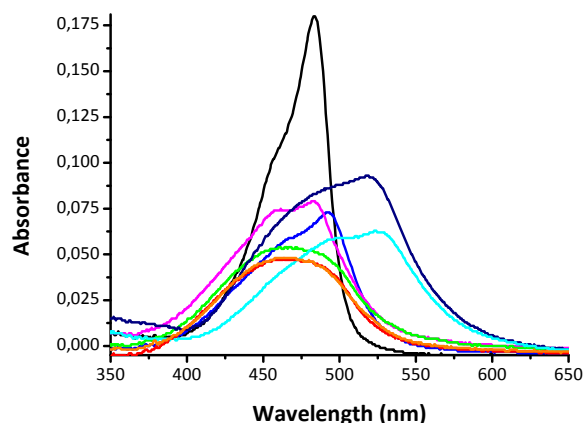


Figure 2.94. Absorption spectra of prodiginine inspired compounds, obatoclax and prodigiosin (2.5  $\mu\text{M}$ ) in  $\text{NaNO}_3$  (102.2 mM  $\text{NaNO}_3$ , I.S. 150 mM,  $\text{NaH}_2\text{PO}_4$  20 mM, pH 7.2). Black trace: **166.HCl**, magenta trace: **167.HCl**, red trace: **168.HCl**, blue trace: **169.HCl**, green trace: **170.HCl**, orange trace: **171.HCl**, navy trace: prodigiosin **8.HCl** and brown trace: obatoclax **65.HCl**.

Once the assays was optimised to avoid the influence of the absorbance of these compounds, lucigenin assays were performed at 0.014 mol% (50 nM). The obtained fluorescence intensities (Figure 2.95) were normalised to  $I_0/I$  and were plotted against time (Figure 2.96). These data were analysed to obtain initial rates ( $I$ ) and half-times ( $t_{1/2}$ ).

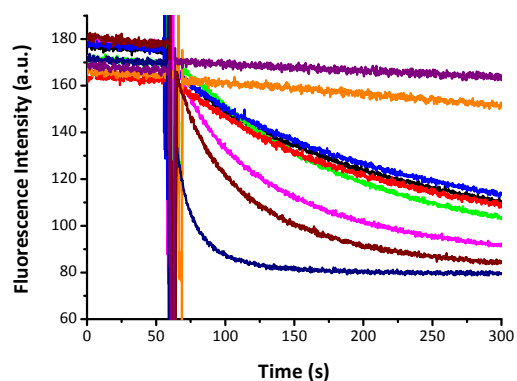


Figure 2.95. Crude fluorescence data of lucigenin assays upon addition of prodiginine inspired compounds, prodigiosin and obatoclax to POPC:Cholesterol (7:3) vesicles, 0.35 mM POPC. Vesicles contained  $\text{NaNO}_3$  (102.2 mM  $\text{NaNO}_3$ , I.S. 150 mM,  $\text{NaH}_2\text{PO}_4$  20 mM, pH 7.2; lucigenin 3 mM) were suspended in  $\text{NaNO}_3$  (102.2 mM  $\text{NaNO}_3$ , I.S. 150 mM,  $\text{NaH}_2\text{PO}_4$  20 mM, pH 7.2). At  $t = 0$  s was added a pulse of NaCl to obtain a final concentration of 10 mM. At  $t = 60$  s the anion carrier was added (0.014 mol% carrier to lipid; 50 nM). Black trace: **166.HCl**, magenta trace: **167.HCl**, red trace: **168.HCl**, blue trace: **169.HCl**, green trace: **170.HCl**, orange trace: **171.HCl**, navy trace: prodigiosin, brown trace: obatoclax and purple trace: blank (10  $\mu\text{L}$  MeOH). Each trace represents the average of at least three different trials, done with at least two different batches of vesicles.

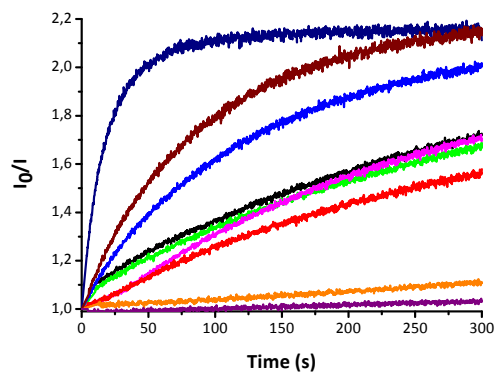


Figure 2.96.  $I_0/I$  normalization of lucigenin assay upon addition of prodiginine inspired compounds, prodigiosin and obatoclax to POPC:Cholesterol (7:3) vesicles, 0.35 mM POPC. Vesicles contained  $\text{NaNO}_3$  (102.2 mM  $\text{NaNO}_3$ , I.S. 150 mM,  $\text{NaH}_2\text{PO}_4$  20 mM, pH 7.2; lucigenin 3 mM) were suspended in  $\text{NaNO}_3$  (102.2 mM  $\text{NaNO}_3$ , I.S. 150 mM,  $\text{NaH}_2\text{PO}_4$  20 mM, pH 7.2). At  $t = 0$  s was added a pulse of NaCl to obtain a final concentration of 10 mM. At  $t = 60$  s the anion carrier was added (0.014 mol% carrier to lipid; 50 nM). Black trace: **166.HCl**, magenta trace: **167.HCl**, red trace: **168.HCl**, blue trace: **169.HCl**, green trace: **170.HCl**, orange trace: **171.HCl**, navy trace: prodigiosin, brown trace: obatoclax and purple trace: blank (10  $\mu\text{L}$  MeOH). Each trace represents the average of at least three different trials, done with at least two different batches of vesicles.

Our data of lucigenin assays, obtained from plotting  $I_0/I$  vs time (Figure 2.96) were analysed to obtain initial rates ( $I$ ) and approximate half-times ( $t_{1/2}$ ). Each curve was fitted with Origin 8 to the previous detailed models. The obtained results are shown in Table 2.19.

Table 2.19. Obtained results from analysis of fluorescence decays and lipophilicities

	$t_{1/2}$ (s) <sup>a</sup>	$[I]$ (s <sup>-1</sup> ) <sup>b</sup>	$[I]$ (s <sup>-1</sup> ) <sup>c</sup>	$[I]$ (s <sup>-1</sup> ) <sup>d</sup>	ALOGPs <sup>e</sup>
<b>166.HCl</b>	181.0	0.0036	0.0036	0.0157	3.38
<b>167.HCl</b>	84.8	0.0086	0.0087	0.0115	4.86
<b>168.HCl</b>	190.4	0.0031	0.0031	0.0012	6.18
<b>169.HCl</b>	177.3	0.0035	0.0035	0.0110	4.93
<b>170.HCl</b>	200.3	0.0040	0.0040	0.0006	6.24
<b>171.HCl</b>	– <sup>f</sup>	0.0003 <sup>g</sup>	0.0003 <sup>g</sup>	0.0003 <sup>g</sup>	7.41
<b>8.HCl</b>	15.4	0.0479	0.0479	0.0643	4.65
<b>65.HCl</b>	62.6	0.0128	0.0128	0.0156	4.15

<sup>a</sup> Eq. 2.17. Data fitted to eq. 2.11. Single exponential decay function

<sup>b</sup> Eq. 2.13. Data fitted to eq. 2.9. Asymptotic exponential function

<sup>c</sup> Eq. 2.15. Data fitted to eq. 2.11. Single exponential decay function

<sup>d</sup> Eq. 2.16. Data fitted to eq. 2.12. Double exponential decay function

<sup>e</sup> One of the lipophilicities calculated using e-dragon

<sup>f</sup> Not determined. It was not possible fit this data to a single exponential decay

<sup>g</sup> Fitted to a lineal function

The values from Table 2.19 showed the same tendency observed in ISE assays. Compound **167.HCl** is the most active carrier of this family, showing the smallest  $t_{1/2}$ . Compound **171.HCl** showed the lower level of activity, likely because of its high lipophilicity. Prodigiosin **8.HCl** and obatoclax **65.HCl** exhibit better anionophoric properties than prodiginine inspired compounds, with smaller  $t_{1/2}$  and higher initial rates. Regarding to the model applied for fitting the data, equations 2.13 and 2.15 gave the same results. The results obtained with equation 2.16, the largest one, differ from the calculated with the other two models. This variation is originated by the presence of the extra term. In the case of prodiginine inspired compounds this difference is higher than for prodigiosin and obatoclax. It could be related to the fact that equation 2.16 finds problems to diverge when the curve needs longer times to reach an asymptotic value.

The family of triazoles offer a good opportunity to test the lipophilicity balance proposed by Davis and *co-workers*.<sup>234</sup> The pairs **167.HCl**/**169.HCl** and **170.HCl**/**168.HCl** contain the same total number of carbon atoms in their aliphatic chains, distributed in a different manner (Figure 2.97). The  $EC_{50}$ ,  $t_{1/2}$  and initial rate values of the **167.HCl** (8 + 2 carbons) are twice better than the obtained for **169.HCl** (6 + 4 carbons). In relation to the other couple **170.HCl**/**168.HCl**, the compound with the binding site nearest to the end of the molecule **168.HCl** (12 + 2 carbons) displays slightly better anionophoric properties than **170.HCl** (8 + 6 carbons).

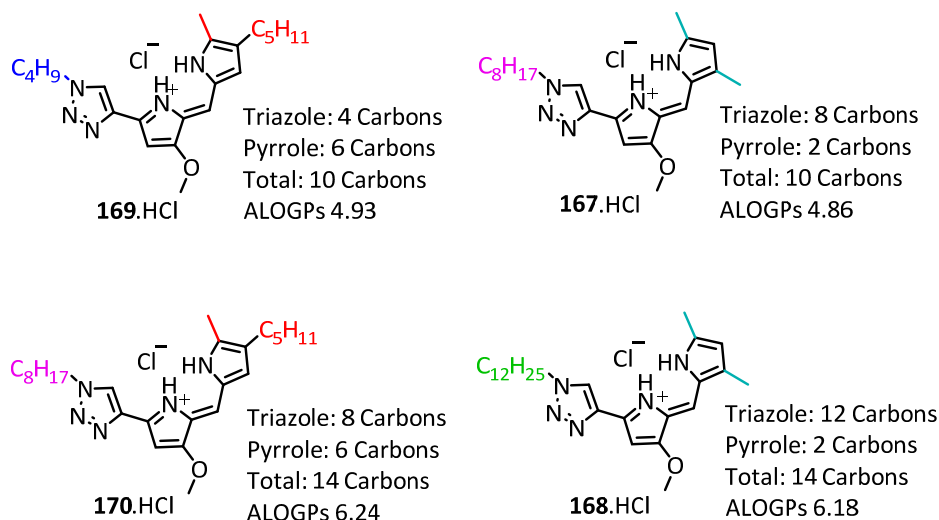


Figure 2.97. Total number of carbon atoms in aliphatic chains.

The ability of triazole analogs to alter the membrane potential was tested in vesicles assays using the safranin O method. This fluorescent probe emits at 580 nm, thus the problem of fluorescence quenching was not found under these conditions, because the emission spectrum of safranin O is not overlapped with the absorption spectra of prodiginine inspired compounds. These experiments are detailed in Chapter IV. In Figure 2.98, it could be observed that the ability of these compounds to alter the membrane potential correlates well with the transport tendency. **167.HCl** displays the best results, meanwhile **171.HCl** is a poor anion carrier.

<sup>234</sup> H. Valkenier, C. J. E. Haynes, J. Herniman, P. A. Gale and A. P. Davis, *Chem. Sci.*, 2014, **5**, 1128–1134.

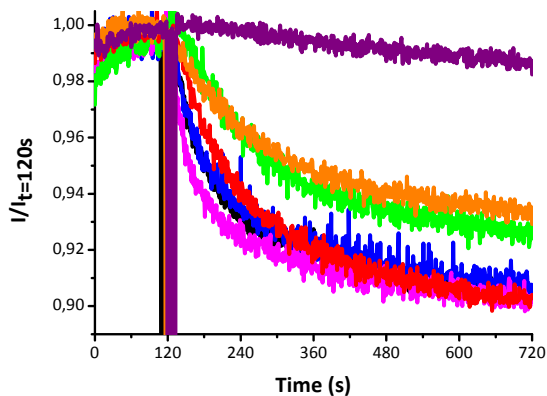


Figure 2.98. Membrane polarization upon addition of prodiginine inspired compounds to POPC vesicles, 0.25 mM. Vesicles contained NaCl (28.8 mM, buffered with  $\text{NaH}_2\text{PO}_4$  5 mM to pH 7.2, I.S. 40 mM) were suspended in  $\text{Na}_2\text{SO}_4$  (9.6 mM, buffered with  $\text{NaH}_2\text{PO}_4$  5 mM to pH 7.2, I.S. 40 mM, and 0.2  $\mu\text{M}$  S.O). At  $t = 120$  s addition of the anion carrier (0.1 mol% carrier to lipid). Black trace: **166.HCl**, magenta trace: **167.HCl**, red trace: **168.HCl**, blue trace: **169.HCl**, green trace: **170.HCl**, orange trace: **171.HCl** and purple trace: blank (10  $\mu\text{L}$  DMSO). Each trace represents the average of at least three different trials, done with at least two different batches of vesicles.

The ability of prodiginine inspired compounds to compensate pH gradients in liposomes was investigated with the fluorescent probe HPTS. Although HPTS emission spectrum is overlapped with the absorption spectra of the tested compounds (Figure 2.92), the working concentrations, 50 nM (0.01 mol% to POPC) and 5 nM (0.001 mol% to POPC), were optimised to avoid interferences in these assays.

All these compounds were shown to compensate pH gradients. Their activity follows a similar trend as in other vesicles assays. **167.HCl** stands out as the most active derivative and **171.HCl** displays poor activity (Figures 2.99 and 2.100).

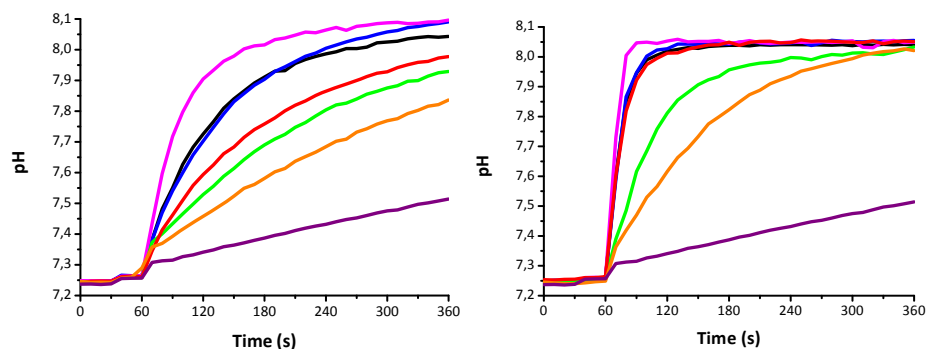


Figure 2.99. Variation of pH upon addition of prodiginine inspired compounds to POPC:cholesterol (7:3) vesicles, 0.5 mM POPC. Vesicles contained  $\text{NaNO}_3$  (126.25 mM  $\text{NaNO}_3$ , 10 mM buffer phosphate pH 7.2, I.S. 150 mM and HPTS 10  $\mu\text{M}$ ) were suspended in  $\text{NaNO}_3$  (126.25 mM  $\text{NaNO}_3$ , 10 mM buffer phosphate pH 7.2 and I.S. 150 mM). At  $t = 30$  s addition of the anion carrier and at  $t = 60$  s addition of 11  $\mu\text{L}$  NaOH 0.5 M. Black trace: **166.HCl**, magenta trace: **167.HCl**, red trace: **168.HCl**, blue trace: **169.HCl**, green trace: **170.HCl**, orange trace: **171.HCl** and purple trace: blank (10  $\mu\text{L}$  DMSO). Each trace represents the average of at least three different trials, done with at least two different batches of vesicles. Left: pH data obtained from the polynomial adjustment at 0.001 mol%. Right: pH data obtained from the polynomial adjustment at 0.01 mol%.

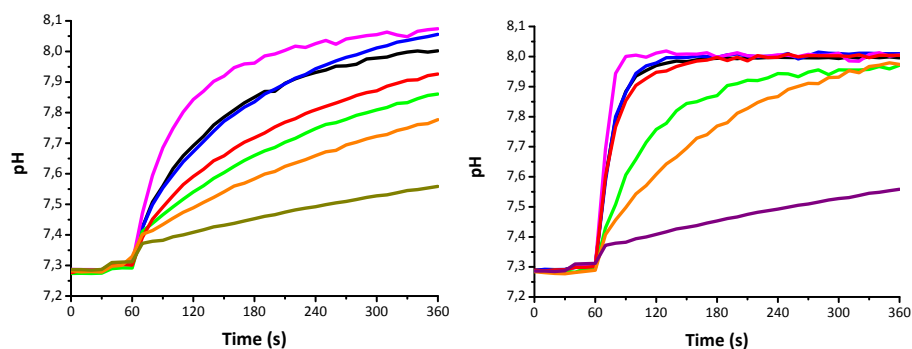
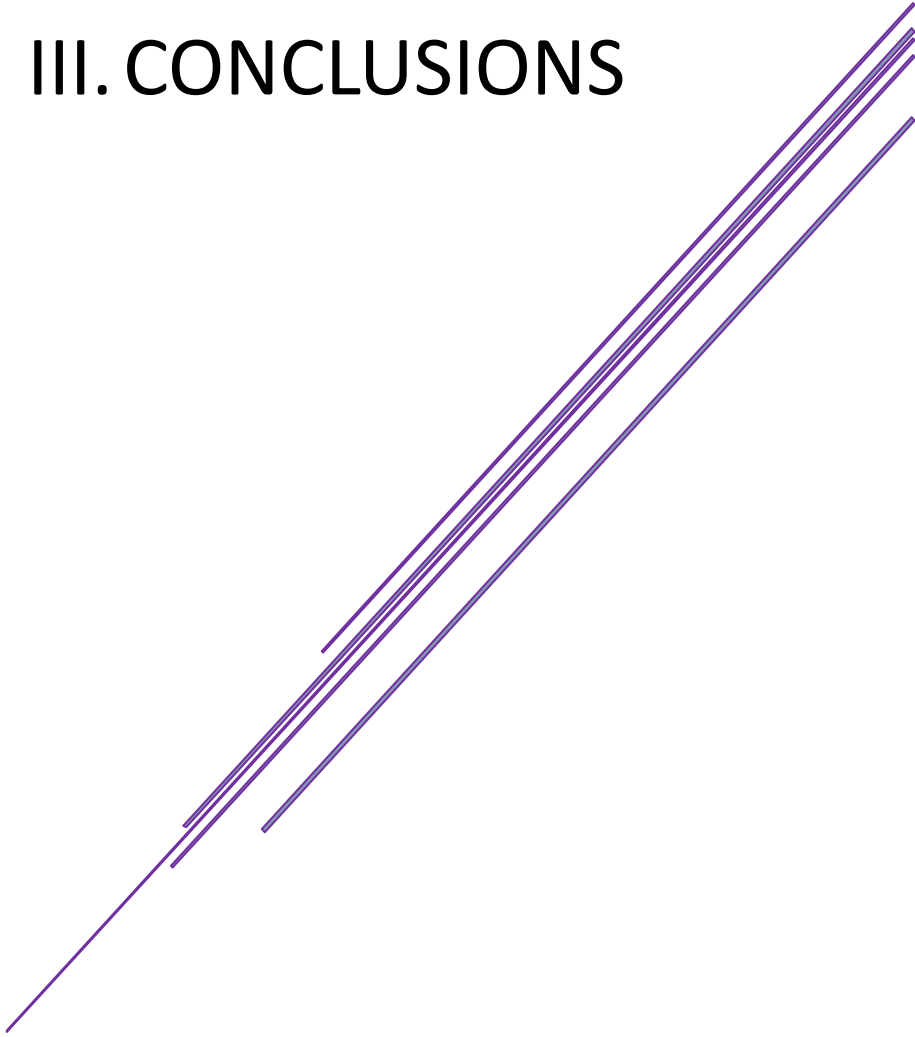


Figure 2.100. Variation of pH upon addition of prodiginine inspired compounds to POPC:cholesterol (7:3) vesicles, 0.5 mM POPC. Vesicles contained  $\text{NaNO}_3$  (126.25 mM  $\text{NaNO}_3$ , 10 mM buffer phosphate pH 7.2, I.S. 150 mM and HPTS 10  $\mu\text{M}$ ) were suspended in  $\text{NaNO}_3$  (126.25 mM  $\text{NaNO}_3$ , 10 mM buffer phosphate pH 7.2 and I.S. 150 mM). At  $t = 30$  s addition of the anion carrier and at  $t = 60$  s addition of 11  $\mu\text{L}$  NaOH 0.5 M. Black trace: **166.HCl**, magenta trace: **167.HCl**, red trace: **168.HCl**, blue trace: **169.HCl**, green trace: **170.HCl**, orange trace: **171.HCl** and purple trace: blank (10  $\mu\text{L}$  DMSO). Each trace represents the average of at least three different trials, done with at least two different batches of vesicles. Left: pH data obtained from the S-Logistic model at 0.001 mol%. Right: pH data obtained from the S-Logistic model at 0.01 mol%.

In principle, this increase in the internal pH could be the result of two different mechanisms of transport. A  $\text{H}^+/\text{NO}_3^-$  symport efflux or a  $\text{NO}_3^-/\text{OH}^-$  antiport.

# III. CONCLUSIONS





In this thesis, three families of anion carriers with potential application as drugs: synthetic tambjamine analogs, tetraheterocyclic transporters and prodiginine inspired compounds have been developed and studied.

The ionophoric activity of all compounds was studied in vesicle models, using different techniques. Quantification of the transport activity was carried out using chloride selective electrode assays. Activities in the range from nM to  $\mu$ M were found. A carrier mechanism, in which the active transporter exchange anions across the phospholipid membrane, is proposed for all studied compounds. Using different fluorescent dyes it is possible to monitor the trafficking of chloride, pH changes and creation of electrochemical gradients as a result of the activity of these compounds in liposomes.

Tambjamine alkaloids constitute a convenient model to develop active anion transporters because of their straightforward synthetic access. Multiple variations involving the enamine substituent, the nature of the heterocycle and the 4-alkoxy substituent were explored. A QSAR analysis of the results highlighted the importance of lipophilicity as a key parameter governing the transport activity of these compounds. An optimal value of lipophilicity can be determined for the different families of compounds. This value shifted depending on other factors involving the structure of the studied compounds.

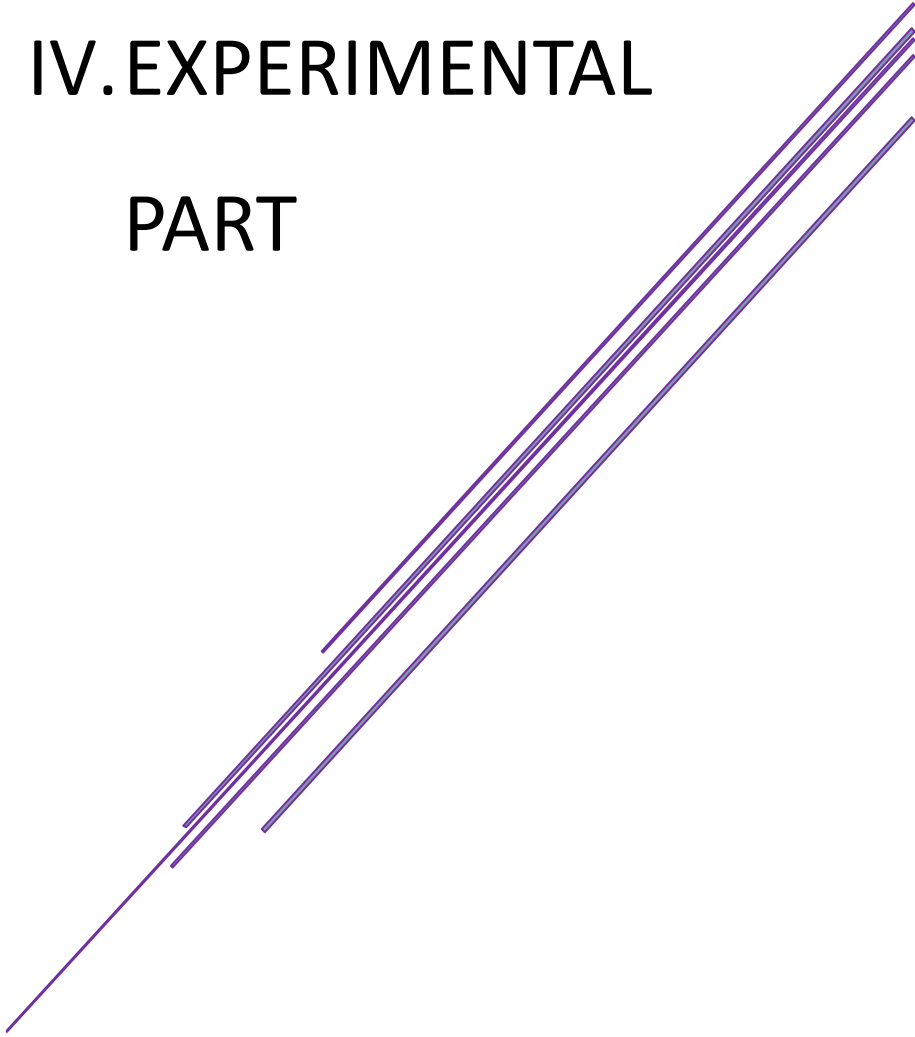
The geometry of the binding site seems to play an important role in the transport process since the replacement of the A ring in the tambjamine scaffold by 2-indole and 7-indole moieties gives rise to different transport efficiencies, when the enamine substituent is maintained.

A family of tetraheterocyclic transporters was developed. These compounds were found to be extremely active anion carriers, rivalling the natural product prodigiosin. This structure is also suitable to develop highly fluorescent BODIPY derivatives.

It is possible to develop active anion transporters inspired in the structure of prodiginines by replacing one of the pyrrole groups by a 1,2,3-triazole heterocycle. This resulted in molecules with similar hydrogen bonding cleft than prodiginines yet different properties, for instance a significantly higher selectivity for the transport of chloride in the chloride/nitrate exchange process compared to the chloride/bicarbonate exchange assay.



# IV. EXPERIMENTAL PART





## 1. GENERAL REMARKS

All reactions involving air sensitive compounds were carried out under a N<sub>2</sub> atmosphere (99.99%). Glassware was oven-dried (120 °C), evacuated and purged with nitrogen.

### 1.1. Starting reagents and solvents

All solvents and starting materials were purchased from commercial suppliers and used without further purification unless otherwise stated. Dry solvents were obtained by distillation and degassed for 15 minutes before being used. POPC and cholesterol were supplied by Sigma Aldrich.

### 1.2. Chromatography

TLC analysis were performed on Al foils coated with silica gel 60 with F<sub>254</sub> indicator and Al foils coated with Aluminum oxide 60 neutral with F<sub>254</sub> indicator. The chromatograms were visualised by UV light (254 nm and 366 nm). Flash column chromatography was carried out on silica gel 60 230–350 mesh or aluminium oxide 90 active neutral 70–230 mesh ASTM, deactivated from Brockman grade I to Brockman grade III. This last one, was obtained by stirring the aluminium oxide with 6% of water, referred to weigh, overnight.

### 1.3. Instrumental techniques

**Nuclear Magnetic Resonance:** NMR were determined on a Varian Mercury-Plus 300 MHz, Varian Inova-400 MHz and Bruker BVT3000 300 MHz spectrometers. Chemical shifts for <sup>1</sup>H NMR are reported in parts per million (ppm) using the residual solvent peak as reference. Coupling constants are reported in Hz. The following abbreviations are used for spin multiplicity: s, singlet; br s, broad singlet; d, doublet; t, triplet; br t, broad triplet; q, quadruplet; br q, broad quadruplet; m, multiplet. Chemical shifts for <sup>13</sup>C{<sup>1</sup>H} NMR are reported in ppm using the residual solvent peak as reference and the multiplicities are determined by DEPT 135 experiments.

**Mass spectrometry:** High Resolution Mass Spectra HRMS were recorded using a Micromass Autospec spectrometer using EI at 70 eV and reported as m/z (relative intensity). GC-MS and low resolution mass spectra (LRMS) measurements were

recorded on an Agilent 6890N/5973 Network GC System, equipped with a HP-5MS column.

**X Ray Diffraction:** Single Crystal X Ray Driffractometer Bruker.

**Fluorescence:** the fluorescence emission was recorded using a HITACHI F-7000 Fluorescence spectrophotometer equipped with stirrer. Two different sorts of cuvettes were used depending on the assay: standard 10 mm quartz glass cells from Hellma Analytics High Precision Cell made of Quartz SUPRASIL or use and throw MAPM-F10-100 labbox cuvettes. All measurements were performed at 25 °C unless specified.

**UV-Vis absorbance:** the UV-Vis spectra were recorded in a HITACHI U-3900 UV-Visible spectrophotometer. Standard 10 mm quartz glass cells from Hellma Analytics High Precision Cell made of Quartz SUPRASIL or use and throw MAPM-F10-100 labbox cuvettes were used. All measurements were performed at 25 °C unless specified.

**Chloride Selective Electrode measurements:** chloride concentration in transport experiments was recorded using a Combination Chloride Electrode HI4107 Hanna Instruments and a Chloride Selective Electrode 96 52 C Crison.

**pH measurements** were made using a CRISON pHmeter 50 14 T.

## 2. SYNTHETIC PROCEDURES

### 2.1. Tambjamine-like transporters synthesis

A variety of tambjamine analogs has been synthesised. They have been developed applying modifications of a previously reported method.

4-benzyloxy-3-pyrrolin-2-one **77b** was prepared from the commercially available 4-methoxy-3-pyrrolin-2-one **77a**, applying modifications over a previously described method.<sup>235</sup> 4-methoxy-3-pyrrolin-2-one was dissolved in 9.3 eq. of benzyl alcohol and 0.12 eq. of MeSO<sub>3</sub>H were added over the mixture. It was heated at 80 °C during 1.5–2 h or until TLC (DCM) showed total consumption of the starting material. Once the reaction had finished, it was cooled at room temperature. The crude was subjected to a flash column chromatography using DCM as mobile phase. Once the benzyl alcohol efflux had finished, the mobile phase polarity was changed to DCM: MeOH (19:1) and **77b** was obtained.

The corresponding pyrrolin-2-one was subjected to a Vilsmeier-Haack reaction with POBr<sub>3</sub> and Diethylformamide (49% yield).<sup>236</sup> The obtained azafulvene **78** was mixed with the corresponding boronic acid under Suzuki-Miyaura cross-coupling conditions to yield the corresponding aldehyde **79** (Scheme 4.1).<sup>237, 238</sup>

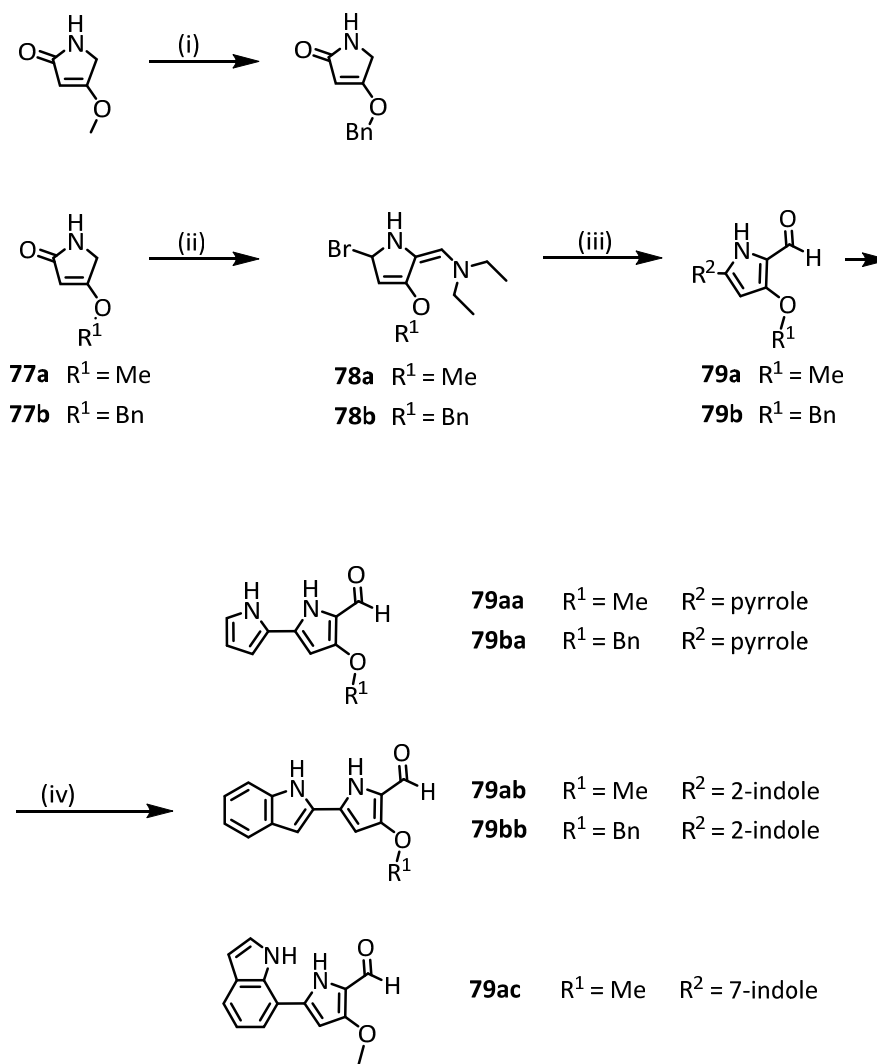
Synthesis of 5-(1H-indol-7-yl)-3-methoxy-1H-pyrrole-2-carbaldehyde **79ac** has not been already reported. (1H-indol-7-yl) boronic acid supplied with the boronic acid unit protected as 4,4,5,5-tetramethyl-1,3,2-dioxaborolan-2-yl (1.1 eq.) was treated with azafulvene **78**. The obtained solid was purified by column chromatography on silica gel (CH<sub>2</sub>Cl<sub>2</sub>/AcOEt 3:1) to yield the corresponding aldehyde **79ac** in moderate to good yields.

<sup>235</sup> Meul, T. (1988), *4-Benzyloxy-3-pyrrolin-2-one, its preparation and use in the synthesis of 2,4-pyrrolidinedione, an antibiotic intermediate*. No. EP252363A119880113. Eur. Pat. Appl.

<sup>236</sup> K. Dairi, S. Tripathy, G. Attardo and J.-F. Lavallée, *Tetrahedron Lett.*, 2006, **47**, 2605–2606.

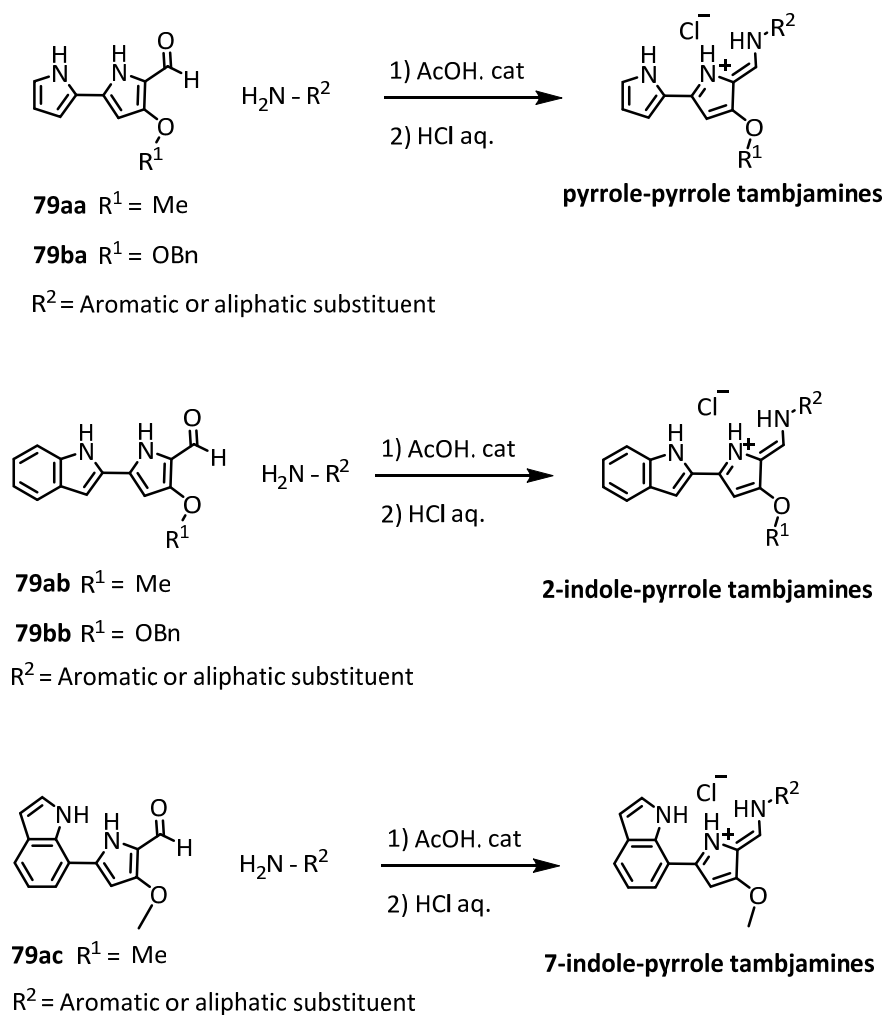
<sup>237</sup> B. Díaz de Greñu, P. Iglesias-Hernandez, M. Espona, D. Quiñero, M.E. Light, T. Torroba, R. Pérez-Tomás and R. Quesada, *Chem. Eur. J.*, 2011, **17**, 14074–14083.

<sup>238</sup> D. M. Pinkerton, M. G. Banwell and A. C. Willis, *Org. Lett.*, 2007, **9**, 5127–5130.



Scheme 4.1. Synthesis of tambjamine precursors.

Tambjamins were prepared in a 50 mL round bottom flask. The corresponding amine (1.3 mmol–5 mmol; 1.3 – 5 eq.) was added over a suspension of the aldehyde (1 mmol) in 10 mL of CHCl<sub>3</sub> or DCE and 40 μL of acetic acid. The mixture was stirred at 60 or 82 °C, depending on the solvent, overnight or until TLC analysis (Hexane:AcOEt 1:1) showed total consumption of the starting material. The reaction was cooled at room temperature. Then, it was diluted with 40 mL of DCM and washed (x3) with HCl 1M (3 x 30 mL). The organic layer was dried over Na<sub>2</sub>SO<sub>4</sub> and evaporated under vacuum to yield the corresponding tambjamine analogs in good to excellent yields, unless a few exceptions (Scheme 4.2).



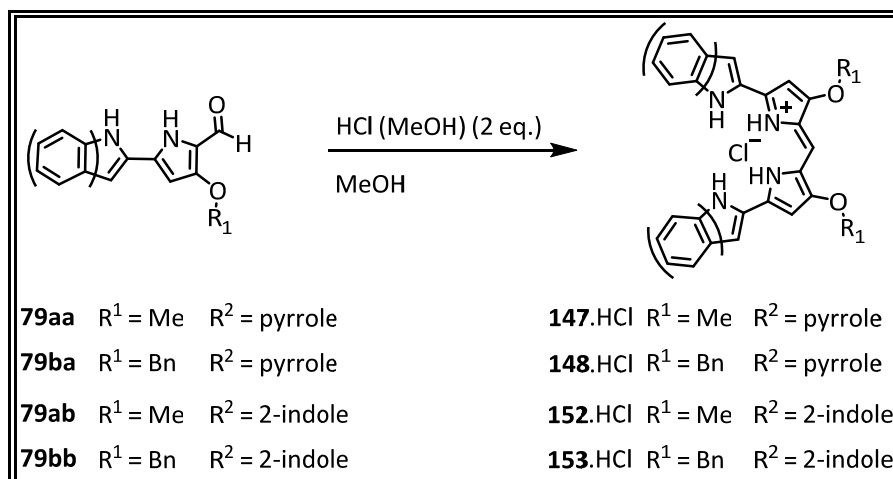
Scheme 4.2. Synthesis of tambjamine analogs

## 2.2. Tetraheterocyclic transporters synthesis

Aldehydes were synthesised as previously described (Scheme 4.1). Compounds **147.HCl–148.HCl** and **152.HCl–153.HCl**, were prepared applying modifications to a previously reported procedure.<sup>239</sup> In a 50 mL round bottom flask, there were added the corresponding aldehyde (0.5 mmol) and MeOH (6 mL). A 0.5 M solution of HCl (in MeOH) (2 eq.) was incorporated, drop by drop, to the obtained aldehyde suspension (Scheme 4.3). Quickly, it was observed a color change from grey/dark

<sup>239</sup> B. Díaz de Greñu, P. Iglesias Hernández, M. Espona, D. Quiñonero, M. E. Light, T. Torroba, R. Pérez-Tomás and R. Quesada, *Chem. Eur. J.*, 2011, **17**, 14074–14083; H. H. Wasserman, D. J. Friedland, D. A. Morrison, *Tetrahedron Lett.* 1968, **9**, 641–644.

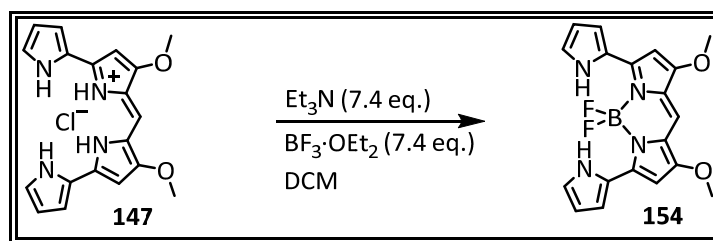
green to dark blue. The reaction was stirred overnight or until TLC analysis (Hexane:AcOEt 1:1) showed total consumption of the starting material. The solvent was evaporated under reduced pressure. The obtained solid was dissolved in 20 mL of DCM and washed with HCl 1M (x3). The organic layer was dried over Na<sub>2</sub>SO<sub>4</sub> and the solvent was removed under reduced pressure. A TLC (Hexane: AcOEt; 1:1). They were crystallised in DCM:hexane and stored.



Scheme 4.3. Synthesis of tetraheterocycles

### 2.3. BODIPY synthesis

In a 100 mL round bottom flask compound **147.HCl** was dissolved in DCM (0.28 mmol per 10 mL; 0.01 mM) and was placed in an ice bath. It was deprotonated with Et<sub>3</sub>N (7.4 eq.). The color changed from dark blue to purple. 15 minutes later, 7.4 eq. of BF<sub>3</sub>·OEt<sub>2</sub> were added drop by drop during 30 minutes. At the end of the addition, the color was blue. After 2 hours, a TLC analysis in DMC showed almost total consumption of the starting material. Some ice was added inside the round bottom flask and the solvent was evaporated in the rotatory evaporator. The remaining water was removed with a glass pipette. The obtained solid was purified by chromatography column using as mobile phase DCM:Hexane 5:1. It was obtained in 34% yield (Scheme 4.4).



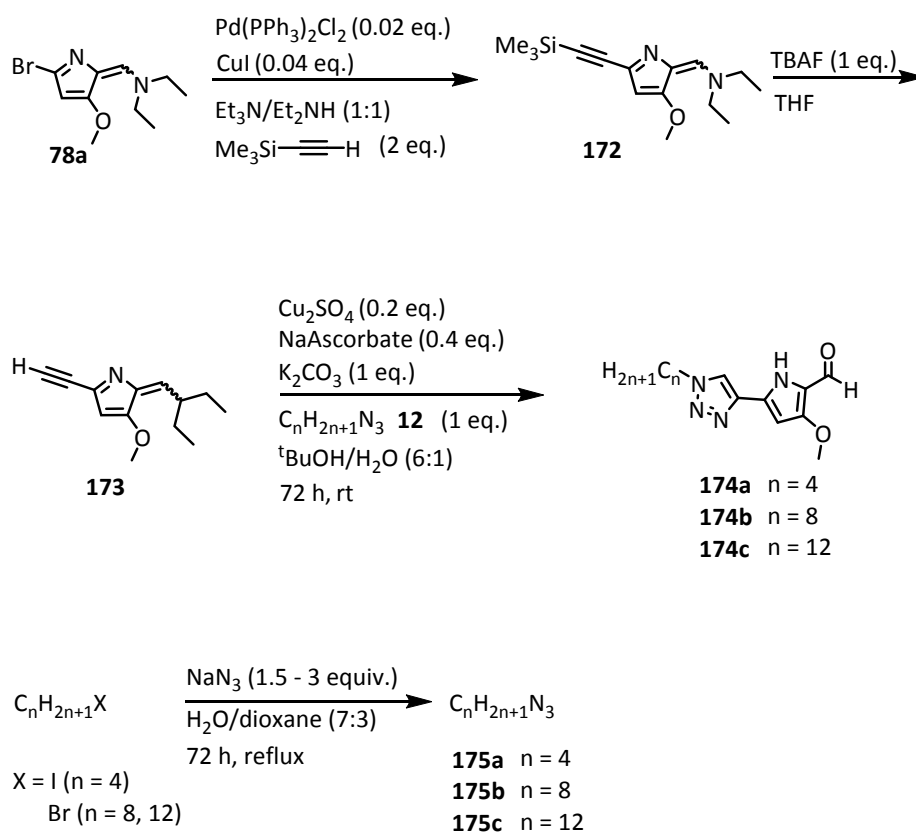
Scheme 4.4. Synthesis of BODIPY

## 2.4. Prodiginine inspired compounds synthesis

Azafulvene **78a** was prepared following the same procedure as in the synthesis of tambjamines. A mixture of compound **78a** (4 mmol), Pd(PPh<sub>3</sub>)<sub>2</sub>Cl<sub>2</sub> (0.02 eq.) and CuI (0.04 eq.) were subjected to vacuum/nitrogen cycles (x3), in to a two-neck schlenk flask. Next the solvents were added (Et<sub>2</sub>NH/Et<sub>3</sub>N (1:1), 10 mL), followed by the alkyne (2 eq.). It was stirred under nitrogen atmosphere at 80 °C overnight. After cooling the reaction, it was diluted with water (80 mL) and extracted with CH<sub>2</sub>Cl<sub>2</sub> (2 × 60 mL). Long times were needed to separate the phases because a dark dense interface was usually obtained. The organic layer was dried over anhydrous Na<sub>2</sub>SO<sub>4</sub> and concentrated at reduced pressure to give compound **172** in 66% yield. **172** was treated with TBAF (1 eq. 1 M solution in THF) in THF at r.t. After three hours the solvent was evaporated and the obtained residue was diluted in DCM (50 mL) and washed with water (x3). The combined organic layers were dried over anhydrous Na<sub>2</sub>SO<sub>4</sub> and evaporated at reduced pressure. They were dissolved in AcOEt and filtered over 2 cm of silica gel under vacuum, with a filter plate (pore 2). The organic layer was concentrated at reduced pressure to yield compound **173** in a 70% yield.

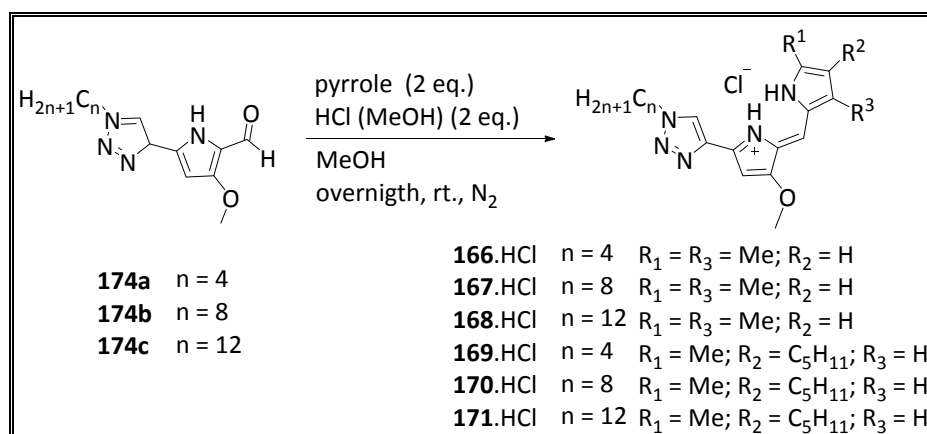
Azides **175**, were synthesised from NaN<sub>3</sub> and the corresponding aliphatic halide in a 250 mL round bottom flask (Scheme 4.5). Over a stirred mixture of water and dioxane (7:3) it was added the corresponding halide (2 mL/mmol). NaN<sub>3</sub> was pulverised and incorporated to the solution (1.5–3 eq.). It was stirred vigorously at 100 °C until <sup>1</sup>H NMR analysis show total consumption of the starting material. The flask was put in an ice-water bath and water was added (10 mL/mmol). It was stirred during 10 minutes. The reaction was extracted with ether (3 x 60 mL) and the combined organic layers were washed once with brine (20 mL/mmol). The ethereous layer was dried over anhydrous Na<sub>2</sub>SO<sub>4</sub> and concentrated at reduced pressure to yield the corresponding azides as colorless oils. The four carbons azide **175a** was stored with solvent (1:1) because otherwise it could be explosive.

Compound **173** was subjected to a CuAAC reaction to yield the corresponding aldehyde precursors of prodiginine inspired compounds. A mixture of the alkyne **173** (5 mmol) and the corresponding azide **175** (1 eq.) was stirred in a schlenk flask. Over that it was added  $\text{CuSO}_4$  (0.2 eq.) solved in the half of the needed water (7 mL),  $t\text{BuOH}$  (33 mL),  $\text{K}_2\text{CO}_3$  (1 eq.), sodium ascorbate (0.4 eq.) and the rest of water (7 mL). The obtained heterogeneous mixture was stirred vigorously from 1-3 days or until TLC ( $\text{CH}_2\text{Cl}_2/\text{AcOEt}$  3:1) analysis indicated complete consumption of reactants. The reaction was diluted with 200 mL of  $\text{NH}_4\text{OH}$ . Thirty minutes later it was extracted with  $\text{Et}_2\text{O}$  (3 x 50 mL). The organic layers were combined and washed once with brine (80 mL). The ethereous layer was dried over anhydrous  $\text{Na}_2\text{SO}_4$  and concentrated under reduced pressure. The solid residue was purified by column chromatography on silica gel ( $\text{CH}_2\text{Cl}_2/\text{AcOEt}$  3:1) to yield the corresponding aldehydes **174** (Scheme 4.5).



Scheme 4.5. Synthesis of triazole-pyrrole aldehydes

The corresponding aldehyde **174** (1 mmol) was placed in a two-neck round bottom flask and subjected to vacuum/nitrogen cycles (x3). Over the solid it was added degassed MeOH (5 mL/mmol), the corresponding pyrrole<sup>240</sup> (2 eq.) and HCl (MeOH) (2 eq.), drop by drop during 15 minutes. The mixture was stirred under nitrogen, at r.t., overnight or until aluminium oxide TLC (Hexane:AcOEt 3:1) analysis indicated total consumption of the starting material. MeOH was evaporated under reduced pressure. The obtained solid was purified by column chromatography using aluminium oxide of Brockman grade III and different mobile phases of hexane/AcOEt, depending on the aliphatic tail length. The corresponding triazole-prodiginine analogs **166–171** were obtained in excellent yields (Scheme 4.6).



Scheme 4.6. Synthesis of triazole-prodigiosin analogs

### 3. VESICLES TRANSPORT ASSAYS

Standard literature procedures were followed to prepare the vesicles used in the transport studies.<sup>241</sup> In all cases, the intra- and extravesicular solutions were buffered to pH 7.2 with NaH<sub>2</sub>PO<sub>4</sub>. The concentration of this salt varies depending on the assay. The ionic strength of both solutions (intra- and extravesicular) was always the same, in order to avoid damages of the vesicle membranes.

<sup>240</sup> Two different pyrroles have been used. 2-methyl-3-pentyl-1H-pyrrole prepared as previously reported by Trofimov, B. A. *et al*, *Chem. Heterocycl. Comp.*, 1985, **21**, 46–49 (Translated from *Khimiya Geterotsiklicheskikh Soedinenii*, 1985, **1**, 59–62) and 2,4-dimethyl-1H-pyrrole commercially available.

<sup>241</sup> R. C. MacDonald, R. I. MacDonald, B. P. M. Menco, K. Takeshita, N. K. Subbarao and L. R. Hu, *Biochim. Biophys. Acta*, 1991, **1061**, 297–303.

### 3.1. Preparation of vesicles

Two different kinds of vesicles were prepared depending on the assay in which they were going to be used. One of them were made only with POPC (1-palmitoyl-2-oleoyl-sn-glycero-3-phosphocholine), and the other were composed by POPC and cholesterol in a 7:3 relationship, respectively. POPC (20 mg/mL = 26.32 mM) and cholesterol (26.32 mM) stock solutions were prepared in chloroform and were kept in the freezer. Below is detailed the vesicle preparation process when two mL of POPC solution are used.

For preparing POPC vesicles, 2 mL of the POPC solution was added to a 5 mL round bottom flask. In the case of POPC:cholesterol (7:3), a mixture of 2 mL of the POPC and 0.6 mL of the cholesterol solutions were added to a 5 mL round bottom flask. The solvent was evaporated using a rotary evaporator (20 °C) and dry overnight under high vacuum. On the next morning, the obtained lipid film was rehydrated with 1 mL of the required internal solution corresponding to each assay, followed by careful vortexing. The obtained lipid suspension, composed of multilamellar vesicles with different sizes, was subjected to seven freezer and thaw cycles (introducing the flask in a dewar with liquid nitrogen followed by immersing it into warm water). In this point, the lipid solution was made of unilamellar vesicles with different sizes. In order to standardize the size, the suspension was extruded through 100 or 200 nm polycarbonate nucleopore membrane using a LiposoFast Basic extruder (Avestin, Inc.).

Once the vesicles were prepared, the next step was removing the non-encapsulated rehydrating solution. There are two different manners of proceeding. One of them consists in placing the lipid suspension in a dialysis membrane and dialysed it against the external required solution (2 x 500 mL). The other one lies in carrying out a Size Exclusion Chromatography (SEC) on a Sephadex G-50 column. Finally, the vesicles suspension was brought to a 10 mL volumetric flask, to obtain a known-concentration lipid solution (5.26 mM for 2 mL of POPC).

$$2 \text{ mL} \cdot \frac{20 \text{ mg POPC}}{1 \text{ mL}} \cdot \frac{1 \text{ mmol POPC}}{760 \text{ mg POPC}} \cdot \frac{1}{10 \text{ mL}} = 5.26 \cdot 10^{-3} \text{ M} = 5.26 \text{ mM POPC}$$

For example, if the POPC concentration in each assay is 0.5 mM in a total volume of 5 mL, each assay contains 475  $\mu$ L of the 5.26 mM solution:

$$C_c \cdot V_c = C_d \cdot V_d \longrightarrow 5.26 \text{ mM} \cdot V_c = 0.5 \text{ mM} \cdot 5000 \mu\text{L} \longrightarrow V_c = 475 \mu\text{L}$$

In a vesicle assay, the transporter concentration could be expressed in molarity or as a function of the POPC amount. For example, in a 0.5 mM lipid assay, 5  $\mu\text{M}$  is equivalent to 1 mol% carrier to POPC.

$$\frac{0.005 \text{ mM carrier}}{0.5 \text{ mM POPC}} \cdot 100 = 1 \text{ mol\% carrier to POPC}$$

### 3.2. Transport assays

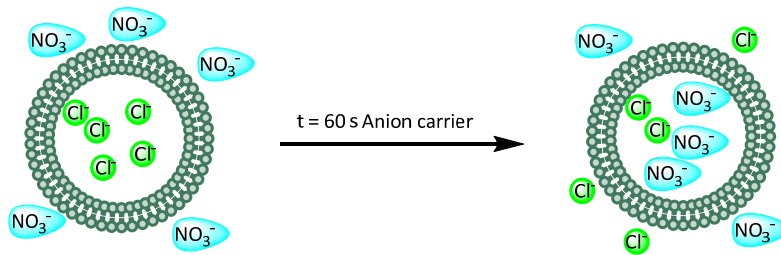
Below are described the conditions applied in the different transmembrane transport assays.

#### 3.2.1. Electrochemical transport assays. Chloride Selective Electrode assays and Hill plots

Potentiometric techniques consist on quantify an ion concentration in solution. This assay is focused on determining the chloride concentration using a Chloride Selective Electrode (Ion Selective Electrode, ISE).

POPC vesicles were prepared as described in the *Section 3.1* of this chapter. The non-encapsulated rehydrating solution was removed by dialysis with the external solution (2 x 500 mL). The intra- and extravesicular composition are outlined below. All ISE assays were carried out using a total volume of 5000  $\mu\text{L}$  and an experiment time of 300 s. Unilamellar vesicles were suspended in the external solution to give a final lipid concentration of 0.5 mM POPC. At  $t = 60$  s (unless other specification), a DMSO solution of the anion carrier was added to the sample. This pulse was never higher than 20  $\mu\text{L}$  in order to avoid influence of the solvent. The chloride efflux out of the vesicles was monitored over time, using the combination chloride electrode. At  $t = 300$  s, a 20  $\mu\text{L}$  pulse of Triton X-10% (v/v) (detergent) was added in order to lyse the vesicles and release all chloride anions. In the data processed step, this total value of chloride anions was considered as 100 % and the rest of dates were calibrated as a function of it.

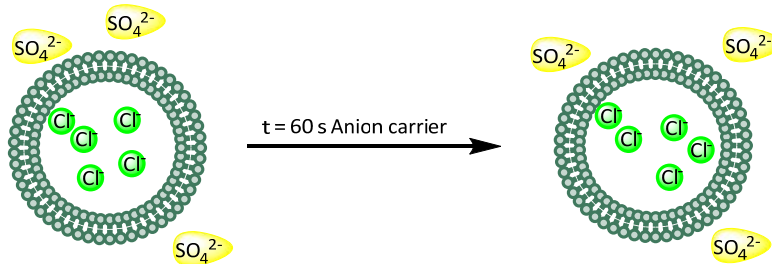
### 3.2.1.1. $\text{NO}_3^-/\text{Cl}^-$ exchange



Scheme 4.7. Schematic representation of the  $\text{NO}_3^-/\text{Cl}^-$  I.S.E. transport assays

- Intravesicular solution: 489 mM NaCl, I.S. 500 mM,  $\text{NaH}_2\text{PO}_4$  5 mM, pH 7.2
- Extravesicular solution: 489 mM  $\text{NaNO}_3$ , I.S. 500 mM,  $\text{NaH}_2\text{PO}_4$  5 mM, pH 7.2
- $t = 0$  s vesicles + buffer
- $t = 60$  s anion carrier addition in DMSO solution
- $t = 300$  s 20  $\mu\text{L}$  Triton X (10% v/v)
- Total time: until stable lecture (30–60 s)

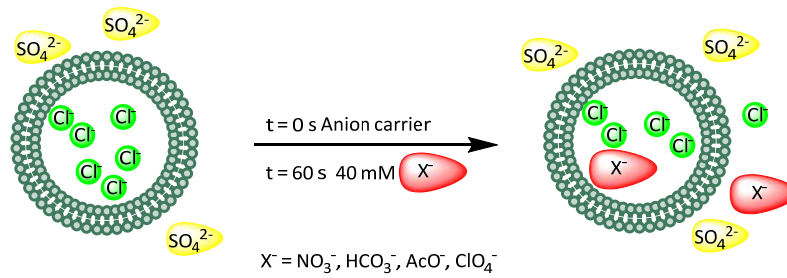
### 3.2.1.2. $\text{SO}_4^{2-}/\text{Cl}^-$ exchange



Scheme 4.8. Schematic representation of the  $\text{SO}_4^{2-}/\text{Cl}^-$  I.S.E. transport assays

- Intravesicular solution: 451 mM NaCl, I.S. 500 mM,  $\text{NaH}_2\text{PO}_4$  20 mM, pH 7.2
- Extravesicular solution: 150 mM  $\text{Na}_2\text{SO}_4$ , I.S. 500 mM,  $\text{NaH}_2\text{PO}_4$  20 mM, pH 7.2
- $t = 0$  s vesicles + buffer
- $t = 60$  s anion carrier addition in DMSO solution
- $t = 300$  s 20  $\mu\text{L}$  Triton X (10% v/v)
- Total time: until stable lecture (30–60 s)

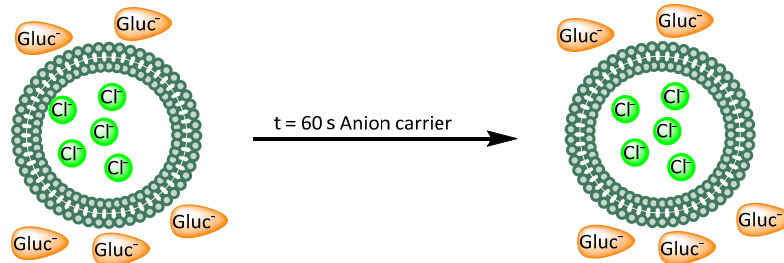
### 3.2.1.3. $\text{HCO}_3^-/\text{Cl}^-$ , $\text{AcO}^-/\text{Cl}^-$ , $\text{ClO}_4^-/\text{Cl}^-$ and $\text{NO}_3^-/\text{Cl}^-$ exchange



Scheme 4.9. Schematic representation of the  $\text{HCO}_3^-/\text{Cl}^-$  I.S.E. transport assays

- Intravesicular solution: 451 mM NaCl, I.S. 500 mM,  $\text{NaH}_2\text{PO}_4$  20 mM, pH 7.2
- Extravesicular solution: 150 mM  $\text{Na}_2\text{SO}_4$ , I.S. 500 mM,  $\text{NaH}_2\text{PO}_4$  20 mM, pH 7.2
- $t = 0 \text{ s}$  vesicles + buffer + anion carrier in DMSO solution (if it is not active in  $\text{Cl}^-/\text{SO}_4^{2-}$  assays, otherwise it is added at  $t = 50 \text{ s}$ )
- $t = 60 \text{ s}$  40 mM  $\text{Na}^+\text{X}^-$  (400  $\mu\text{L}$  of  $\text{Na}^+\text{X}^-$  500 mM; prepared in the external buffer)
- $t = 300 \text{ s}$  20  $\mu\text{L}$  Triton X (10% v/v)
- Total time: until stable lecture (30–60 s)

### 3.2.1.4. Gluconate $^-/\text{Cl}^-$ exchange



Scheme 4.10. Schematic representation of the Gluconate $^-/\text{Cl}^-$  I.S.E. transport assays

- Intravesicular solution: 489 mM NaCl, I.S. 500 mM,  $\text{NaH}_2\text{PO}_4$  5 mM, pH 7.2
- Extravesicular solution: 489 mM NaGluconate, I.S. 500 mM,  $\text{NaH}_2\text{PO}_4$  5 mM, pH 7.2
- $t = 0 \text{ s}$  vesicles + buffer
- $t = 60 \text{ s}$  anion carrier addition in DMSO solution

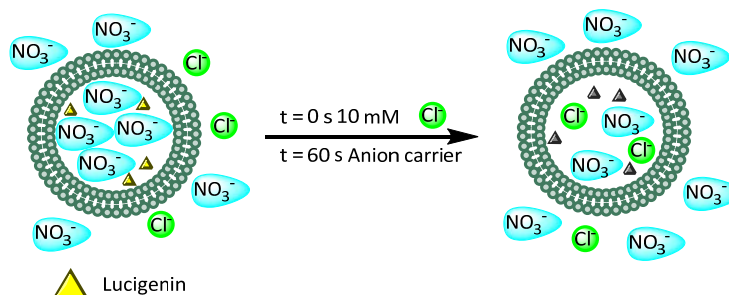
- $t = 300 \text{ s}$  20  $\mu\text{L}$  Triton X (10% v/v)
- Total time: until stable lecture (30–60 s)

### 3.2.2. Photochemical transport assays. Fluorescence probes

Luminescence phenomena are highly sensitive to environment changes. These assays are based on some fluorophores which fluorescence varies as a function of changes in different variables such as concentration (carboxyfluorescein), pH (HPTS), membrane potential (safranin O) or the presence of some ions (lucigenin is selectively quenched by chloride), previously mentioned in Chapter I.

POPC and POPC:cholesterol (7:3) vesicles were used in these experiments. They were prepared as described in the Section 4.1 of this chapter. The non-encapsulated rehydrating solution was removed by SEC, using as mobile phase the external buffer. The intra- and extravesicular compositions are outlined below. Use and throw cuvettes were used in these assays. The total volume was 2500  $\mu\text{L}$ . Vesicles were suspended in the external solution and the final lipid composition, as well as, the solvent in which the anion carrier was added depend on de fluorescent probe. Unless other specification, the anion carrier was added at  $t = 60 \text{ s}$ . The fluorescence changes were monitored over time (the working wavelength depends on the fluorescence probe) and finally the data were processed as convenient.

#### 3.2.2.1. Lucigenin based assays



Scheme 4.11. Schematic representation of lucigenin transport assays

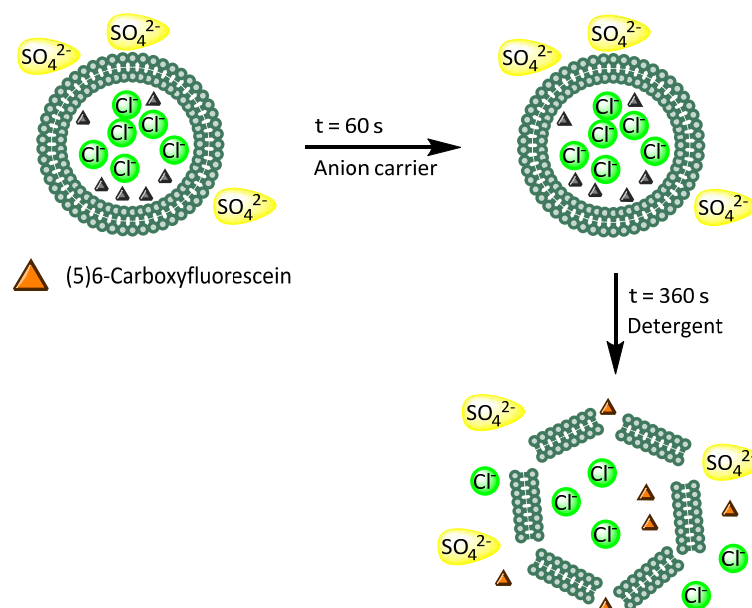
- POPC:cholesterol (7:3) vesicles 0.5 mM in POPC
- Intravesicular solution: 102.2 mM  $\text{NaNO}_3$ , I.S. 150 mM,  $\text{NaH}_2\text{PO}_4$  20 mM, pH 7.2; Lucigenin 3 mM
- Extravesicular solution: 102.2 mM  $\text{NaNO}_3$ , I.S. 150 mM,  $\text{NaH}_2\text{PO}_4$  20 mM, pH 7.2

- $t = 0$  s vesicles + buffer + 10 mM NaCl (100  $\mu$ L of NaCl 250 mM; prepared in the external buffer)
- $t = 60$  s anion carrier addition in MeOH solution.
- Total time 360 s
- $\lambda_{\text{exc}} = 372$  nm;  $\lambda_{\text{exc}} = 503$  nm

#### Data processed

The obtained data were processed as described in Chapter II (Section 2.5).

#### 3.2.2.2. 5(6)-Carboxyfluorescein based assays



Scheme 4.12. Schematic representation of carboxyfluorescein transport assays

- POPC vesicles 0.025 or 0.05 mM
- Intravesicular solution: 451 mM NaCl, I.S. 500 mM,  $\text{NaH}_2\text{PO}_4$  20 mM, pH 7.2; carboxyfluorescein 50 mM
- Extravesicular solution: 150 mM  $\text{Na}_2\text{SO}_4$ , I.S. 500 mM,  $\text{NaH}_2\text{PO}_4$  20 mM, pH 7.2
- $t = 0$  s vesicles + buffer
- $t = 60$  s anion carrier addition in DMSO solution
- $t = 360$  detergent. The fluorescence was recorded 2 more minutes

- Total time = 480 s
- $\lambda_{\text{exc}} = 490 \text{ nm}$ ;  $\lambda_{\text{exc}} = 520 \text{ nm}$

**Data processed**

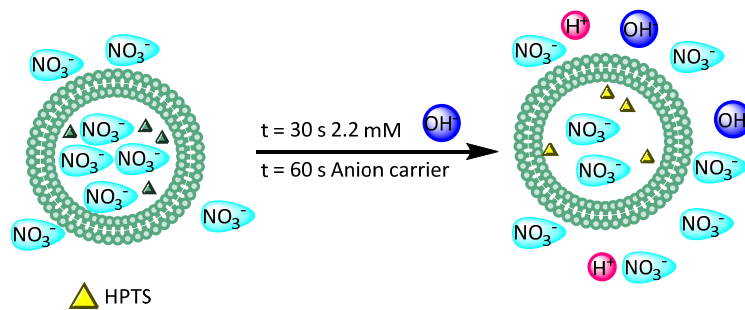
Equation 4.1 is applied to the obtained data.

$$\text{CF leakage} = \left[ \frac{I_t - I_0}{I_{\text{máx}} - I_0} \right]_{\lambda = 520 \text{ nm}}$$

$I_t \rightarrow$  fluorescence intensity at time t  
 $I_0 \rightarrow$  fluorescence intensity at time 0  
 $I_{\text{máx}} \rightarrow$  maximum fluorescence intensity observed after addition of detergent.

Equation 4.1. CF leakage vs spectrophotometric relation of fluorescence intensity

**3.2.2.3. HPTS based assays**



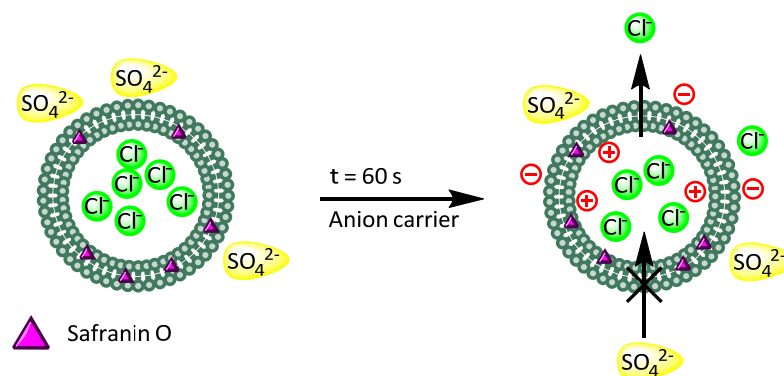
Scheme 4.13. Schematic representation of HPTS transport assays

- POPC:cholesterol (7:3) vesicles 0.5 mM in POPC
- Intravesicular solution: 126.2 mM  $\text{NaNO}_3$ , I.S. 150 mM,  $\text{NaH}_2\text{PO}_4$  10 mM, pH 7.2; HPTS 10  $\mu\text{M}$
- Extravesicular solution: 126.2 mM  $\text{NaNO}_3$ , I.S. 150 mM,  $\text{NaH}_2\text{PO}_4$  10 mM, pH 7.2
- $t = 0 \text{ s}$  vesicles + buffer
- $t = 30 \text{ s}$  a pulse of NaOH (11  $\mu\text{l}$  of 0.5 M) to obtain a 2.2 mM final concentration
- $t = 60 \text{ s}$  anion carrier addition in DMSO solution.
- Total time 360 s
- $\lambda_{\text{exc}} = 403 \text{ nm}$  and 460 nm simultaneously;  $\lambda_{\text{exc}} = 510 \text{ nm}$

**Data processed**

The obtained data were processed as described in Chapter II (Section 2.5).

## 3.2.2.4. Safranin O based assays



Scheme 4.14. Schematic representation of safranin O transport assays

- POPC vesicles 0.25 mM
- Intravesicular solution: 28.8 mM NaCl, I.S. 40 mM, NaH<sub>2</sub>PO<sub>4</sub> 5 mM, pH 7.2
- Extravesicular solution: 19.6 mM Na<sub>2</sub>SO<sub>4</sub>, I.S. 40 mM, NaH<sub>2</sub>PO<sub>4</sub> 5 mM, pH 7.2
- The internal solution non encapsulated is not removed
- t = 0 s vesicles + buffer + Safranin O 0.2 μM (0.08 mol % to lipid) (5 μL 0.1 mM prepared in the external buffer).
- t = 120 s anion carrier addition in DMSO solution
- Total time = 600 s
- λ<sub>exc</sub> = 520 nm; λ<sub>exc</sub> = 580 nm

**Data processed**

The obtained data were plotted as  $I/I_{t=120s}$  against time.

**4. TITRATION AND JOB PLOT ANALYSIS**

This technique let us know the anions and receptor stoichiometry. It gives information about the selectivity between different anions and let us calculate the binding constant values.

<sup>1</sup>H NMR titrations were made using as solvent DMSO-*d*<sub>6</sub> with 0.5% H<sub>2</sub>O. 1 mL of a 0.005–0.01 M solution of the studied anion carrier (receptor) was prepared in a vial. 0.5 mL of this solution were added to a NMR tube. Using the remaining 0.5 mL,

a solution of the desired anion (guest) was prepared (~ 0.1 M). Small aliquots of the guest solution were added to the NMR tube until a 6:1 receptor:guest ratio was reached. After each addition, it was stirred vigorously and a  $^1\text{H}$  NMR spectrum was recorded. Working in this way, implies an increasing concentration of the guest while the receptor concentration remains constant.  $^1\text{H}$  NMR chemical shift was calibrated to the solvent peak. The data of the affected signal/s were fitted to a 1:1 binding model using WinEQNMR2 software in order to obtain the association constants.<sup>242</sup>

## 5. CALCULATION OF LUCIGENIN STERN VOLMER CONSTANTS

The fluorescence dynamic quenching is described by the Stern-Volmer equation (equation. 2.8, described in Chapter II). Lucigenin follows a dynamic quenching mechanism.

$$\frac{I_0}{I} = 1 + K_{SV} \cdot [Q] \quad \text{Equation 2.8}$$

Six different Stern Volmer constants of lucigenin were calculated under different conditions. Lucigenin solutions were prepared in accordance with the following specifications.

- $\text{NaNO}_3$  88.2 mM, phosphate buffer 5 mM, pH 7.2, I.S. 100 mM. Lucigenin 0.02 mM
- $\text{NaNO}_3$  88.2 mM, phosphate buffer 5 mM, pH 7.2, I.S. 100 mM. Lucigenin 0.001 mM
- $\text{Na}_2\text{SO}_4$  17.6 mM, phosphate buffer 20 mM, pH 7.2, I.S. 100 mM. Lucigenin 0.02 mM
- $\text{Na}_2\text{SO}_4$  17.6 mM, phosphate buffer 20 mM, pH 7.2, I.S. 100 mM. Lucigenin 0.001 mM
- $\text{NaNO}_3$  489 mM, phosphate buffer 5 mM, pH 7.2, I.S. 500 mM. Lucigenin 0.02 mM
- $\text{NaNO}_3$  489 mM, phosphate buffer 5 mM, pH 7.2, I.S. 500 mM. Lucigenin 0.001 mM

---

<sup>242</sup> M. J. Hynes, *J. Chem. Soc. Dalton*, 1993, 311-312.

The measurements were carried out using a HITACHI F-7000 Fluorescence spectrophotometer equipped with stirrer. A stir bar was placed inside the use and throw cuvette with an initial volume of lucigenin solution of 1.3 mL. Successive additions of NaCl, prepared in the corresponding lucigenin solution in order to avoid dilution, were added. The fluorescence spectra after each addition was recorded at 503 nm after exciting at 372 nm. The Stern Volmer constants,  $K_{SV}$  ( $M^{-1}$ ) were determined from the slope of plotting  $I_0/I$  vs the chloride (quencher) concentration (M). Where  $I_0$  is the lucigenin fluorescence in absence of quencher and  $I$  is the fluorescence after each addition.

## 6. pKa MEASUREMENTS

A  $5 \cdot 10^{-6}$  M solution of the studied compound was prepared in a 12 mL (vial), in a mixture 4:1 DMSO–H<sub>2</sub>O (v/v) (0.1 M NaCl) at 25 °C. The pH was adjusted to ~ 5 using HCl 1M (in 0.1 M NaCl). Increasing aliquots of NaOH 1M (in 0.1 M NaCl) were then added. After each addition a portion of the solution was passed to a quartz cuvette and its absorbance spectra was recorded. This aliquot of solution was returned to the vial and a pulse of NaOH (1M) was added to increase the pH. This procedure was followed until pH ~ 10. pKa values were determined from a plot of log (ionization ratio) vs pH (equation 4.2).

$$\text{Log} \left( \frac{A - A_{A^-}}{A_{AH} - A} \right) = -\text{pH} + \text{pKa} \quad \text{equation 4.2}$$

Where:

- A is the absorbance at a time, (it was used  $\lambda_{\text{abs, max}}$  of protonated form)
- $A_{A^-}$  is the absorbance of the neutral form, at its  $\lambda_{\text{abs, max}}$  of non protonated form
- $A_{AH}$  is the absorbance of the protonated form, at its  $\lambda_{\text{abs, max}}$  of protonated form